PRECIPITATION FACTORS LEADING TO ARC CLOUD FORMATION

Final Report

October 1985 - April 1987

Principal Investigator: K. C. Brundidge

Texas A&M University

College Station, Texas 77843-3146

Prepared for George C. Marshall Space Flight Center

under Grant NAG8-043

PREFACE AND ACKNOWLEGEMENTS

This report represents the combined efforts of three graduate students and the Principal Investigator. Accordingly, it is in three sections with separate indexing for each section.

The section titles are as follows:

1. Factors Leading to the Formation of Arc Cloud Complexes.
2. Convective Cell Development and Propagation in a Mesoscale Complex.
3. Nighttime Atmospheric Stability Changes and their Effects on the Temporal Intensity of a Mesoscale Convective Complex.

Section 1 represents the main thrust of the effort as stated in the contract. The others developed as we went along. Section 3 is an incomplete study at the time of this report but was to the stage that some preliminary results could be given.

The authors are grateful for the sponsorship of this work by the National Aeronautics and Space Administration under Grant NAG8-043. Special thanks is given to Dr. James Arnold of the Atmospheric Sciences Division, Space Science Laboratory of the Marshall Space Flight Center who guided the Principal Investigator into a study of mesoscale convective systems during the brief period he spent with the Atmospheric Science Division. Gratitude also is expressed to Mr. Paul Meyer for his devoted efforts to procure synoptic data and satellite imagery used in these studies and for his assistance in the use of the McIDAS system at the Marshall Space Flight Center.

FACTORS LEADING TO THE FORMATION OF ARC CLOUD COMPLEXES

Mark John Welshinger
and
Kenneth C. Brundidge

Texas A&M University
College Station, Texas

Prepared for George C. Marshall Space Flight Center

under Contract NAG8-043

ABSTRACT

Factors leading to the formation of arc cloud complexes

A total of 12 mesoscale convective systems (MCSs) were investigated. The duration of the gust front, produced by each MCS, was used to classify the MCSs. Category 1 MCSs were defined as ones that produced a gust front and the gust front lasted for more than 6 h. There were seven category 1 MCSs in the sample. Category 2 MCSs were defined as ones that produced a gust front and the gust front lasted for 6 h or less. There were four category 2 MCSs. The MCS of Case 12 was not categorized because the precipitation characteristics were similar to a squall line, rather than an MCS. All of the category 1 MCSs produced arc cloud complexes (ACCs), while only one of the category 2 MCSs produced an ACC. To determine if there were any differences in the characteristics between the MCSs of the two categories, composite analyses were accomplished. The analyses showed that there were significant differences in the characteristics of category 1 and 2 MCSs. Category 1 MCSs, on average, had higher thunderstorm heights, greater precipitation intensities, colder cloud top temperatures and produced larger magnitudes of surface divergence than category 2 MCSs. It was deduced that the more pronounced characteristics of category 1 MCSs played an important role in the conversion of an MCS to an ACC.

ACKNOWLEDGMENTS

The authors thank Dr. Aylmer H. Thompson, whose helpful comments aided tremendously in the preparation of this report. Mrs. Jacquelyn V. Strong typed the manuscript.

The National Aeronautics and Space Administration sponsored this research through Contract NAG8-043 under the auspices of the Atmospheric Sciences Division, Space Sciences Laboratory, Marshall Space Flight Center. Special thanks are extended to Mr. Paul Meyer for his assistance in procuring satellite images and other data through the McIDAS system at the Marshall Space Flight Center.

TABLE OF CONTENTS

LIST OF TABLES

LIST OF FIGURES

LIST OF FIGURES (Continued)

LIST OF FIGURES (Continued)

CHAPTER I

INTRODUCTION

Since the launch of the first operational weather satellite in February 1966 (Schnapf, 1982), satellite observations and interpretation have become increasingly important in the areas of weather research and operational forecasting. One reason is that geostationary satellite imagery is the only meteorological observing tool that can follow the evolution of clouds from the synoptic scale down to the cumulus scale. Therefore, it can depict atmospheric activity which is up to two orders of magnitude smaller than can be resolved by conventional meteorological observations. This unique ability of the satellite provides the meteorologist a mechanism to infer weather events down to the mesoscale.

A well-known phenomenon which occurs as a thunderstorm propagates past a station is the rise and oscillation of the surface pressure. Downdrafts descending from thunderstorm cells are the source of the air forming the cold dome over the ground, which leads to the rise in surface pressure (Byers and Braham, 1949; Fujita, 1959, 1963). If the downdrafts of cold air are strong enough and last for a sufficient time, an organized high pressure system develops at the surface. This high pressure system is called the "mesohigh."

Purdom (1973), using satellite imagery, showed that the leading edge of a mesohigh appeared as an arc-shaped line of convective clouds moving out in all directions from a dissipating thunderstorm area. The

---

The citations on the following pages follow the style of the Journal of the Atmospheric Sciences.

arc-shaped cloud line, normally composed of cumulus, cumulus congestus, or cumulonimbus clouds, has been named the "arc cloud" (Purdom, 1973, 1976, 1979). As the leading edge of the cold air spreads outward from the storm area, it undercuts and lifts the warmer, moister air ahead of it and the arc cloud is formed.

In many ways, the structure of the leading edge of the cold air associated with the arc cloud (also referred to as the mesoscale outflow boundary) resembles a true cold front. Byers and Braham (1948) remarked that the "air mass discontinuity acts as a miniature cold front and that the movement of this pseudofront has a marked influence on the initial formation of new cells." Normally, abrupt changes in wind direction and speed, called the gust front, rapid cooling and rising pressure, sometimes called the density surge line (Sinclair and Purdom, 1982, 1984), pressure surge line (Fujita, 1955), or pressure jump line (Tepper, 1950a), accompany the passage of the outflow boundary.

Large, long-lived convective weather systems are most commonly referred to as mesoscale convective systems (MCSs). Maddox (1980) has described a specific type of MCS which he has named the "mesoscale convective complex." The definition is presented in Table 1. The definition is based on the areal extent and duration of specific cloud top temperatures observed in enhanced Geostationary Operational Environmental Satellite (GOES) infrared (IR) imagery.

The MCC, an organized meso-α scale convective system (Orlanski, 1975), is nocturnal in nature and occurs most frequently during the warm season months, March through September (Maddox, 1980; Maddox et al., 1982; Rodgers et al., 1983; Rodgers et al., 1985). Maddox surmises that

Table 1. Mesoscale convective complex (MCC) definition. The definition is based upon analysis of enhanced IR satellite imagery (after Maddox, 1980).

	Physical Characteristics
Size:	A. Cloud shield with IR temperature less than or equal to -32°C must have an area greater than or equal to 100,000 km^2.
	B. Interior cold cloud region with temperature less than or equal to -52°C must have an area greater than or equal to 50,000 km^2.
Initiate:	Size definitions A and B first satisfied.
Duration:	Size definitions A and B must be met for a period greater than or equal to 6 h.
Maximum extent:	Contiguous cold cloud shield (IR temperature less than or equal to -32°C) reaches maximum size.
Shape:	Eccentricity (minor axis/major axis) greater than or equal to 0.7 at time of maximum extent.
Terminate:	Size definitions A and B no longer satisfied.

during the genesis stage MCCs entrain mid-level, potentially cool environmental air, which produces strong, evaporationally-driven downdrafts, surface mesohighs and outflow boundaries. Similar results were obtained by Zipser (1969) in his study of a tropical convective system which developed during the Line Islands Experiment. Zipser concluded that the evaporationally-driven downdrafts had mid-tropospheric origins, somewhere between 60 kPa and 40 kPa, where environmental air of equivalent potential temperature similar to that at the surface was located.

In the development stage of an MCC, a merging of the mesohighs of individual thunderstorms produces a single large mesohigh. Vertical motions along the forward edge of the spreading, cooler air generate the arc cloud. However, the arc cloud is on a larger time and space scale than the gust front for an individual thunderstorm. The large mesohigh and surrounding arc cloud have been collectively termed an arc cloud complex (ACC) by Brundidge (1983).

The dissipation stage of the MCC is characterized by a rapid demise of the intense convection. One reason Maddox (1980) gives for the dissipation is that "the cold air dome beneath the system may become so intense that the surface convergence zone moves away from the region of mean mesoscale ascent into a region of mid- and upper-level sibsidence."

ACCs can last for many hours. Even after the demise of the MCC (or more generally the MCS), the cool air and outflow boundary may still be evident. As Maddox (1980) states, "Although the MCC rapidly loses its meso-α scale organization, the cool air and outflow boundary at the surface may persist for many hours." Sinclair and Purdom (1982) believe that the regeneration of weak precipitation along portions of the arc,

coupled with sub-cloud evaporation is one explanation for an arc cloud line being able to maintain its identity as a single feature for several hours.

Because of the long life-span of some ACCs, a chain of storm events often occurs, leading to the formation of other MCSs. Miller (1984), in a case study of an ACC, found convection along the arc cloud at different times during its life, which eventually resulted in the formation of an MCS much larger than the ACC. Bartels (1983), in a study of a dual MCC, showed that an outflow boundary associated with the western MCC was related to an MCC type system that developed over Oklahoma during the following afternoon.

Fritsch et al. (1981) showed that MCCs produce widespread regions of measureable rainfall and that they account for a significant portion of growing-season rainfall over much of the United States' corn and wheat belts. Maddox (1980) stated that many MCCs produce locally intense rainfalls and flash flooding. In Bartels' (1983) study, rains from the western MCC resulted in flash flooding. Evacuations were required in Springfield, MO and Joplin, MO, as some homes had water 3 ft deep. Since ACCs can develop into new MCCs, the ACC can be related to the occurrence of flash floods.

ACCs are often the forerunners of severe weather. Tepper (1950b) reported a case of tornado formation at the intersection of two pressure jump lines. Fujita (1963) and Miller (1972) stress the importance of intersecting boundaries, stating that these areas are favored locations for severe weather development. Using satellite imagery, Purdom (1974) showed that the intersection of an arc cloud with other existing

boundaries locates an area for new convection to develop. If atmospheric conditions are favorable, severe weather often forms at the point of intersection.

As well as the increased threat of severe weather, the ACC is a dangerous source of potential aircraft accidents (Greene, 1977). In an observational study of outflow boundaries, Goff (1976) found a wide variation between one gust front case and another. However, the updrafts along the gust front were generally concentrated in a region a few kilometers wide, with vertical motions as high as 6 to 7 m s^{-1}. Sinclair and Purdom (1984) found similar vertical motions during aircraft penetrations of the density surge line (DSL). They found upward vertical motion, with peaks as high as 10 m s^{-1}, at the DSL interface region. Between 2 and 7 km behind the DSL, a distinct transition was found from upward to downward vertical motions. Vertical motions in the sinking air ranged from -3 to -3 m s^{-1}. Therefore, if an aircraft were on final approach and encountered an outflow boundary, the extreme change in vertical motions over such a short distance across the DSL might lead to an aircraft accident (Sinclair and Purdom, 1984).

In summary, the importance of ACCs is that they can develop into new MCSs, they can be associated with the initiation of severe weather and their associated wind shear can lead to potential aircraft mishaps. The study of ACCs must include detailed studies of the entity which produces them, namely, MCSs, if our ability to forecast their occurrence is to improve. It is well-known that some MCSs produce well-defined, extremely-potent ACCs, whils others do not. What characteristics are different in MCSs that produce ACCs compared to the MCSs that yield no

ACC?

Byers and Braham (1948) showed that rain at the surface was in the downdraft area of thunderstorm cells. They also showed that the maximum intensity of rain at the surface and the maximum intensity of associated surface divergence have a very high correlation (see Fig. 1). That is, an area of heavy rain at the surface coincides with an area of strong divergence in the surface winds. The divergence is caused by the downdrafts spreading out across the ground.

In a case study of three ACCs, Brundidge (1984) hypothesized that the appearance of the arc cloud is a direct result of heavy rainfall on the south side of an MCS. This agrees with the findings of Byers and Braham (1948). From their findings, it logically follows that heavy precipitation can create strong downdrafts and subsequently a strong gust front and mesohigh. The presence of the gust front and mesohigh, in turn, is revealed in the magnitude of the surface divergence and the pattern of the surface divergence field. Therefore, heavy precipitation on the south side of an MCS can create strong downdrafts, which lead to a strong gust front and mesohigh, and eventually an arc cloud forms along the leading edge of the gust front.

Woodley et al. (1972), in their study of rainfall estimation from satellite cloud photographs, discovered several important facts about rain clouds. Two facts pertinent to this study are:

1. Clouds with cold tops in the IR imagery produce more rainfall than those with warmer tops.

2. The highest and coldest clouds form where the thunderstorms are most vigorous and the rain heaviest.

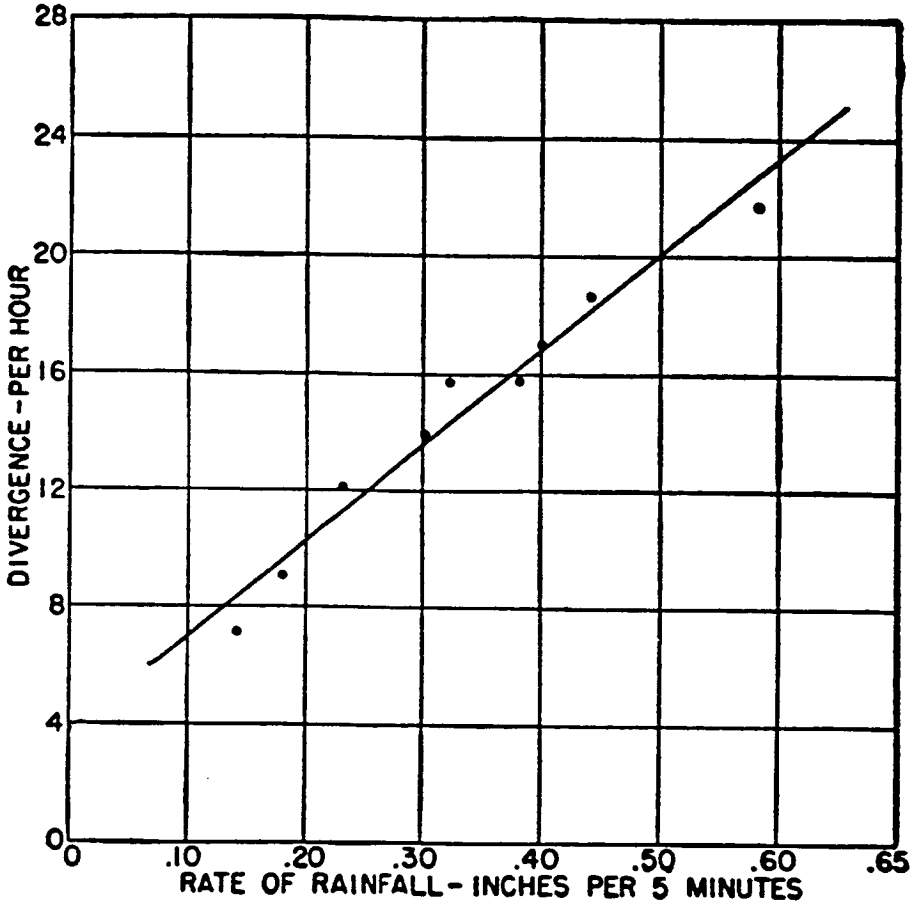

Fig. 1. Relationship between maximum intensity of rain and the maximum intensity of associated surface divergence. The line through the scatter of points is the linear regression line for the distribution. The correlation coefficient is 0.98 (after Byers and Braham, 1949).

Gagin et al. (1985) attempted to provide a comprehensive formulation of the dependence between the depth of the convective cells and their gross precipitation features. In their study, they concluded that taller cells produce larger total rain volumes by virtue of their greater rainfall intensities, their longer duration as precipitating entities and their larger precipitating areas.

Based on the studies cited above, it appears that precipitation patterns and rates, cloud top temperatures, thunderstorm heights and surface divergence patterns are interrelated and seem to play an important role for the conversion of an MCS to an ACC. It has been the purpose of this study to compare these features between MCSs that become ACCs and ones that do not. Research of this type will enable us to understand better the occurrence of ACCs and may provide the signatures manifested in satellite and radar observations which would permit forecasting the development of significant arc clouds.

CHAPTER II

RESEARCH PROCEDURES

Products Used in the Study

Several products and sources of information were used to aid in this investigation of arc cloud complexes. These were as follows:

1. The records of hourly precipitation from the climatological networks of raingauges obtained from the National Climatic Data Center (NCDC) located in Asheville, North Carolina. Figs. 2-10 show the locations by states of the various raingauges used in this study. The data received from the NCDC were plotted and analyzed on the state maps to determine patterns and rates of rainfall.

2. Sectional surface maps corresponding to the time and location of the MCSs were plotted and analyzed. Patterns in the temperature, pressure and wind fields helped ascertain the existence and strength of gust fronts.

3. Hourly radar summary charts from the National Weather Service (NWS) were used to provide comparisons of the precipitation pattern at the surface among the various MCSs. They also were used to obtain the maximum thunderstorm height, within the MCS, which occurred at the radar observation time (normally 35 min past each hour).

4. GOES imagery was used for:

    a. An aid in determining the existence of an arc cloud.

    b. Determining the duration of the arc cloud, if one existed. This aided in the classification of the MCS. The classifications of the MCSs will be discussed later.

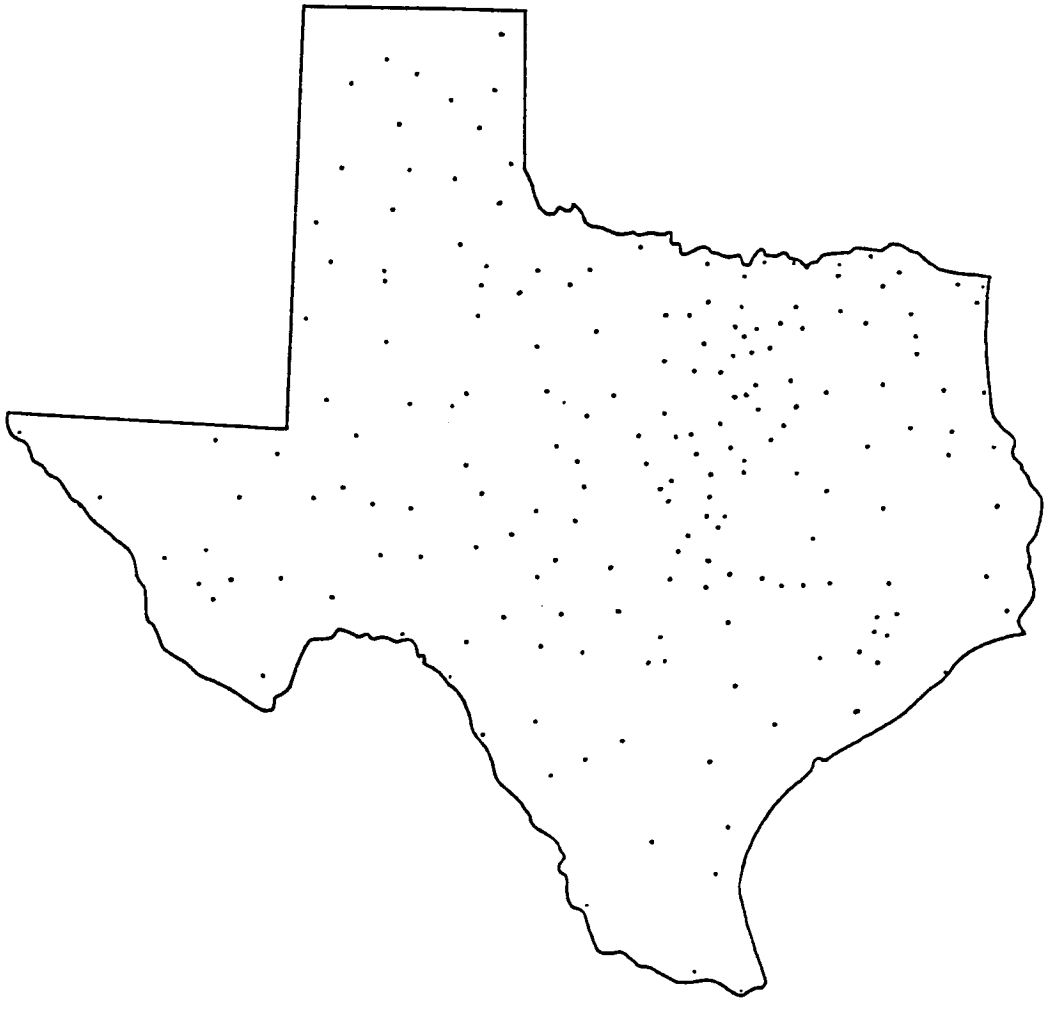

Fig. 2. Location of the climatological raingauge network in Texas.

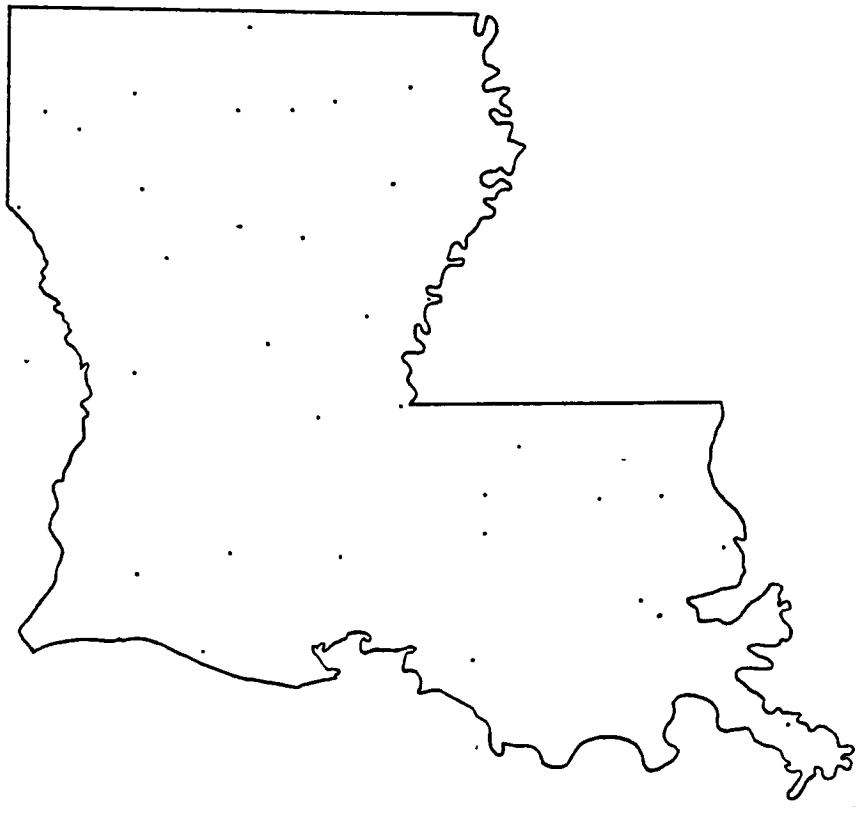

Fig. 3. Location of the climatological raingauge network in Louisiana.

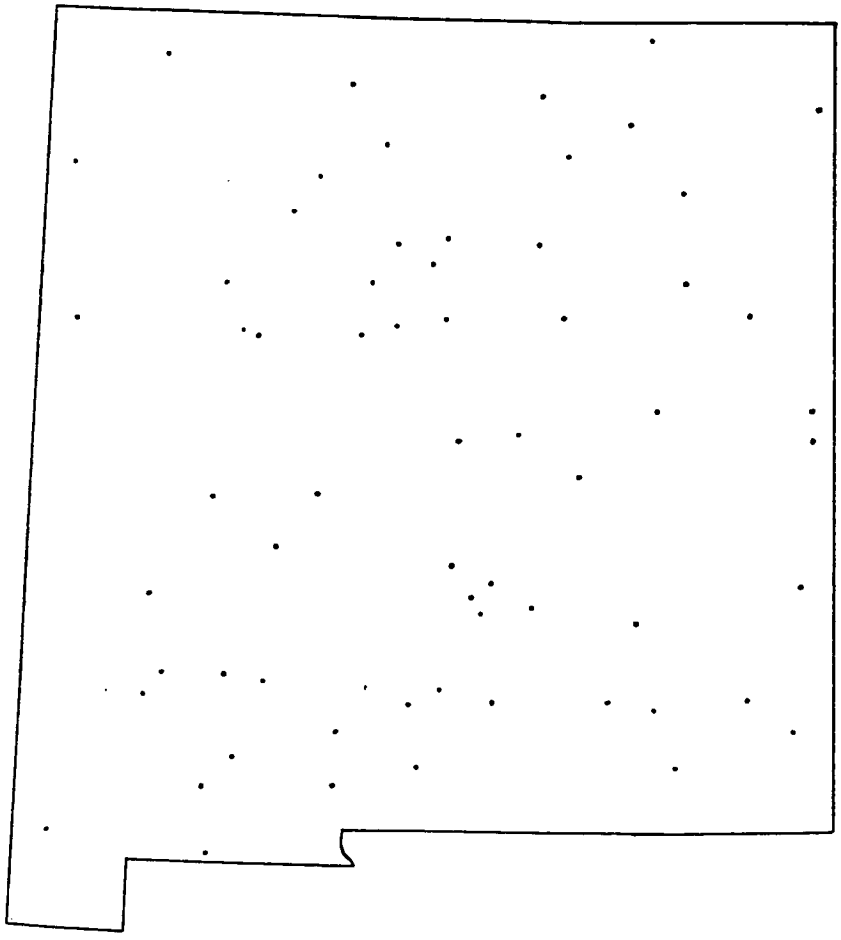

Fig. 4. Location of the climatological raingauge network in New Mexico.

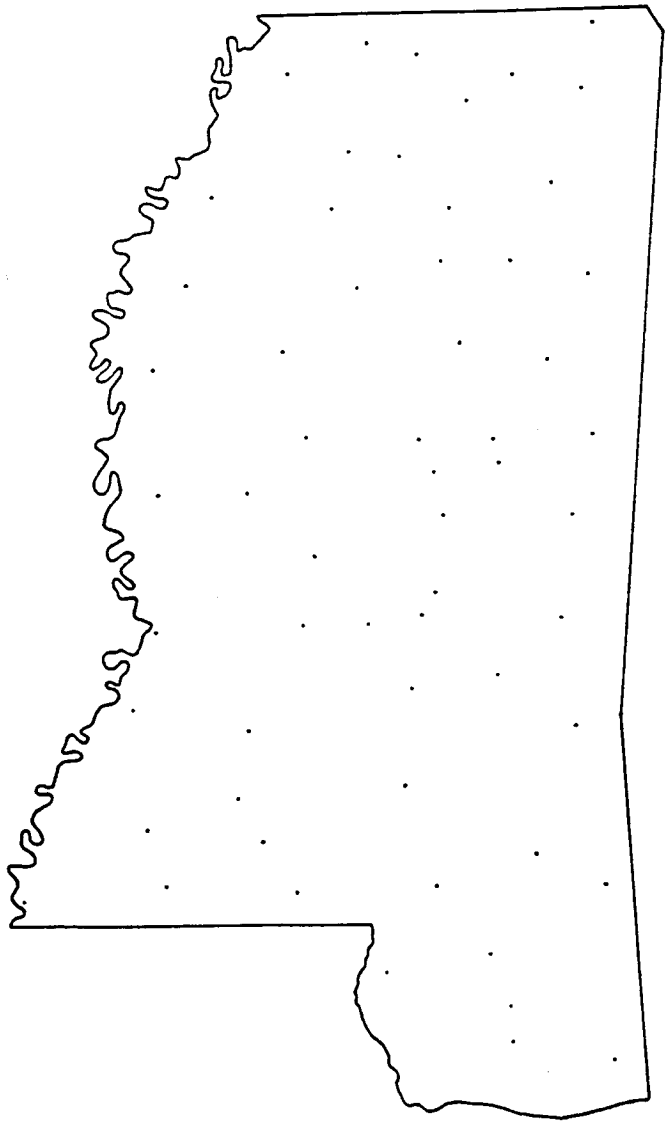

Fig. 5. Location of the climatological raingauge network in Mississippi.

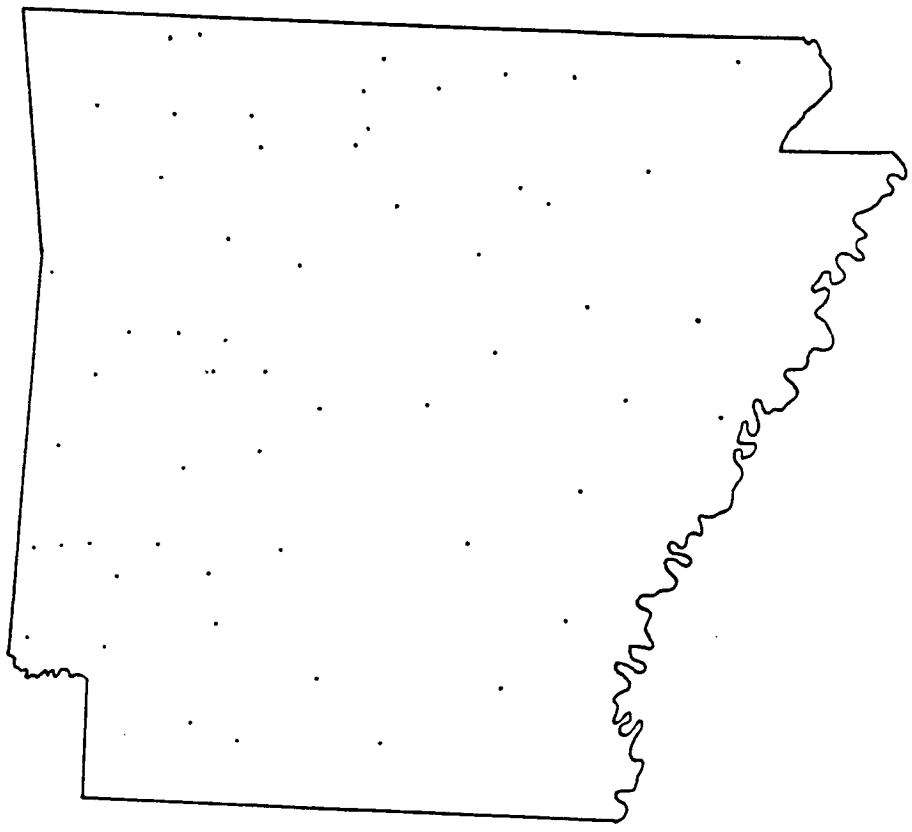

Fig. 6. Location of the climatological raingauge network in Arkansas.

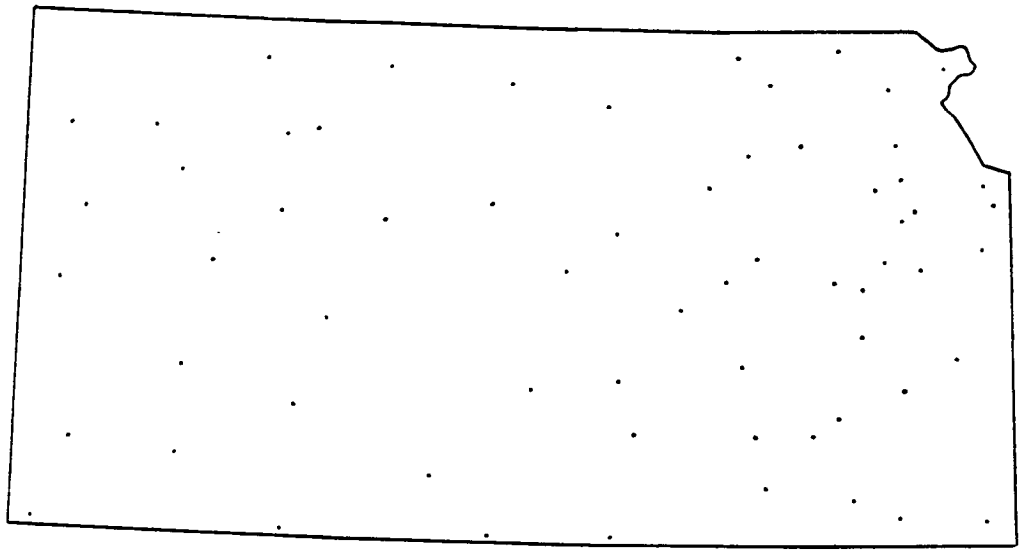

Fig. 7. Location of the climatological raingauge network in Kansas.

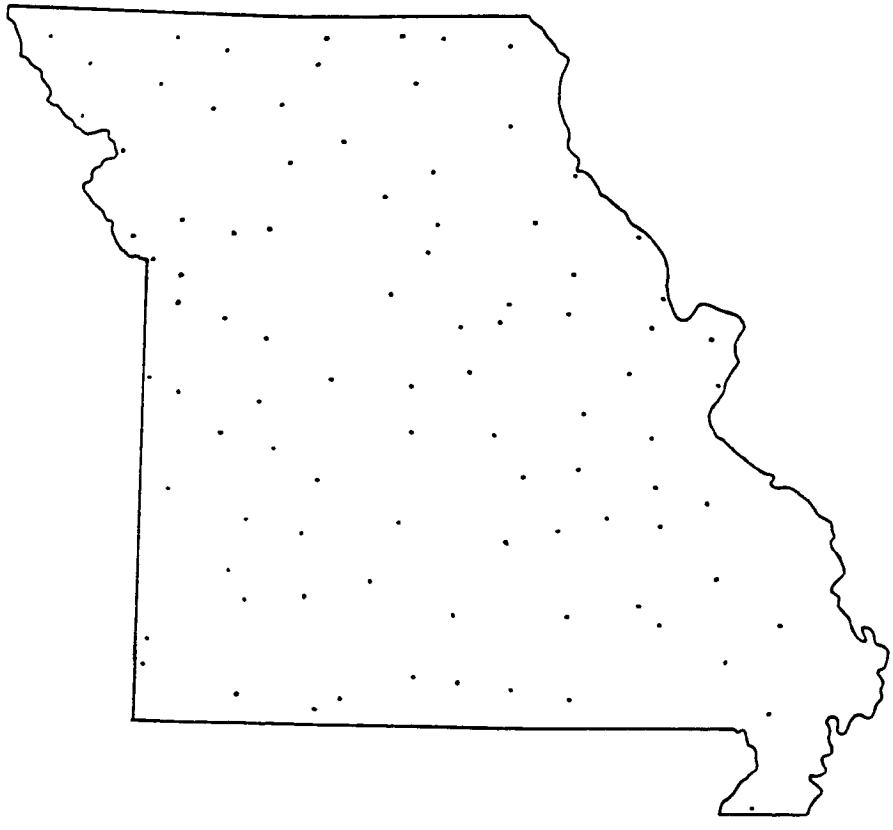

Fig. 8. Location of the climatological raingauge network in Missouri.

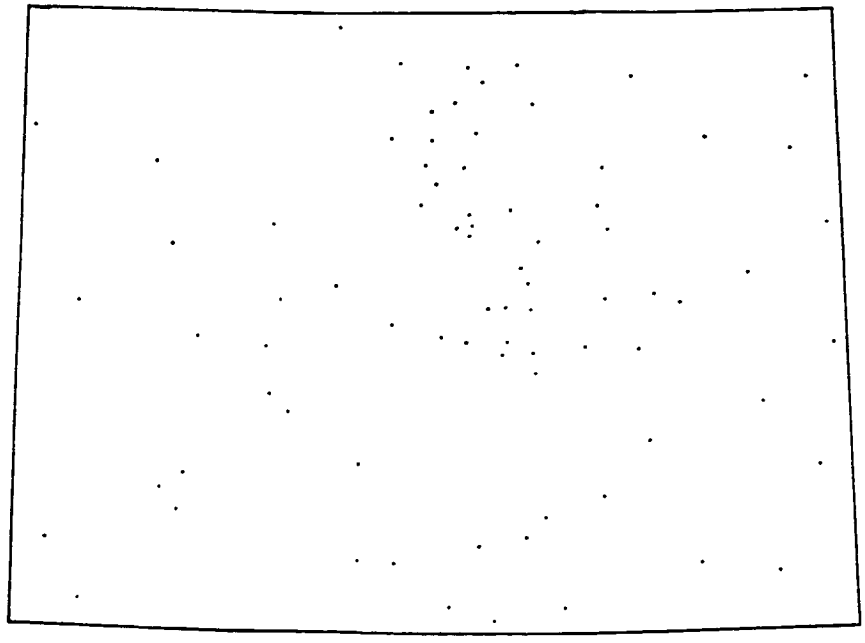

Fig. 9. Location of the climatological raingauge network in Colorado.

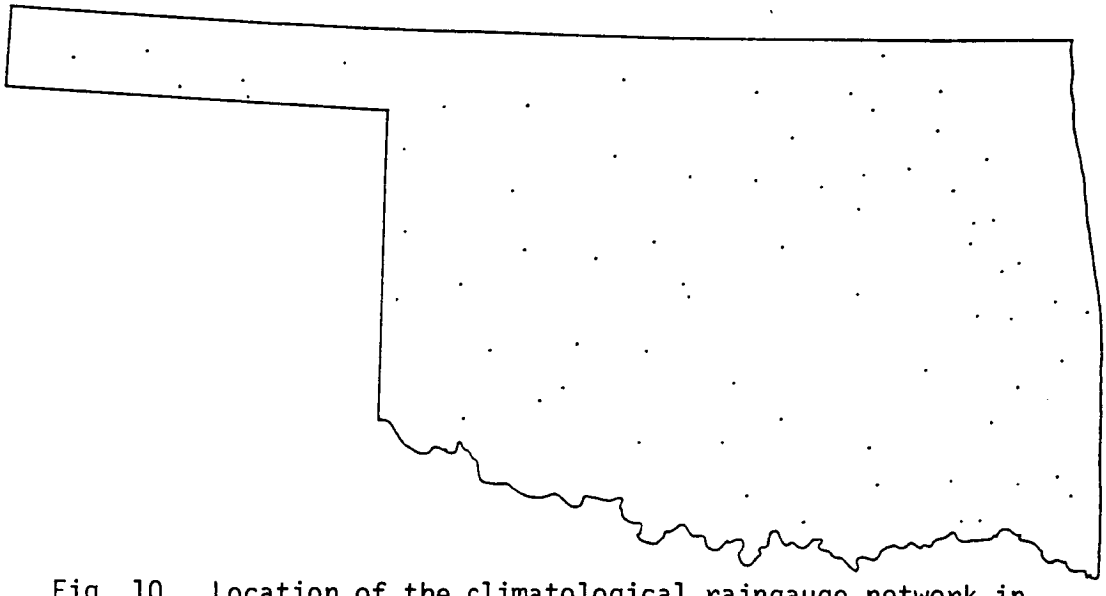

Fig. 10. Location of the climatological raingauge network in Oklahoma.

5. The Man-Computer Interactive Data Access System (McIDAS) of the Atmospheric Sciences Division of the Systems Dynamic Laboratory, Marshall Space Flight Center, provided the following products:

a. Hourly surface divergence patterns.[1]

b. Hourly contoured analysis of the cloud top temperatures as determined from the GOES IR imagery.[1]

c. Hourly surface equivalent potential temperature analysis.[1]

d. Additional satellite images.

e. A computer printout, on an hourly basis, of the size of the MCS as it appears in the satellite IR imagery. The size is referenced to the number of pixels that are contained within four specific temperature ranges: -32°C to -98°C; -52°C to -98°C; -58°C to -98°C; -62°C to -98°C.

Overview

A total of 12 cases was chosen for this study. Three publications were primarily used in selecting the various cases (Maddox et al., 1982; Rodgers et al., 1983, 1985). These articles were annual summaries of the times and locations of MCCs that occurred during 1981, 1982 and 1983. The MCSs that were chosen were studied by Brundidge (1983, 1984) and Miller (1984) and were known to produce ACCs. The cases that were finally included in this study are listed in Table 2. Also, dates and details of the life cycles of each event are listed. Of the cases selected, most of the MCSs originate or terminate in Texas. This

[1]The analysis and contours by the McIDAS are computer products obtained objectively by use of the Barnes (1973) interpolation scheme.

Table 2. Mesoscale convective systems (MCSs) included in study. Initiate and terminate times are after Maddox et al., 1982; Rodgers et al., 1983, 1985.

Case number	Date	Time (GMT)		
		Initiate	Maximum extent**	Terminate
1	10/11 Apr 81	2315/10	0300/11	0531/11
2	9 May 81	0115/09	0500/09	1015/09
3	27 May 81	0515/27	1000/27	1400/27
4	17 May 82	0030/17	0400/17	0730/17
5	19 May 82	*	0900/19	*
6	10/11 Jun 82	2245/10	0700/11	1530/11
7	26 Jun 82	*	1100/26	*
8	27 Jun 82	0800/27	0900/27	1400/27
9	28/29 Jun 82	2230/28	0200/29	0430/29
10	20 May 83	0130/20	0800/20	1300/20
11	11 Jun 83	0530/11	0900/11	1200/11
12	14 Jun 83	0130/14	0600/14	1600/14

*These cases were not MCCs; therefore, initiate and terminate times were not available.

**The times listed are the maximum extent of the area, as depicted on IR satellite imagery, with temperatures $\leq$ -62°C. This information was determined by the use of McIDAS.

stipulation was employed because of the denser climatological rainguage network in Texas, compared to the other states (see Figs. 2-10).

Each case was carefully analyzed to determine if a gust front existed. Hourly surface maps, hourly surface divergence patterns provided by the McIDAS and satellite pictures, both visual and IR, were used to determine the existence and duration of a gust front.

The various MCSs were then categorized as follows:

1. MCS produces gust front and the gust front persists more than 6 h. This is referred to as a category 1 MCS.

2. MCS produces gust front and the gust front persists for 6 h or less. This is referred to as a category 2 MCS.

After the cases were categorized, each case was further analyzed for the following characteristics associated with the MCS:

1. Maximum hourly surface divergence.

2. Coldest hourly cloud top temperature.

3. Maximum hourly point precipitation rates.

4. Sum of the three largest hourly precipitation rates. An explanation of this analysis procedure is as follows. Assume an MCS produced the following rainfall rates, for a particular hour, at six climatological rainguage sites: 0.8, 2.2, 1.5, 0.3, 1.7 and 2.0 in h^{-1}. The sum of the three largest precipitation rates, for this hour, would be 2.2 + 2.0 + 1.7 = 5.9 in h^{-1}. By using this analysis technique, an areal coverage of the heavy precipitation is inferred, rather than just at a single point.

5. Maximum hourly thunderstorm height.

Finally, composite analyses of the five characteristics were

accomplished for each category. The composites were used to determine significant differences between the categories. The differences suggested some possible causative factors that aid in the formation of ACCs.

CHAPTER III

DIVISION OF MCSs INTO CATEGORIES

Category 1 MCSs

Category 1 MCSs are defined as follows: The MCS produces a gust front and the gust front persists more than 6 h. Seven MCSs are classified in this category. The seven MCSs are from Cases 2, 3, 4, 7, 8, 10 and 11. A brief discussion of the synoptic situation and storm characteristics associated with each category 1 MCS follows.

Case 2: 9 May 1981

During the late afternoon of 8 May 1981, a cluster of thunderstorms developed over north central Texas. By 0115 GMT 9 May 1981, the cluster of storms had conglomerated and an MCC was initiated. Fig. 11 shows the 50 kPa analysis for 1200 GMT 9 May 1981. A short-wave trough extended through the central United States. This flow pattern had contributed to the production of the MCC. The precipitation pattern at 0235 GMT is depicted in the NWS radar summary chart (Fig. 12). The large precipitation area in north central Texas, associated with the MCC, developed on the north side of a warm front. The warm front was evident in the 0300 GMT surface θ_e analysis, which was obtained by use of the McIDAS. The tight gradient of the θ_e isolines in northern Texas, indicating the presence of the warm front, is shown in Fig. 13.

By 0500 GMT, a mesohigh and strong gust front first appeared in the surface pressure analysis (not shown). The gust front was located in northeastern Texas and was moving southeast. As it passed Shreveport,

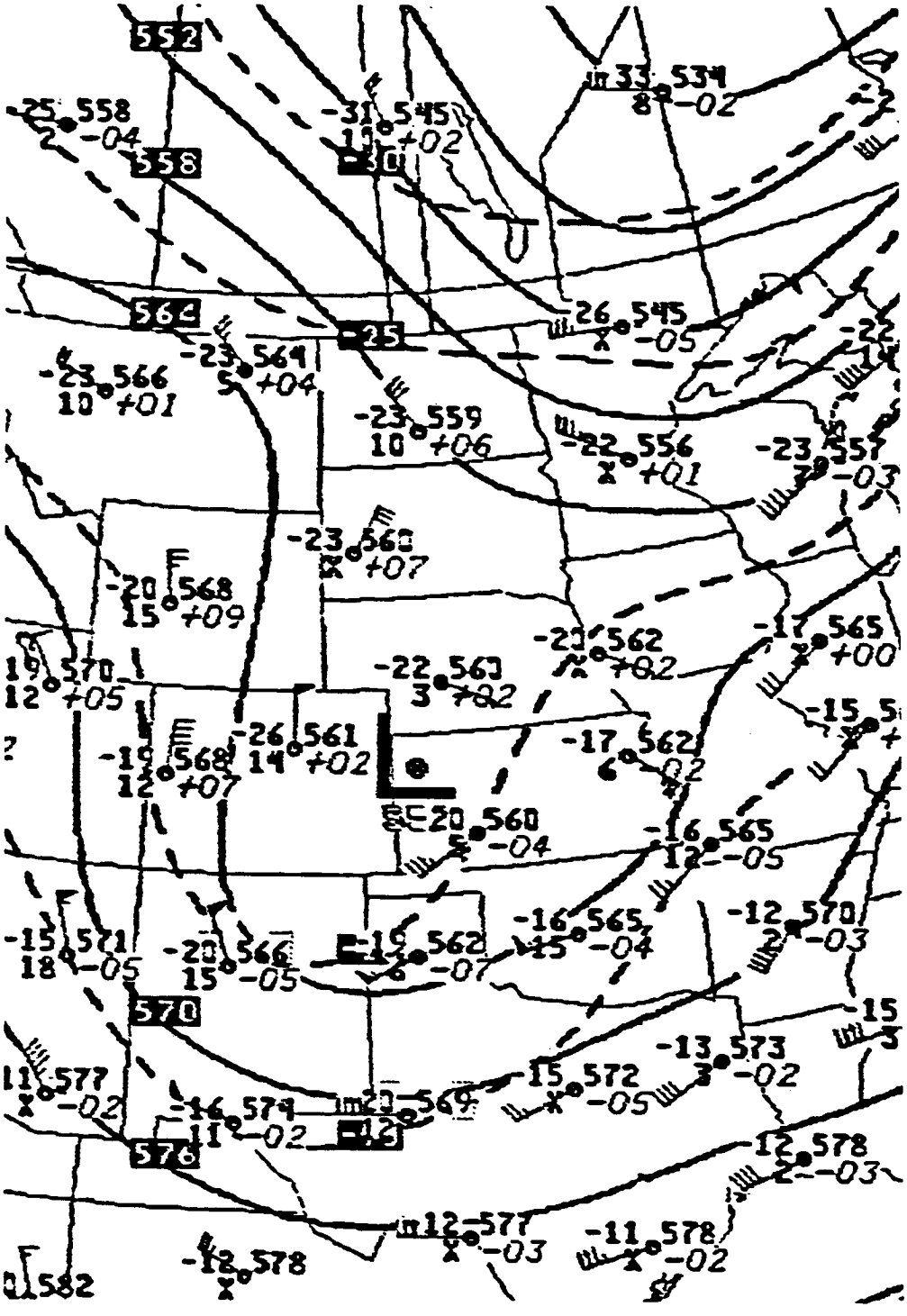

Fig. 11. 50 kPa height (dm) and temperature (°C) fields for 1200 GMT 9 May 1981. Height contours (solid lines) are every 60 m; isotherms (dashed lines) are every 5°C.

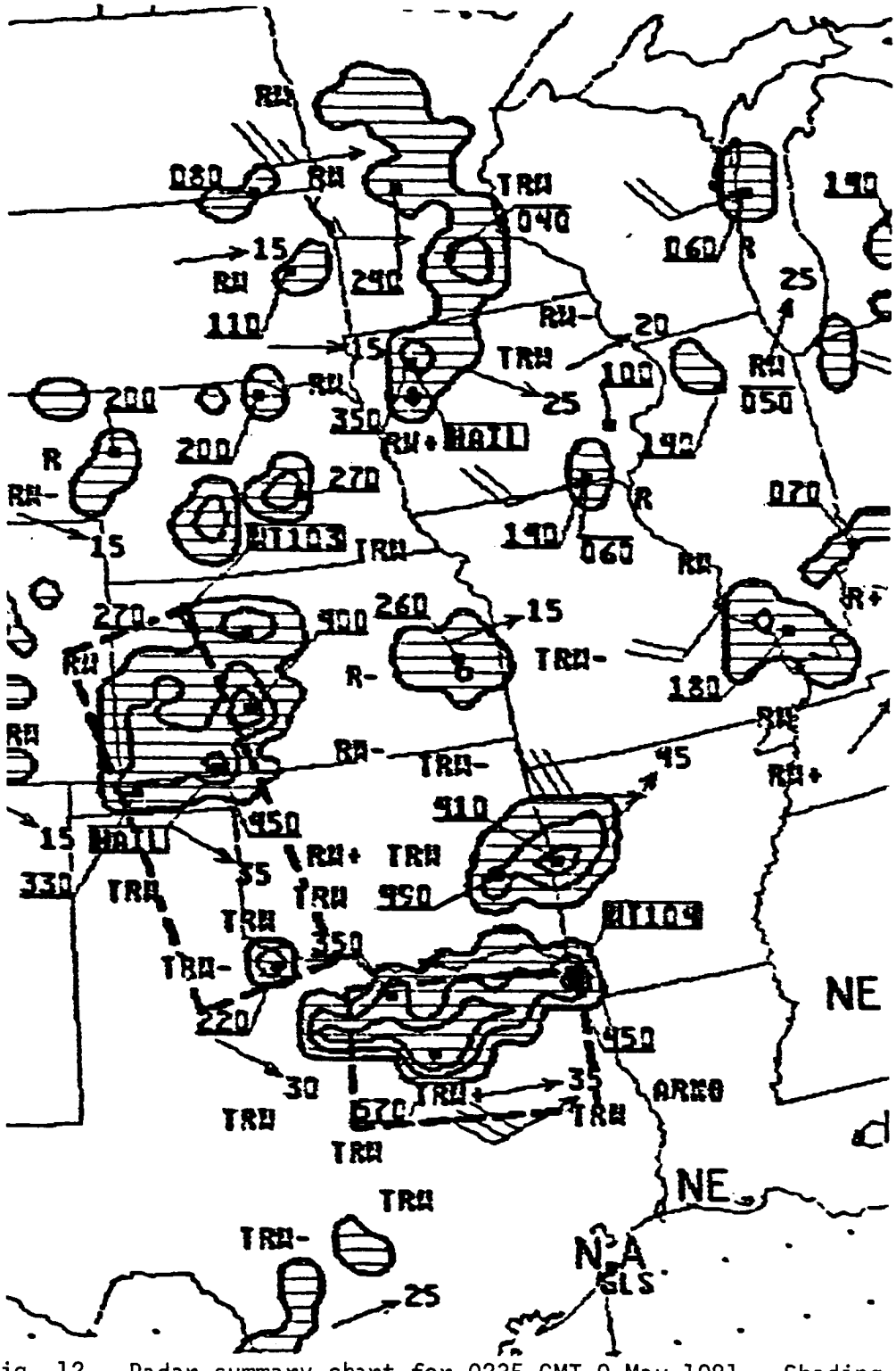

Fig. 12. Radar summary chart for 0235 GMT 9 May 1981. Shading indicates echo areas. Contours at echo intensities 1, 3, and 5; echo heights are in hundreds of feet; cell movement given at end of arrows in knots; area and line movement given by pennant with full barb = 10 kt.

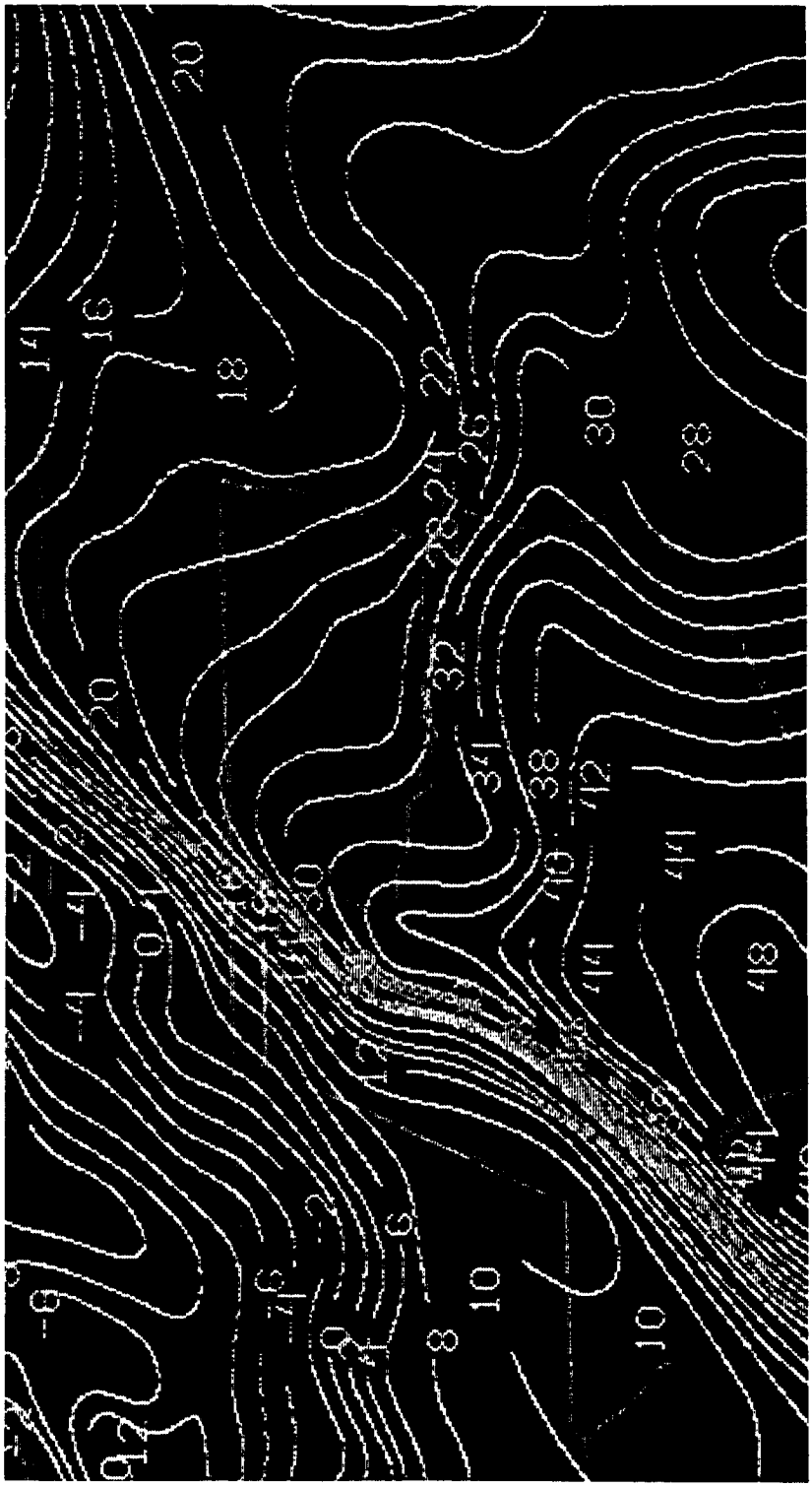

Fig. 13. Surface θ_e (°C) field for 0300 GMT 9 May 1981.

LA (SHV), a peak wind of 35 kt was recorded (0723 GMT). The strong, gusty wind was one of the indicators that the gust front was quite powerful. Even near termination of the MCC, at 1000 GMT, a strong meso-high and gust front were still evident in the surface pressure analysis (see Fig. 14). Since the pressures to the rear of the gust front were higher than the environmental pressures ahead of it, the gust front would be expected to remain quite active (Miller, 1972). In fact, the 1300 GMT visible satellite image, shown in Fig. 15, still showed evidence of the gust front and mesohigh. Convection had formed along the leading edge of the gust front in southern Louisiana, while subsidence associated with the mesohigh had created partial clearing in central Louisiana.

The characteristics associated with this MCC were very pronounced and are shown in Table 3. In the few hours after the initiation of the MCC (the initiation of the MCC was 0115 GMT), the maximum hourly thunderstorm heights were quite impressive. The heights from 0135 GMT to 0535 GMT, were 60,000, 57,000, 55,000, 55,000, and 53,000 ft, respectively. The hourly surface divergence remained large after the maximum extent of the MCC. In fact, the largest magnitude of the surface divergence was reached at 0800 GMT (3×10^{-5} s^{-1}), 3 h after the maximum extent of the MCC. The maximum sum of the three largest hourly point precipitation rates was 5.96 in h^{-1}. Similarily, the largest hourly maximum point precipitation rate was 2.2 in h^{-1}. Of particular interest, is the fact that the sum of the three largest hourly point precipitation rates, stayed above 1.5 in h^{-1} for eight consecutive hours. The coldest hourly cloud top temperatures, during the few hours after

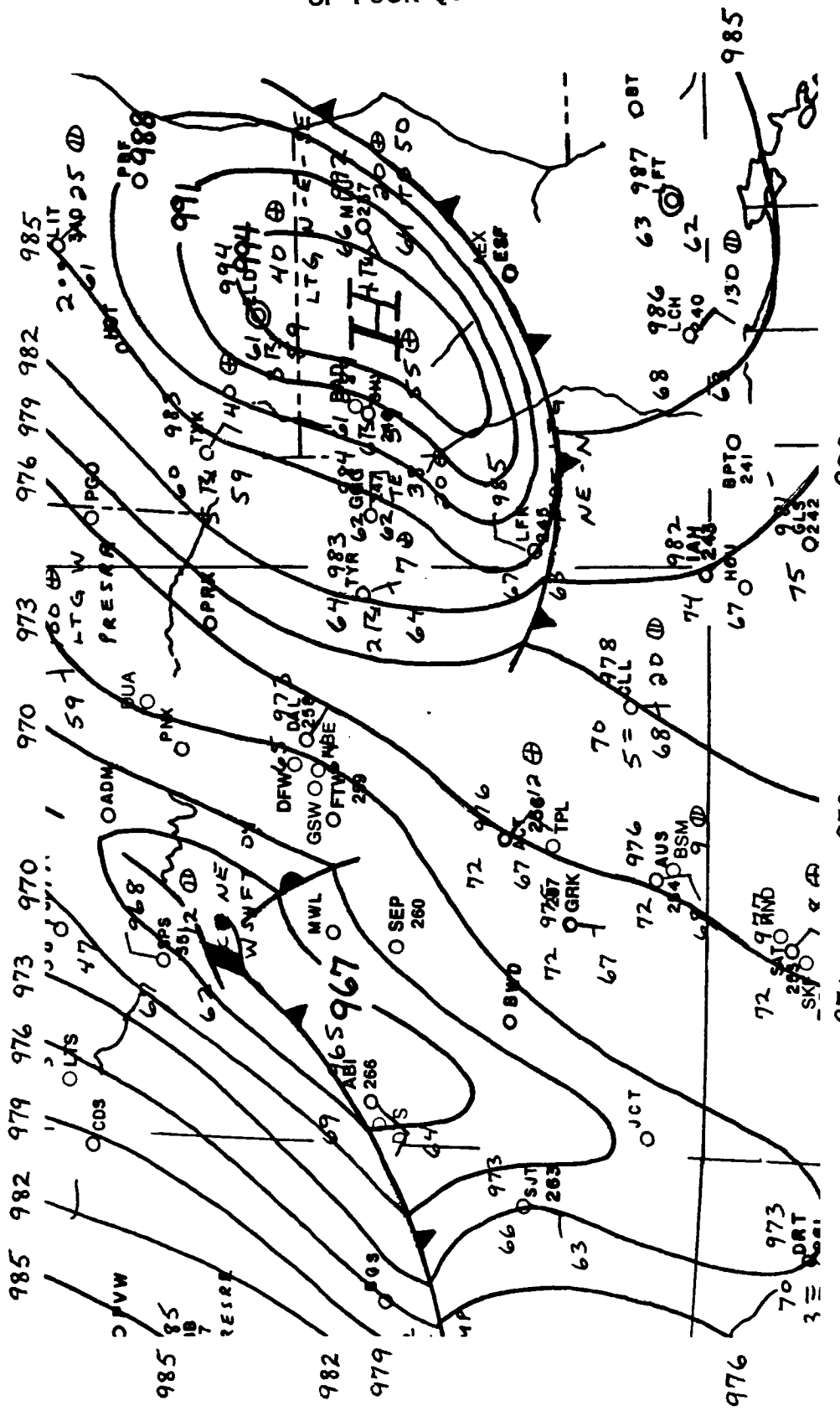

Fig. 14. Surface pressure field for 1000 GMT 9 May 1981. Altimeter setting contours are every 0.03 in Hg. The gust front, located in eastern Texas and central Louisiana, is denoted by a cold front symbol. Note: 982 corresponds to an altimeter setting of 29.82 in Hg.

Fig. 15. GOES visible image for 1300 GMT 9 May 1981.

Table 3. Characteristics associated with the MCC of Case 2 (8/9 May 1981). The maximum thunderstorm heights were determined at approximately 35 min past each hour. Dashes indicate that the parameter was not determined.

Time (GMT)	Maximum thunderstorm height (x 100 ft)	Maximum surface divergence (x 10^{-5} s^{-1})	Sum of the three largest precipitation rates (in h^{-1})	Maximum point precipitation rate (in h^{-1})	Coldest cloud top temperature (°C)
2300		-	-	-	-
	540				
0000		-	0.66	0.40	-
	550				
0100		-	2.50	1.30	-
	600				
0200		1	5.00	1.50	-63
	570				
0300		1	3.05	1.25	-63
	550				
0400		1	5.96	2.20	-63
	550				
0500		1	2.10	1.10	-68
	530				
0600		2	2.40	0.90	-68
	520				
0700		3	2.40	1.40	-63
	470				
0800		3	2.45	1.45	-63
	480				
0900		2	1.30	0.70	-58
	420				
1000		2	0.73	0.58	-
	400				
1100		-	0.30	0.40	-
	-				
1200		-	0.10	0.10	-
	-				
1300		-	0.00	0.00	-
	-				

MCC initiation, were quite cold, as was expected in view of the great heights of the thunderstorms.

Case 3: 27 May 1981

By 0515 GMT 27 May 1981, an MCS over southeastern Oklahoma had reached the critical size criteria of the MCC definition. The 50 kPa pattern associated with this MCC is reproduced in Fig. 16. Notice the trough-ridge-trough configuration; with ridging located over the area of the MCC. This pattern was quite different from the previous case. However, at the surface, conditions were very similar to that of Case 2. Although the NWS's surface analysis (not shown) did not depict a frontal boundary near the MCC, the surface θ_e analysis for 0900 GMT (Fig. 17) indicated a distinct contrast of air masses. This contrast of air masses was also evident prior to the MCC formation, indicating that it was not an MCC-produced phenomenon. The ambient surface air temperature and surface dew point temperature for two stations, Enid, OK (END) and Waco, TX (ACT), are used to illustrate the contrast of air masses. Enid's ambient surface air temperature and surface dew point temperature for 0900 GMT were 10°C and 13°C, respectively, while at the same time, Waco's were 24°C and 22°C. A definite contrast of air masses existed across the MCC.

About 2 h after the initiation of the MCC, a mesohigh and gust front formed near the Oklahoma/Texas borders and subsequently moved rapidly southeast. Once again, the strength of the gust front was revealed by the strong and gusty winds which it produced. At 0935 GMT, as the gust front passed Dallas, TX (DAL), a peak wind of 45 kt was

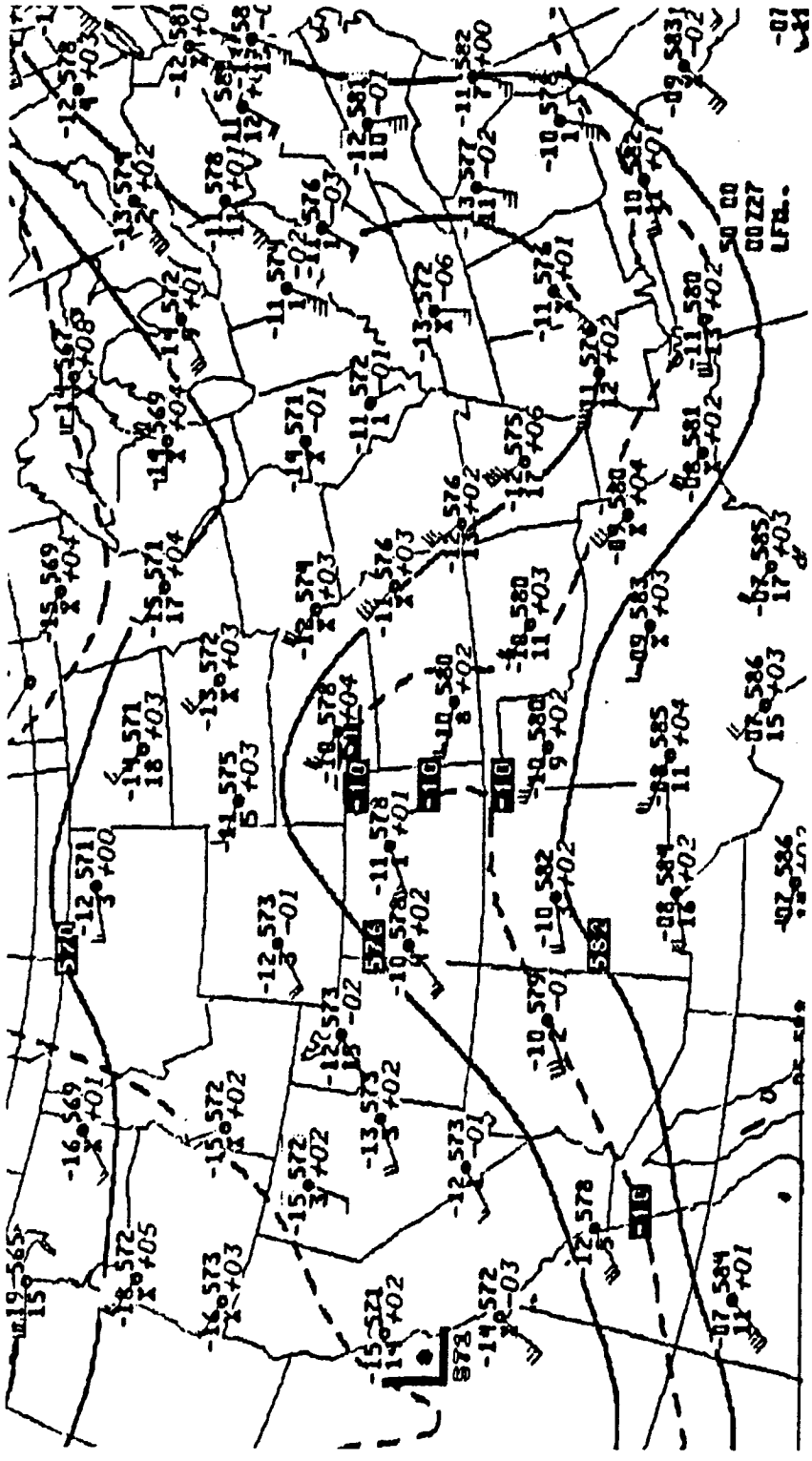

Fig. 16. 50 kPa height (dm) and temperature (°C) fields for 0000 GMT 27 May 1981. Height contours (solid lines) are every 60 m; isotherms (dashed lines) are every 5°C.

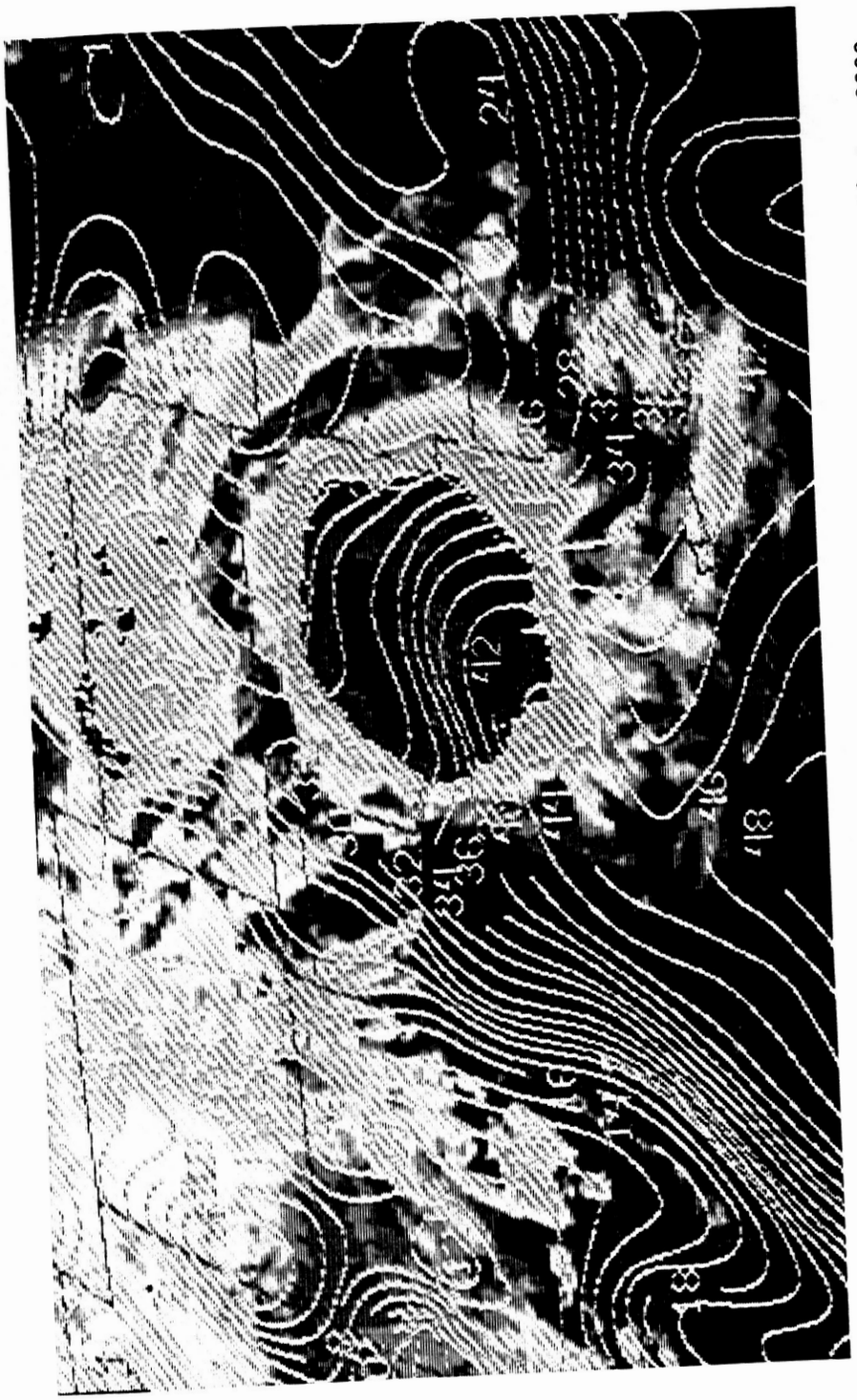

Fig. 17. Surface θ_e (°C) field overlaid upon GOES image (MB enhancement) for 0900 GMT 27 May 1981.

recorded.

Upon close inspection of the first visible satellite pictures for the day (1200 to 1300 GMT), an arc cloud, separated from the parent storm, was perceived. Fig. 18 shows the visible satellite picture for 1500 GMT. By this time, the arc cloud had nearly reached the Gulf coast of eastern Texas. After this time, the arc cloud weakened and was no longer discernable in the satellite images after 1800 GMT.

Characteristics associated with the MCC are given in Table 4. Most of the characteristics were not as pronounced as those of the MCC in Case 2. However, they were significantly stronger than the characteristics of the MCSs classified in category 2, as will be shown later. Two characteristics of the MCC for this case are worth emphasizing. Even after the termination of the MCC (1400 GMT), the maximum surface divergence increased to 3×10^{-5} s^{-1} (at 1400 and 1500 GMT), compared to 2×10^{-5} s^{-1} of the previous 6 h. Also, notice that the sum of the three largest precipitation rates stayed at or above 1.5 in h^{-1} for 6 h. It may be recalled that for Case 2, this condition existed for 8 h.

Case 4: 17 May 1982

A storm area formed in Kansas and western Oklahoma on 16 May 1982. This storm area developed on the east side of a stationary front as analyzed by the NWS (not shown). The front extended from South Dakota to the Texas panhandle and beyond to the southeast corner of New Mexico. Fig. 19 shows the 50 kPa analysis for 1200 GMT 16 May 1982. The trough located over Arizona and New Mexico moved eastward and initiated the formation of the storm area. By 0030 GMT 17 May 1982 the storm area was

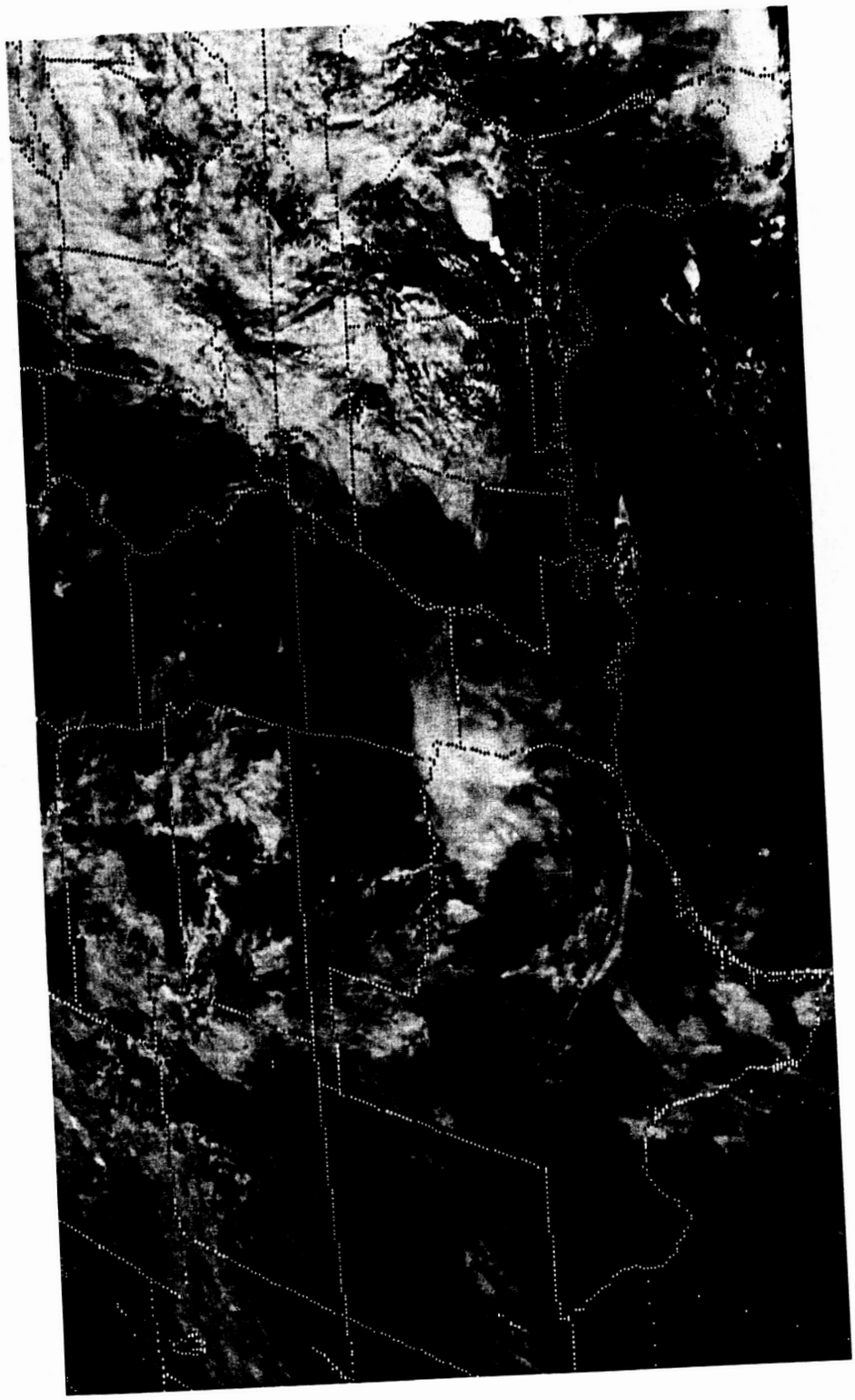

Fig. 18. GOES visible image for 1500 GMT 27 May 1981.

Table 4. Characteristics associated with the MCC of Case 3 (27 May 1981). The maximum thunderstorm heights were determined at approximately 35 min past each hour. Dashes indicate that the parameter was not determined.

Time (GMT)	Maximum thunderstorm thunderstorm (x 100 ft)	Maximum surface divergence (x $10^{-5}s^{-1}$)	Sum of the three largest precipitation rates (in h^{-1})	Maximum point precipitation rate (in h^{-1})	Coldest cloud top temperature (°C)
0400		-	0.60	0.50	-
	520				
0500		-	1.00	0.50	-
	550				
0600		3	1.00	0.70	-
	580				
0700		3	0.73	0.43	-73
	560				
0800		2	1.59	1.30	-68
	520				
0900		2	1.50	0.60	-73
	550				
1000		2	2.70	0.99	-68
	480				
1100		2	2.93	1.13	-68
	470				
1200		2	2.50	0.90	-68
	320				
1300		2	1.61	1.01	-
	250				
1400		3	0.60	0.20	-
	160				
1500		3	0.60	0.20	-
	-				
1600		-	0.10	0.10	-
	-				

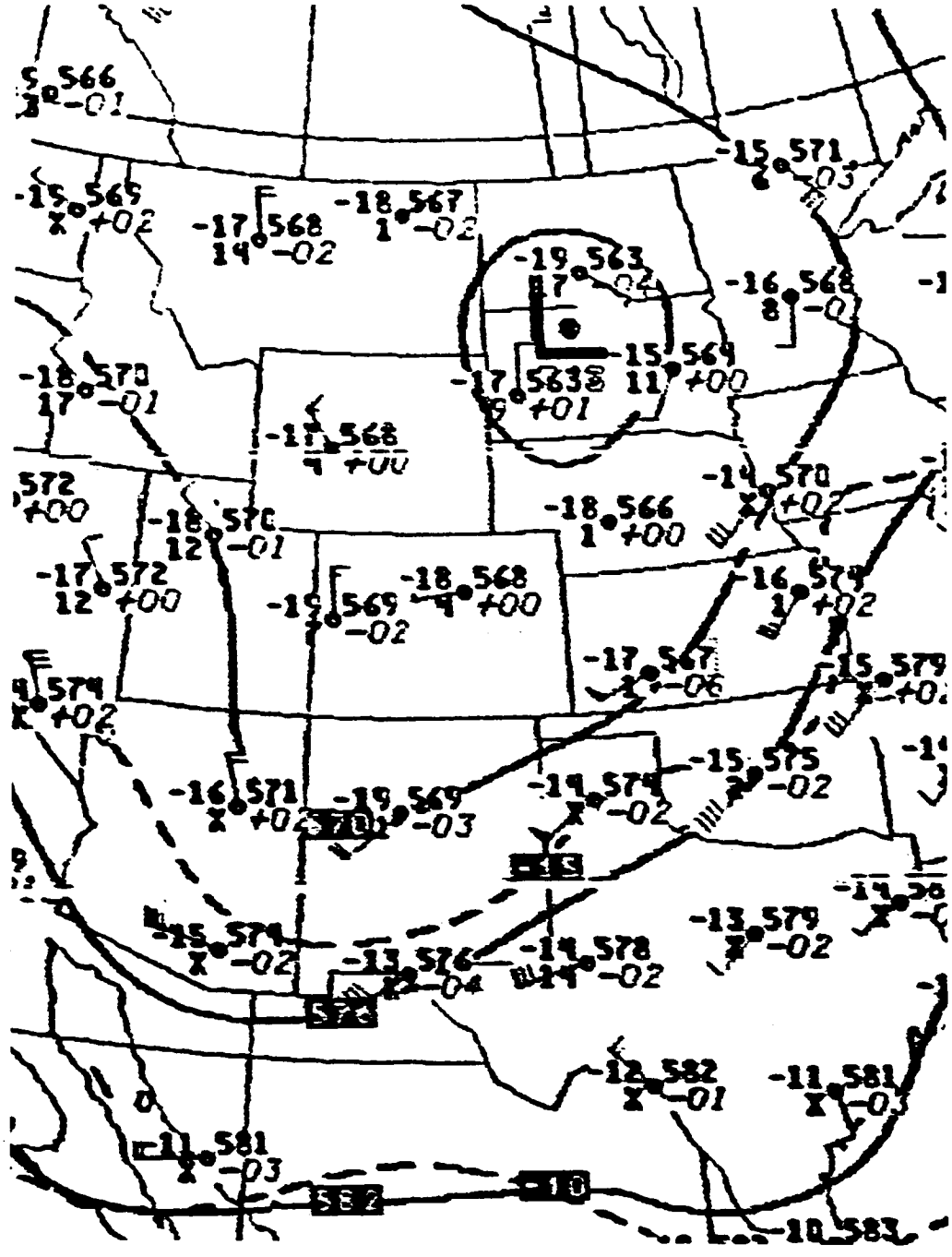

Fig. 19. 50 kPa height (dm) and temperature (°C) fields for 1200 GMT 16 May 1982. Height contours (solid lines) are every 60 m; isotherms (dashed lines) are every 5°C.

large enough to be classified as an MCC. Fig. 20 shows the MCC at 0415 GMT, near the time of maximum extent. About 2 h earlier, at 0200 GMT, a mesohigh and gust front formed. The gust front extended from Chanute, KS (CNU) to Oklahoma City, OK (OKC) to Lubbock, TX (LBB).

The gust front associated with this MCC was very strong, producing gusty winds and severe weather. At 0300 GMT, along the leading edge of the gust front, Fort Sill, OK (FSI) reported a tornado to the west. The following stations reported wind gusts greater than 34 kt as the gust front passed: Oklahoma City, OK (0233 GMT, 35 kt); Tulsa, OK (0436 GMT, 35 kt); Wichita Falls, TX (0506 GMT, 37 kt); McAlester, OK (0640 GMT, 36 kt); Dallas, TX (0830 GMT, 35 kt).

Fig. 21 shows the GOES IR image, with the MB enhancement curve, for 1000 GMT. The thunderstorms had weakened considerably and the MCC had already terminated. At this time, however, the gust front and large mesohigh were still very pronounced, as depicted in the surface analysis shown in Fig. 22. The mesohigh encompassed southeast Oklahoma and most of northern Texas. It was about this time that an arc cloud in the IR imagery first became discernible.

Eventually, a massive ACC formed. Fig. 23 shows the arc cloud, located in Texas, at 1832 GMT. The arrows point to its leading edge. The arc cloud finally lost its identity in the satellite images around 2200 GMT.

Table 5 shows the characteristics associated with this MCC. The maximum thunderstorm height of 65,000 ft occurred at 0135 GMT. This correlated quite well with the maximum point rainfall rate, which occurred during the hour ending at 0200 GMT. The behavior of the values

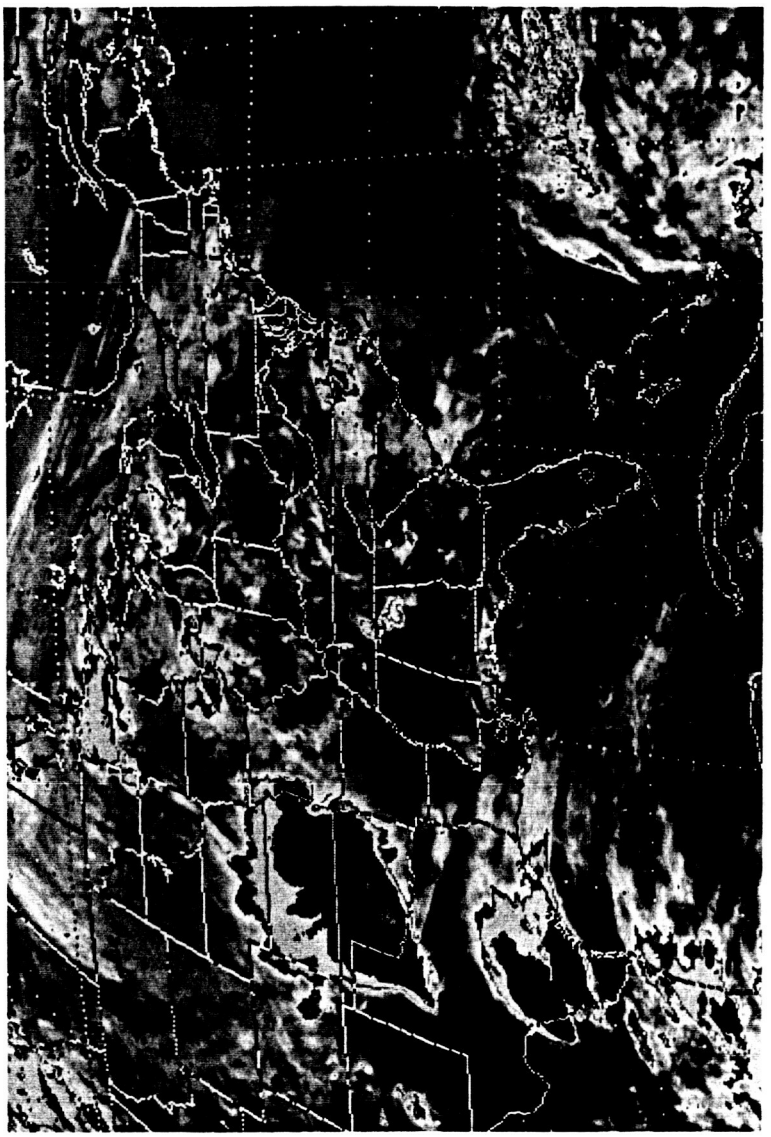

Fig. 20. GOES IR image with MB enhancement for 0415 GMT 17 May 1982.

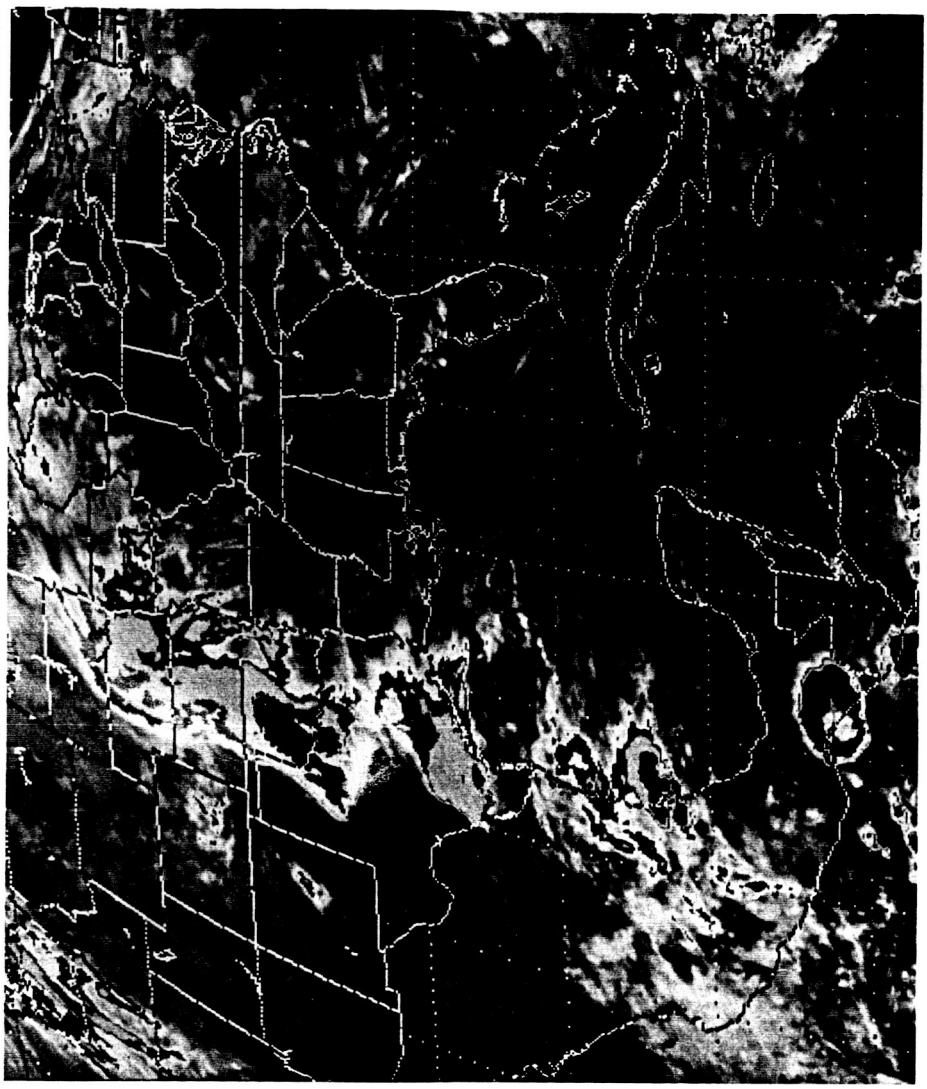

Fig. 21. GOES IR image with MB enhancement for 1000 GMT 17 May 1982.

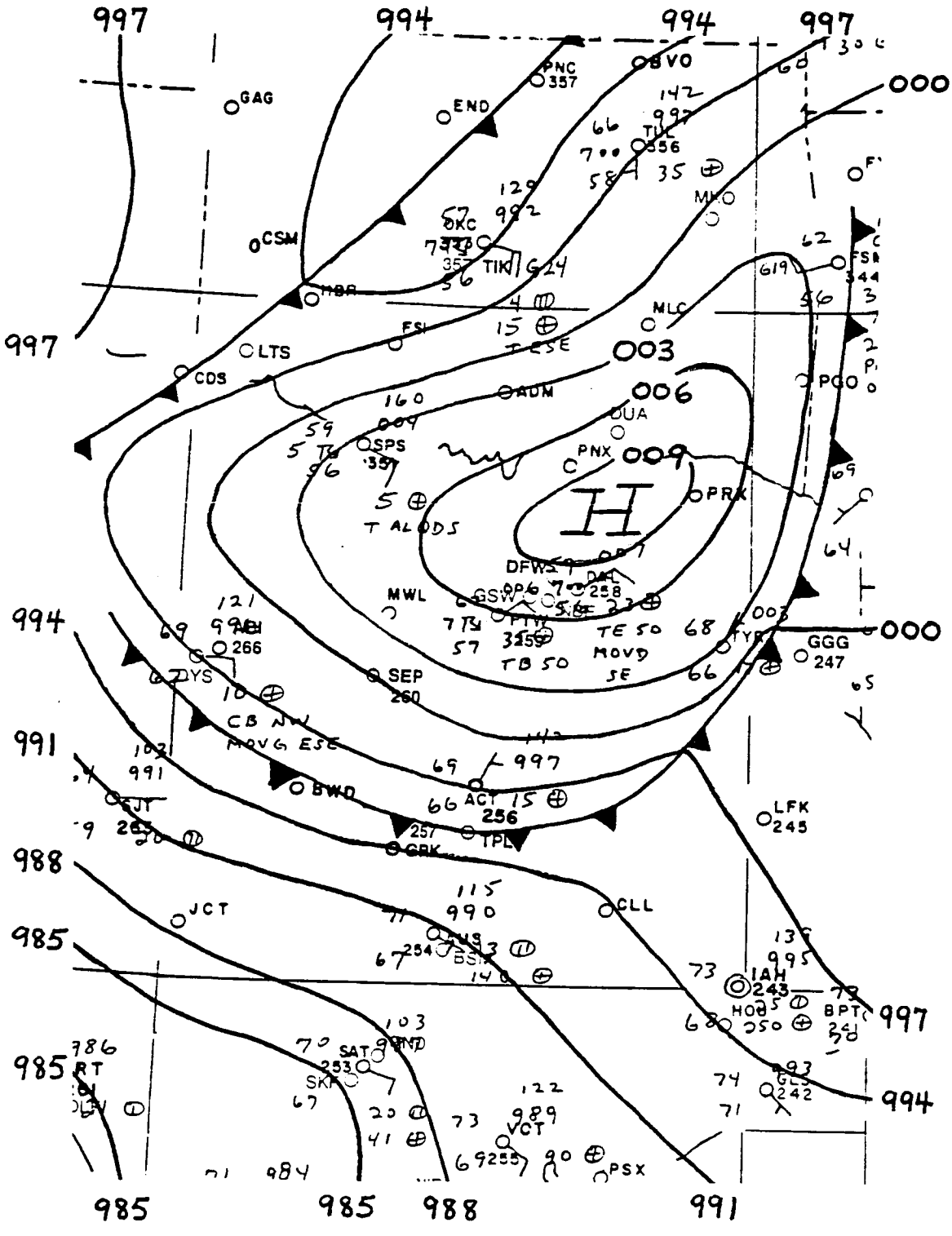

Fig. 22. Surface pressure field for 1000 GMT 17 May 1982. Altimeter setting contours are every 0.03 in Hg. The gust front, located in northeastern Texas and western Arkansas, is denoted by a cold front symbol.

Fig. 23. GOES visible image for 1832 GMT 17 May 1982.

Table 5. Characteristics associated with the MCC of Case 4 (16/17 May 1982). The maximum thunderstorm heights were determined at approximately 35 min past each hour. Dashes indicate that the parameter was not determined.

Time (GMT)	Maximum thunderstorm height (x 100 ft)	Maximum surface divergence (x 10^{-5} s^{-1})	Sum of the three largest precipitation rates (in h^{-1})	Maximum point precipitation rate (in h^{-1})	Coldest cloud top temperature (°C)
2300		-	2.20	1.70	-
	590				
0000		-	3.83	1.80	-
	620				
0100		1	3.29	1.76	-73
	650				
0200		2	2.80	2.30	-73
	530				
0300		4	2.90	1.40	-68
	510				
0400		2	3.20	1.10	-68
	520				
0500		2	2.74	0.94	-68
	550				
0600		2	3.58	1.50	-63
	580				
0700		3	2.50	1.10	-63
	630				
0800		4	3.00	1.10	-
	420				
0900		4	1.52	0.60	-
	410				
1000		4	1.40	0.70	-
	400				
1100		3	1.78	0.90	-
	390				
1200		4	2.73	1.63	-
	-				
1300		5	1.52	0.60	-
	-				
1400		4	1.39	0.75	-
	-				

of the sums of the three largest hourly rainfall rates was similar to the previous cases. The sum of the rainfall rates stayed above 1.5 in h^{-1} for 11 straight hours, compared to 8 and 6 h for Cases 2 and 3, respectively. Very cold cloud top temperatures were associated with the early stages of the MCC, with temperatures as low as -73°C. As expected, the large mesohigh, created by the downdrafts of the thunderstorms, was associated with strong surface divergence. The maximum of 5×10^{-5} s^{-1} occurred at 1300 GMT.

Of the 12 cases included in this study, the MCC of this case produced the largest ACC.

Case 7: 26 June 1982

During the afternoon of 25 June 1982, convection developed to the lee of the Rockies and moved eastward. During the evening hours an MCS developed over the western plains stretching from the Texas panhandle to southwestern South Dakota. Wetzel et al. (1983) described a similar sequence of events. They found that afternoon orogenic thunderstorms, such as those that develop along the foothills of the Rockies, often move eastward and provide the beginnings of significant Plains mesosystems.

The synoptic setting leading to the formation of the MCS was described by Miller (1984). At 50 and 30 kPa, the MCS developed near the inflection point downstream of a short-wave trough and in an area of cold advection. The flow at both 30 and 20 kPa was diffluent over the MCS, indicating the liklihood of convergence below. At both 70 and 85 kPa there was slight warm advection near the MCS. Thus, the troposphere

was undergoing destabilization due to differential advection.

Two gust fronts were produced by the MCS. The first gust front formed around 0600 GMT 26 June 1982 and dissipated by 1500 GMT. The second gust front was first detected in the surface analysis at 1100 GMT and dissipated around 2200 GMT. Fig. 24 is the surface analysis for 1200 GMT and shows both gust fronts. The gust fronts are denoted by cold front symbols.

Both gust fronts moved to the southeast and eventually produced arc clouds. Evidence of the first arc cloud could first be detected in the IR satellite imagery at 0830 GMT. The second arc cloud was first visible in the satellite images at 1430 GMT and eventually grew into a large ACC. Fig. 25 shows the second arc cloud, extending from central Oklahoma to north central Texas and then southwestward to the southeast portions of New Mexico, at 1832 GMT.

Table 6 shows the characteristics associated with this MCS. The maximum hourly thunderstorm heights oscillated, corresponding to the formation of the two arc clouds. The heights fell drastically, from 54,000 ft to 41,000 ft, between 0735 GMT and 0935 GMT, bracketing the time the first arc cloud appeared. Similarily, between 1335 GMT and 1535 GMT, the heights fell from 48,000 ft to 34,000 ft, again around the time of arc cloud formation. The coldest cloud top temperatures oscillated in a similar fashion. The sum of the three largest precipitation rates stayed above 1.5 in h^{-1} from 0300 to 0800 GMT, a total of 6 h. The only exception to this was the hour ending at 0600 GMT, where it appeared likely that the heavy precipitation fell between the climatological raingauge sites. After this period of heavy precipitation, the

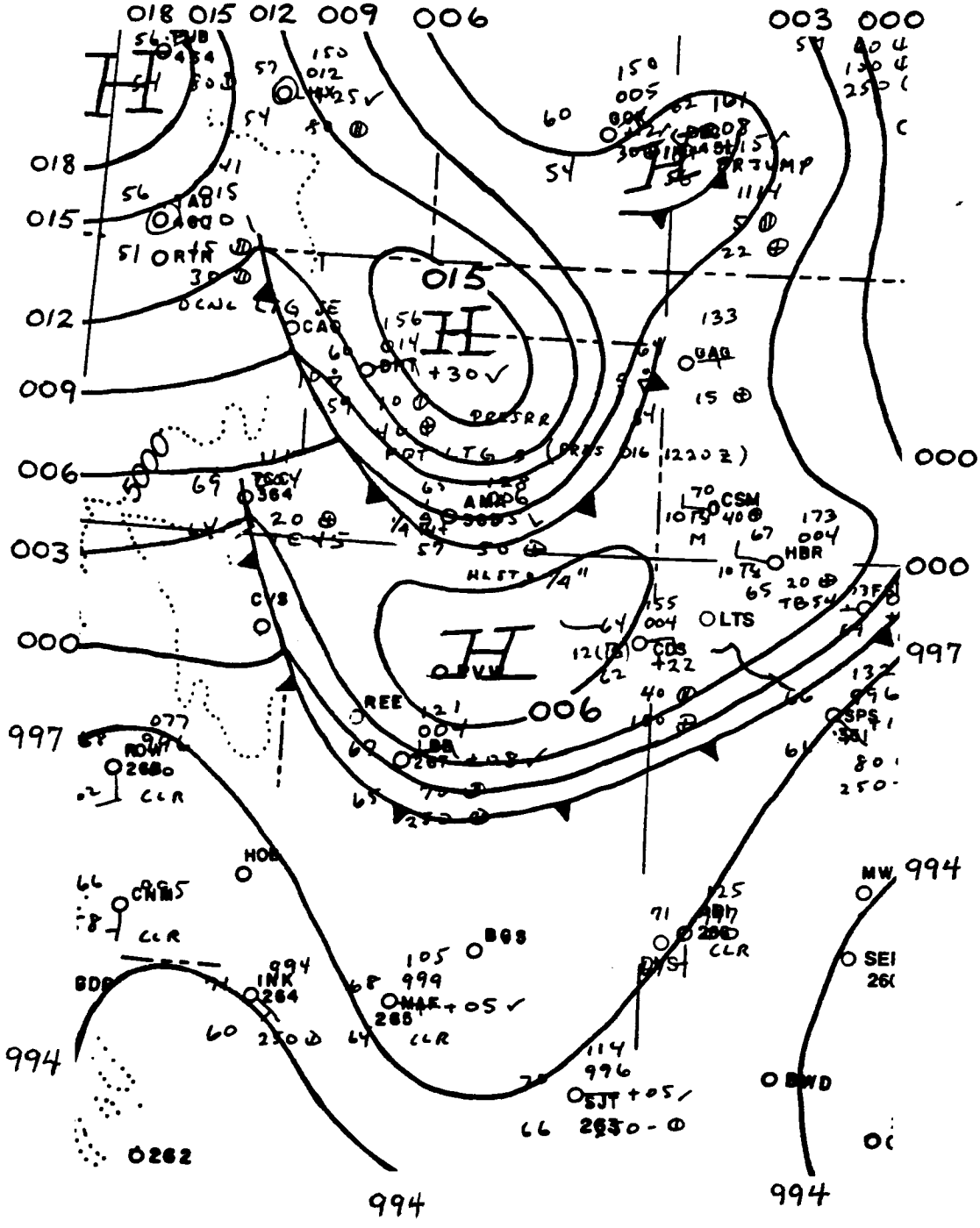

Fig. 24. Surface pressure field for 1200 GMT 26 June 1982. Altimeter setting contours are every 0.03 in Hg. The gust fronts are denoted by cold front symbols.

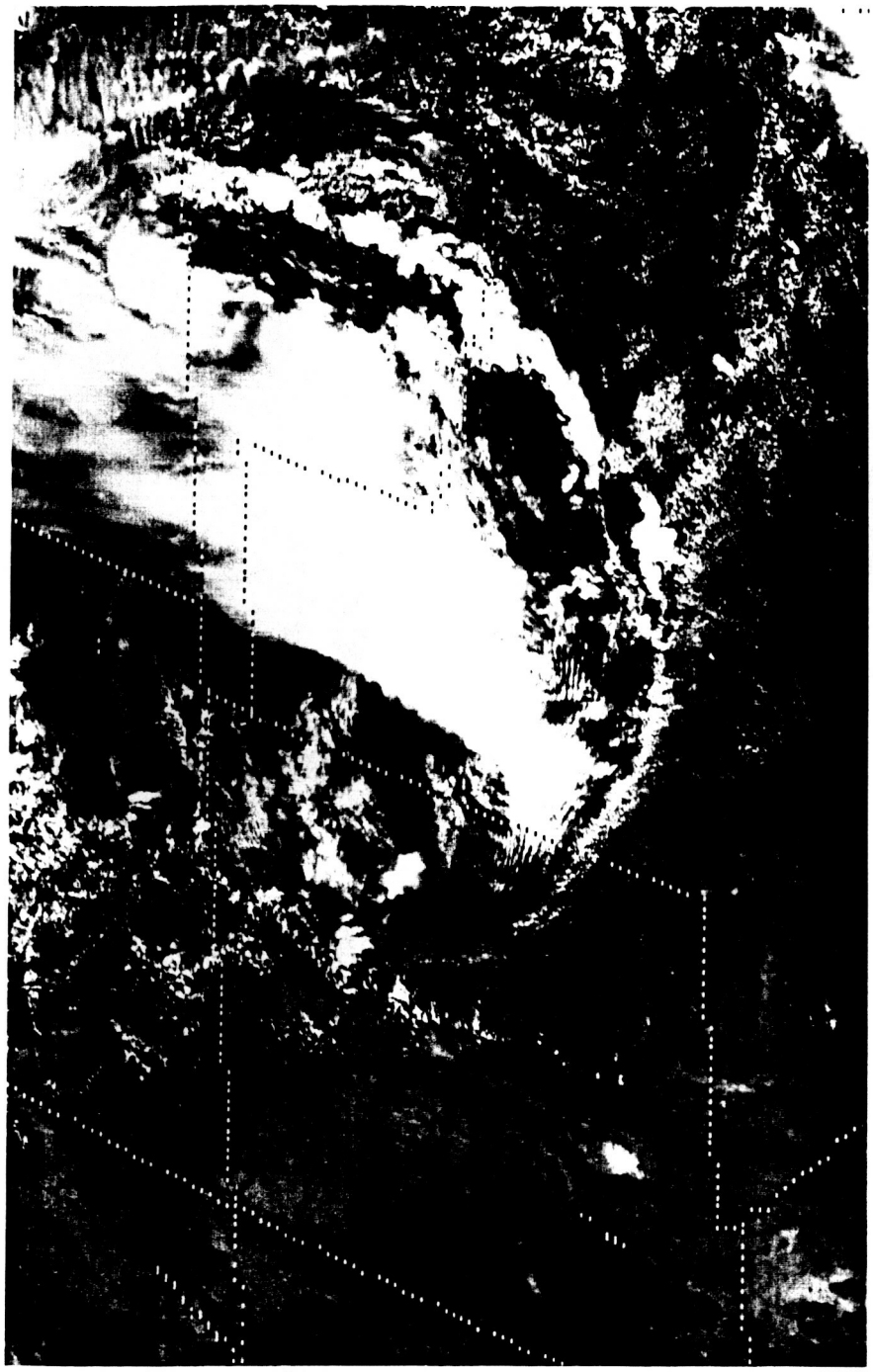

Fig. 25. GOES visible image for 1832 GMT 26 June 1982.

Table 6. Characteristics associated with the MCS of Case 7 (26 June 1982). The maximum thunderstorm heights were determined at approximately 35 min past each hour. Dashes indicate that the parameter was not determined.

Time (GMT)	Maximum thunderstorm height (x 100 ft)	Maximum surface divergence (x 10^{-5} s^{-1})	Sum of the three largest precipitation rates (in h^{-1})	Maximum point precipitation rate (in h^{-1})	Coldest cloud top temperature (°C)
0000	-	-	1.40	0.90	-
0100	-	-	0.50	0.20	-
0200	-	-	0.50	0.20	-
0300	-	-	1.88	0.80	-
0400	-	-	1.54	0.61	-
0500	550	-	1.50	0.50	-
0600	600	-	0.70	0.44	-
0700	540	-	2.00	1.10	-
0800	540	-5	1.51	0.90	-68
0900	480	2	1.26	0.60	-63
1000	410	1	1.36	0.60	-63
1100	400	1	1.25	0.60	-68
1200	400	1	1.94	1.25	-68
1300	480	3	0.81	0.50	-68
1400	480	3	0.80	0.60	-68
1500	450	4	1.63	0.90	-63
1600	340	-	0.50	0.20	-
1700	-	-	0.30	0.10	-
	-				

first arc cloud formed. Another peak in the sum of the three largest precipitation rates occurred the hour ending at 1500 GMT (1.63 in h^{-1}). This seemed to correspond with the formation of the second arc cloud.

Case 8: 27 June 1982

During the afternoon of 26 June 1982, the large arc cloud discussed in the previous case intersected with an east-west oriented line of cumulus and formed an MCS over western Texas. The MCS moved southeast, reached its most intense stage around 0330 GMT 27 June 1982 and slowly dissipated thereafter. Only a weak gust front and mesohigh were produced by the MCS.

Another MCS developed during the afternoon of 26 June 1982. This MCS developed to the lee of the Rockies in northeast New Mexico and essentially followed the same movement as the first MCS. Fig. 26 shows both MCSs at 0700 GMT 27 June 1982. The eastern MCS was dissipating, while the western MCS was still intensifying. By 0800 GMT, the western MCS was large enough to be classified as an MCC.

The western MCC produced a much stronger gust front and mesohigh compared to the eastern MCS. This was clearly evident in the surface pressure field for 1200 GMT, presented in Fig. 27. The remains of the mesohigh produced by the eastern MCS were still apparent and were located southeast of Austin, TX (AUS). The central pressure of this mesohigh was approximately 29.97 in of mercury. The mesohigh produced by the western MCC had a central pressure of about 30.13 in of mercury. The strength of the western mesohigh and gust front was reflected in San Angelo's (SJT) winds, which gusted to 45 kt during the passage of the

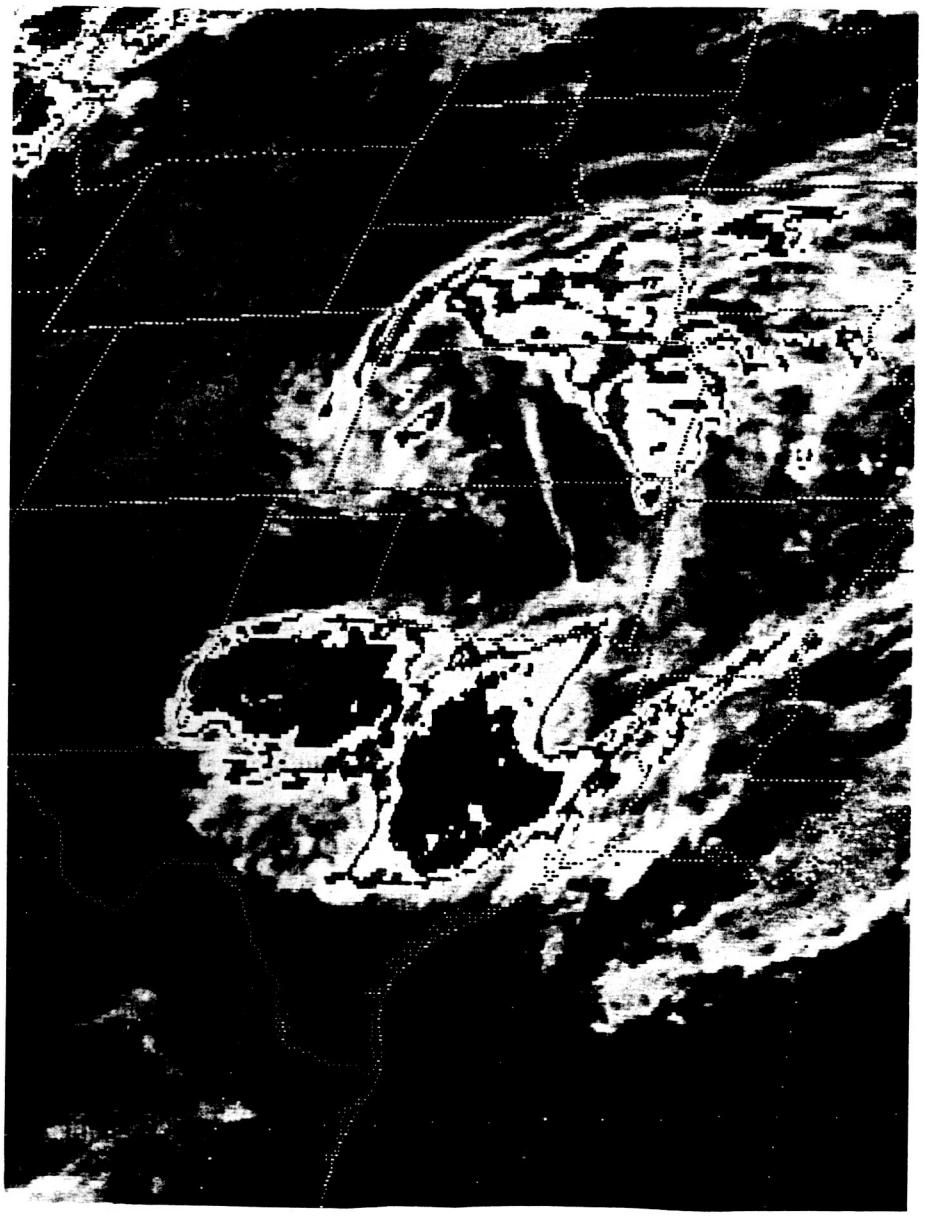

Fig. 26. GOES IR image with MB enhancement for 0700 GMT 27 June 1982.

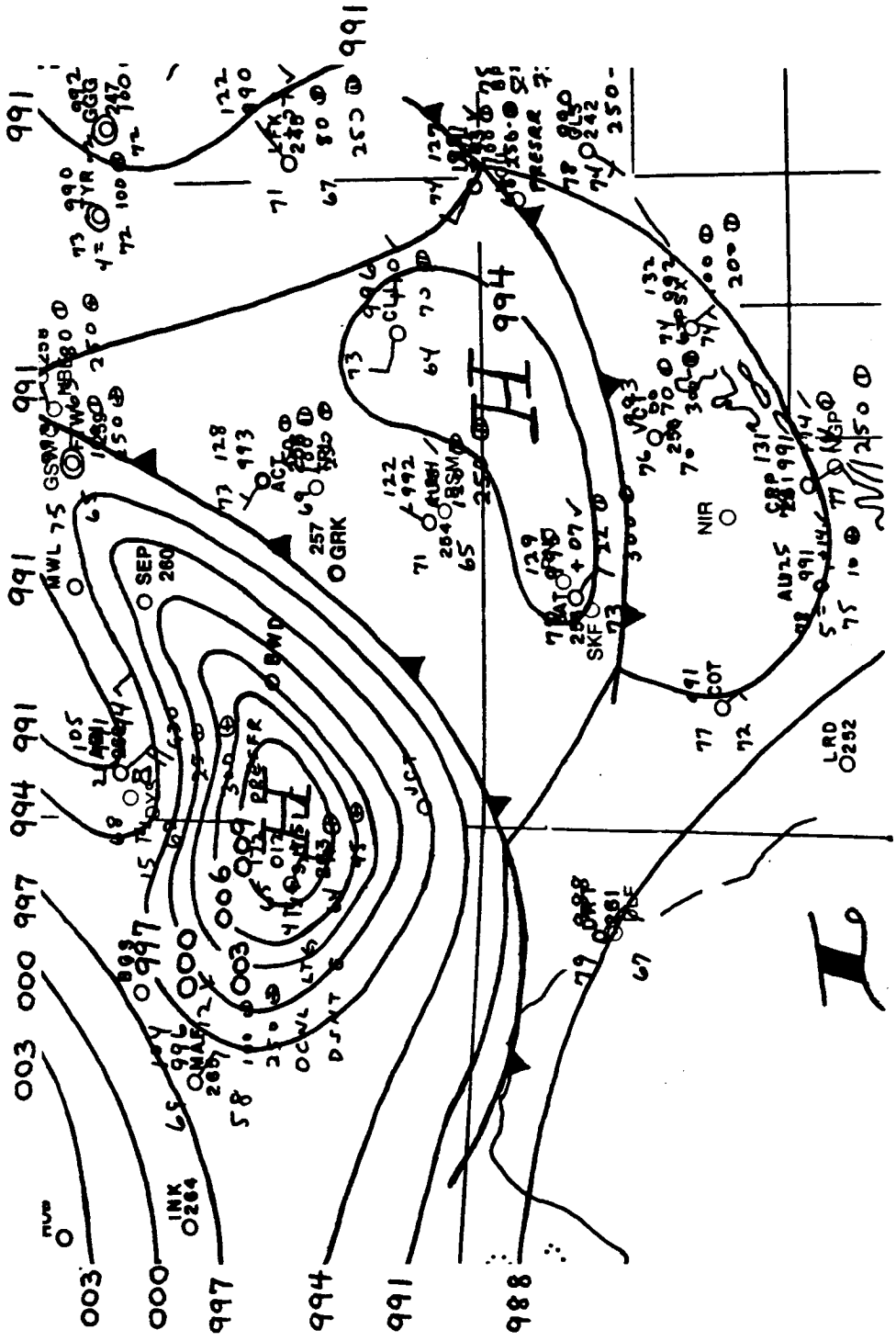

Fig. 27. Surface pressure field for 1200 GMT 27 June 1982. Altimeter setting contours are every 0.03 in Hg. The gust fronts are denoted by cold front symbols.

gust front (0958). An arc cloud, associated with the gust front and separated from the main MCS cloud shield, first became evident in the satellite images at 1200 GMT.

The characteristics of the western MCC are similar to the previous category 1 MCSs and are displayed in Table 7. Dramatic characteristic changes occurred around the time of arc cloud formation. The maximum hourly thunderstorm heights dropped from 48,000 ft at 1135 GMT to 30,000 ft at 1335 GMT, the sum of the three largest precipitation rates fell from 3.72 in h^{-1} at 1100 GMT to 0.9 in h^{-1} at 1300 GMT, the maximum point precipitation rate reduced from 1.5 to 0.5 in h^{-1} and the coldest cloud top temperatures warmed from -73 to -58°C. Two other interesting features are seen in the characteristics associated with the MCC. The magnitude of the maximum surface divergence remained large after the maximum extent of the MCC (0900 GMT). Also, the sum of the three largest precipitation rates stayed above 1.5 in h^{-1} for 7 h, excluding the hour ending at 0800 GMT, when it appeared the heavy precipitation fell between reporting climatological raingauge sites. Therefore, heavy precipitation fell over a significant area for a long time, preceding the formation of the arc cloud.

Case 10: 20 May 1983

On the afternoon and evening of 19 May 1983, an enormous convective storm system evolved from the merger of several smaller MCSs. The initial thunderstorms developed around 2000 GMT 19 May 1983, just to the east of a north-south dry line, which was located in western Texas. Another almost equally vigorous system developed 2 h later in northeast

Table 7. Characteristics associated with the MCC of Case 8 (27 June 1982). The maximum thunderstorm heights were determined at approximately 35 min past each hour. Dashes indicate that the parameter was not determined.

Time (GMT)	Maximum thunderstorm height (x 100 ft)	Maximum surface divergence (x 10^{-5} s^{-1})	Sum of the three largest precipitation rates (in h^{-1})	Maximum point precipitation rate (in h^{-1})	Coldest cloud top temperature (°C)
0000	-	-	0.80	0.80	-
0100	500	-	0.90	0.50	-
0200	500	-	0.10	0.10	-
0300	470	-	0.20	0.10	-
0400	490	-	0.20	0.10	-
0500	540	-	0.01	0.01	-
0600	520	3	2.30	1.60	-73
0700	520	4	2.00	1.00	-68
0800	500	5	0.85	0.50	-73
0900	500	3	1.85	0.90	-73
1000	500	2	2.49	1.30	-73
1100	480	3	3.72	1.50	-73
1200	330	2	1.69	0.90	-68
1300	300	3	0.90	0.50	-58
1400	260	4	0.60	0.20	-
1500	450	4	0.30	0.10	-
1600	490	-	0.32	0.20	-
1700	530	-	-	-	-

Texas in the vicinity of a weak warm front. By 0130 GMT 20 May 1983, the two MCSs merged into an MCC. The 50 kPa analysis for 0000 GMT 20 May 1983 is shown in Fig. 28. This flow configuration, termed the "New Orleans Type" (Belville and Stewart, 1983), consisted of a deep trough and closed circulation over the southwest United States. This pattern is often responsible for early spring heavy rainfall events in the southeast (Belville and Stewart, 1983).

By 0400 GMT, a mesohigh and gust front, located in southeast Texas, were evident in the surface analysis (not shown). The gust front was an important factor influencing the National Severe Storms Forecast Center to issue Tornado Watch Number 179 at 0458 GMT. The watch bulletin stated that an outflow boundary, located from Lufkin, TX, west-southwest to south of San Antonio, TX, would be the focus for continued development of very strong thunderstorms. As the gust front interacted with the very unstable airmass, numerous reports of severe weather were reported. Two examples were wind gusts of 53 kt at San Antonio at 0453 GMT and a confirmed tornado at Houston's Intercontinental Airport at 0720 GMT. After 0900 GMT, the southern portion of the gust front moved into the northwest Gulf of Mexico. However, the northern portion was still discernable in the surface analysis as it passed stations in Louisiana. For instance, Lake Charles reported a wind gust of 40 kt at 0928 GMT and Lafayette's winds changed from calm at 1100 GMT to a westerly component of 10 kt at 1200 GMT.

At 1200 GMT an arc cloud was discernable in the visible satellite image. Fig. 29 shows the arc cloud, at 1300 GMT, extending from southeastern Louisiana into the northwest Gulf of Mexico. At this time, the

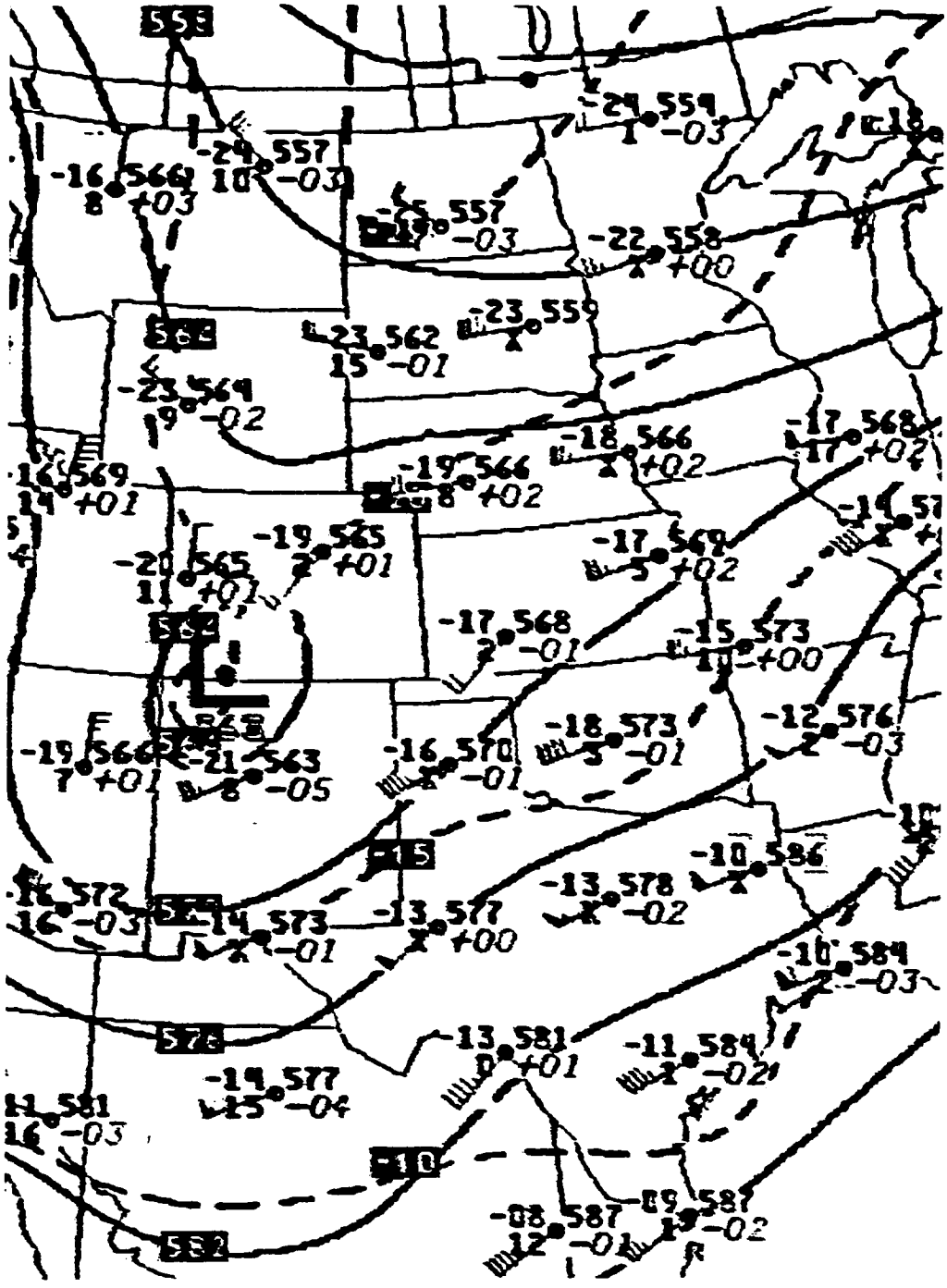

Fig. 28. 50 kPa height (dm) and temperatures (°C) fields for 0000 GMT 20 May 1983. Height contours (solid lines) are every 60 m; isotherms (dashed lines) are every 5°C.

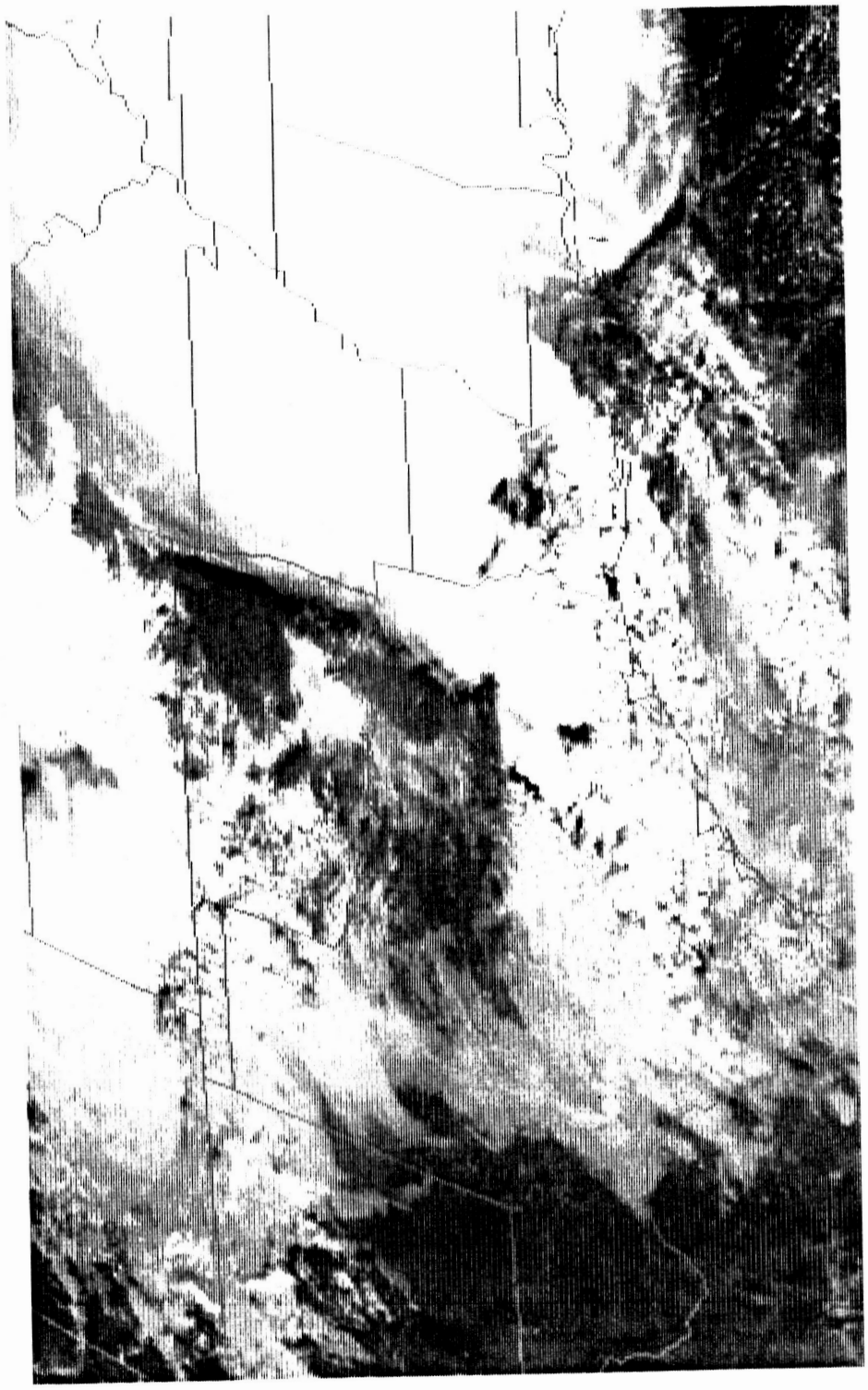

Fig. 29. GOES visible image for 1300 GMT 20 May 1983.

NWS's surface analysis depicted a cold front extending from the Tennessee Valley southwestward to southeast Texas (not shown). Normally, pronounced clearing occurs behind arc clouds. The lack of clearing in southeast Texas (see Fig. 29) can be partially explained by the presence of the existing cold front.

The characteristics associated with the MCC are displayed in Table 8. The extreme intensity of the MCC is obvious. The highest reported thunderstorm height of 66,000 ft was reached at 0635 GMT. The largest point precipitation rate and the maximum sum of the three largest hourly precipitation rates, of 2.1 in h^{-1} and 4.10 in h^{-1}, respectively, occurred at 0700 GMT, just before the time of maximum extent of the storm. Also, the sum of the three largest hourly precipitation rates stayed above 1.5 in h^{-1} for 5 straight hours. The only exception to this occurred the hour ending at 0600 GMT, when it again appeared that the heavy precipitation fell between the climatological raingauge sites. This was determined by following the movement of the coldest cloud tops on satellite images and by keeping continuity of the most intense precipitation. The coldest cloud top temperatures of -78°C occurred at both 0700 and 0800 GMT. It should be noted that the decrease of the maximum hourly surface divergence after 1000 GMT, was probably due to the lack of wind reports behind the gust front as it moved into the Gulf of Mexico.

Case 11: 11 June 1983

On the evening of 10 June 1983, thunderstorms formed over eastern New Mexico and western Texas ahead of a short-wave trough in the

Table 8. Characteristics associated with the MCC of Case 10 (20 May 1983). The maximum thunderstorm heights were determined at approximately 35 min past each hour. Dashes indicate that the parameter was not determined.

Time (GMT)	Maximum thunderstorm height (x 100 ft)	Maximum surface divergence (x 10^{-5} s^{-1})	Sum of the three largest precipitation rates (in h^{-1})	Maximum point precipitation rate (in h^{-1})	Coldest cloud top temperature (°C)
0000		2	-	-	-
	-				
0100		4	-	-	-63
	-				
0200		2	-	-	-63
	-				
0300		2	0.40	0.40	-63
	610				
0400		2	0.70	0.40	-68
	630				
0500		2	2.65	1.00	-73
	640				
0600		1	1.20	0.80	-73
	660				
0700		0	4.10	2.10	-78
	550				
0800		1	2.74	1.20	-78
	520				
0900		1	2.16	0.92	-73
	540				
1000		2	0.99	0.43	-73
	420				
1100		0	0.87	0.40	-68
	330				
1200		0	0.15	0.10	-63
	350				
1300		0	0.21	0.10	-58
	350				
1400		-	0.40	0.20	-
	320				
1500		-	0.71	0.40	-
	-				
1600		-	0.06	0.06	-
	-				

mid-troposphere. At 0000 GMT 11 June 1983, the short-wave trough was evident in the 50 kPa analysis and extended from western Kansas to southwestern New Mexico (Fig. 30). At the surface, the storms developed to the east of a dry line and in an area of strong convergence, with magnitudes as large as -3×10^{-5} s^{-1}, as determined by the McIDAS. The thunderstorms expanded and at 0530 GMT an MCC was initiated.

At 0800 GMT, a gust front and mesohigh developed. As the gust front passed Wichita Falls, TX, a wind gust of 44 kt was reported.

By 1300 GMT, an arc cloud was evident in the visible satellite image (Fig. 31). The arc cloud extended from southeastern Oklahoma to central Texas. At 1600 GMT, the gust front and mesohigh were still discernible in the surface analysis and the arc cloud was clearly evident in the satellite images (not shown).

Table 9 shows the characteristics associated with the MCC. Although the characteristics were not as pronounced as some of the previous category 1 MCSs, heavy precipitation fell for a significant time. The sum of the three largest hourly precipitation rates stayed above 1.5 in h^{-1} for five consecutive hours.

Category 2 MCSs

Category 2 MCSs are defined as follows: The MCS produces a gust front and the gust front persists for 6 h or less. Four MCSs are classified in this category. The four MCSs are from Cases 1, 5, 6 and 9. A brief discussion of the synoptic situation and storm characteristics associated with each category 2 MCS follows.

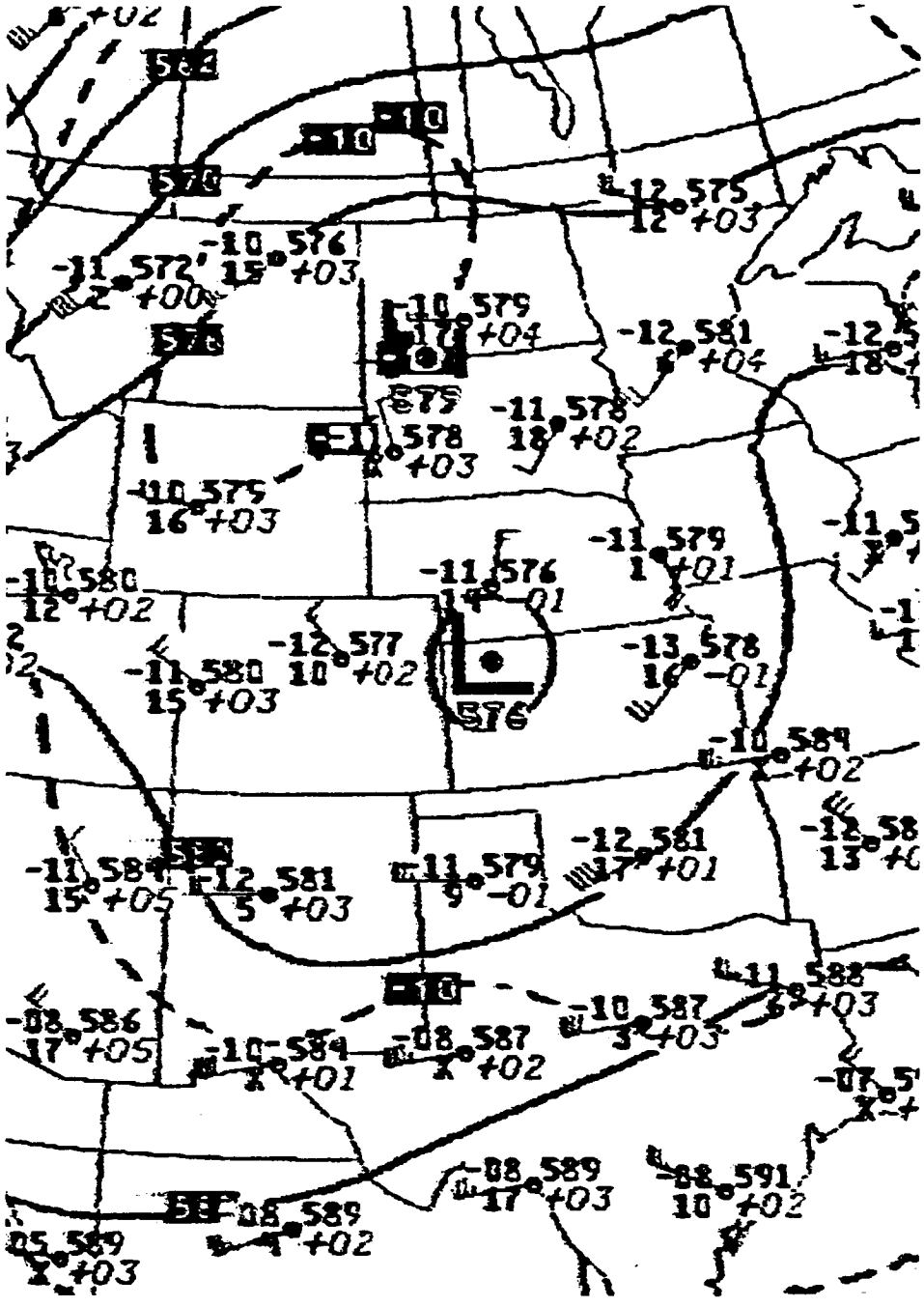

Fig. 30. 50 kPa height (dm) and temperature (°C) fields for 0000 GMT 11 June 1983. Height contours (solid lines) are every 60 m; isotherms (dashed lines) are every 5°C.

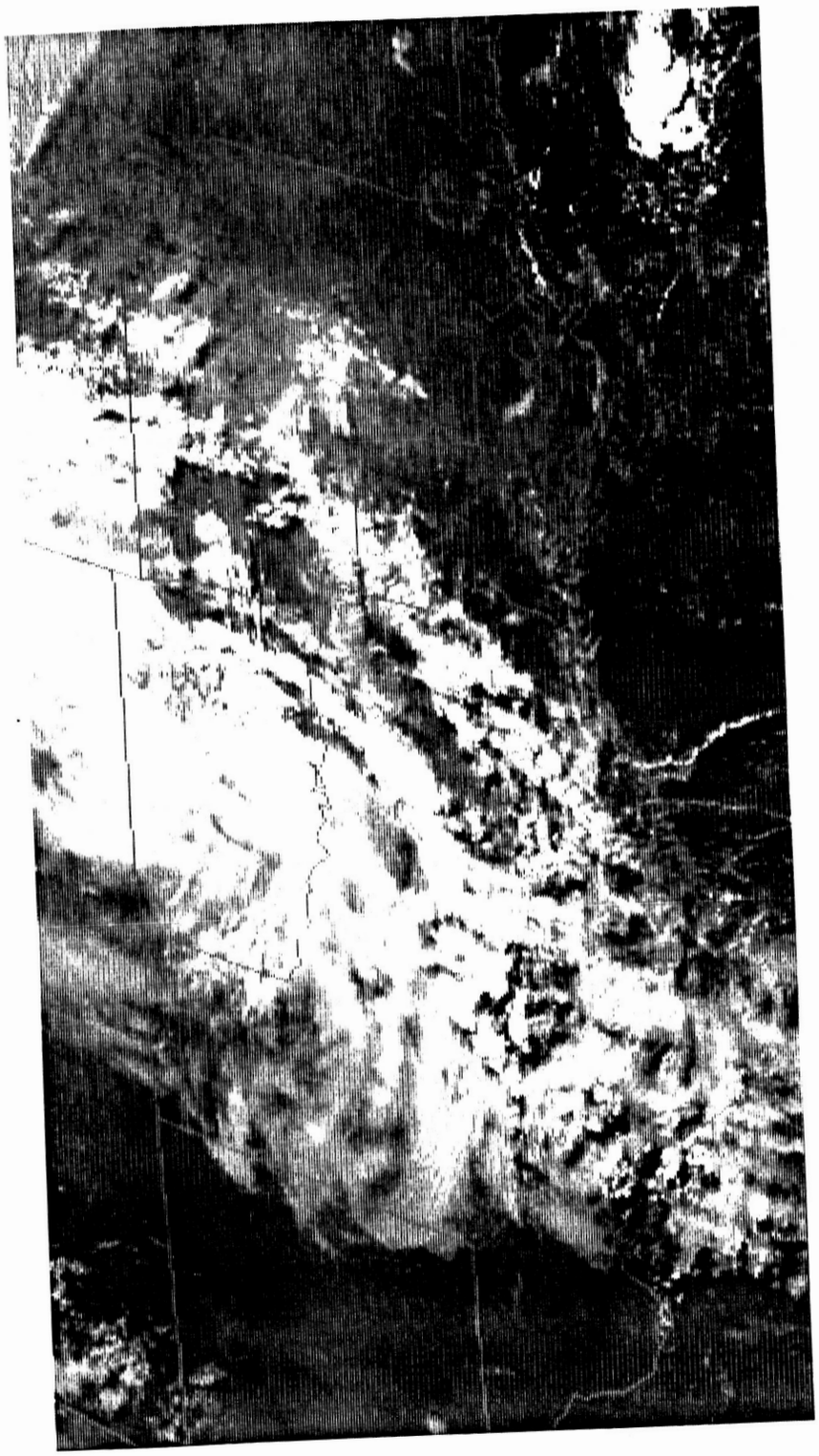

Fig. 31. GOES visible image for 1300 GMT 11 June 1983.

Table 9. Characteristics associated with the MCC of Case 11 (11 June 1983). The maximum thunderstorm heights were determined at approximately 35 min past each hour. Dashes indicate that the parameter was not determined.

Time (GMT)	Maximum thunderstorm height (x 100 ft)	Maximum surface divergence (x 10^{-5} s^{-1})	Sum of the three largest precipitation rates (in h^{-1})	Maximum point precipitation rate (in h^{-1})	Coldest cloud top temperature (°C)
0200	-	-	0.16	0.10	-
0300	-	-	1.12	0.50	-
0400	500	-3	0.67	0.40	-58
0500	510	-3	1.10	0.60	-58
0600	520	-1	2.30	0.90	-63
0700	510	-3	1.80	0.70	-63
0800	450	-2	1.60	0.60	-63
0900	440	3	2.00	0.90	-68
1000	390	1	1.55	0.60	-63
1100	320	2	1.08	0.50	-58
1200	310	2	0.88	0.44	-58
1300	300	-	0.01	0.01	-
1400	300	-	0.30	0.10	-

Case 1: 10/11 April 1981

On 10 April 1981 an MCC developed over the Texas panhandle during the late afternoon. It developed along a stationary front, which extended from southeastern Minnesota to north central Kansas and then southward to the Texas panhandle. Convection occurred all along this front (see Fig. 32). The MCC developed in response to a short wave in the mid-troposphere. Of course, a number of other conditions must have co-existed to support MCC development, such as lower tropospheric warm advection, ample moisture and convective instability (Maddox, 1981). Fig. 33 shows the 70 kPa analysis for 0000 GMT 11 Apr 1981. The short wave trough line is clearly evident, located over the western portion of the Texas panhandle.

By 0200 GMT 11 Apr 1981, an organized surface high pressure system and gust front, produced by the downdrafts of the thunderstorms associated with the MCC, first appeared. Fig. 34 shows the surface analysis for 0300 GMT. The gust front, denoted by the cold front symbols, was located from just west of Oklahoma City, OK (OKC), to Fort Sill, OK (FSI) and southwestward to just south of Childress, TX (CDS). Note the west wind at Hobart, OK (HBR) and the southeastern winds at Amarillo, TX (AMA) and Dalhart, TX (DHT). These diverging winds are a typical pattern associated with the presence of the mesohigh and gust front. Fig. 32 shows the surface divergence field overlaid upon the GOES IR imagery, both for 0300 GMT. A well-organized divergence pattern, with magnitudes up to 4×10^{-5} s^{-1}, was centered over the northeastern Texas panhandle.

The MCC terminated at 0531 GMT (see Table 2, page 19). The gust front quickly lost its identity and by 0700 GMT was no longer evident in

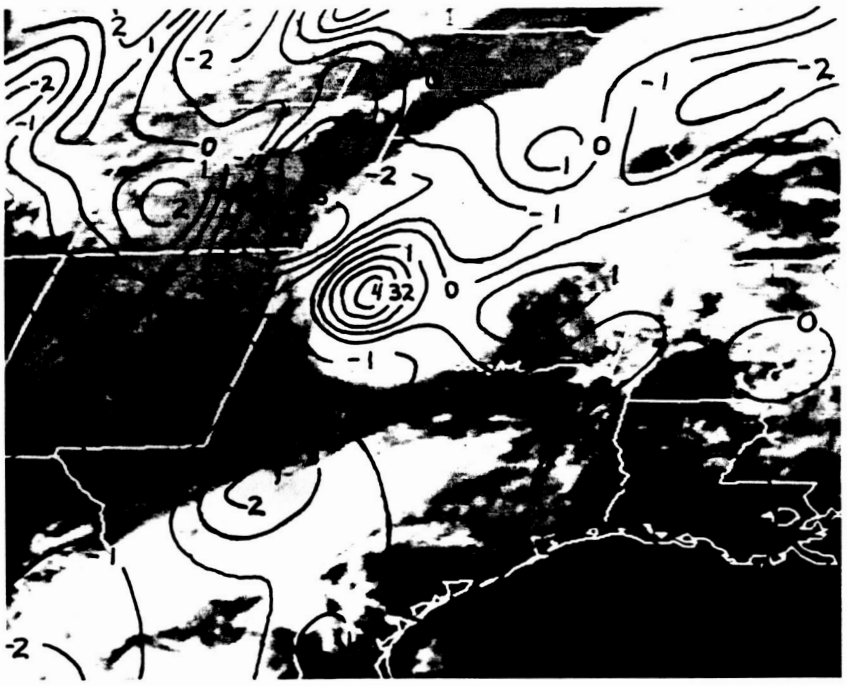

Fig. 32. Surface divergence field overlaid upon GOES IR image for 0300 GMT 11 April 1981. Values are times 10^{-5} s^{-1} and isolines are drawn at an increment of 1 x 10^{-5} s^{-1}.

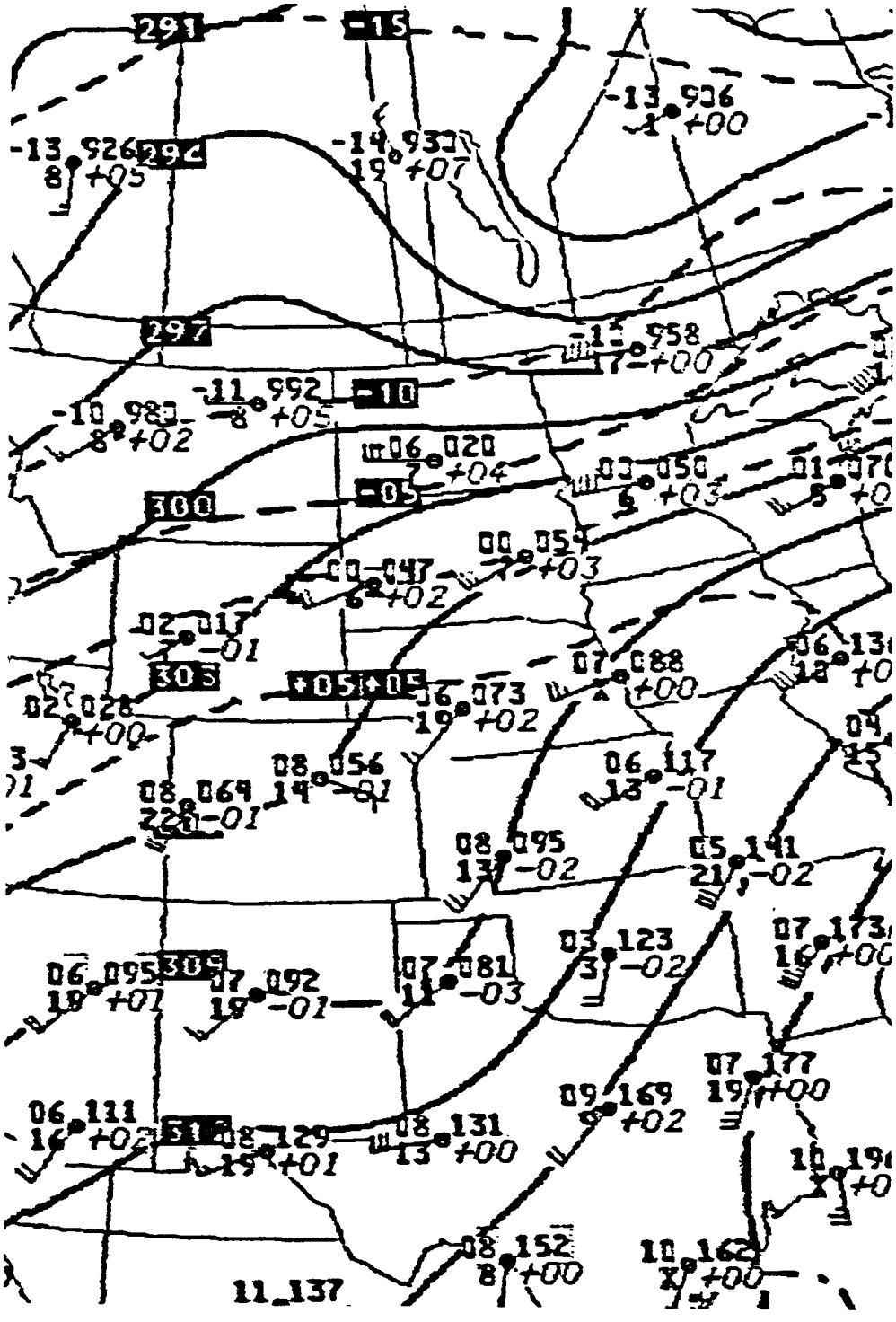

Fig. 33. 70 kPa height (dm) and temperature (°C) fields for 0000 GMT 11 April 1981. Height contours (solid lines) are every 30 m; isotherms (dashed lines) are every 5°C.

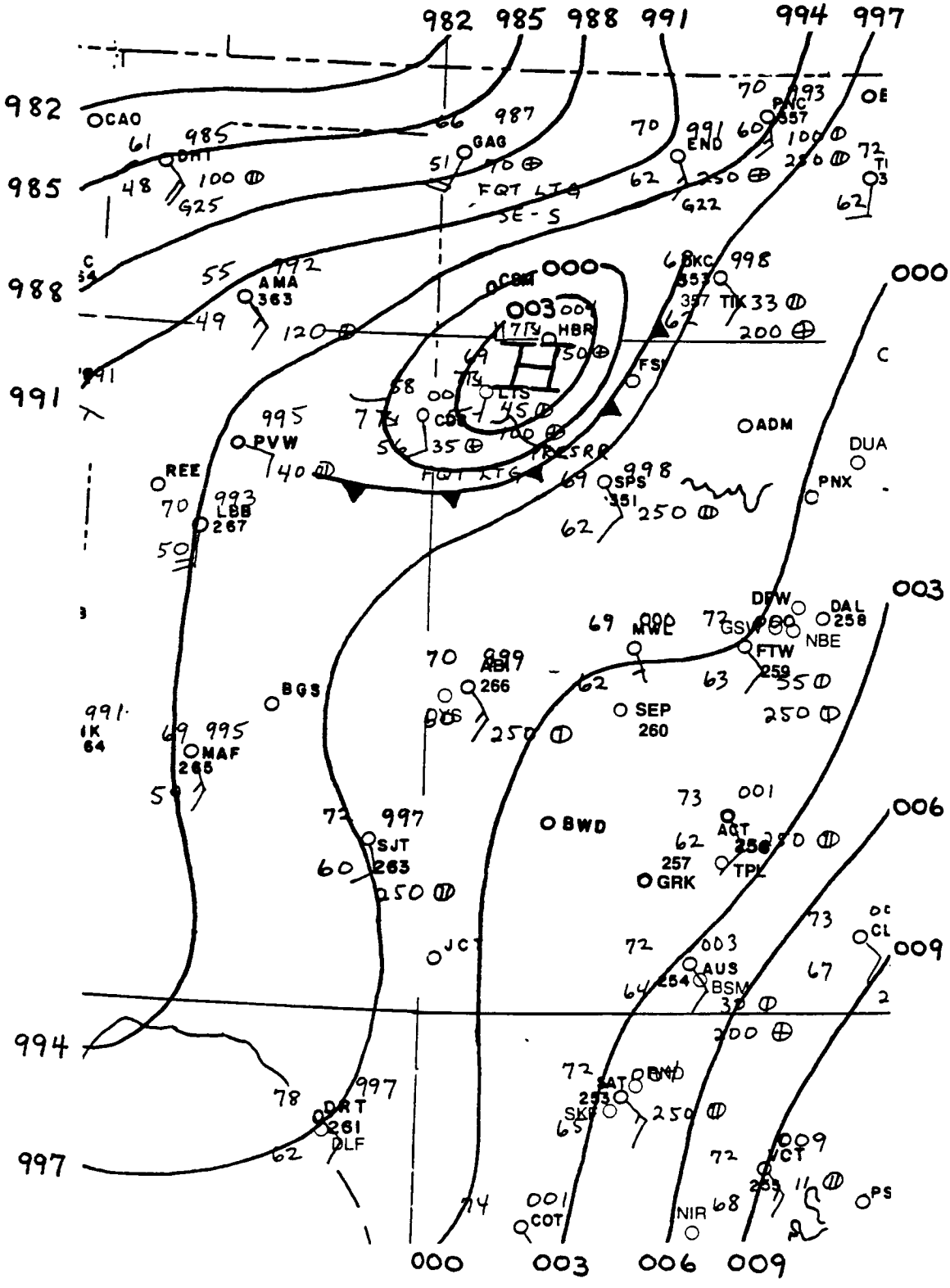

Fig. 34. Surface pressure field for 0300 GMT 11 April 1981. Altimeter setting contours are every 0.03 in Hg. The gust front is denoted by a cold front symbol.

the surface analysis (not shown). Therefore, the gust front lasted for 5 h, from 0200 to 0700 GMT. No arc cloud was ever apparent in the satellite images.

Table 10 shows specific characteristics associated with this MCC. The maximum thunderstorm height of 56,000 ft occurred at 0435 GMT. After the termination of the MCC, as expected, the heights quickly lowered. The hourly surface divergence reached its maximum at 0200 and 0300 GMT, near the time of maximum extent (see Table 2) of the system, as measured by the number of pixels in the IR satellite imagery contained by the -62°C isotherm. The surface divergence slowly weakened thereafter, which indicated the gust front was also weakening. The maximum sum of the three largest hourly precipitation rates and the largest point precipitation rate were 1.5 in h^{-1} and 1.0 in h^{-1}, respectively. These rainfall rates are rather light compared to the MCSs classified in category 1. The coldest hourly cloud top temperatures followed a similar pattern as the maximum hourly thunderstorm tops; a rapid warming of the temperatures, which corresponds to a lowering of the thunderstorm heights, occurred shortly after termination of the MCC.

Case 5: 19 May 1982

During the nighttime hours of 19 May 1982, two MCSs developed over western Kansas and western Oklahoma. The first MCS began forming around 0030 GMT and subsequently dissipated around 0800 GMT. The second MCS, the one of most importance for this study, formed around 0800 GMT, in western Oklahoma and dissipated by 1300 GMT. Fig. 35 shows the GOES IR image at 0800 GMT. The first MCS, now dissipated, was located in

Table 10. Characteristics associated with the MCC of Case 1 (10/11 April 1981). The maximum thunderstorm heights were determined at approximately 35 min past each hour. Dashes indicate that the parameter was not determined.

Time (GMT)	Maximum thunderstorm height (x 100 ft)	Maximum surface divergence (x 10^{-5} s^{-1})	Sum of the three largest precipitation rates (in h^{-1})	Maximum point precipitation rate (in h^{-1})	Coldest cloud top temperature (°C)
2300	510	-	0.59	0.40	-
0000	500	-	0.50	0.20	-63
0100	460	2	0.00	0.00	-63
0200	510	4	0.30	0.20	-63
0300	490	4	1.40	0.80	-63
0400	560	3	1.50	1.00	-63
0500	530	2	1.17	0.50	-63
0600	500	2	0.62	0.40	-58
0700	430	2	0.30	0.10	-
0800	300	2	0.50	0.30	-
0900	-	1	0.13	0.10	-
1000	-	1	0.10	0.10	-

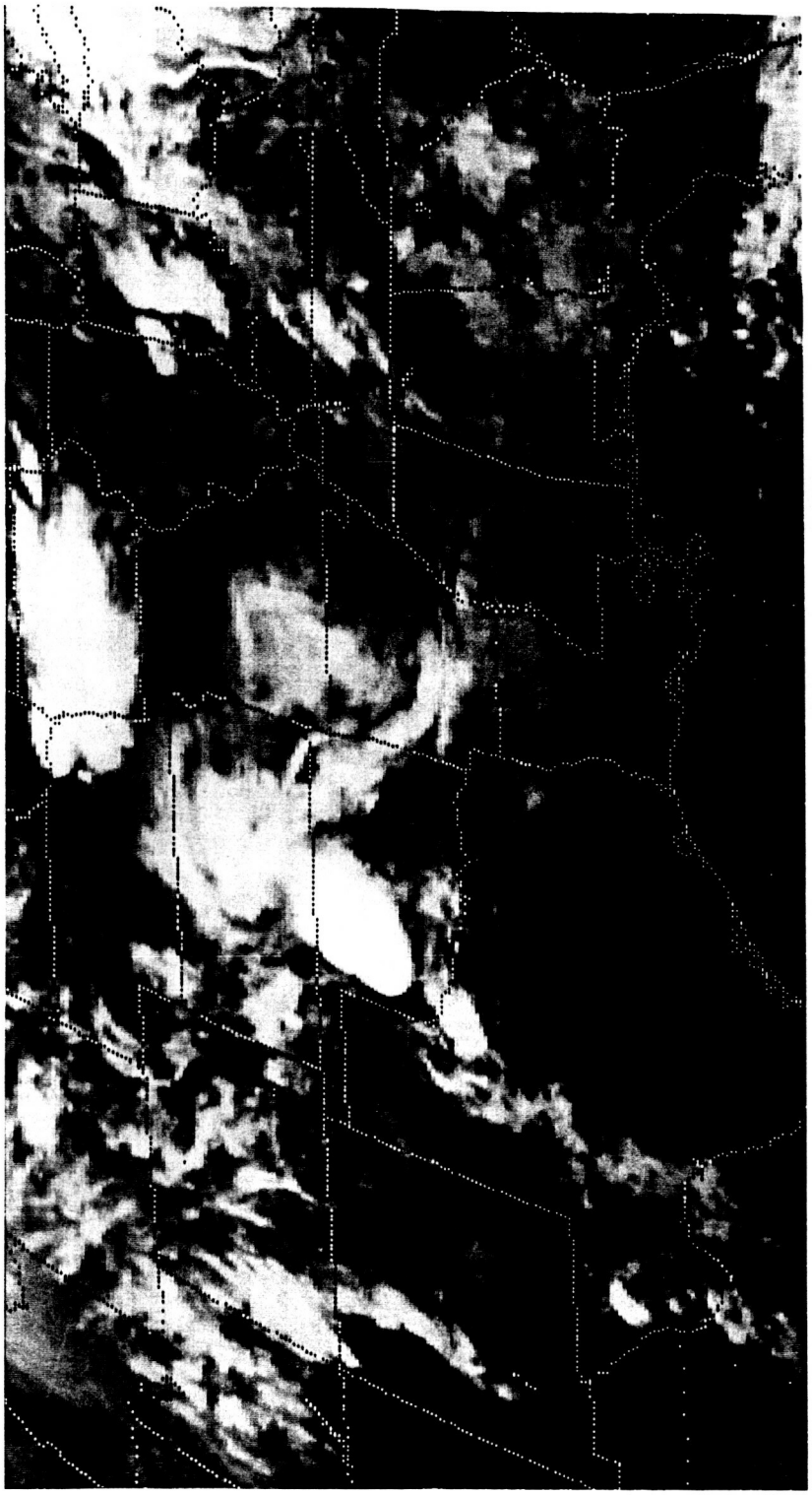

Fig. 35. GOES IR image for 0800 GMT 19 May 1982.

central Kansas. The second MCS, in the development stage, was located in western Oklahoma.

The mid-tropospheric flow pattern, associated with the development of the MCSs, is depicted in the 50 kPa analysis, Fig. 36. A deepening, negatively tilted trough, encompassed the western United States. However, the axis of a weak ridge was located just to the west of the development region. There was no indication in the flow, over the development region, of a weak embedded trough, which normally accompanies the formation of MCSs. This might have been one factor which led to the short duration of the MCSs.

A weak mesohigh and gust front, associated with the second MCS, appeared over western Oklahoma at 1000 GMT. By 1100 GMT, evidence of a small arc cloud could be seen in the GOES IR image. However, the gust front, mesohigh and arc cloud were undetectable in the surface analysis and satellite images after 1600 GMT.

Brundidge (1983) also studied this case. He gave three reasons for the short life and relative unimportance of this arc cloud:

1. The cold-air layer at the ground was very shallow, amounting to only about 200 m in depth.

2. The wind in the shallow layer had no northerly component; therefore, the outflow was not undercutting and lifting the warm, moister, surface air in northern Texas to maintain convection.

3. It appeared that the storm was simultaneously raining itself out and drawing drier air into the system, thus reducing the energy supply.

Table 11 shows the characteristics associated with primarily the

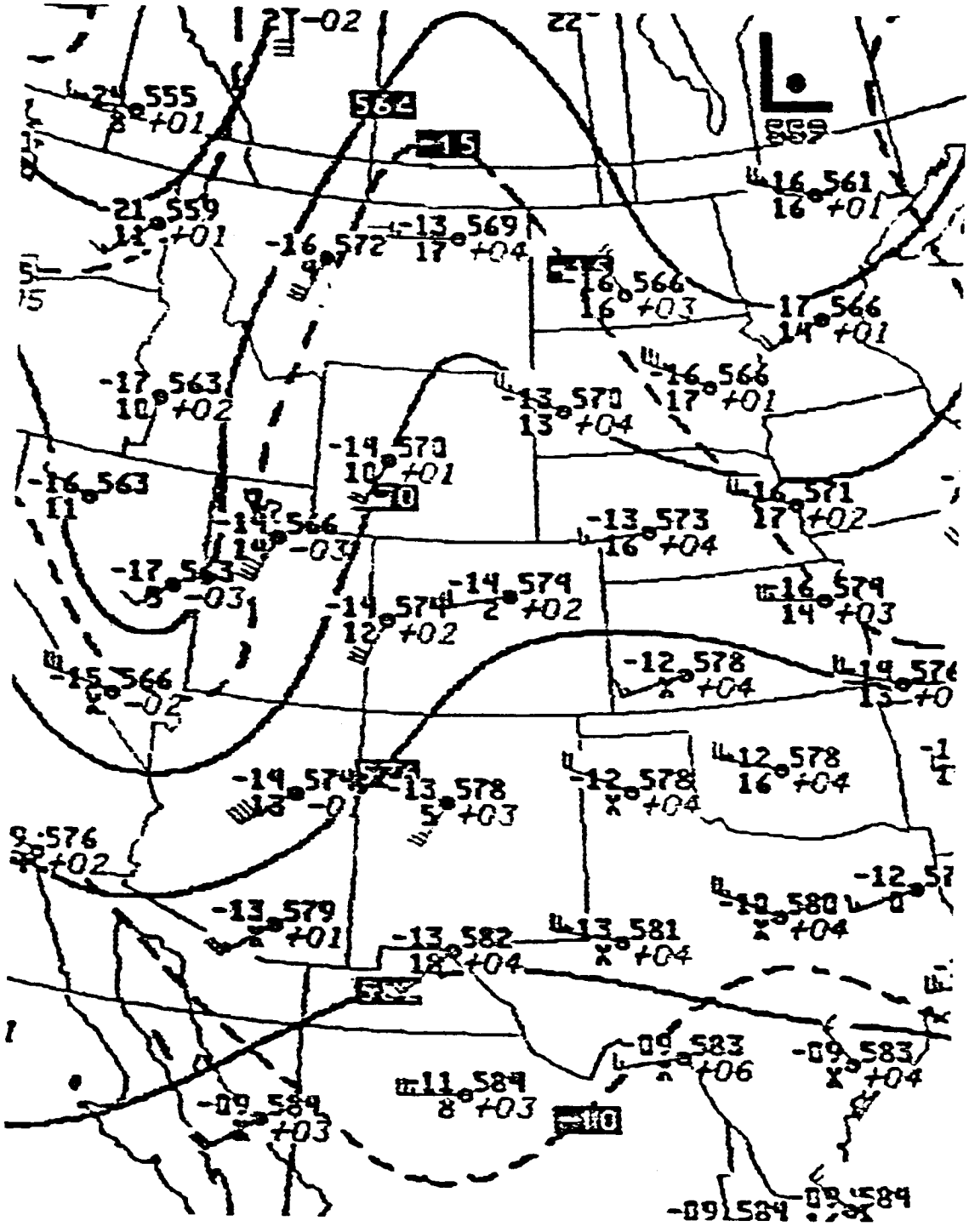

Fig. 36. 50 kPa height (dm) and temperature (°C) fields for 0000 GMT 19 May 1982. Height contours (solid lines) are every 60 m; isotherms (dashed lines) are every 5°C.

Table 11. Characteristics associated with the MCS of Case 5 (19 May 1982). The maximum thunderstorm heights were determined at approximately 35 min past each hour. Dashes indicate that the parameter was not determined.

Time (GMT)	Maximum thunderstorm height (x 100 ft)	Maximum surface divergence (x 10^{-5} s^{-1})	Sum of the three largest precipitation rates (in h^{-1})	Maximum point precipitation rate (in h^{-1})	Coldest cloud top temperature (°C)
0300		-	0.08	0.05	-
	490				
0400		3	0.08	0.08	-63
	460				
0500		3	0.12	0.09	-63
	420				
0600		1	0.32	0.17	-63
	490				
0700		1	0.52	0.32	-63
	490				
0800		1	0.23	0.20	-63
	450				
0900		-1	1.19	1.10	-63
	420				
1000		0	1.05	0.60	-63
	380				
1100		0	1.50	1.00	-63
	400				
1200		1	0.30	0.10	-58
	350				
1300		-	0.70	0.50	-
	310				
1400		-	0.10	0.10	-
	290				

second MCS. However, any characteristics given before 0800 GMT were associated with the first MCS. Similar to Case 1, the characteristics were very weak. For the second MCS, the maximum thunderstorm height was only 45,000 ft and the maximum surface divergence was only 1 x 10^{-5} s^{-1}. The maximum sum of the three largest hourly rainfall rates was 1.5 in h^{-1}, the same as Case 1. Also, the largest hourly point precipitation rate was only 1.1 in h^{-1}, compared to 1.0 in h^{-1} for Case 1. Lastly, the coldest cloud top temperature was only -63°C.

Case 6: 10/11 June 1982

A very large MCC formed over western Texas on 10 June 1982. At 50 kPa, near zonal flow existed over the development area at 0000 GMT 11 June 1982 (Fig. 37). At the same time, very strong warm advection was present at both 85 and 70 kPa (not shown). Maddox (1983), in view of the quasi-geostrophic equations (in particular the tendency and omega equations), noted that the MCC develops in a region of upward vertical motion and that the upward motion "is primarily a reflection of strong low-level warm advection rather than of strong differential PVA."

The lifetime of the MCC, initiation to termination, was 2245 GMT 10 June 1982 to 1530 GMT 11 June 1982. Analysis of the cloud top temperatures, provided by the McIDAS and the plotted precipitation rates, revealed that the MCC actually consisted of two separate MCSs. The first MCS developed in the Texas panhandle and moved into southwest Oklahoma. The most intense phase of the MCS lasted from approximately 0300 to 0800 GMT. Fig. 38 shows the surface divergence overlaid upon the GOES IR imagery with MB enhancement, both for 0700 GMT. According

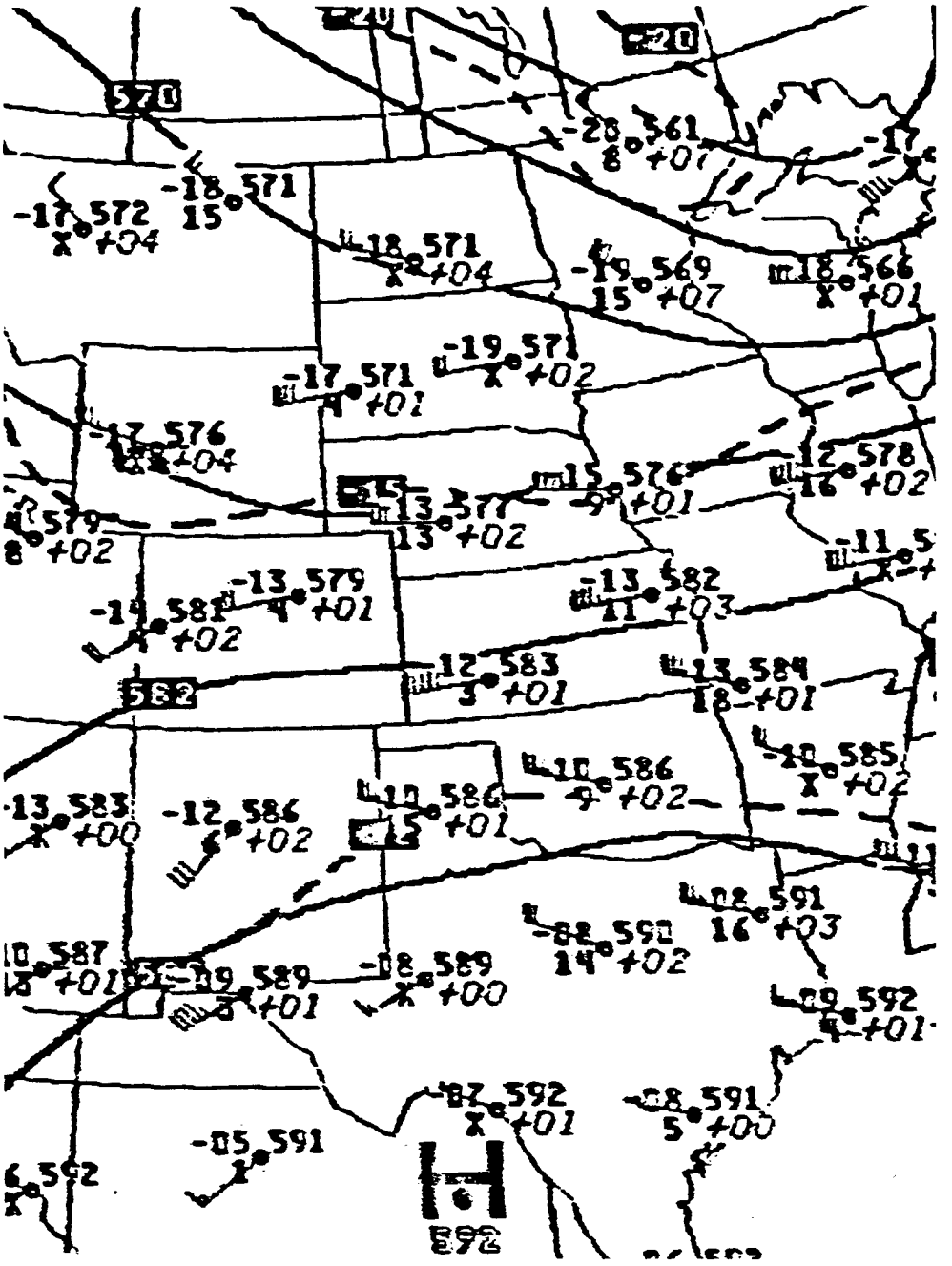

Fig. 37. 50 kPa height (dm) and temperature (°C) fields for 0000 GMT 11 June 1982. Height contours (solid lines) are every 60 m; isotherms (dashed lines) are every 5°C.

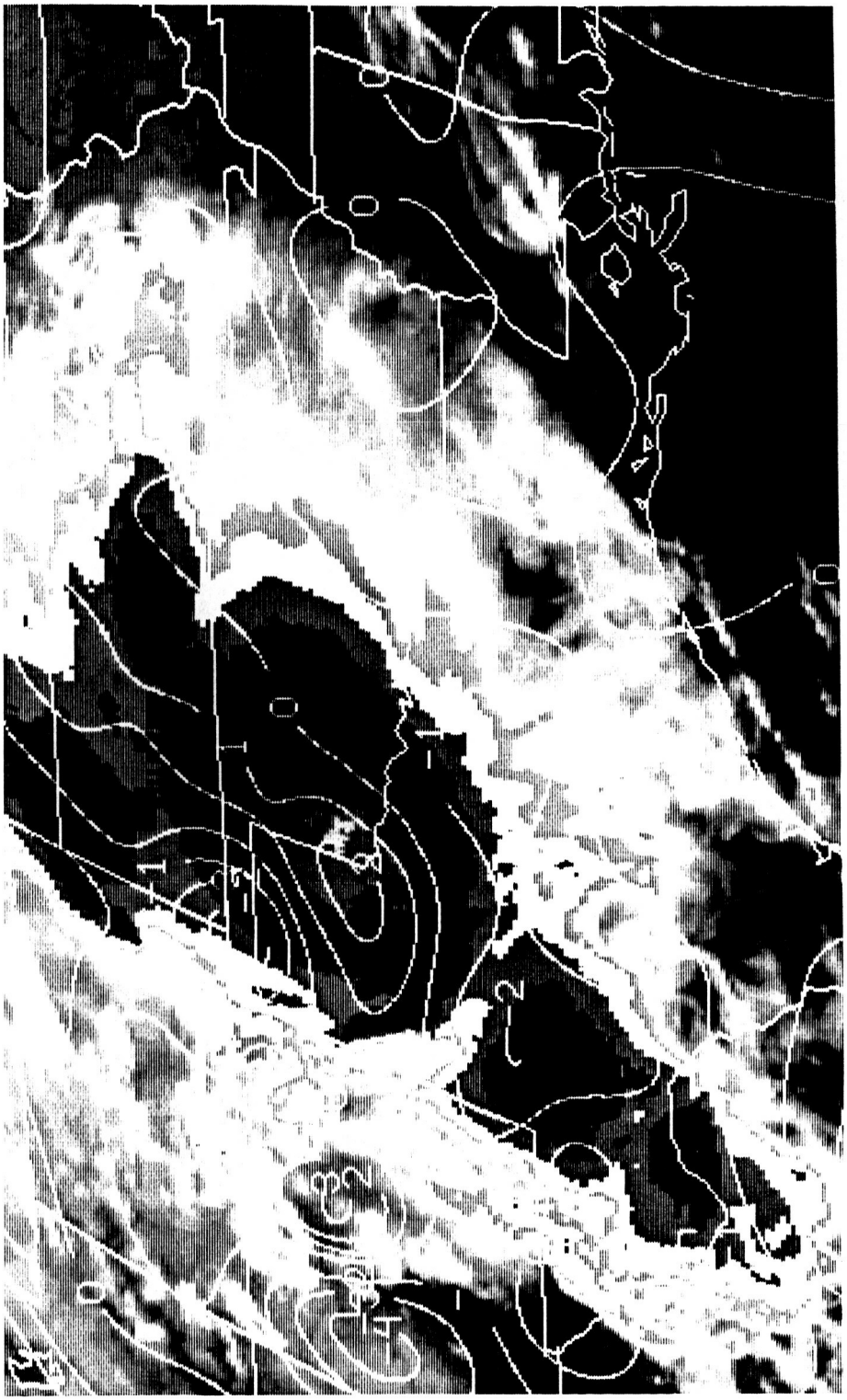

Fig. 38. Surface divergence field overlaid upon GOES IR image for 0700 GMT 11 June 1982. Values are times 10^{-5} s^{-1} and isolines are drawn at an increment of 1 x 10^{-5} s^{-1}.

to the MB enhancement curve, the large black area in the Texas panhandle and in western Oklahoma, corresponds to cloud top temperatures between -58°C and -62°C. The repeat gray area and the whitish area, enclosed by the black area, represent the coldest cloud top temperatures. Therefore, the maximum thunderstorm tops associated with the first MCS were located in the eastern portions of the Texas panhandle and in southwestern Oklahoma. An organized mesohigh and gust front, produced by this MCS, appeared in the surface analysis at 0500 GMT (Fig. 39). After the demise of the MCS, the mesohigh and gust front weakened. By 1000 GMT, the mesohigh and gust front were ill-defined in the surface analysis. The second MCS developed in northeastern Oklahoma, around the time the first MCS was terminating. The mesohigh and gust front associated with the second MCS were much weaker than those produced by the first MCS. No arc cloud was produced by either MCS.

The characteristics of the first MCS are displayed in Table 12. The sum of the three largest hourly precipitation rates stayed above 1.5 in h^{-1} for only 3 h. Of the two precious MCSs classified in category 2, this sum stayed at or above 1.5 in h^{-1} for only 1 h. Another interesting feature is exhibited in the trend of the maximum hourly surface divergence. The magnitudes of the divergence were strong, as high as 4×10^{-5} s^{-1}, before the demise of the mesohigh and gust front. However, after 1000 GMT, the divergence weakened, which corresponded to the weakening of the mesohigh and gust front.

Case 9: 28/29 June 1982

A short-lived MCC developed over northeastern Texas during the

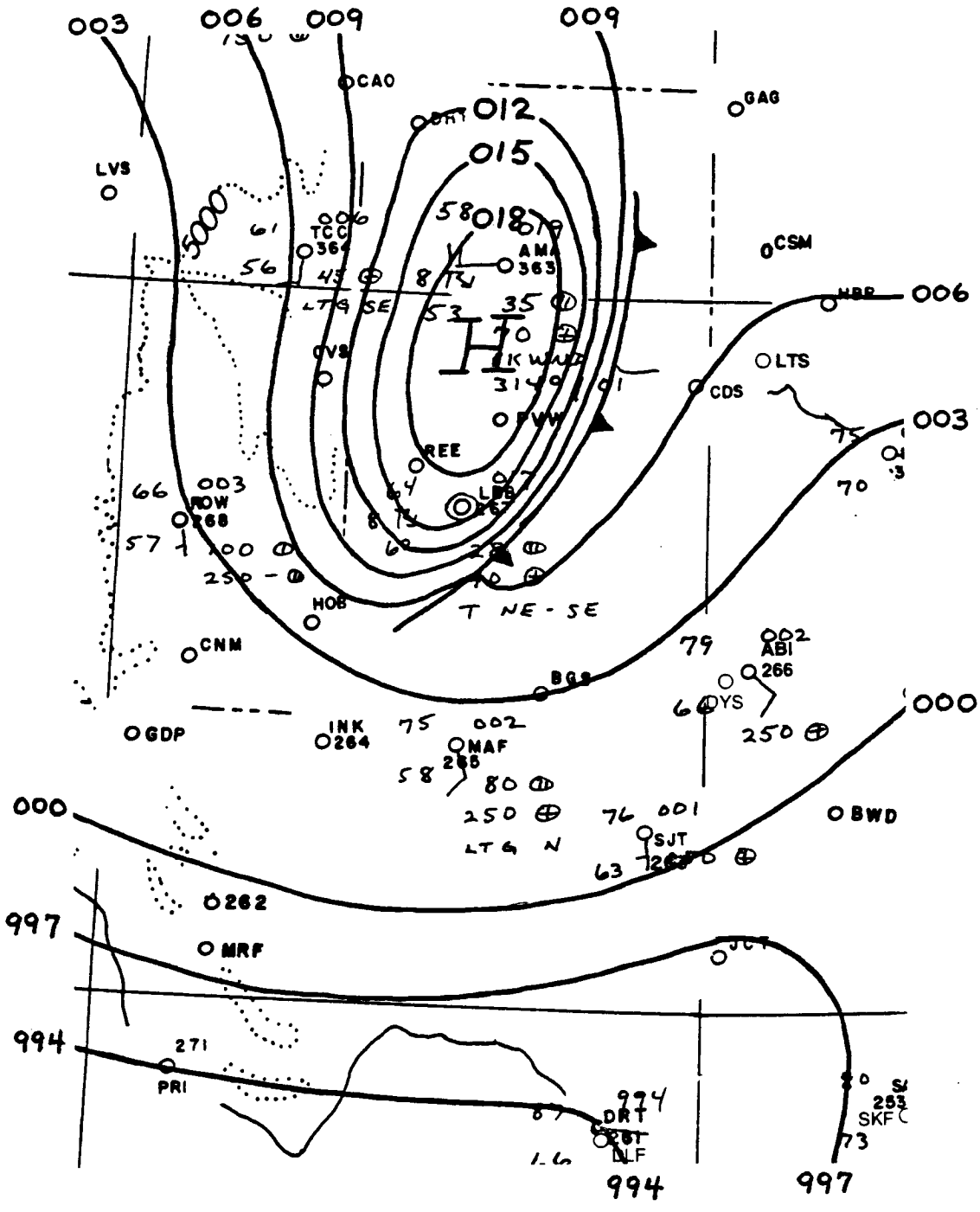

Fig. 39. Surface pressure field for 0500 GMT 11 June 1982. Altimeter setting contours are every 0.03 in Hg. The gust front is denoted by a cold front symbol.

Table 12. Characteristics associated with the MCC of Case 6 (11 June 1982). The maximum thunderstorm heights were determined at approximately 35 min past each hour. Dashes indicate that the parameter was not determined.

Time (GMT)	Maximum thunderstorm height (x 100 ft)	Maximum surface divergence (x 10^{-5} s^{-1})	Sum of the three largest precipitation rates (in h^{-1})	Maximum point precipitation rate (in h^{-1})	Coldest cloud top temperature (°C)
0100	-	-	1.40	1.00	-
0200	520	-	0.40	0.20	-
0300	530	-	1.20	1.00	-
0400	550	2	1.32	0.70	-73
0500	540	4	1.99	0.90	-73
0600	550	3	2.59	1.30	-73
0700	500	2	1.83	0.70	-73
0800	460	3	0.91	0.31	-73
0900	480	4	1.40	0.70	-68
1000	410	3	1.40	0.70	-68
1100	340	1	0.57	0.20	-
1200	380	2	0.22	0.10	-
1300	400	1	0.29	0.10	-

afternoon of 28 June 1982. Fig. 40 depicts the 50 kPa analysis for 0000 GMT 29 June 1982. This was near the initiation time of the MCC. An upper level trough was associated with the MCC and a very pronounced ridge was situated to the west. At 85 kPa, warm air advection (i.e., quasi-geostrophically forced upward motion) was evident over eastern Texas (not shown). Absolute moisture contents within the air mass feeding the MCC were high. For instance, at 85 kPa, the moisture content for Victoria, TX (VCT) was 11 g kg^{-1} at 0000 GMT 29 June 1982. Maddox (1982), in a composite study of 10 MCCs, described a similar synoptic setting for the development of MCCs.

At 0000 GMT 29 June 1982, a gust front and mesohigh appeared in the surface analysis (Fig. 41). The MCC terminated at 0430 GMT (see Fig. 42). By 0500 GMT the gust front and mesohigh had virtually disappeared in the surface analysis (Fig. 43). The weakness of the gust front, during its lifetime, was verified by the lack of strong winds as it passed reporting weather stations. The strongest wind gust was only 15 kt, which occurred at both Lufkin, TX (LFK) and College Station, TX (CLL). No arc cloud was produced by this MCC.

The characteristics associated with the MCC are depicted in Table 13. The maximum hourly thunderstorm heights were impressive, reaching 58,000 ft at 0135 GMT. However, the heights quickly lowered after 0235 GMT. The maximum surface divergence reached magnitudes of 3×10^{-5} s^{-1} at 0400 and 0500 GMT and then rapidly weakened. The sum of the three largest hourly precipitation rates and the maximum hourly point precipitation rates were quite large before 0100 GMT, but dramatically dropped thereafter. As the precipitation rates decreased, the coldest cloud top

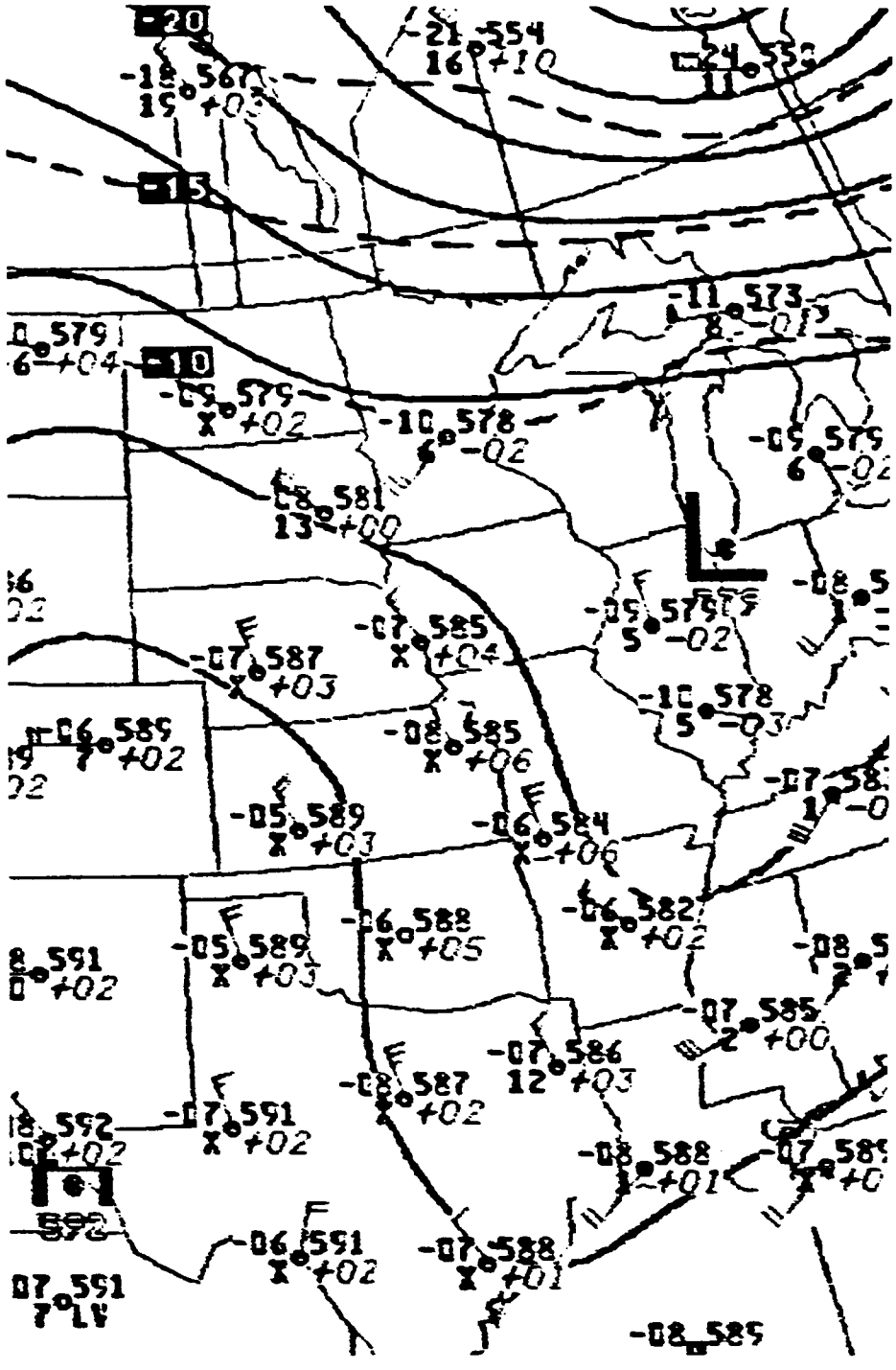

Fig. 40. 50 kPa height (dm) and temperature (°C) fields for 0000 GMT 29 June 1982. Height contours (solid lines) are every 60 m; isotherms (dashed lines) are every 5°C.

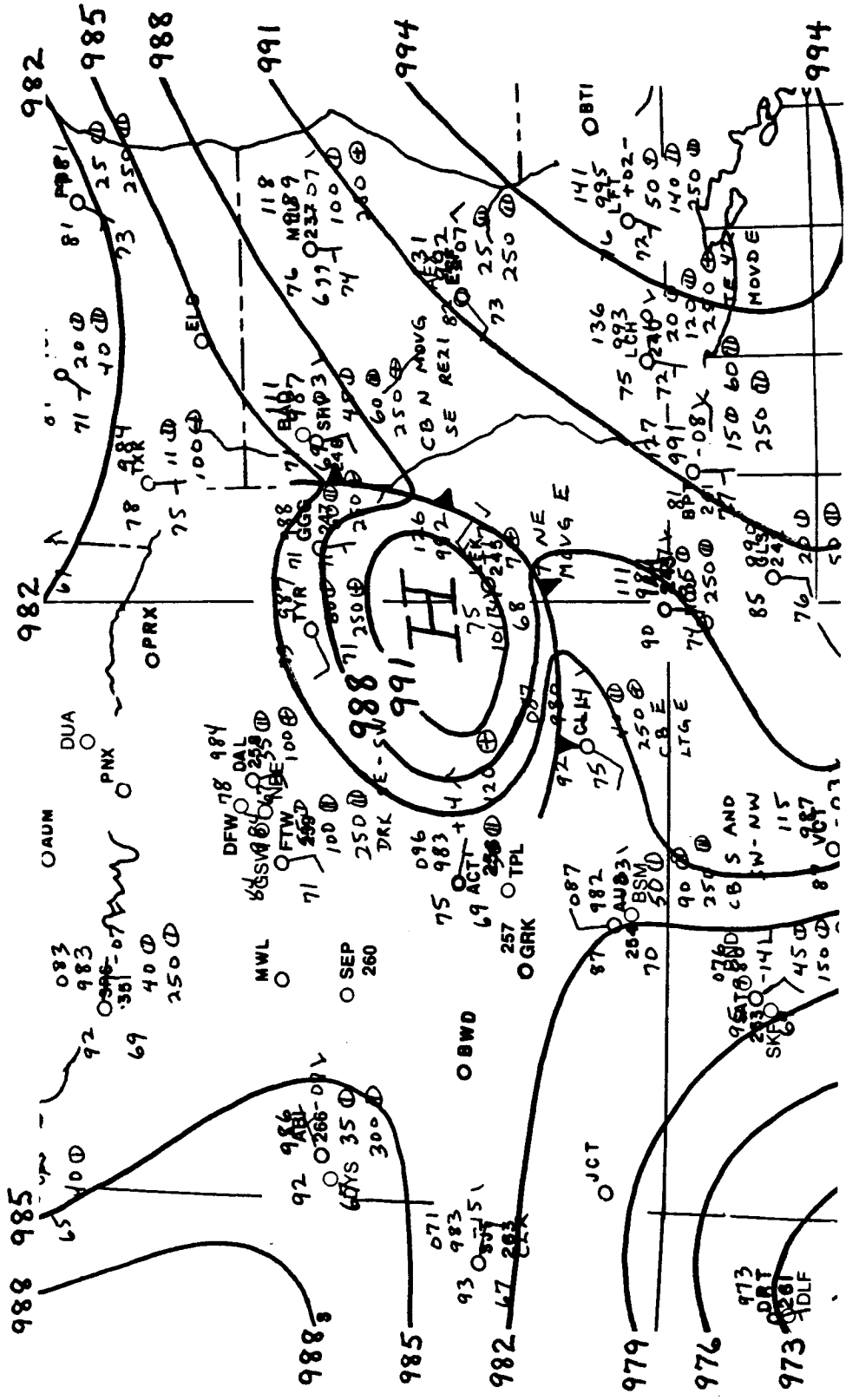

Fig. 41. Surface pressure field for 0000 GMT 29 June 1982. Altimeter setting contours are every 0.03 in Hg. The gust front is denoted by a cold front symbol.

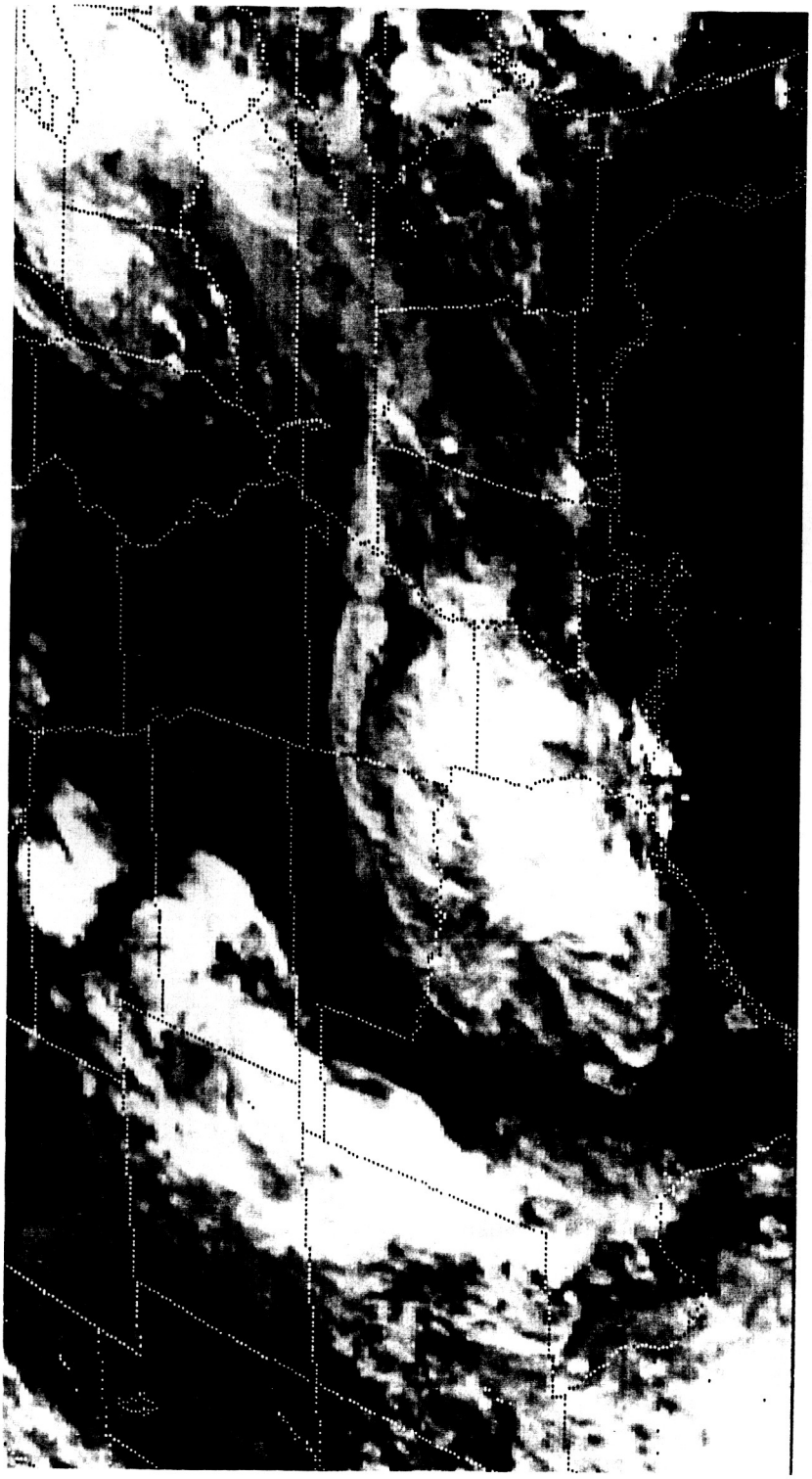

Fig. 42. GOES IR image for 0430 GMT 29 June 1982.

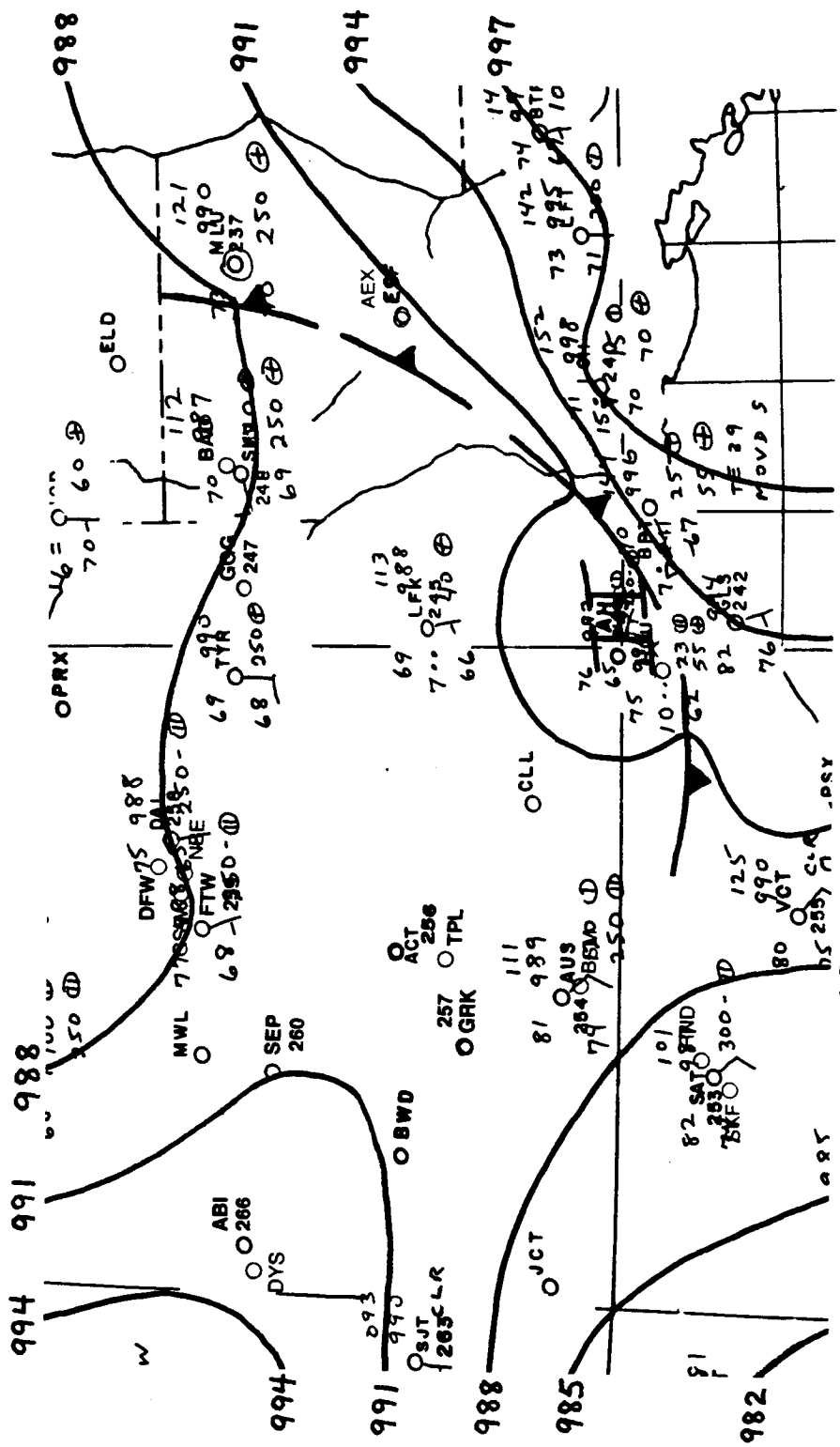

Fig. 43. Surface pressure field for 0500 GMT 29 June 1982. Altimeter setting contours are every 0.03 in Hg. The gust front is denoted by a cold front symbol.

Table 13. Characteristics associated with the MCC of Case 9 (28/29 June 1982). The maximum thunderstorm heights were determined at approximately 35 min past each hour. Dashes indicate that the parameter was not determined.

Time (GMT)	Maximum thunderstorm height (x 100 ft)	Maximum surface divergence (x 10^{-5} s^{-1})	Sum of the three largest precipitation rates (in h^{-1})	Maximum point precipitation rate (in h^{-1})	Coldest cloud top temperature (°C)
2100	510	-	2.72	1.62	-
2200	500	-2	2.46	0.90	-73
2300	570	0	1.80	1.00	-73
0000	550	1	0.99	0.40	-68
0100	580	0	1.60	1.30	-73
0200	550	1	0.60	0.40	-68
0300	450	2	0.50	0.30	-63
0400	420	3	0.88	0.48	-58
0500	340	3	0.23	0.17	-53
0600	360	1	0.40	0.20	-
0700	-	-1	0.20	0.10	-
0800	-	-	0.10	0.10	-
0900	-	-	0.10	0.10	-

temperatures warmed, which agrees with the findings of Gagin et al. (1985).

Case 12: 14 June 1983

During the afternoon of 13 June 1983, convection formed along a strong cold front, which was located through the central United States. An MCC developed near the southern portions of the cold front. By 0600 GMT 14 June 1983 it had reached its maximum extent. At this time, the MCC engulfed north central Texas and most of Oklahoma.

The precipitation pattern produced by the MCC was not typical of most MCCs. Heavy precipitation associated with the MCC fell exclusively along the cold front. Close inspection of the plotted hourly precipitation revealed that no precipitation fell along the southern edge of the MCC cloud shield. This was rather unusual, as many instances of an arc-shaped band of heavy precipitation along the southern portions of MCCs have been reported (Maddox, 1980, 1981; Leary and Rappaport, 1982; Howard and Maddox, 1983; and Bartels, 1983). Bartels (1983) stated, "Throughout the MCC life-cycle the most intense rainfall occurred near its southern periphery." Maddox (1980) argues that the most intense convective elements occur along the convergence zone produced by the interaction of the outflow boundary and the low-level inflow. This convergence zone occurs along the southern portion of the MCC. An example of this arc-shaped precipitation band, produced by the MCC from Case 2, is shown in Fig. 44. The arc-shaped band of heavy precipitation was located from eastern Texas to central Louisiana. Also, notice the circular shape in the overall precipitation pattern that was produced by

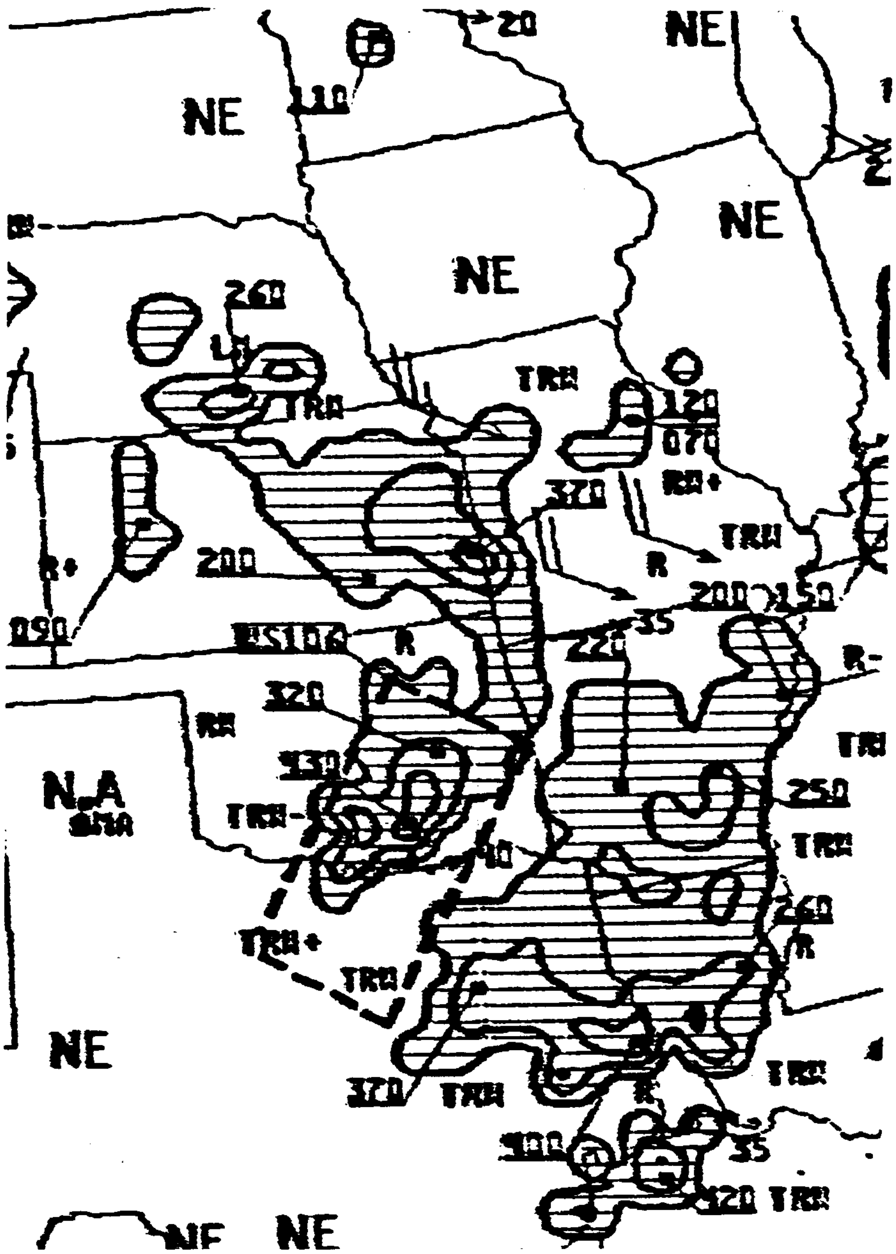

Fig. 44. Radar summary chart for 1035 GMT 9 May 1981. Shading indicated echo areas. Contours at echo intensities 1, 3, and 5; echo heights are in hundreds of feet; cell movement given at end of arrows in knots; area and line movement given by pennant with full barb = 10 kt.

the MCC of Case 2. This is typical of MCCs because of their circular shape, imposed by the MCC definition (refer to Table 1, page 3). In contrast, the precipitation pattern produced by the MCC of this case was markedly different. Fig. 45 displays this pattern and also shows the approximate location of the MCC cloud shield (scalloped area). There was no arc-shaped line of heavy precipitation on the southern periphery of the MCC. In fact, there was no precipitation falling there at all. Also, the overall precipitation pattern was much more elongated, like that produced by squall lines.

In summary, the precipitation pattern produced by the MCC of this case resembled that of a squall line, rather than an MCC. Therefore, this MCC was not classified in category 1 or 2 and was not used in the composite analyses (see next section).

Significant Events Associated with Category 1 and 2 MCSs

Table 14 summarizes the times that the following events occurred for both category 1 and 2 MCSs:

1. Maximum extent of the MCS.

2. First appearance of the gust front and mesohigh in the surface analysis.

3. First appearance, if any, of an arc cloud in the satellite images. In most cases, the first appearance of an arc cloud could only be determined by visible satellite images. It is extremely difficult to detect their existence in the IR images because arc clouds are normally composed of low, warm clouds. Therefore, the actual time of arc cloud formation could have been earlier than the time indicated in Table 14.

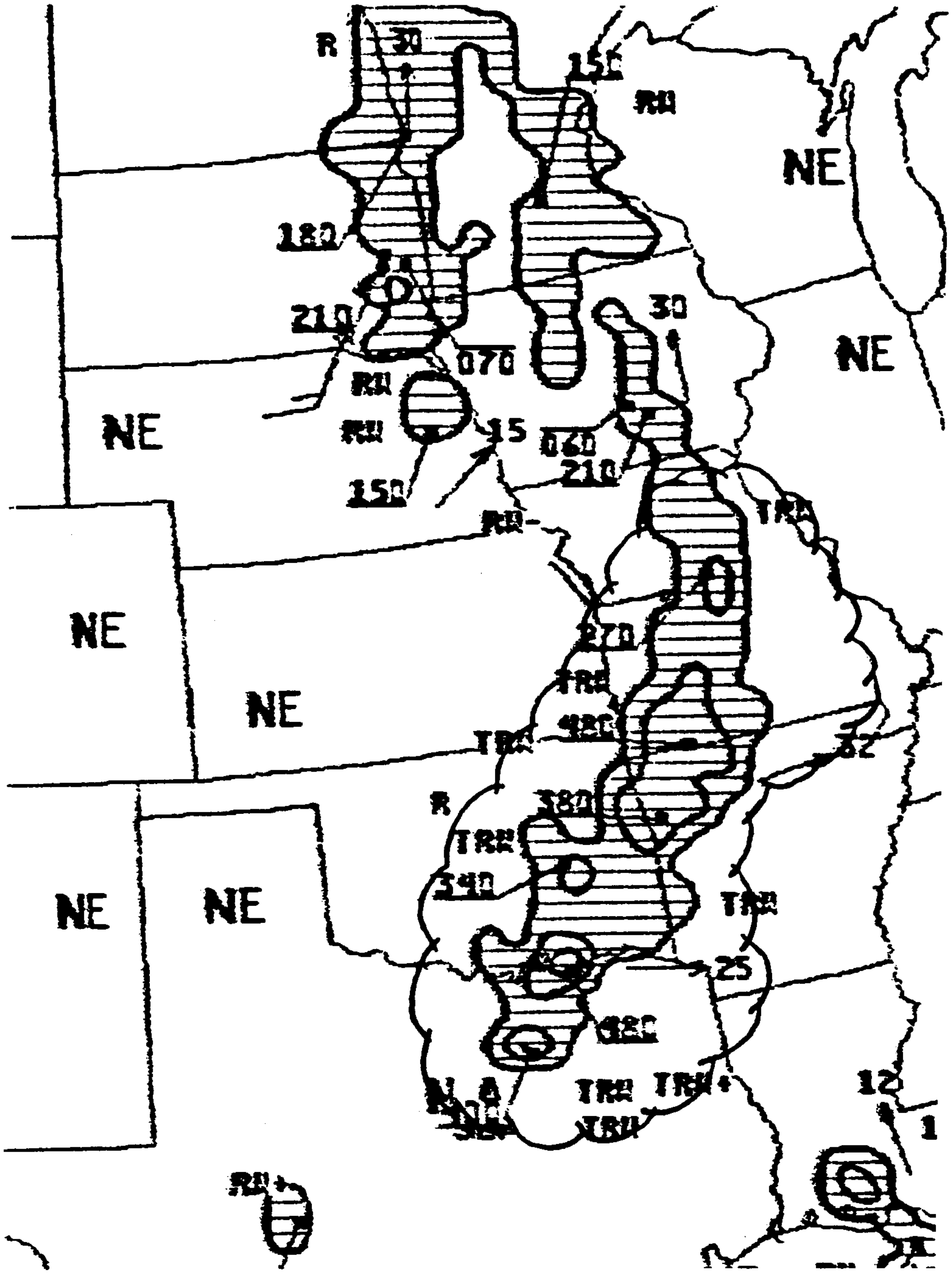

Fig. 45. Radar summary chart for 1035 GMT 14 June 1983. Shading indicates echo areas. Contours at echo intensities 1, 3, and 5; echo heights are in hundreds of feet; cell movement given at end of arrows in knots; area and line movement given by pennant with full barb = 10 kt. The scalloped area represents the approximate location of the MCC cloud shield at 1000 GMT 14 June 1983.

C-2

Table 14. Summary of significant events associated with category 1 and 2 MCSs. Time of MCS maximum extent, gust front/mesohigh first appearance in hourly surface analyses and arc cloud first appearance and termination, as determined by satellite imagery are listed.

Case number	Maximum extent (GMT)	Gust front/ mesohigh (GMT)	Arc cloud began (GMT)	Arc cloud ended (GMT)
		Category 1 MCSs		
2	0500	0500	1200	1800
3	1000	0700	1230	1800
4	0400	0200	1000	2200
7	1100	1100	1430	2200
8	0900	0800	1200	2100
10	0800	0400	1200	1800
11	0900	0800	1200	1800
		Category 2 MCSs		
1	0300	0200	none	none
5	0900	1000	1100	1600
6	0700	0500	none	none
9	0200	0000	none	none

4. The arc cloud, if any, became indistinguishable in the satellite images.

As seen in Table 14, all category 1 MCSs produced arc clouds. These MCSs, by definition, produced gust fronts that persisted for more than 6 h. In contrast, only one of the category 2 MCSs produced an arc cloud. These MCSs, by definition, produced gust fronts of shorter duration, lasting 6 h or less.

CHAPTER IV

COMPOSITE ANALYSES

To determine any differences between the MCSs of the two categories, composite analyses of the five following characteristics were accomplished:

1. Maximum hourly thunderstorm height.
2. Maximum hourly surface divergence.
3. Sum of the three largest precipitation rates.
4. Maximum hourly point precipitation rate.
5. Coldest hourly cloud top temperature.

Method of the Composite Analyses

The maximum extent of each MCS was determined by the McIDAS (see Table 2, page 19). The time of maximum extent, as defined in this research, occurred when the area, as depicted in IR satellite imagery, with temperatures less than or equal to -62°C, reached its maximum size.

For the composite analyses, the time of maximum extent was referred to as the zero (0) hour or zero (0) reference time. That is, this time was used as a reference time for all MCSs and determined when all the MCSs were at the same stage in their life-history. The hours before the maximum extent were defined as minus (-) hours and the hours after the maximum extent were defined as plus (+) hours. For example, the maximum extent time of the MCC for Case 1 was 0300 GMT 11 April 1981. Therefore, 0300 GMT was referred to as the zero (0) reference hour. 0400, 0500 and 0600 GMT were referred to as +1, +2 and +3 hours, respectively.

The MCS characteristic, "maximum hourly point precipitation," will be used as an example to demonstrate the method employed to accomplish the composite analyses. Assume the MCSs of Cases 2, 3, 4, 7, 8, 10 and 11 (category 1 MCSs) had maximum point precipitation rates of 1.10, 1.00, 0.90, 0.50, 0.50, 1.50 and 1.50 in h^{-1}, respectively, at hour +1 (1 h after maximum extent). The composite analysis, for this hour, would be the average of the precipitation rates (1.00 in h^{-1}). This procedure was applied for several hours before and after the maximum extent.

Results of the Composite Analyses

Composite analyses of the five characteristics were accomplished for the MCSs of category 1. The results of the composite analyses are displayed in the following five figures (thin solid lines). Similarly, composite analyses of the five characteristics were accomplished for the MCSs of category 2. These results are also shown in the following five figures (thick solid lines).

Fig. 46 graphically displays the results of the composite analysis for the maximum hourly thunderstorm heights. In the hours before the maximum extent time, category 1 MCSs, on average, had higher maximum thunderstorm heights, compared to the MCSs of category 2. This was especially true from -2 to -6 h (2 to 6 h before the time of maximum extent). This is the critical time period for the formation of the gust front, as the gust front and mesohigh usually form within the few hours before the maximum extent time of the MCS (see Table 14, page 88). In the hours after maximum extent, the differences in the maximum

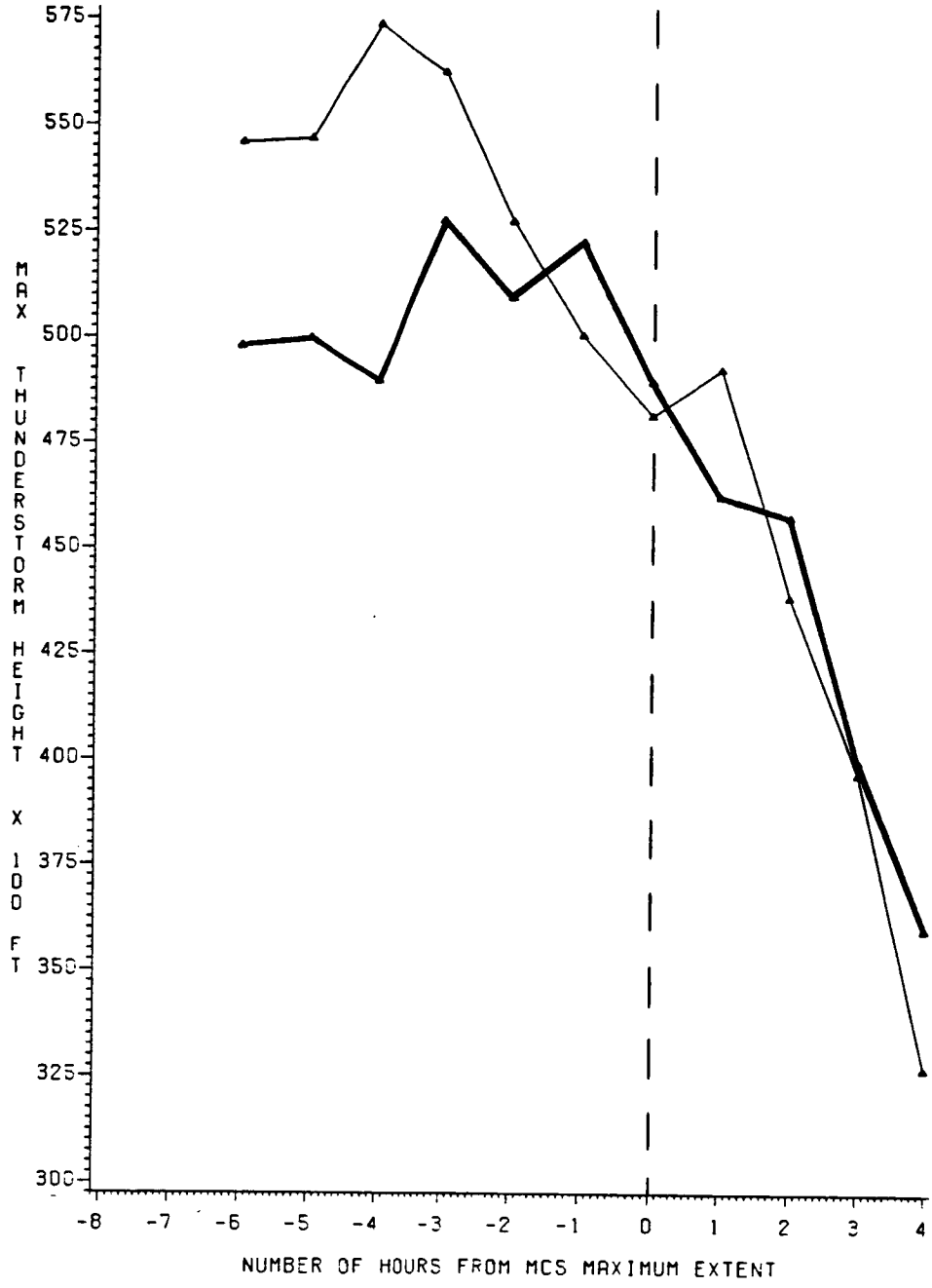

Fig. 46. Composite of the maximum hourly thunderstorm tops of category 1 (thin line) MCSs and category 2 (thick line) MCSs. Minus (-) hours are before MCS maximum extent and plus (+) hours are after MCS maximum extent.

thunderstorm heights of category 1 and 2 MCSs became negligible.

Fig. 47 depicts the results of the composite analysis of the maximum hourly surface divergence. The most striking result from the analysis occurred from hours +2 to +5. For category 2 MCSs, the divergence decreased from 2.25×10^{-5} s^{-1} at hour +2 to 1.00×10^{-5} s^{-1} at hour +5. The opposite occurred for category 1 MCSs. The divergence increased from 2.43×10^{-5} s^{-1} at hour +2 to 3.40×10^{-5} s^{-1} at hour +5. The increasing magnitude of the maximum surface divergence associated with category 1 MCSs, from hours +2 to +5, may be misleading. A possible explanation of the increase, which occurred after MCS maximum extent, is as follows. During this period, the gust front for category 1 MCSs was still well-defined and continued to propagate away from its initial formative location, thus affecting an increasing number of weather stations. Therefore, at hour +5, the surface divergence associated with the gust front/mesohigh was calculated from a greater number of reliable winds, compared to the calculation at hour +2. This could have led to an apparent increase in the magnitude of the surface divergence, as calculated by the McIDAS. Divergence values as large as 10^{-4} s^{-1} have been measured in a mesonetwork of instruments (Ulanski and Garstang, 1978). The most significant result of the composite analysis is that at hour +5, the magnitude of the maximum surface divergence associated with category 1 MCSs was much larger than the magnitude of the maximum surface divergence associated with category 2 MCSs.

Fig. 48 depicts the composite analysis of the sum of the three largest precipitation rates. There was a distinct difference between the precipitation rates of the two categories. With the exception of

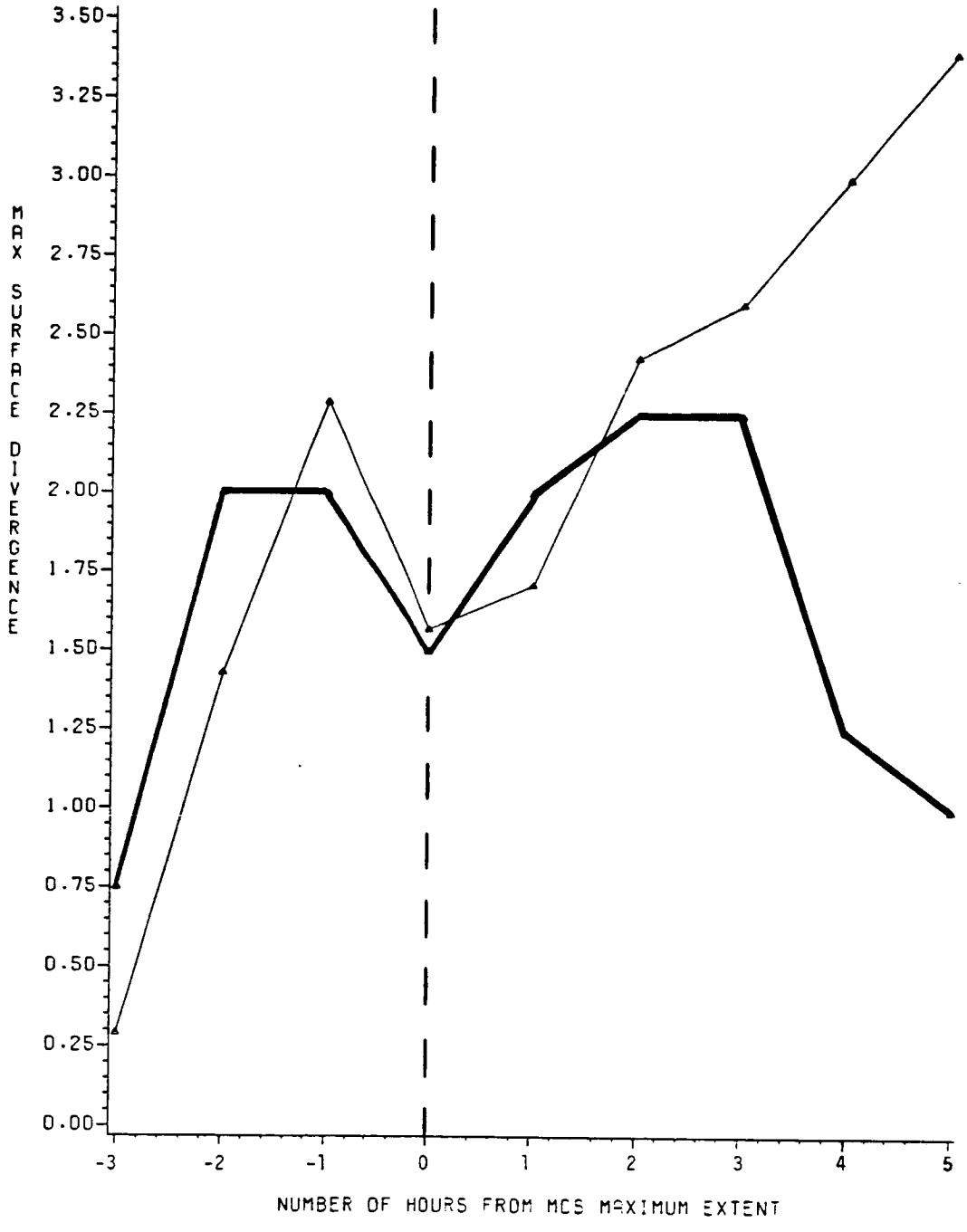

Fig. 47. Composite of the maximum hourly surface divergence of category 1 (thin line) MCSs and category 2 (thick line) MCSs. Minus (-) hours are before MCS maximum extent and plus (+) hours are after MCS maximum extent. Divergence values have units of 10^{-5} s^{-1}.

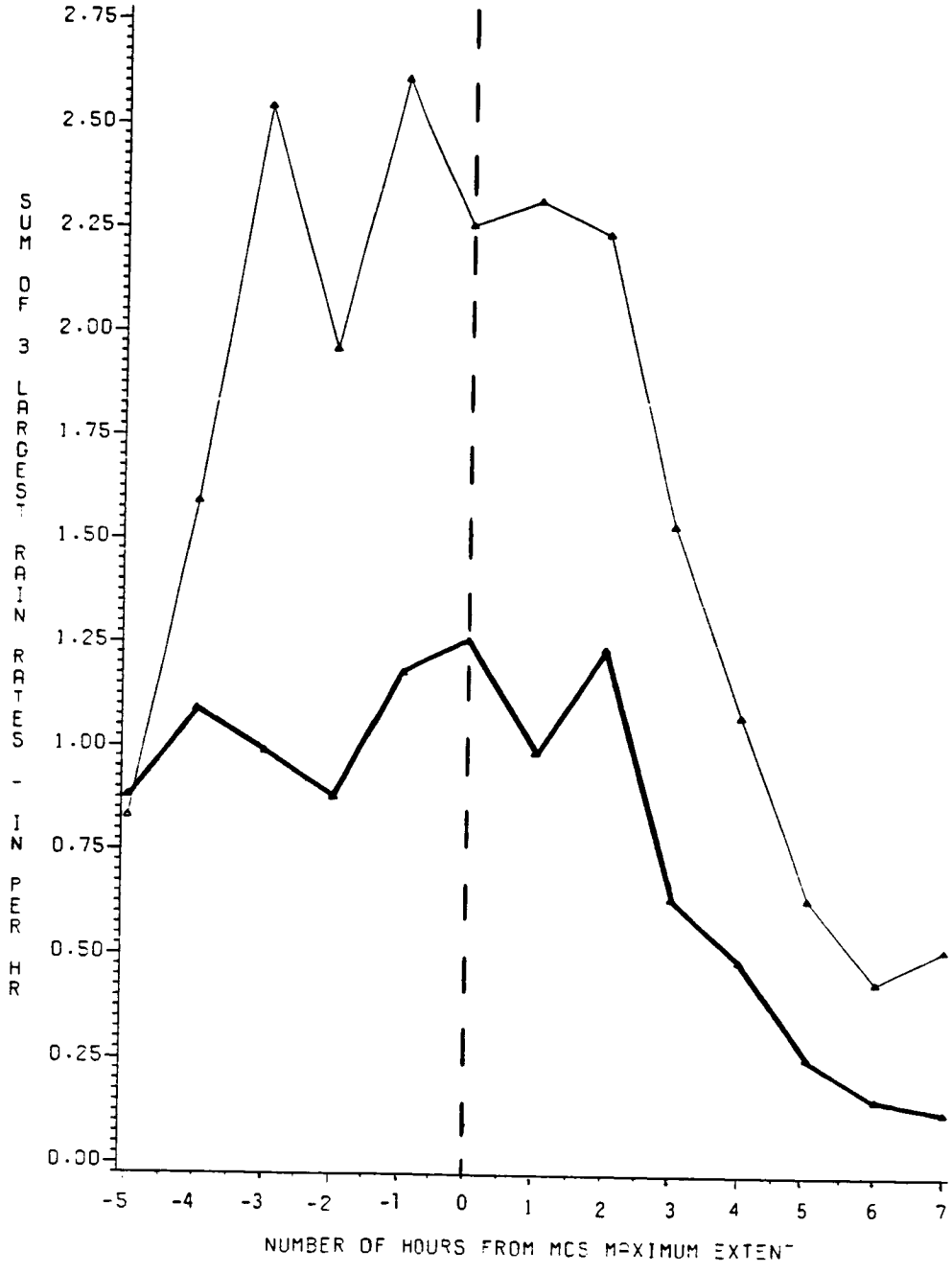

Fig. 48. Composite of the sum of the three largest precipitation rates of category 1 (thin line) MCSs and category 2 (thick line) MCSs. Minus (-) hours are before MCS maximum extent and plus (+) hours are after MCS maximum extent.

hour -5, the sum of the three largest precipitation rates was significantly higher for category 1 MCSs. In fact, in the 8 h of heaviest precipitation, from -4 to +3, the average sum of the three largest precipitation rates of category 1 MCSs was more than double that of category 2 MCSs (2.13 in h^{-1} to 1.03 in h^{-1}). This would imply that category 1 MCSs produced significantly higher rainfall rates, over an area, than the MCSs of category 2.

The intense precipitation associated with category 1 MCSs persisted for a longer period, compared to the heaviest precipitation associated with the MCSs of category 2. The sum of the three largest precipitation rates, produced by the MCSs of Cases 2, 3, 4, 7, 8, 10 and 11 (category 1 MCSs), stayed above 1.5 in h^{-1} for 8, 6, 11, 6, 7, 5 and 5 h, respectively. However, the sum of the three largest precipitation rates, produced by the MCSs of Cases 1, 5, 6 and 9 (category 2 MCSs), stayed above 1.5 in h^{-1} for 1, 1, 3 and 3 h, respectively. Thus, the sum of the three largest precipitation rates stayed above 1.5 in h^{-1} for an average of almost 7 h for category 1 MCSs and only 2 h for category 2 MCSs. Therefore, category 1 MCSs produced more intense precipitation rates over an area, for a longer period, compared to category 2 MCSs.

Fig. 49 shows the results of the composite analysis for the maximum hourly point precipitation rates. This analysis verifies that category 1 MCSs produced, on average, more intense rainfall rates than category 2 MCSs. As seen in Fig. 49, the higher precipitation rates of category 1 MCSs were maintained throughout the entire time period of the composite analysis. In the 8 h of heaviest precipitation, from -4 to +3, the average maximum point precipitation rate of category 1 MCSs was almost

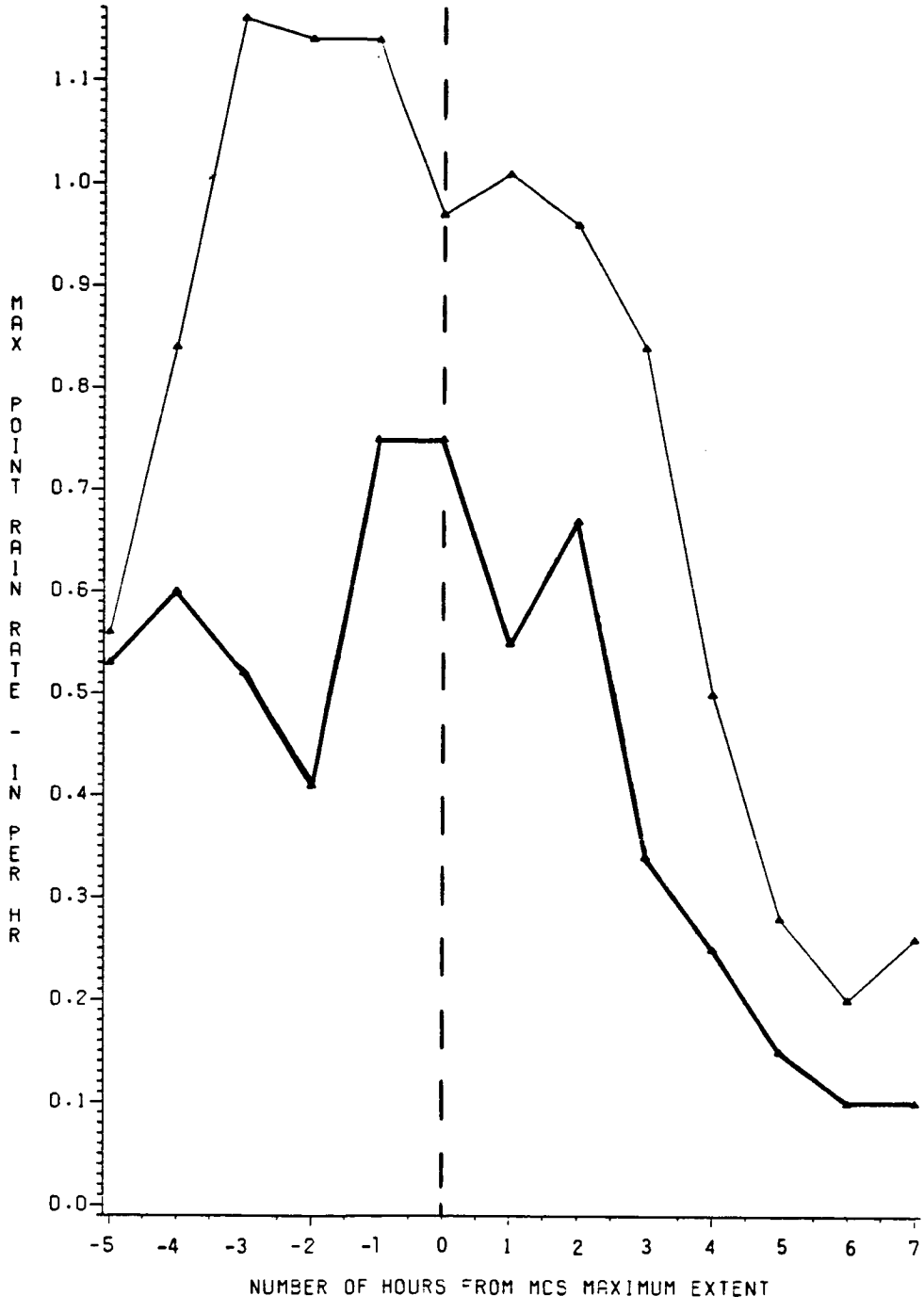

Fig. 49. Composite of the maximum hourly point precipitation rates of category 1 (thin line) MCSs and category 2 (thick line) MCSs. Minus (-) hours are before MCS maximum extent and plus (+) hours are after MCS maximum extent.

double that of category 2 MCSs (1.01 in h^{-1} to 0.57 in h^{-1}).

Fig. 50 represents the results of the composite analysis for the coldest hourly cloud top temperatures. Category 1 MCSs, on average, had colder cloud top temperatures, compared to the MCSs of category 2.

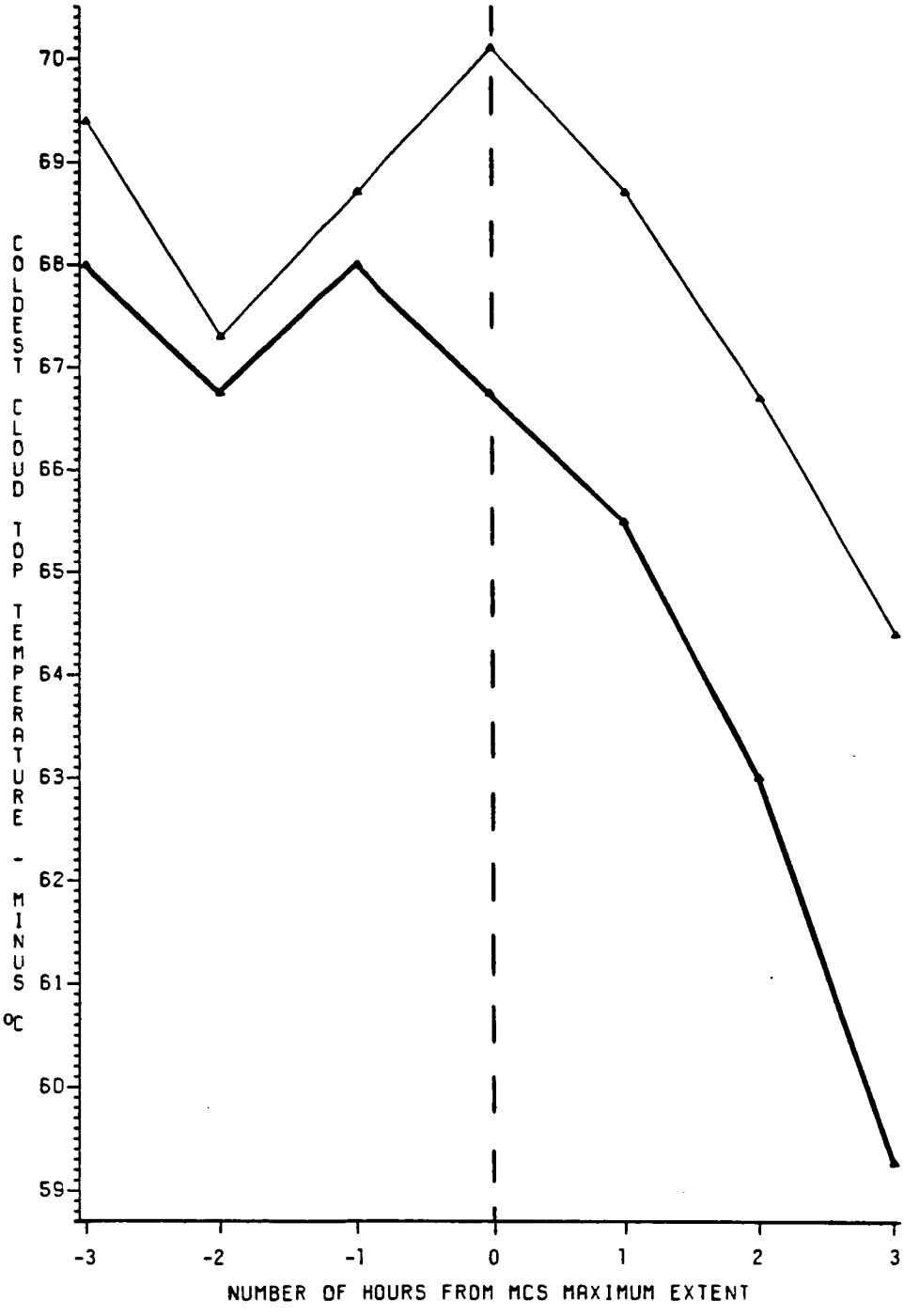

Fig. 50. Composite of the coldest hourly cloud top temperatures for category 1 (thin line) MCSs and category 2 (thick line) MCSs. Minus (-) hours are before MCS maximum extent and plus (+) hours are after MCS maximum extent.

CHAPTER V

SUMMARY

Category 1 and 2 MCSs have significant differences in their characteristics. This contention is supported by the results of the composite analyses. It appears these differences aid in producing stronger, longer-lasting gust fronts in category 1 MCSs. In turn, since all category 1 MCSs produced arc clouds and only one category 2 MCS produced an arc cloud (see Table 14, page 88), the strength and duration of the gust front seems to be an important factor in whether an arc cloud forms.

A summary of the differences in the category 1 and 2 MCSs follows:

1. Category 1 MCSs, on average, produce more intense precipitation rates than category 2 MCSs. In the hours of heaviest precipitation, the average sum of the three largest precipitation rates of category 1 MCSs is more than double that of category 2 MCSs. For this study, this average sum for category 1 and 2 MCSs was 2.13 in h^{-1} to 1.03 in h^{-1}, respectively. During this same period, the average maximum point precipitation rate of category 1 MCSs is nearly double that of category 2 MCSs. For this study, the average maximum point precipitation rate for category 1 and 2 MCSs was 1.01 in h^{-1} to 0.57 in h^{-1}, respectively. Also, the intense precipitation associated with category 1 MCSs persists for a longer period, compared to the heaviest precipitation associated with the MCSs of category 2. For instance, the sum of the three largest precipitation rates stayed above 1.5 in h^{-1} for an average of almost 7 h for category 1 MCSs and only 2 h for category 2 MCSs.

2. The maximum hourly surface divergence, on average, associated

with category 1 MCSs, is stronger than the divergence associated with category 2 MCSs, for the hours +2 to +5.

3. In the hours from -2 to -6, the critical hours for gust front formation, category 1 MCSs, on average, have higher maximum thunderstorm heights than category 2 MCSs, as determined at 35 min past each hour. During this period, the average maximum thunderstorm heights for category 1 and 2 MCSs are 55,000 and 51,000 ft, respectively.

4. The coldest hourly cloud top temperatures of category 1 MCSs, on average, are colder than those in category 2.

The gust front, on average, formed approximately 1.5 h prior to the MCS maximum extent, as determined from Table 14. Using this information, coupled with the results shown in Fig. 46-50, for category 1 MCSs, the following becomes apparent:

1. The gust front, on average, forms approximately 2 h after the maximum thunderstorm heights are reached (see Fig. 46).

2. The time of formation of the gust front corresponds to the period of maximum precipitation intensity (see Figs. 48-49).

3. The formation of the gust front takes place during a period of increasing magnitude of the surface divergence (see Fig. 47). The increasing surface divergence corresponds to the period of maximum precipitation intensity (see Figs. 48-49). This correlation (see Fig. 1) agrees with the findings of Byers and Braham (1949).

4. The formation of the gust front corresponds to a decrease in the coldest cloud top temperatures (see Fig. 50).

The arc cloud, on average, formed approximately 4 h after MCS maximum extent, as determined from Table 14. As mentioned earlier, the

appearance of the arc cloud was determined, in most cases, by inspection of the visible satellite images. Undoubtedly, some of the arc clouds formed during the period when only IR satellite images were available. During this period the arc cloud would be undetectable, in most cases, because arc clouds normally consist of low, warm clouds. Taking this into account, the arc cloud, on average, probably formed approximately 3 h after MCS maximum extent. Using this information, coupled with the results shown in Figs. 46-50, for category 1 MCSs, the following becomes apparent:

1. The arc cloud forms during a period of rapidly falling thunderstorm heights (see Fig. 46).

2. The arc cloud forms as the precipitation intensity dramatically lowers (see Figs. 48-49).

3. The arc cloud forms during a period when the magnitude of the maximum surface divergence remains large (see Fig. 47).

4. The arc cloud forms during a period of rapid warming of the cloud top temperatures (see Fig. 50).

Using the radar summary charts from the NWS, a composite analysis of the maximum hourly radar reflectivity intensity for category 1 and 2 MCSs was accomplished. The determination of intensity was done by an intensity processor known as the Digital Video Integrator and Processor (D/VIP). Contours on the radar summary charts correspond to the 1, 3 and 5 D/VIP levels. D/VIP level 1 corresponds to "light" precipitation, D/VIP level 3 corresponds to "heavy" precipitation and D/VIP level 5 corresponds to "intense" precipitation (U.S. Department of Commerce, 1980). This analysis was done because the results could be used by

operational meteorologists, since this information is readily available.

Fig. 51 depicts the results of the composite analysis of the maximum hourly radar reflectivity intensity. From hours -5 to -2, both category 1 and 2 MCSs produced D/VIP level 5 radar reflectivities. However, from hours -2 to +1, the maximum reflectivities produced by category 2 MCSs dropped below D/VIP level 4, on average, while category 1 MCSs maintained D/VIP level 5.

Using the above information, the following criteria are given as guidance, to the operational meteorologist, in forecasting the occurrence of gust fronts and arc clouds:

1. The gust front, on average, forms approximately 1.5 h before maximum extent of the MCS.

2. If the gust front persists for more than 6 h, it is likely an arc cloud will form. The arc cloud, on average, forms approximately 3 h after maximum extent of the MCS.

3. The arc cloud forms while the thunderstorm heights are rapidly falling.

4. The arc cloud forms while the coldest cloud top temperatures are rapidly warming.

5. Lastly, it seems likely that an arc cloud will form if the maximum D/VIP level remains at level 5 through hour +1 (1 h after MCS maximum extent). Caution should be used when using this criterion alone, as the MCS of Case 1, which did not produce an arc cloud, produced D/VIP level 5 reflectivities through hour +3. However, using this criterion with the other guidelines, should prove more useful. For example, even though the MCS of Case 1 produced D/VIP level 5

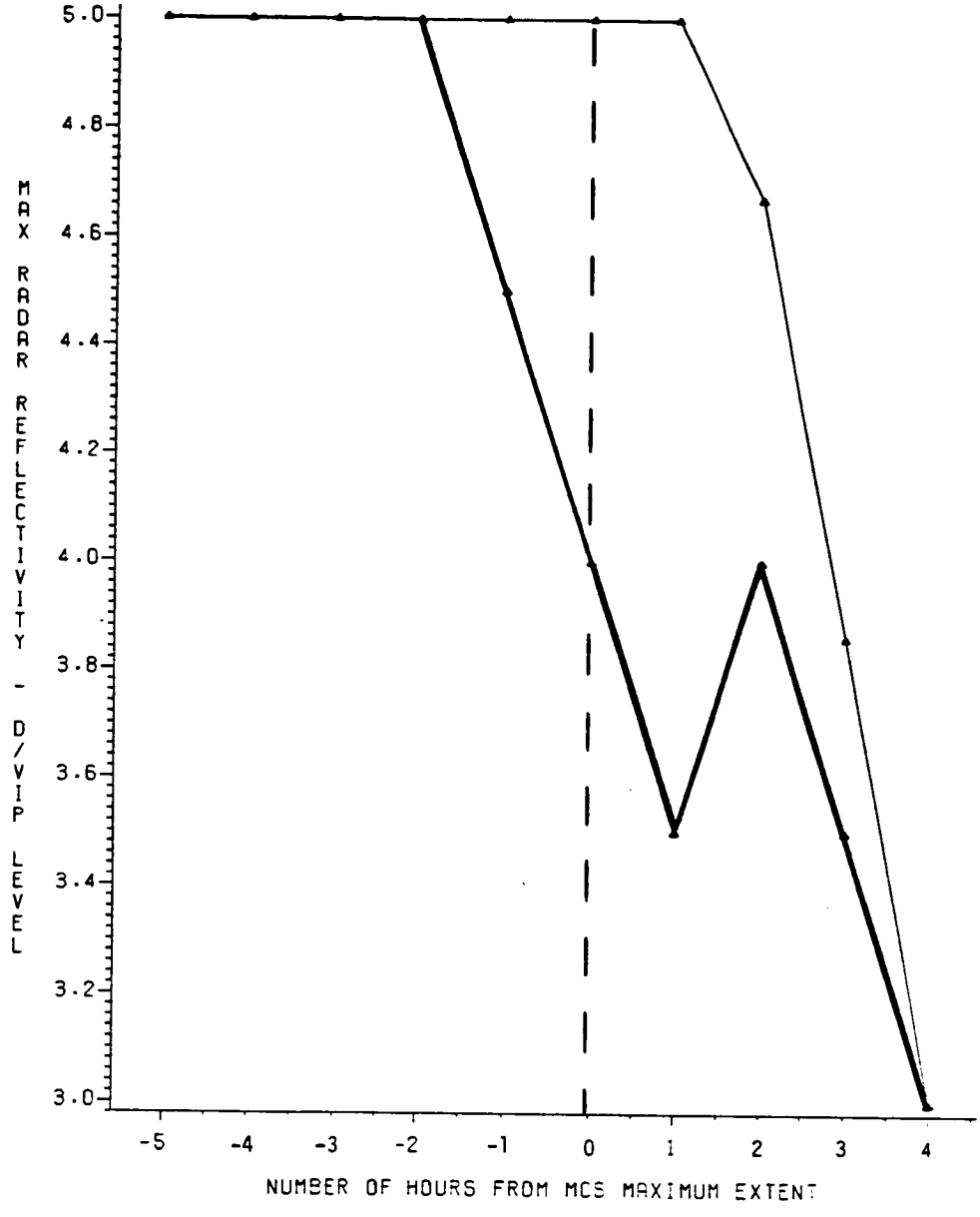

Fig. 51. Composite of the maximum hourly radar reflectivity intensity of category 1 (thin line) MCSs and category 2 (thick line) MCSs. Minus (-) hours are before MCS maximum extent and plus (+) hours are after MCS maximum extent.

reflectivities through hour +3, the gust front only lasted for 5 h, therefore, it is unlikely an arc cloud will form.

REFERENCES

Barnes, S. L., 1973: Mesoscale objective map analysis using weighted time-series observations. NOAA Tech. Memo. ERL NSSL-62, NTIS COM-73-10781, 60 pp.

Bartels, D. L., 1983: Internal structure and evolution of a dual mesoscale convective complex. Preprints, 5th Conf. on Hydrometeorology, Tulsa, OK, Amer. Meteor. Soc., 97-102.

Belville, J. D., and N. O. Stewart, 1983: Extreme rainfall events in Louisiana: The "New Orleans Type." Preprints, 5th Conf. on Hydrometeorology, Tulsa, OK, Amer. Meteor. Soc., 284-290.

Brundidge, K. C., 1983: Investigation of the arc cloud complex. Research Reports - 1983 NASA/ASEE Summer Faculty Fellowship Program, George C. Marshall Space Flight Center, Huntsville, AL, 23 pp.

_____, 1984: Precipitation factors leading to arc cloud formation. NASA Proposal, Texas A&M University, College Station, TX, 14 pp.

Byers, H. R., and R. R. Braham, Jr., 1948: Thunderstorm structure and circulation. J. Meteor., 5, 71-86.

_____, and _____, 1949: The Thunderstorm. U.S. Dept. of Commerce, Weather Bureau, Washington, D. C., 282 pp.

Fritsch, J. M., R. A. Maddox and A. B. Barnston, 1981: The character of mesoscale convective complex precipitation and its contribution to warm season rainfall in the U.S. Preprints, 4th Conf. on Hydrometeorology, Reno, NV, Amer. Meteor. Soc., 94-99.

Fujita, T., 1955: Result of detailed synoptic studies of squall lines. Tellus, 7, 405-436.

_____, 1959: Precipitation and cold air production in mesoscale thunderstorm systems. J. Meteor., 16, 454-466.

_____, 1963: Analytical mesometeorology: A review. Meteor. Monogr., 5, 77-122.

Gagin, A., D. Rosenfeld and R. E. Lopez, 1985: The relationship between height and precipitation characteristics of summertime convection cells in south Florida. J. Atmos. Sci., 42, 84-94.

Goff, R. C., 1976: Vertical structure of thunderstorm outflows. Mon. Wea. Rev., 104, 1429-1440.

Greene, G. E., 1977: Wind shear characterization. U.S. Fed. Aviation Admin., Washington, D.C., Report No. FAA-RD-77-33, 120 pp.

Howard, K., and R. A. Maddox, 1983: Precipitation characteristics of two mesoscale convective systems. Preprints, 5th Conf. on Hydrometeorology, Tulsa, OK, Amer. Meteor. Soc.

Leary, C. A., and E. N. Rappaport, 1982: Internal structure of a mesoscale convective complex. Preprints, 21st Conf. Radar Meteor., Edmonton, Alberta, Canada, Amer. Meteor. Soc., 70-77.

Maddox, R. A., 1980: Mesoscale convective complexes. Bull. Amer. Soc., 61, 1374-1387.

_____, 1981: The structure and lifecycle of midlatitude mesoscale convective complexes. Ph.D. dissertaion, Colorado State University, 171 pp.

_____, 1982: Forecasting mesoscale convective complexes over the central United States. Preprints, 12th Conf. Severe Local Storms, San Antonio, TX, Amer. Meteor. Soc., 180-183.

_____, 1983: Large-scale meteorological conditions associated with midlatitude, mesoscale convective complexes. Mon. Wea. Rev., 111, 1475-1493.

_____, D. M. Rodgers and K. W. Howard, 1982: Mesoscale convective complexes over the United States during 1981. Mon. Wea. Rev., 110, 1501-1514.

Miller, R. C., 1972: Notes on Analysis and Severe-Storm Forecasting Procedures of the Air Force Global Weather Service, Tech. Rep. 200 (Rev.), Air Weather Service, Scott Air Force Base, IL, 190 pp.

Miller, R. L., 1984: The arc cloud complex: A case study. Masters Thesis, Texas A&M Univ., College Station, TX, 101 pp.

Orlanski, I., 1975: A rational subdivision of scales of atmospheric processes. Bull. Amer. Meteor. Soc., 56, 527-530.

Purdom, J. F. W., 1973: Picture of the month: Mesohigh and satellite imagery. Mon. Wea. Rev., 101, 180-181.

_____, 1974: Satellite imagery applied to the mesoscale surface analysis and forecast. Preprints, 5th Conf. Weather Forecasting and Analysis, St. Louis, MO, Amer. Meteor. Soc., 63-68.

_____, 1976: Some uses of high-resolution GOES imagery in the mesoscale forecasting of convection and its behavior. Mon. Wea. Rev., 104, 1474-1483.

Purdom, J. F. W., 1979: The development and evolution of deep convection. Preprints, 11th Conf. Severe Local Storms, Kansas City, MO, Amer. Meteor. Soc., 143-150.

Rodgers, D. M., K. W. Howard and E. C. Johnston, 1983: Mesoscale convective complexes over the United States during 1982. Mon. Wea. Rev., 111, 2363-2369.

_____, M. J. Magnano and J. H. Arns, 1985: Mesoscale convective complexes over the United States during 1983.. Mon. Wea. Rev., 113, 888-901.

Schnapf, A., 1982: The development of the TIROS global environmental satellite system. NASA Conf. Pub. 2227, Meteorological Satellites-Past, Present, and Future, 20th Aerospace Sciences Meeting, AIAA, Orlando, FL, Jan., 1982, 7-16.

Sinclair, P. C., and J. F. W. Purdom, 1982: Integration of research aircraft data and 3 minute interval GOES data to study the genesis and development of deep convective storms. Preprints, 12th Conf. Severe Local Storms, San Antonio, TX, Amer. Meteor. Soc., 269-271.

_____, and _____, 1984: Aircraft penetrations of arc cloud lines. Preprints, Satellite Meteorology/Remote Sensing and Applications, Clearwater Beach, FL, Amer. Meteor. Soc., 160-163.

Tepper, M., 1950a: A proposed mechanism of squall lines: The pressure jump line. J. Meteor., 7, 21-29.

_____, 1950b: On the origins of tornadoes. Bull. Amer. Meteor. Soc., 31, 311-314.

Ulanski, S. L., and M. Garstang, 1978: The role of surface divergence and vorticity in the life cycle of convective rainfall. Part I: Observation and analysis. J. Atmos. Sci., 35, 1047-1062.

U. S. Department of Commerce, 1980: National Weather Service Radar Code User's Guide, NOAA, National Weather Service publication, Silver Spring, Maryland, 179 pp.

Wetzel, P. J., W. R. Cotton and R. L. McAnelly, 1983: A long-lived mesoscale convective complex. Part I: The mountain generated component. Mon. Wea. Rev., 111, 1893-1918.

Woodley, W. L., B. Sancho and A. H. Miller, 1972: Rainfall Estimation from Satellite Cloud Photographs. NOAA Tech. Memo. ERL OD-11, 43 pp.

Zipser, E. J., 1969: The role of organized unsaturated convective downdrafts in the structure and rapid decay of an equitorial disturbance. J. Appl. Meteor., 8, 799-814.

CONVECTIVE CELL DEVELOPMENT AND PROPAGATION IN A MESOSCALE CONVECTIVE COMPLEX

Yoo-Shin Ahn

and

Kenneth C. Brundidge

Texas A & M University

College Station, Texas

Prepared for George C. Marshall Space Flight Center

under Contract NAG 8-043

ABSTRACT

A case study was made of the mesoscale convective complex (MCC) which occurred over southern Oklahoma and northern Texas on 27 May 1981. This storm moved in an eastsoutheasterly direction and during much of its lifetime was observable by radars at Oklahoma City, OK. and Stephenville, TX. It was found that the direction of cell (VIP level 3 or more reflectivity) propagation was somewhat erratic but approximately the same as the system (VIP level 1 reflectivity) movement and the ambient wind. New cells developed along and behind the gust front making it appear that once the MCC is initiated, a synergistic relationship exists between the gust front and the MCC. The relationship between rainfall patterns and amounts and the infrared (IR) temperature field in the satellite imagery were examined. The 210°K isotherm of GOES IR imagery was found to encompass the rain area of the storm. The heaviest rainfall was in the vicinity of the VIP level 3 cells and mostly contained within the 205°K isotherm of GOES IR imagery.

ACKNOWLEDGEMENTS

The authors are grateful the support for this work provided by the George C. Marshall Space Flight Center under Grant NAG. 8-043.

TABLE OF CONTENTS

LIST OF TABLES

LIST OF FIGURES

I.INTRODUCTION

For many years, meteorologists had believed that thunderstorms occurred in two basic forms: air mass storms represented by isolated cells and squall lines involving many cells organized into a line However, as pointed out by Purdom (1979), the advent of the Geostationary Operational Environmental Satellite (GOES) has enabled meteorologists generally to see a variety of atmospheric events not distinguishable by ordinary synoptic observations. In particular, a third mode of thunderstorm activity has been recently discovered. It has been found that many summertime storms are organized aggregations of thunderstorm cells which Maddox (1980b) has called mesoscale convective complexes (MCCs).

Through examination of satellite imagery it has been found that thirty or more MCCs may occur in the United States during the months March through September (Maddox, 1980b; Maddox et al., 1982; Merritt and Fritsch, 1984; Rodgers et al., 1983; Rodgers et al., 1985). These systems may produce severe weather such as hail, tornadoes, damaging winds and flash flooding (Bosart and Sanders, 1981); however, they also have been found to be the main source of summertime rainfall over the crop lands of the mid-west (Fritsch et al., 1981).

MCCs have a distinctive appearance in satellite imagery. They appear as a nearly circular mass of cloud covering an area of 100,000 km^2 or more and at a temperature less than or equal to $-32^{\circ}C$. The complete definition of an MCC is presented in Table 1. Whereas they may start in

the afternoon or evening MCCs primarily are nocturnal systems which reach maximum intensity sometime after midnight and may not dissipate until after sunrise (Maddox, 1980a). Frequently during the dissipating stage, the MCC produces an arc cloud (Purdom, 1973, 1976; Gurka, 1976) which moves outward from the MCC and may play a role in new storm development the following day.

The problem of understanding the movement and internal dynamics of thunderstorms and thunderstorm systems has been the subject of much research of the years Byers and Braham (1949) found that small radar echoes moved with the cloud layer-mean wind. However, Zehr and Purdom (1982) did not find this wind to be a reliable indicator of storm motion. Newton and Fankhauser (1975) stuied storm motion as related to storm size They found that small- to medium-sized storms generally move to the left of the mean vector wind in the troposphere while large storms with diameters of about 20-30 km generally move to the right of the mean wind.

Observational studies which have been made of multi-cell systems (Fujita and Brown, 1958; Heymsfield and Schotz, 1985; Marwitz, 1972) have shown that such systems simultaneously move and maintain themselves by a process called "discrete propagation". In this process, new cells develop on the right flank of the storm area and move toward the left flank where they dissipate. This produces a complex of cells which as a whole moves to the right of the individual cell motion. Figure 1 shows three distinct propagation models as described by Marwitz (1972) for three different multi-cell storm systems. In Fig. 1a, the individual

TABLE 1. Mesoscale Convective Complex (MCC) definition. The definition is based upon analysis of enhanced IR satellite imagery (after Maddox, 1980b).

Physical Characteristics	
Size:	A: Cloud shield with IR temperature $\leq -32°C$ must have an area $\geq 100{,}000$ km^2 B Interior cold cloud region with temperature $\leq -52°C$ must have an area $\geq 50{,}000$ km^2
Initiate:	Size definitions A and B are first satisfied
Duration:	Size definitions A and B must be met for a period ≥ 6 h
Maximum extent:	Contiguous cold cloud shield (IR temperature $\leq -32°C$) reaches maximum size
Shape:	Eccentricity (minor axis/major axis) ≥ 0.7 at time of maximum extent
Terminate:	Size definitions A and B are no longer satisfied

whole cells, represented by ovals, propagate continuously in the direction of the mean wind coupled with discrete propagation to the right of the mean wind. The cells in Fig. 1b propagate both continuously and discretely to the right of the mean wind, which provides a large angular departure of storm motion from the mean wind. The third possibility in Fig. 1c is one in which continuous propagation is to the left of the mean wind but the offsetting discrete propagation to the right results in overall storm motion in the same direction as the mean wind. Numerical simulation studies such as those by Miller (1978) and Wilhelmson and Chen (1982) also show the tendency for discrete propagation to control storm motion. As pointed out by Wilhelmson and Chen, how the individual cells move relative to the mean vector wind in the cloud layer bears on the rate at which moisture can be supplied to them for continued growth.

The studies of multi-cell systems cited above did not involve the use of satellite imagery. Therefore, it is not clear to what extent the results may be applicable to MCCs which, as noted before are defined on the basis of satellite imagery using criteria developed by Maddox (1980b). MCCs are large enough in scale to generally encompass several observing sites at any given time; however, the internal processes are sub-synoptic and therefore not easily determined It is safe to say that these processes are poorly understood. Several questions may be asked:

a. How are MCCs maintained during the nighttime hours when no surface heating is occurring to destabilize the boundary layer?

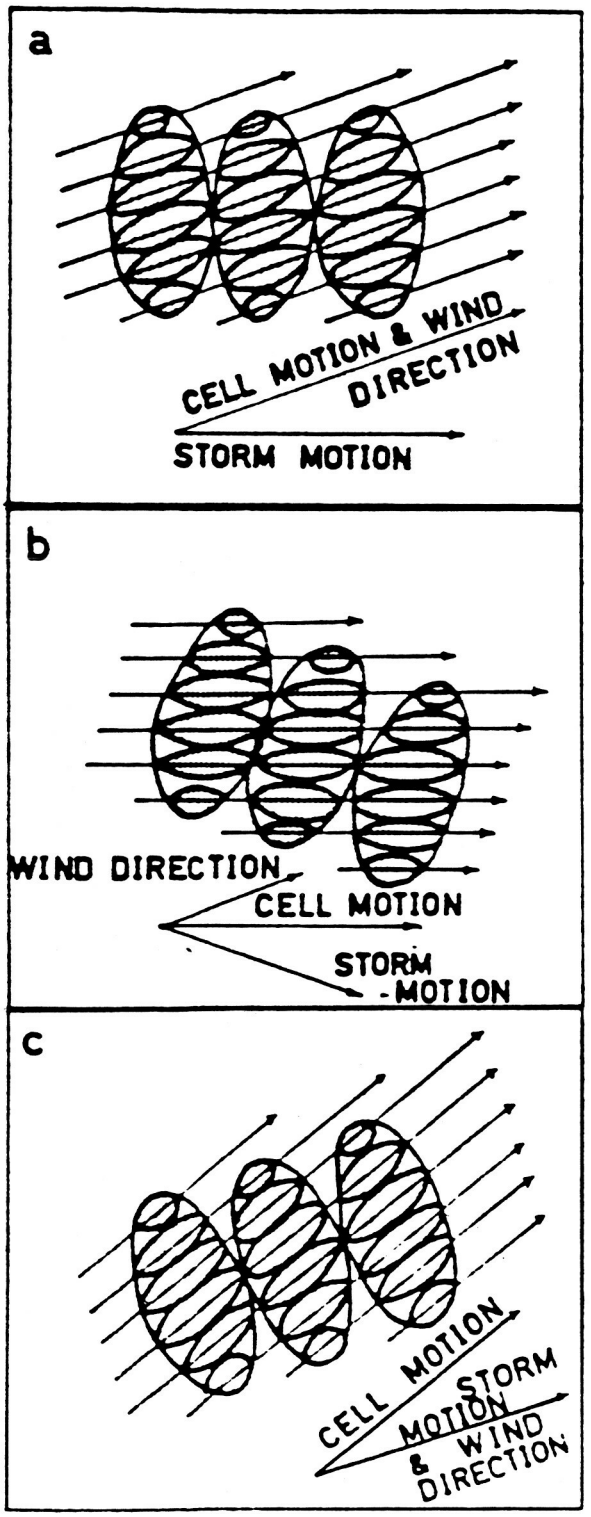

Fig. 1. Schematic models of multi-cell storm propagation (from Marwitz, 1972).

b. Do new cells develop on the interior of an MCC in a random fashion at the intersections of outflow boundaries, as occurs with air mass storms? Or is cell development related to the meso-β scale outflow boundary of the system as a whole?

c. How do the movement of individual cells and the movement of the system as a whole relate to one another and to the mean cloud-layer wind?

At present, answers to these questions can only be inferred from inadequate observations. Maddox and Howard (1983) have urged the use of satellite imagery and radar observations in combination to obtain a better understanding of the precipitation structure of middle-latitude mesosystems, to improve understanding of the life cycle of MCCs as an aid to forecasting them, and to provide better estimates of rainfall patterns and amounts based on cloud-top IR temperature structure The study described here was this approach to focus on the problem areas described above in a case study of the MCC which occurred over southern Oklahoma and northern Texas on 27 May 1981. This storm moved in a southeasterly direction and during much of its lifetime was observed simultaneously by radars at Oklahoma City (OKC), OK. and Stephenville (SEP), TX.

II. RESEARCH PROCEDURES

The data used and the procedures followed in this study are as follows.

a Radar films for 27 May 1981 for the OKC and SEP radar sites were obtained from the National Climatic Data Center, Asheville, North Carolina. These films, with frames at one minute intervals, were examined to determine the history of cell development and movement. For this purpose a "cell" was defined to be a reflectivity region at a Video Integrator Processor (VIP) level of 3 or more. The system as a whole was defined as all the area enclosed by the VIP level 1 reflectivity value. The relationships between the manually digitized radar (MDR) code, which is used for the hourly radar summary maps provided by the National Weather Service (NWS), VIP levels, and storm intensity levels are shown in Table 2

b. The rawinsonde soundings at OKC and SEP at 1200 GMT were used to determine the mean wind structure during the mature stages the storm.

c The records of hourly precipitation from the climatological networks of raingauges were obtained from the National Climatic Data Center. Figures 2 and 3 show the locations of the recording raingauges in Texas and Oklahoma, respectively. These data were plotted and analyzed on the state maps.

d. Sectional surface maps corresponding to the time and location of the MCC were plotted and analyzed. Microbarograph traces and Weather

TABLE 2. Description of Manually Digitized Radar (MDR) Code (After Foster and Reap 1973).

Code No.	Maximum Observed VIP Values	Coverage In Box	Maximum Rainfall Rate (in./hr.)	Intensity Category
0	No Echoes			
1	1	Any Vip 1	.1	Weak
2	2	$\leq$ 50% of VIP 2	.1- .5	Moderate
3	2	> 50% of VIP 2	.5-1.0	Moderate
4	3	$\leq$ 50% of VIP 3	1.0-2.0	Strong
5	3	> 50% of VIP 3	1.0-2.0	Strong
6	4	$\leq$ 50% of VIP 3 and 4	1.0-2.0	Very Strong
7	4	> 50% of VIP 3 and 4	1.0-2.0	Very Strong
8	5 or 6	$\leq$ 50% of VIP 3,4,5, and 6	2.0	Intense or Extreme
9	5 or 6	> 50% of VIP 3,4,5, and 6	2.0	Intense or Extreme

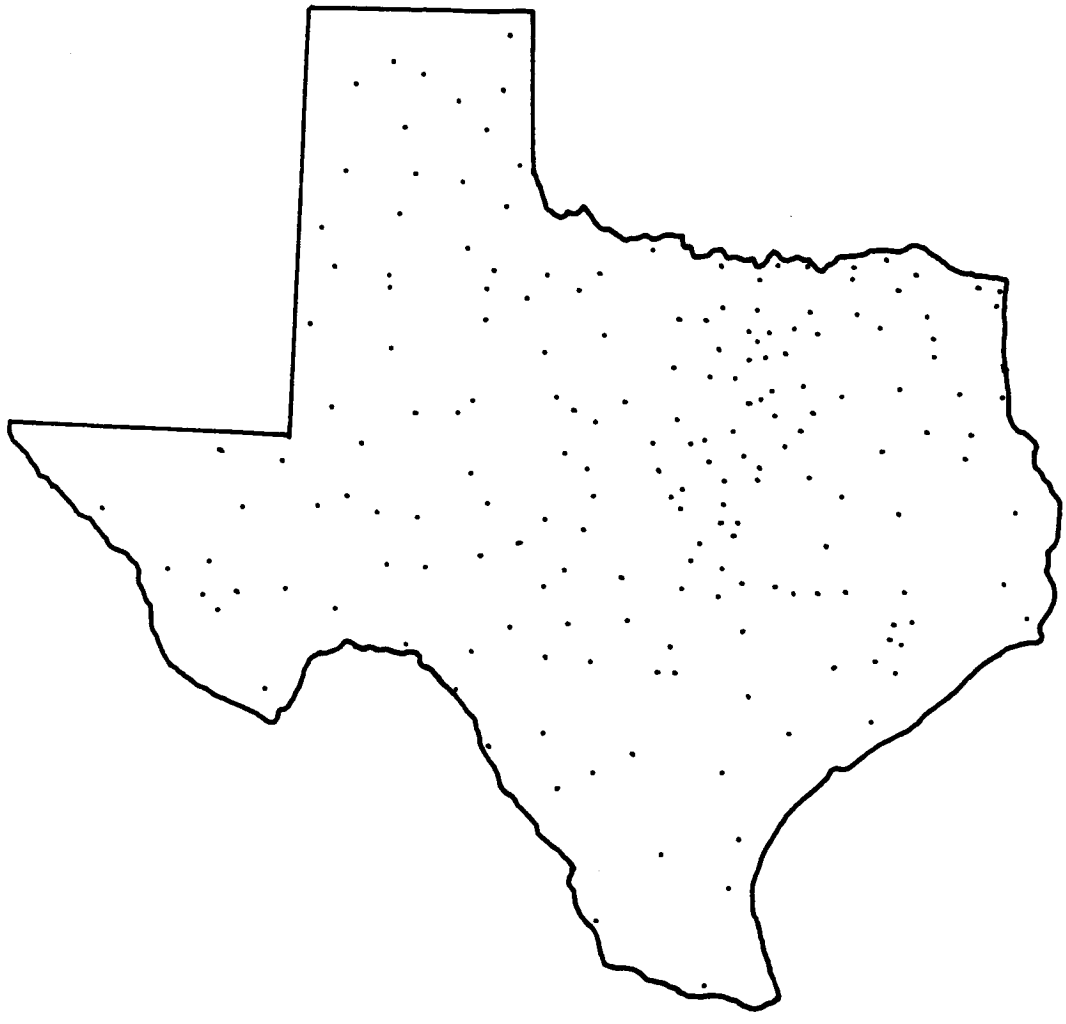

Fig. 2. The climatological network of rainguages in Texas.

Fig. 3. The climatological network of rainguages in Oklahoma.

Bureau/Army/Navy (WBAN) records from stations in Oklahoma and northern Texas obtained from the National Climatic Data Center were utilized in this analysis. Gust front position and propagation were more accurately determined with this information and related to radar echo structure and precipitation patterns.

e. The Man-Computer Interactive Data Access System (McIDAS) of the Atmospheric Sciences Division of the Systems Dynamic Laboratory, National Aeronautics and Space Administration Marshall Space Flight Center, was used to obtain hourly, contoured analyses of the cloud top temperature as determined from the GOES IR imagery. This information was combined with the raingauge data.

III. SYNOPTIC CONDITIONS AND STORM HISTORY

The MCC of 27 May 1981 started with isolated thunderstorms over the Texas and Oklahoma panhandles on the afternoon of 26 May. These storms grew in size and intensity and amalgamated. During the evening of the 26th (0100 to 0340 GMT, 27 May) there were two reports of funnel clouds and four reports of tornadoes preceeded by golfball-sized hail associated with this storm. These reports came from Briscoe, Motley and Cottle Counties in northwestern Texas very near the Oklahoma border.

Shortly before midnight (0515 GMT, 27 May 1981) the storm system met the criteria for an MCC stated in Table 1. By this time the center of the storm lay roughly on the Red River between OKC and SEP. The maximum extent of the MCC, defined in terms of the area enclosed by the 210 K isotherm depicted in the IR satellite imagery was reached at 1000 GMT on 27 May Reports of hail came from the northern Texas Archer and Tarrant Counties at 0900 GMT and 1055 GMT, respectively. A windstorm was reported in Fannin County at 0935 GMT.

The termination of the storm as an MCC came at 1400 GMT in the northeastern corner of Texas; however, the system continued to produce precipitation until 1600 GMT.

Figures 4 and 5 show the 70 kPa and 50 kPa analyses for 0000 GMT, 27 May 1981. There is evidence, particularly at 70 kPa of a weak, short-wave trough moving through the long-wave ridge over the area in which the MCC developed. Gurka (1976) found that many summertime, mesoscale systems producing gust fronts observable as arc clouds in

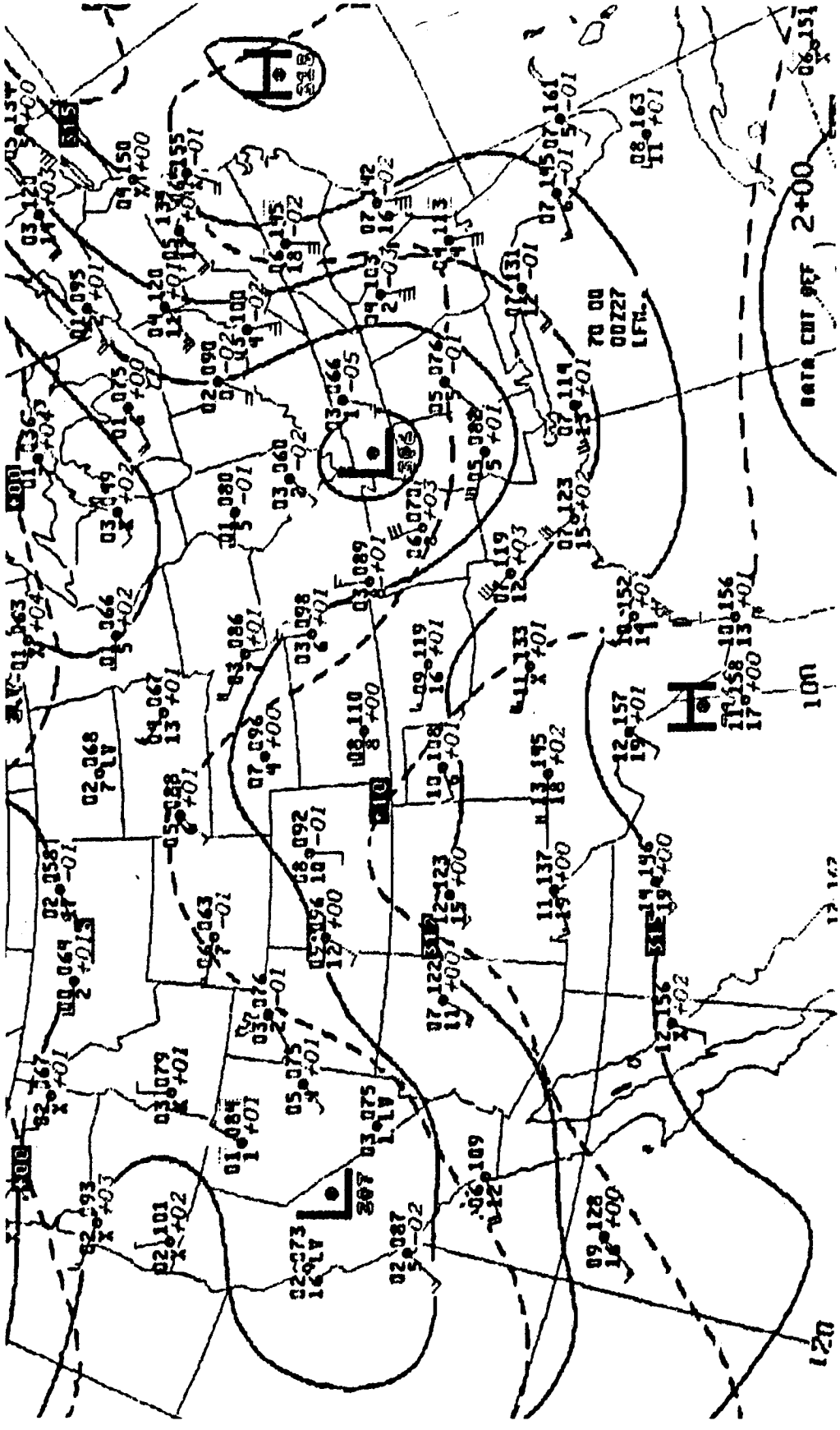

Fig. 4. Synoptic analysis at 70 kPa for 0000 GMT, 27 May 1981. Geopotential height lines are solid, isotherms are dashed.

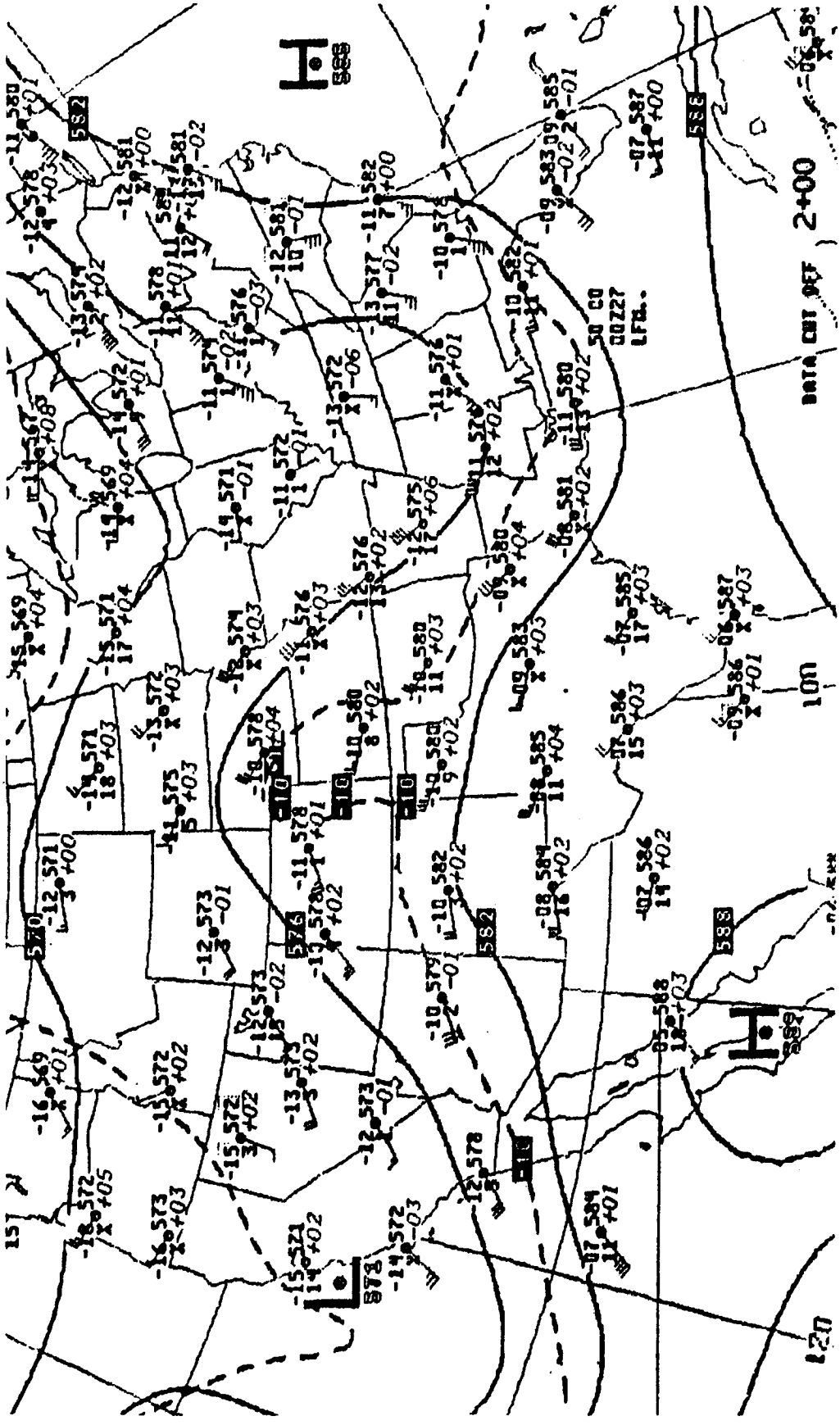

Fig. 5. Synoptic analysis at 50 kPa for 0000 GMT, 27 May 1981. Isolines as described in Fig. 4.

satellite imagery formed in short-wave troughs imbedded in northwesterly flow aloft. The low level warm advection indicated in Fig. 4 may have contributed to the initiation of the MCC. A mesoscale warm pocket is also seen over the area in the 50 kPa analysis.

At 0600 GMT, a mesohigh and strong gust front first appeared in the surface pressure analysis. The gust front, which will be examined later, was located across the Oklahoma/Texas border and was moving southeastward. As it passed Dallas (DAL), TX., a peak wind of 45 kt was one of the indicators that the gust front was quite powerful. Even near termination of the MCC, at 1400 GMT, a strong mesohigh and gust front were still evident in the surface pressure analysis (see Fig 6).

The GOES visible image for 1500 GMT is shown in Fig. 7. Only wide-spread layer-cloud precipitation was occurring at this time. The arc cloud produced by this MCC can be seen in Fig. 7 to be approaching the Gulf Coast of eastern Texas. The arc cloud finally vanished from the satellite images after 1800 GMT.

Other characteristics of this MCC as determined by Welshinger (1985) are shown in Table 3.

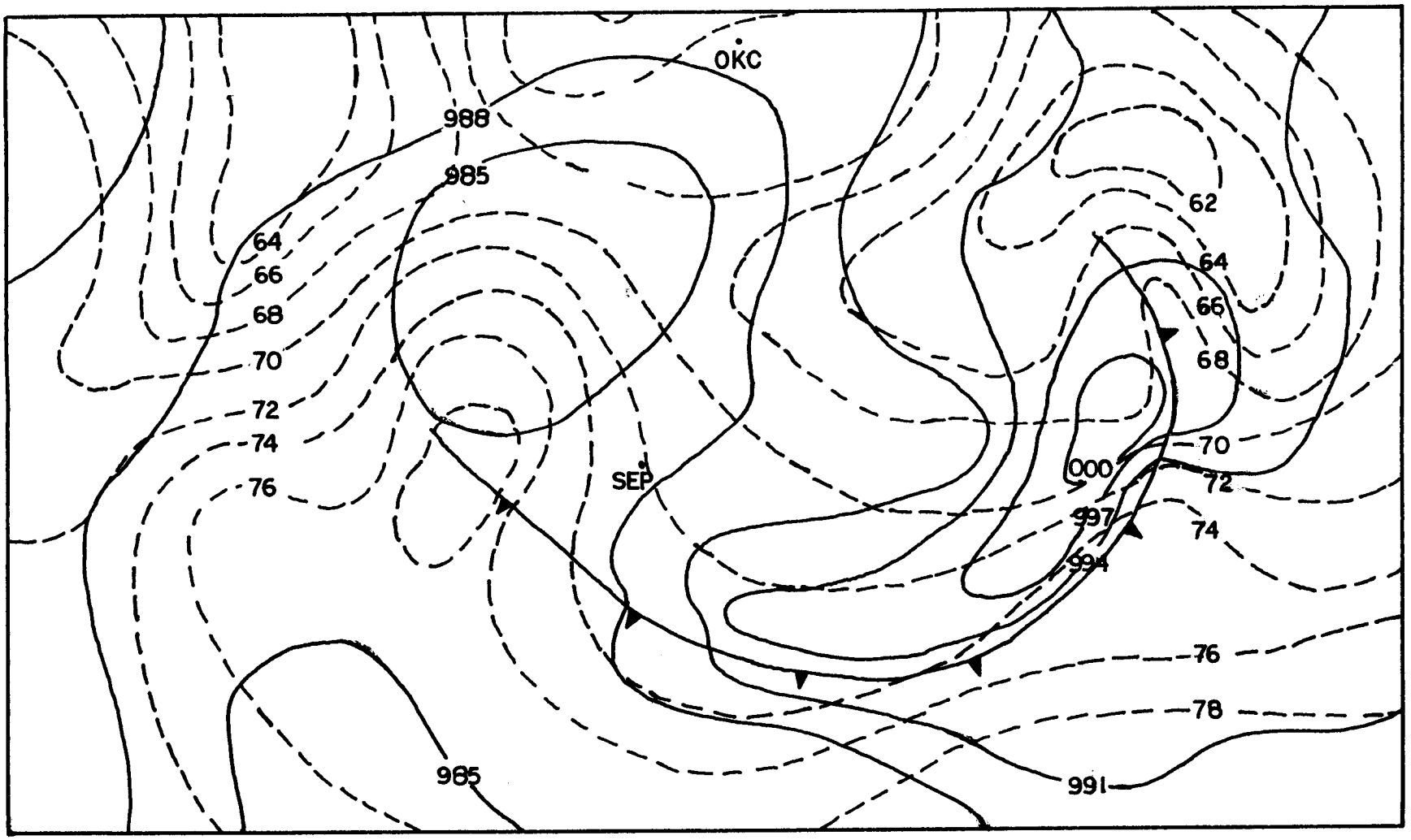

Fig. 6. Surface synoptic analysis at 1400 GMT, 27 May 1981. Pressure contuors are altimeter setting values at 0.03 in Hg increments, isotherms are dashed. The gust front is denoted by cold front symbols.

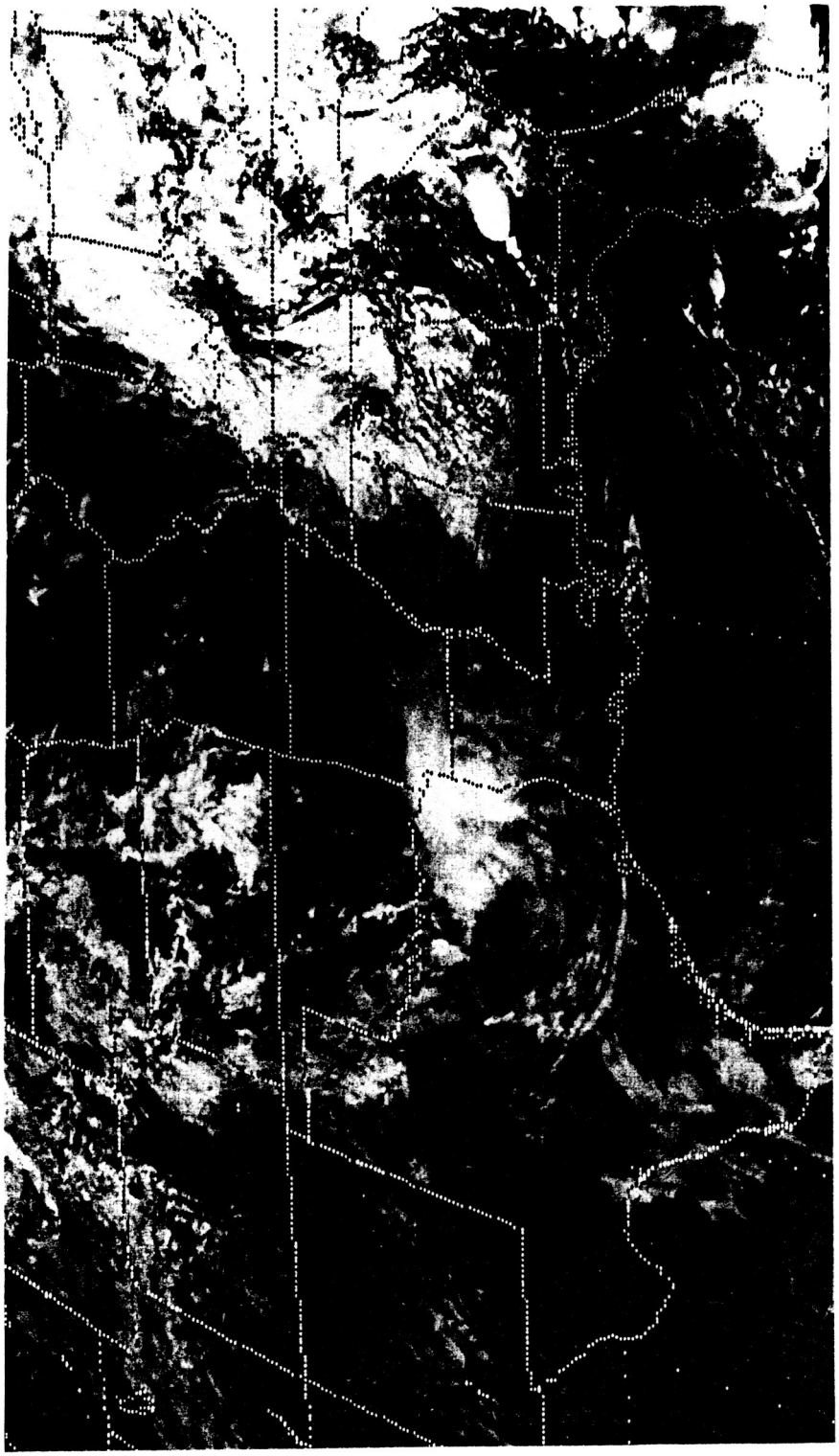

Fig. 7. GOES visible image for 1500 GMT 27 May 1981.

TABLE 3. Characteristics associated with the MCC of 27 May 1981. The maximum thunderstorm heights were determined at approximately 35 min past each hour. Dashes indicate that the parameter was not determined (Welshinger, 1985).

Time (GMT)	Maximum thunderstorm height (x 100 ft)	Maximum surface divergence (x 10^{-5} s)	Sum of the three largest precipitation rates (in/h)	Maximum point precipitation rate (in/h)	Coldest cloud top temperature (°C)
0400	520	-	0.60	0.50	-
0500	550	-	1.00	0.50	-
0600	580	3	1.00	0.70	-
0700	560	3	0.73	0.43	-73
0800	520	2	1.59	1.30	-68
0900	550	2	1.50	0.60	-73
1000	480	2	2.70	0.99	-68
1100	470	2	2.93	1 13	-68
1200	320	2	2.50	0.90	-68
1300	250	2	1.61	1 01	-
1400	160	3	0.60	0.20	-
1500	-	3	0.60	0.20	-
1600	-	-	0.10	0.10	-

IV. STORM MOTION

Figures 8a and b show time sections of the radar echoes at VIP level 1 covering the period from 0000 to 1558 GMT 27 May 1981 at 1 h intervals. This is a composite representation using data obtained simultaneously at OKC and SEP. Due to the elevation angle and the position of the storm between the two radars, data from the southern part and northern part were attenuated for OKC and SEP, respectively Thus, compositing was necessary in order to get the complete picture. The displacement of the echoes seen in the figure are in part real and in part due to the analysis technique. The radar echoes at 60 min intervals were plotted with respect to the radar station located on the upper sloping line which was oriented from 295 to 115°. After the echoes at a given time were plotted, the station was shifted 20 n mi along this line, and the procedure was then repeated. The station positions and the echoes were labeled with letters related to the time of the observation, as indicated in the figure. Sloping solid straight lines were then drawn connecting individual cells and conglomerations of cells in time. The hatching of the system at 1458 and 1558 GMT was done simply for better identification because it was slow and very small at these times. It must be stated that not all the VIP level 1 echoes that existed at each of the times given in Fig. 8a and b are shown. Only those associated with the main storm area and which existed for at least 1 h were considered.

The time sequence of the echoes reveals interesting features that

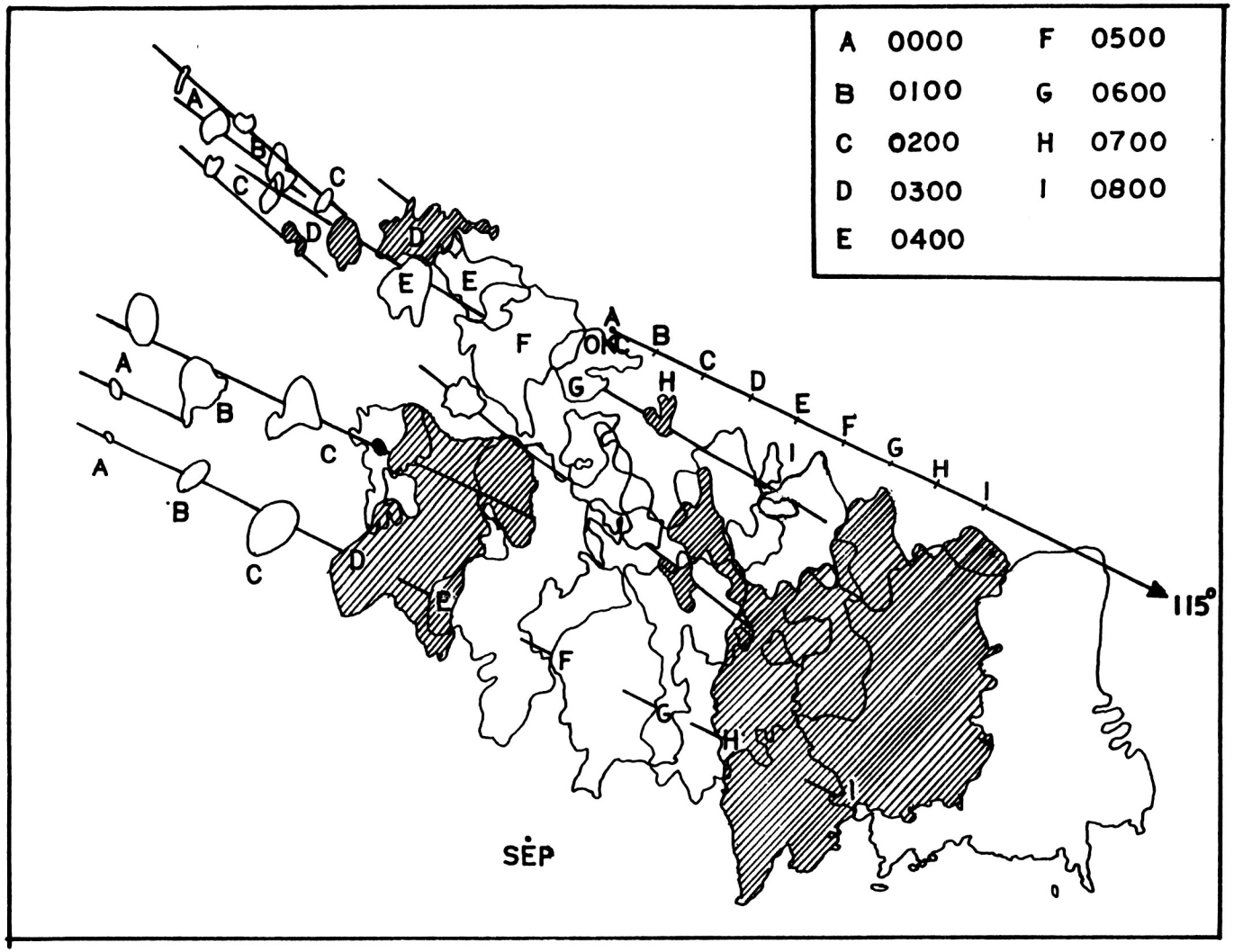

Fig. 8a. VIP level 1 cell outlines at hourly intervals from 0000 to 0800 GMT. Lettered, solid line originating at OKC shows path along which radars were displaced with time for analysis purposes.

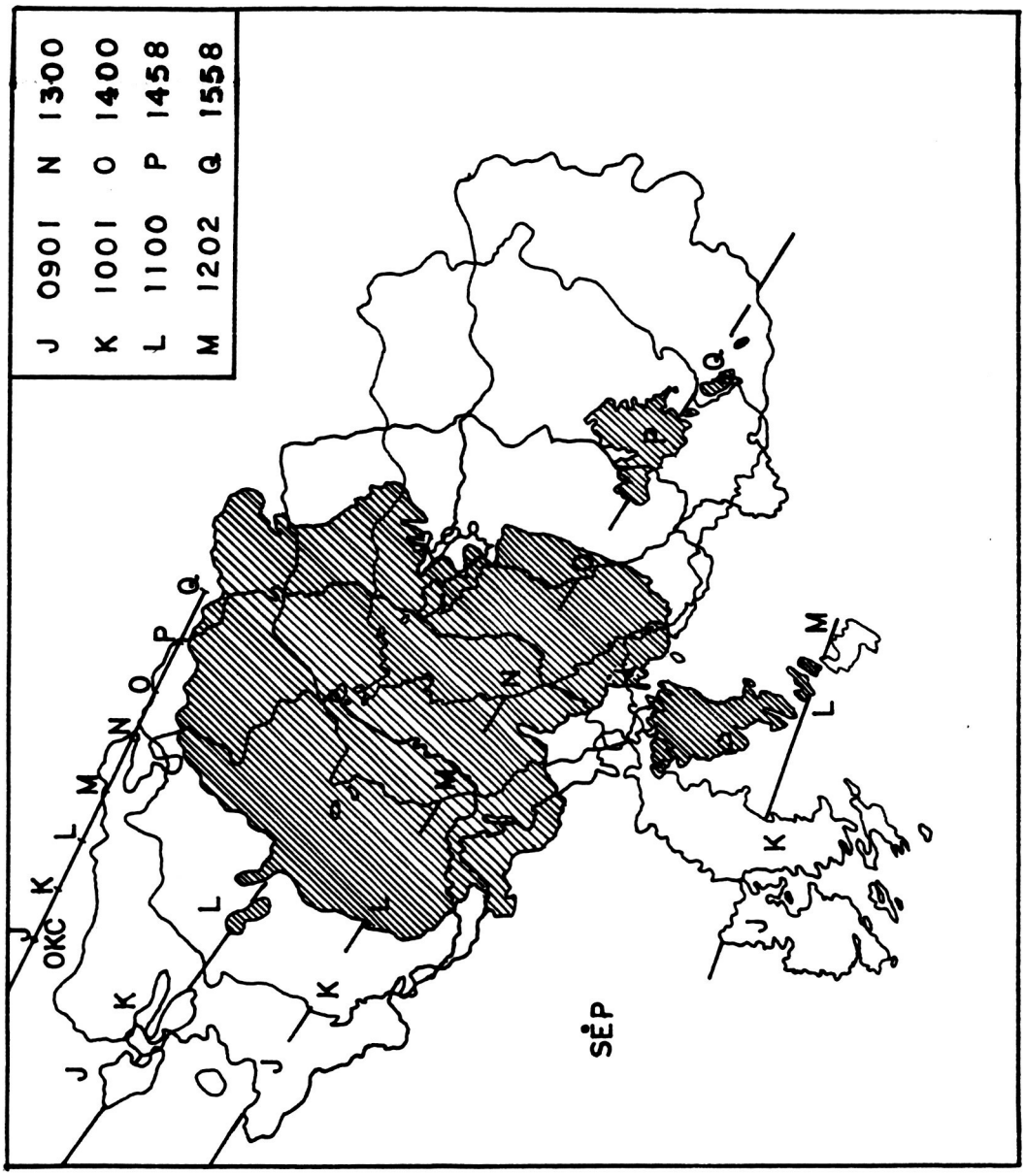

Fig. 8b. As in Fig. 8a except from 0901 to 1558 GMT.

might not be detected with a casual study of the individual echo photographs. It may be noted how the VIP 1 echoes grew in size and merged as the time approached 0515 GMT, the time at which the storm qualified as an MCC. Examination of the figure also indicates the movement of the VIP level 1 echoes varied somewhat from time to time both in direction and speed. However, overall the movement was in the same direction as that chosen for the displacement of the radars, from 295° at a speed of 11 ms^{-1}.

Time sections of the VIP level 3 or more radar reflectivity, covering the period from 0120 to 1240 GMT 27 May 1981 are shown in Fig. 9a and b. The radar echoes at 20 min intervals were plotted by again using a moving coordinate system with a 20 n mi displacement. The station and the echoes were labeled with letters related to the time of the observation. Somewhat erratic cell motion is seen in this figure in that some of these cells moved to left of the storm motion which others moved to the right. Whereas in general, the VIP 3 cells moved at about the same speed as the overall storm (VIP level 1) some cells (hatched in Fig. 9b) which developed starting a 0821 GMT moved at 20 ms^{-1}. When they first appeared, they were located on the west side of the system. By 1240 GMT, they were almost at the middle, southern part of the system.

A careful examination of Fig. 9 also reveals that the appearance of new cells, or vanishing of old cells, did not take place in a consistent fashion. For example, new cells appeared on the north side of the developing system at 0341 GMT, 0400 GMT and 0440 GMT. Some of

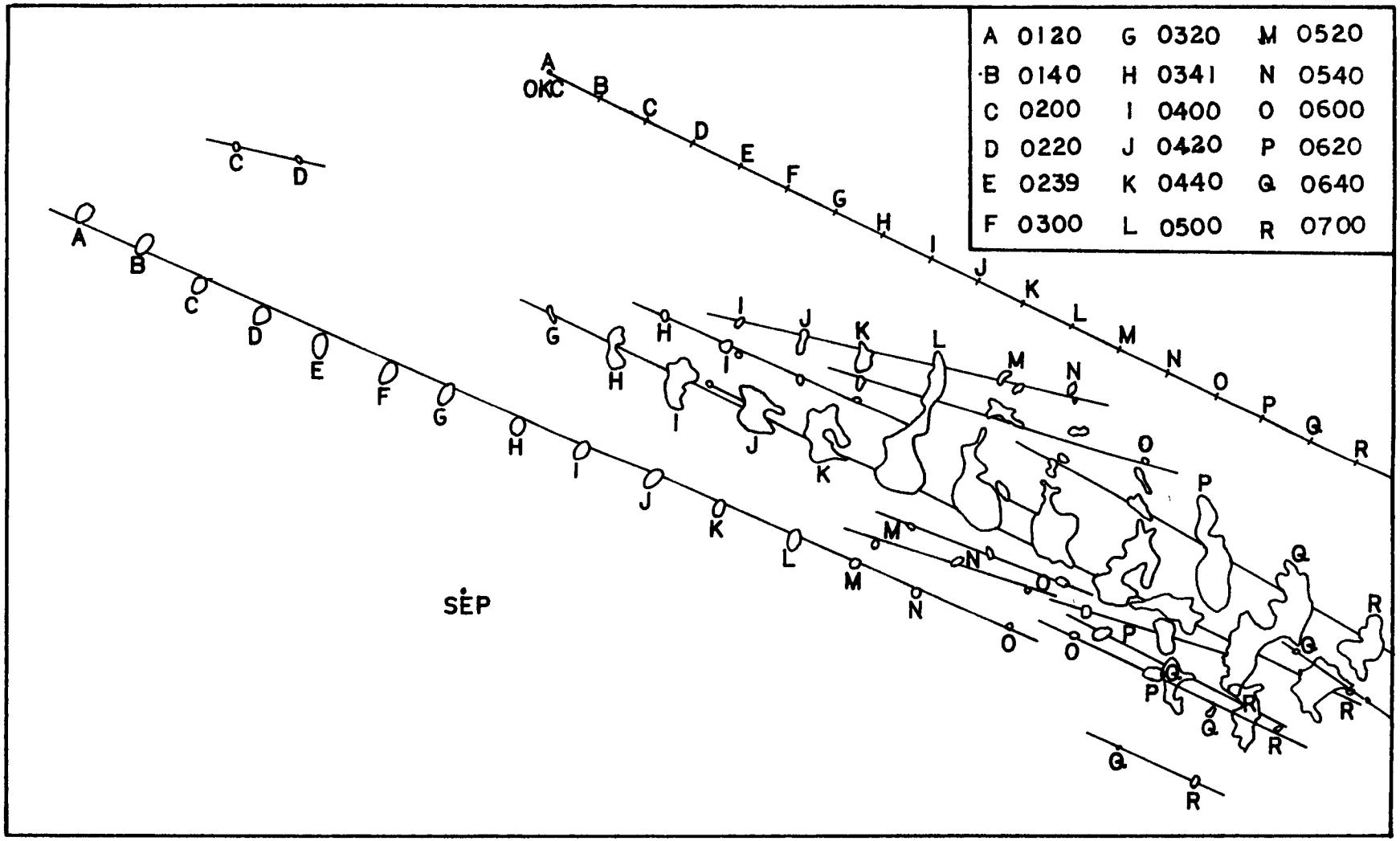

Fig. 9a. VIP level 3 cell outlines at 20 min intervals from 0120 to 0700 GMT. Solid line through OKC shows displacement path of radars.

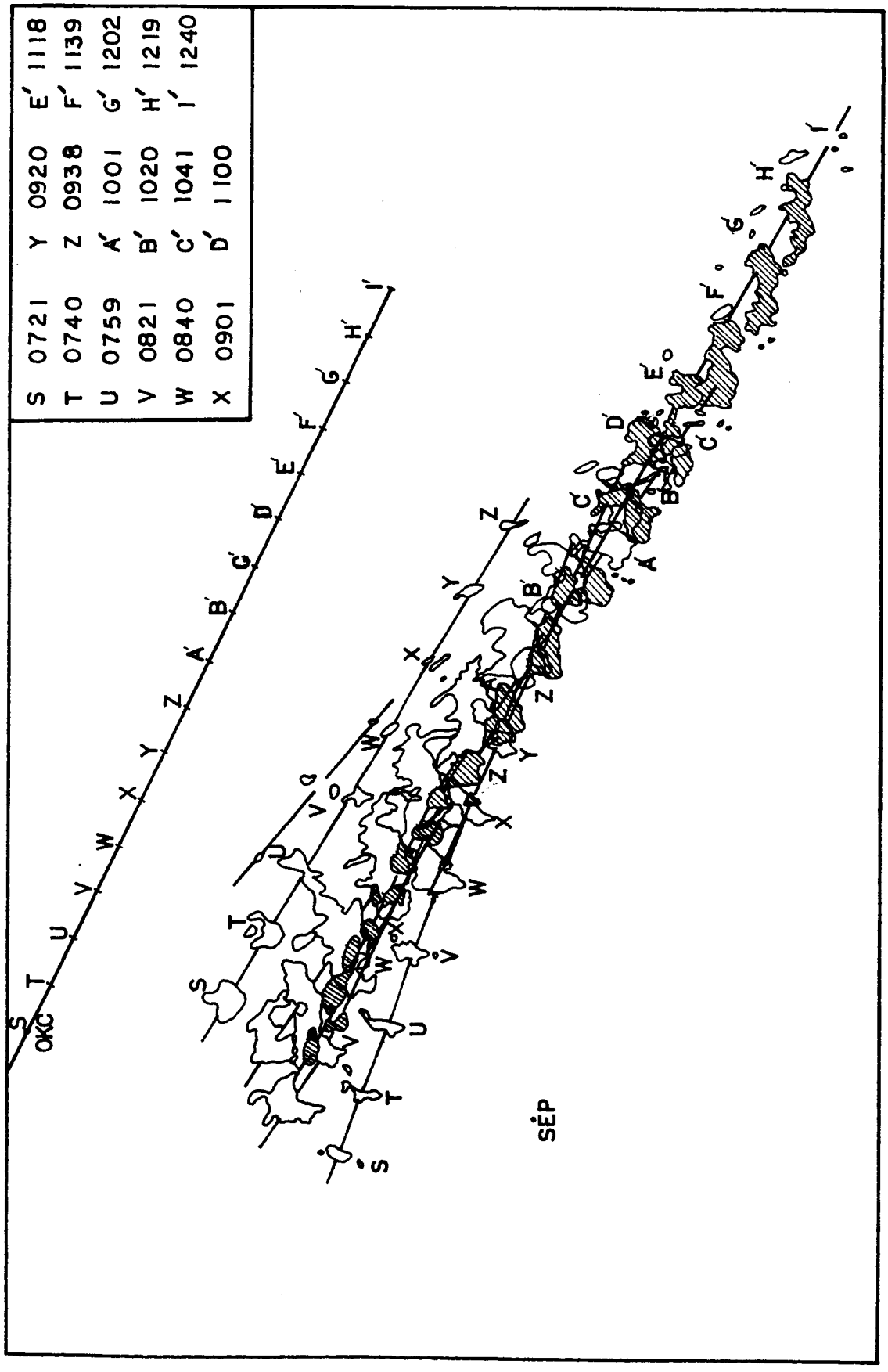

Fig 9b. As in Fig. 9a except from 0721 to 1240 GMT.

these eventually dissipated. Likewise, new cells appeared on the south side of the system at 0520 GMT, 0600 GMT and 0620 GMT Again, some of these cells dissipated. New cell development also took place to the rear of the primary convective line, starting around 0821 GMT. Thus a consistent pattern of cell development on one side of the storm and dissipation on the other side, such as found by Marwitz (1972) did not occur in this case.

The mean wind flow in the vicinity of storm was determined from 1200 GMT rawinsonde measurements at OKC and SEP. This observation time was chosen because it was closest to the time of maximum extent of the MCC, 1000 GMT.

Figure 10 is a hodograph plot of the winds at OKC and SEP at the 85, 70, 50, 30 and 20 kPa levels. The average propagation vector of the storm (and the VIP level 3 cells), from 295 at 11 ms^{-1}, also is indicated. This speed is moderate compared with some reported in the literature (Maddox and Howard, 1983).

The mean cloud -layer wind vector and mass-weighted mean wind vector also are shown in Fig. 10. The mean cloud-layer wind was calculated by first determining the mean vector wind for each station over the layer from 85 to 20 kPa, and then averaging the resulting two vectors. The mass-weighted wind was calculated in the same way but using the relationship

$$V_m = \frac{\sum_{i=1}^{N} \rho_i V_i}{\sum_{i=1}^{N} \rho_i}$$

where ρ is density and the summations extended from 85 to 20 kPa. It is

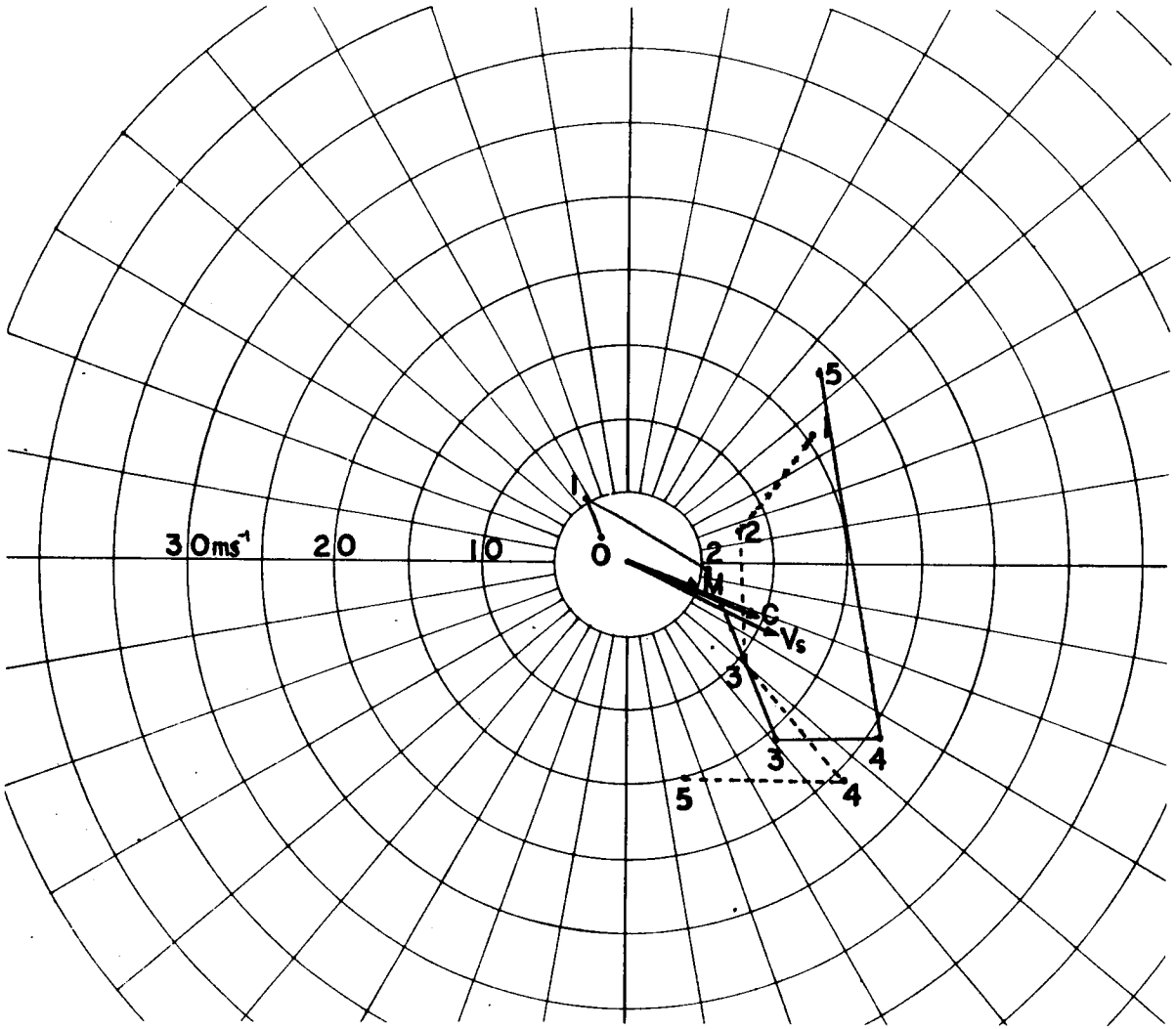

0. Surface
1. 850 mb
2. 700 mb
3. 500 mb
4. 300 mb
5. 200 mb

Fig. 10. Hodographs at 1200 GMT for OKC (solid) and SEP (dashed). Winds are shown for the surface and mandatory pressure levels from 35 to 20 kPa. Storm motion V_S, the cloud-layer wind C and the mass-weighted vector M are plotted.

seen that the mass-weighted vector has the same direction as the mean cloud-layer wind vector but is smaller in magnitude. On the other hand, the mean cloud layer wind matches very well with the storm vector, allowing for errors in wind observations and determination of echo displacements. Zehr and Purdom (1982) found that the direction of the mean cloud layer wind is usually very similar to the 50 kPa wind. It can be seen that this match is close for SEP but not as good at OKC. Likewise, the 1 km-50 kPa shear vector found as an indicator of the MCC motion by McAnelly and Cotton (1986)does not work well for this MCC.

The observed winds at OKC and SEP in comparison with the storm motion show that the relative motion of the air at and below 70 kPa was into the storm from the front and right flanks; this continuous supply of low-level moist air no doubt contributed to the maintenance of the storm. At and above 50 kPa, dryer environmental air was entering the system from the left and rear flanks.

Figure 11 again shows the VIP level 1 echoes; however, this representation differs from that shown in Fig. 8a and b in several ways. First, in this representation, the echoes have not been translated relative to the radar sites, thus their true positions as a function of time relative to OKC and SEP are shown. Secondly, the letters in Fig. 11 show the instantaneous position of the echo centers; therefore, the confusing overlapping of echo areas appearing in Fig. 8a and b is eliminated. Finally, Fig. 11 shows all VIP level 1 echoes, regardless of lifetime or position, at the given times Thus, echoes outside the main storm area are shown, e. g. note the echoes at 1202

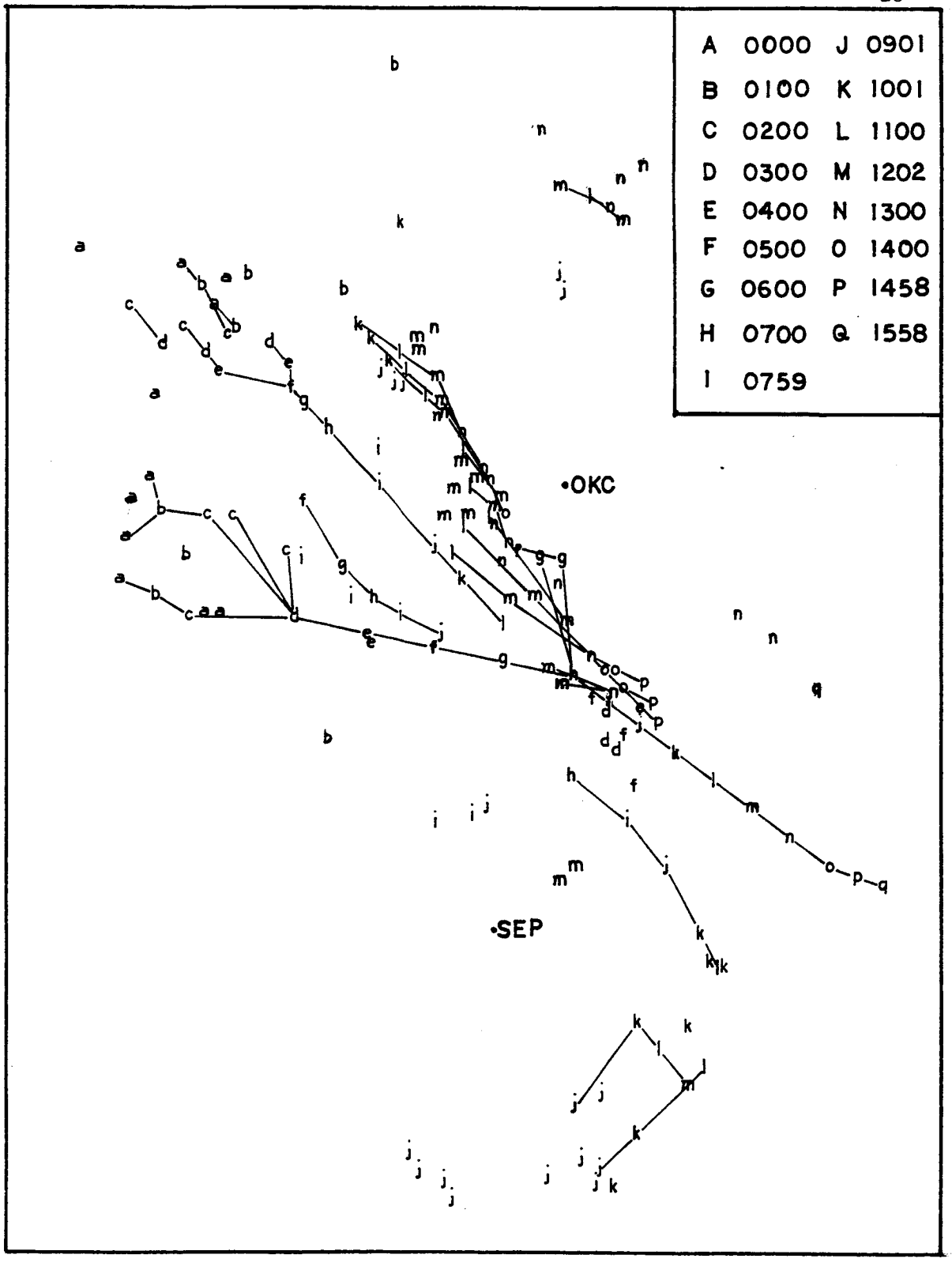

Fig. 11. VIP level 1 cell centroid positions at hourly intervals from 0000 to 1558 GMT. Variations in propagation direction through the lifetime of the storm are evident.

GMT appearing to the north and west of OKC.

This figure shows somewhat more clearly how the tracks of the echoes varied in direction through the lifetime of the storm. About 0901 GMT, new VIP level 1 echoes developed to the south of the main storm area and moved toward the northeast. In all likelihood, these echoes were related to warmer clouds and their motion was a result of the low-level flow.

V. NEW CELL DEVELOPMENT

One objective of the study was to examine how new cells (VIP level 3 or more) developed in relation to the gust front of the system as a whole. Figure 12 shows the trajectories of selected VIP level 3 cell centers in conjunction with the positions of the gust front in time. Many of the cells shown in Fig. 9 are not included here. The gust front positions were determined from the combination of WBAN logs and microbarograph traces from selected stations coupled with sectional surface observations.

The simultaneous positions of the cells and the gust front in time are labeled with letters at approximately 1 h intervals, as in previous figures. The gust front was not identifiable until after the storm had become an MCC. Thereafter, it was found on the eastern, southern, and western extremities of the VIP level 1 echo field- more will be said about this relationship later. Figure 12 again shows the great variability in the trajectories of the cells. Furthermore, it shows that new cells developed along and behind the gust front, and either dissipated quickly or translated toward the southeast along with the gust front for several hours before dissipating. In some instances, merging of cells occurred.

One interesting phenomenon which can be seen to some extent in Fig. 12 is the tendency of the region of greatest reflectivity to appear as a line oriented in a somewhat south to north direction in the early life of the MCC. Note the cells labeled A at 0600 GMT. In this case, as

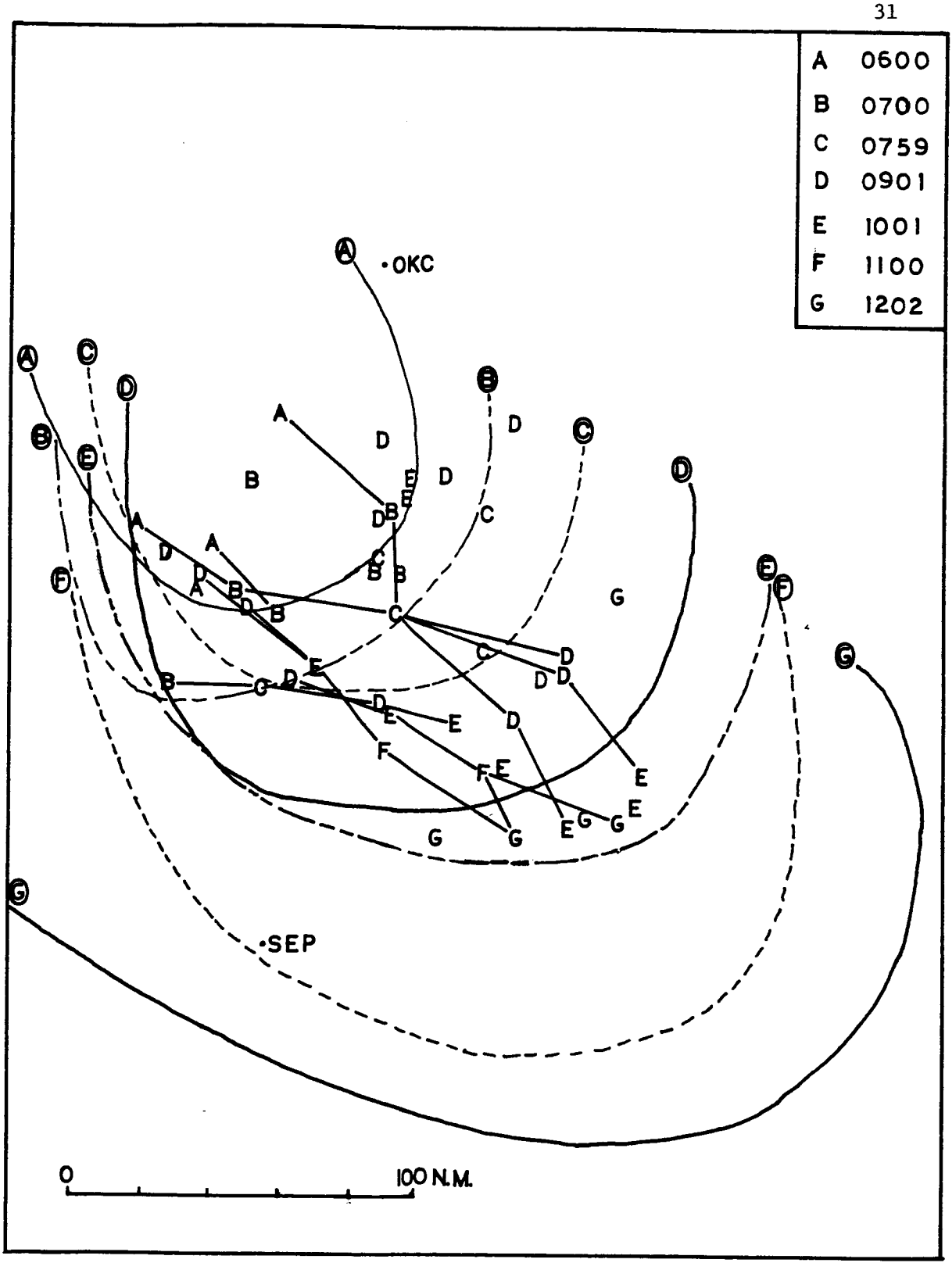

Fig. 12. Gust front and level 3 cell positions at hourly intervals.

time went on, older cells progressed southeastward while new cells developed behind the less-mobile, western side of the gust front- see the cells labeled D at 0901 GMT. Consequently, the maximum reflectivity became oriented along a more west-east line. This phenomenon also has been observed by Howard and Maddox (1983) and Bartels and Rockwood (1983) In the first case, the western end of the line eventually developed into a second MCC. After the time of the maximum extent of the MCC at 1000 GMT, it is seen in Fig. 12 that the gust front accelerated and no new cell development occurred after 1202 GMT.

Although it cannot be ascertained with certainty with these observation, it appears likely that the gust front plays a significant role in the development of new VIP level 3 (or more) cells, as suggested by Maddox (1980b). At some time it moves outward so far from the primary convective activity that the associated low-level horizontal convergence no longer can maintain the storm.

VI. RADAR DATA DETAILS

The echoes seen in Fig. 13 at 1 h intervals from 0100 to 1558 GMT illustrate the important evolutionary features of the MCC. Outer solid lines denote the VIP level 1 systems, and hatched regions denote the cells with VIP level 3 or more reflectivity. The blackened region at 0200 GMT and later times denotes no radar echo as a consequence of attenuation. At 0300 GMT the precipitation amount was 0.3 in at McLean, TX. These precipitation values represent accumulated amounts over the previous hour from the climatological networks of raingauges. The dot in the figure shows both the location of the precipitation and the decimal point. The storm was growing and at 0400 GMT moderate rainfall had occurred at Altus, OK. Over the hour from 0300 to 0400 GMT this incipient MCC produced funnel clouds and tornadoes in Texas.

The storm intensified rapidly and met MCC criteria by 0515 GMT. The expansion in area of the system is apparent from comparison of Figs. 13 e and f. Moderate rainfall occurred during the initiation time. The northeast to southwest oriented line of cells (VIP level 3 or more reflectivity) continued to move eastward for several hours (Fig. 13d-g), with the northern cells moving somewhat faster on convergent tracks. About three quarters of an hour after the initiation of the MCC, a mesohigh and gust front formed across the Oklahoma/Texas border and subsequently moved southeastward. As the MCC intensified, scattered rainfall occurred, and moderate to heavy rainfall was reported in the vicinity of the VIP level 3 cells. During the merging of the discrete

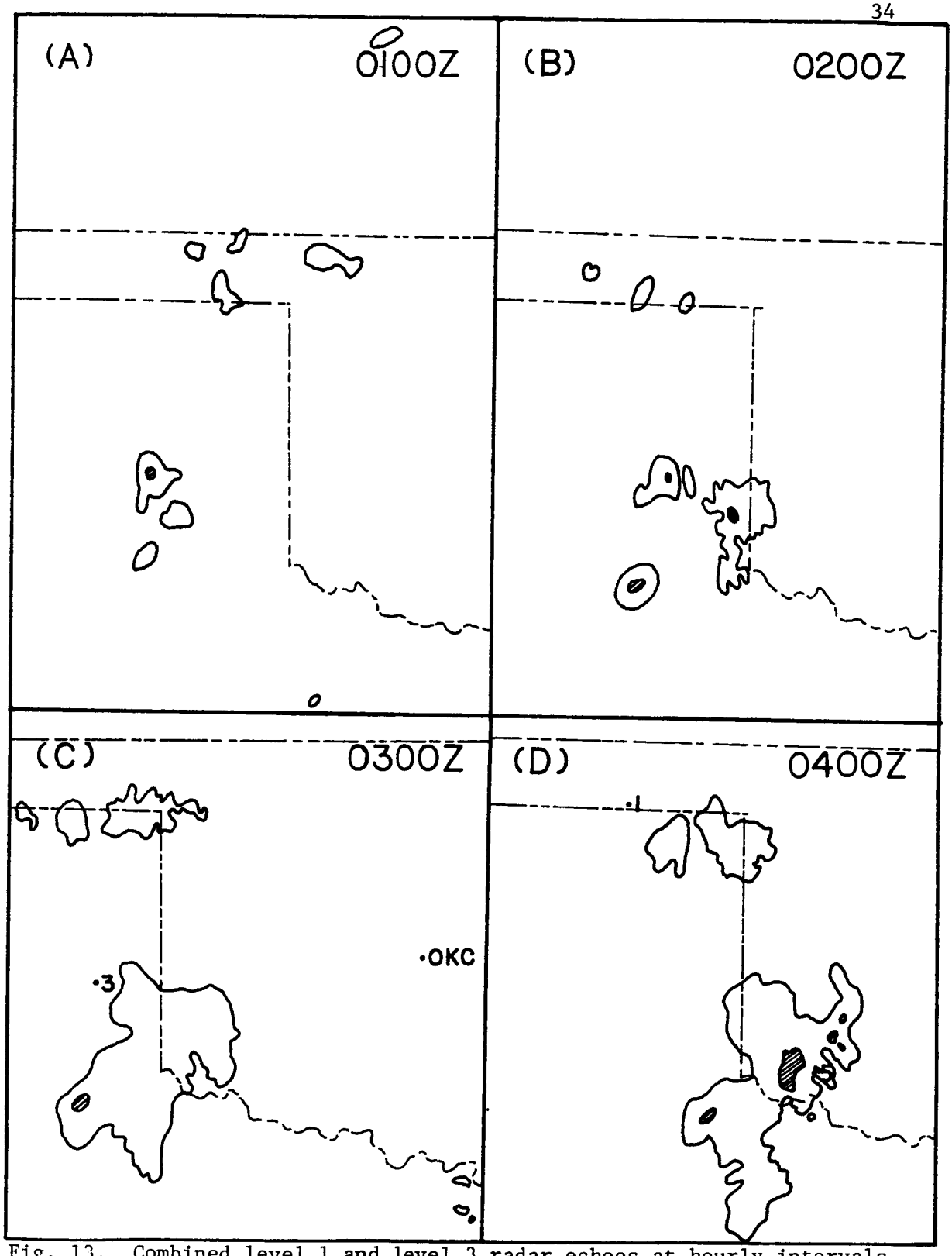

Fig. 13. Combined level 1 and level 3 radar echoes at hourly intervals from 0100 to 1558 GMT. Outer contours represent VIP level 1 echoes; level 3 echoes are hatched. One-hour accumulated rainfall amounts from recording rainguages are shown. Starting with 0600 GMT, the gust front is denoted by cold front sysmbols. Blackened areas indicate radar attenuation.

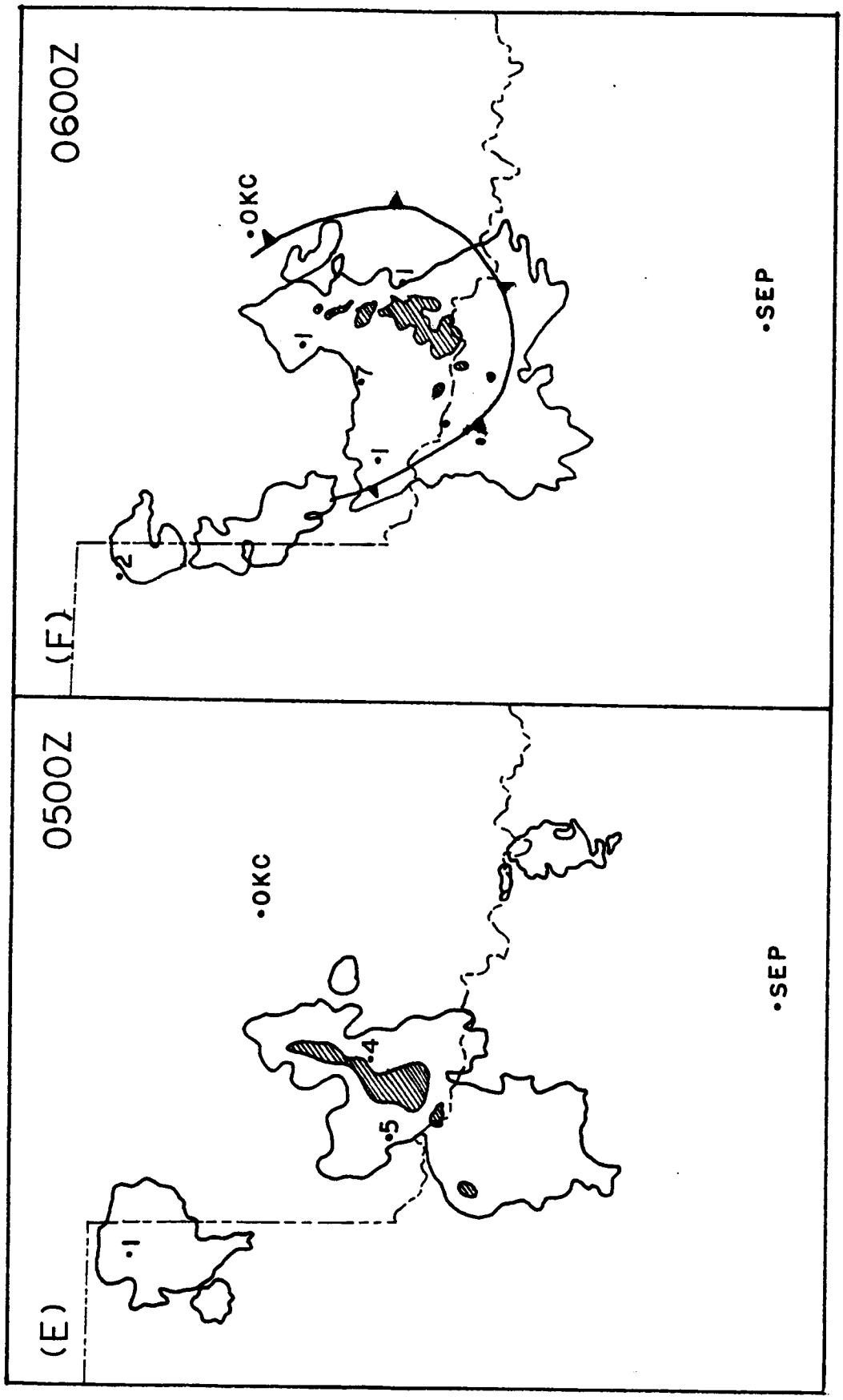

Fig. 13. (Continued)

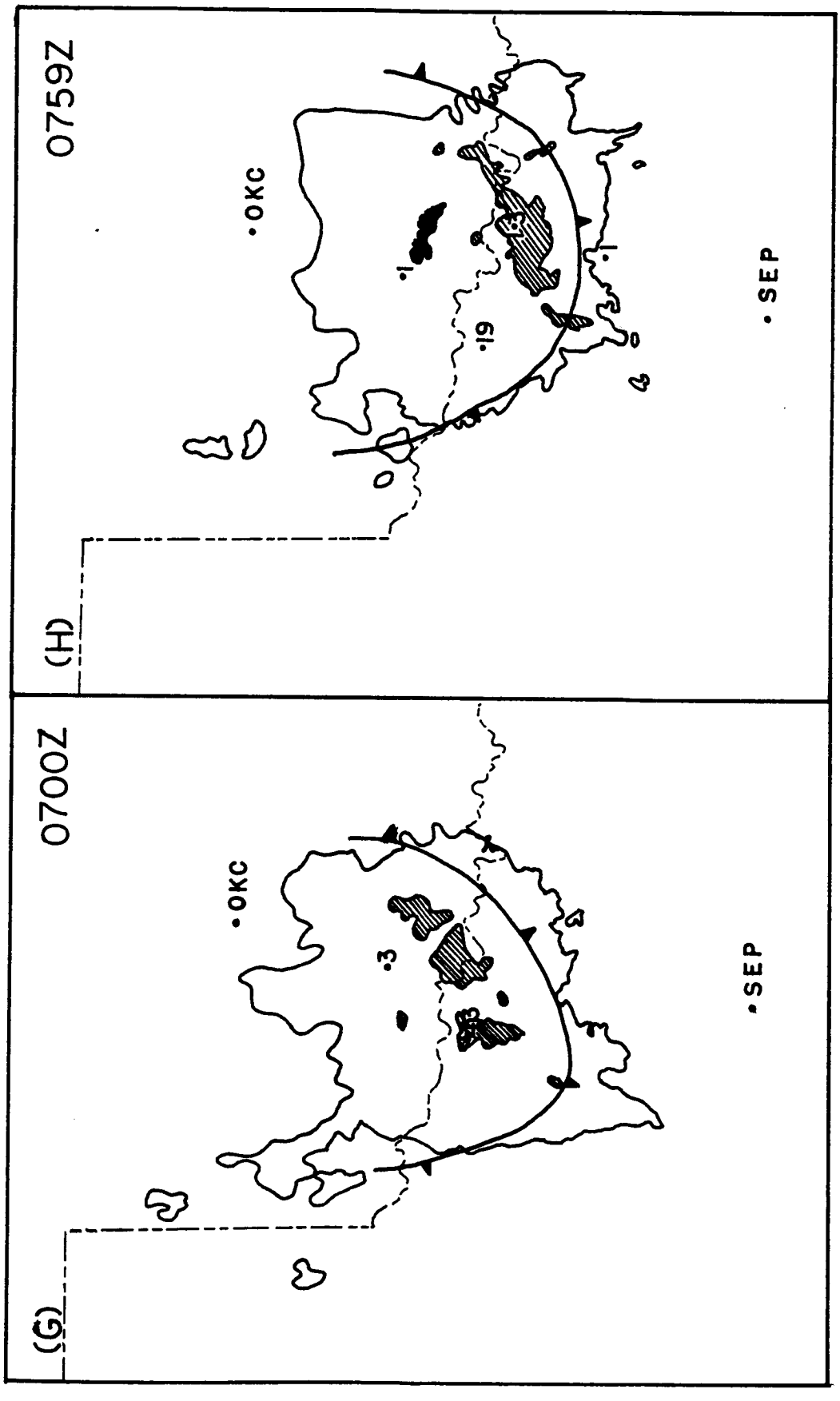

Fig. 13. (Continued)

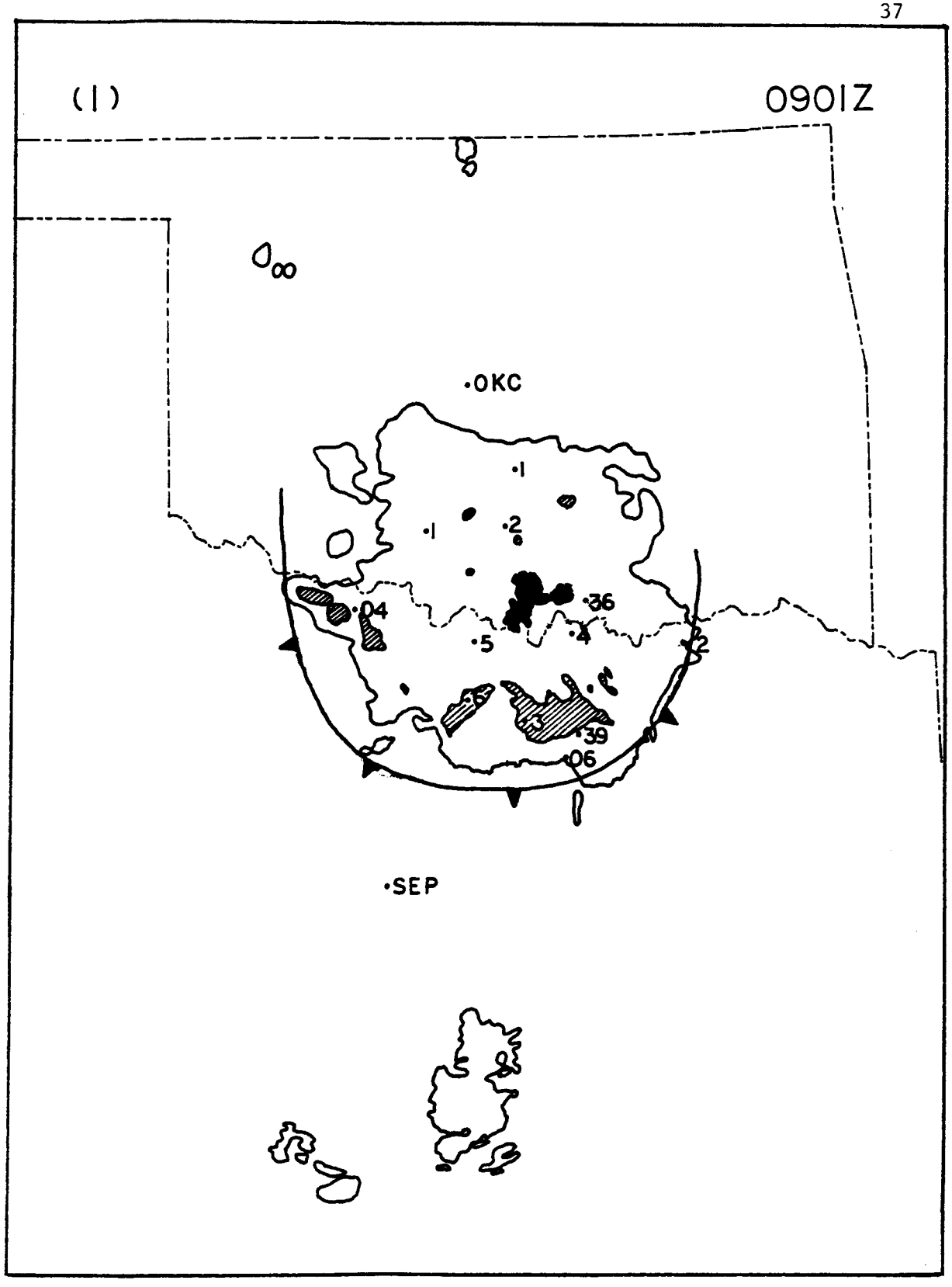

Fig. 13. (Continued)

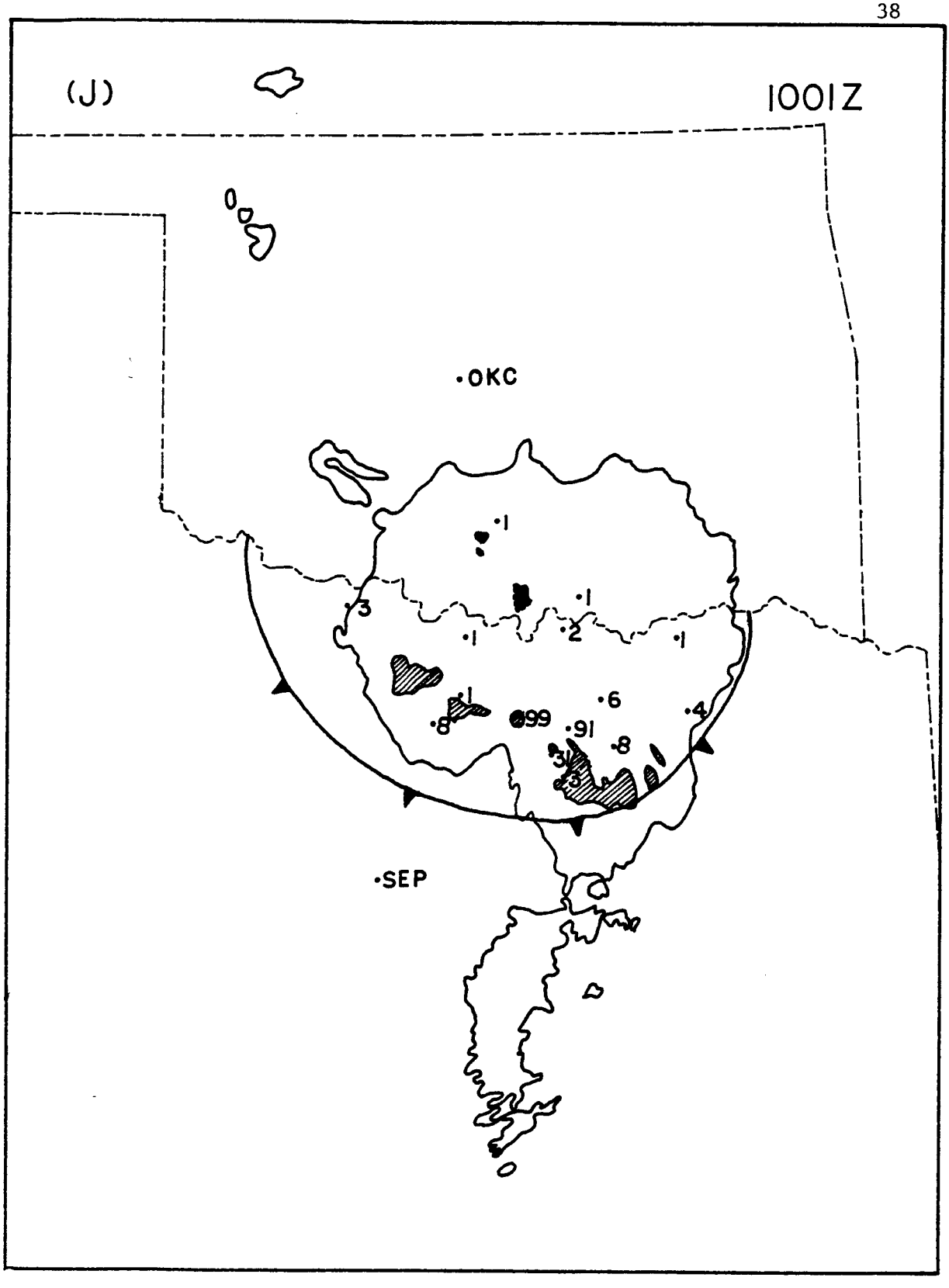

Fig. 13. (Continued)

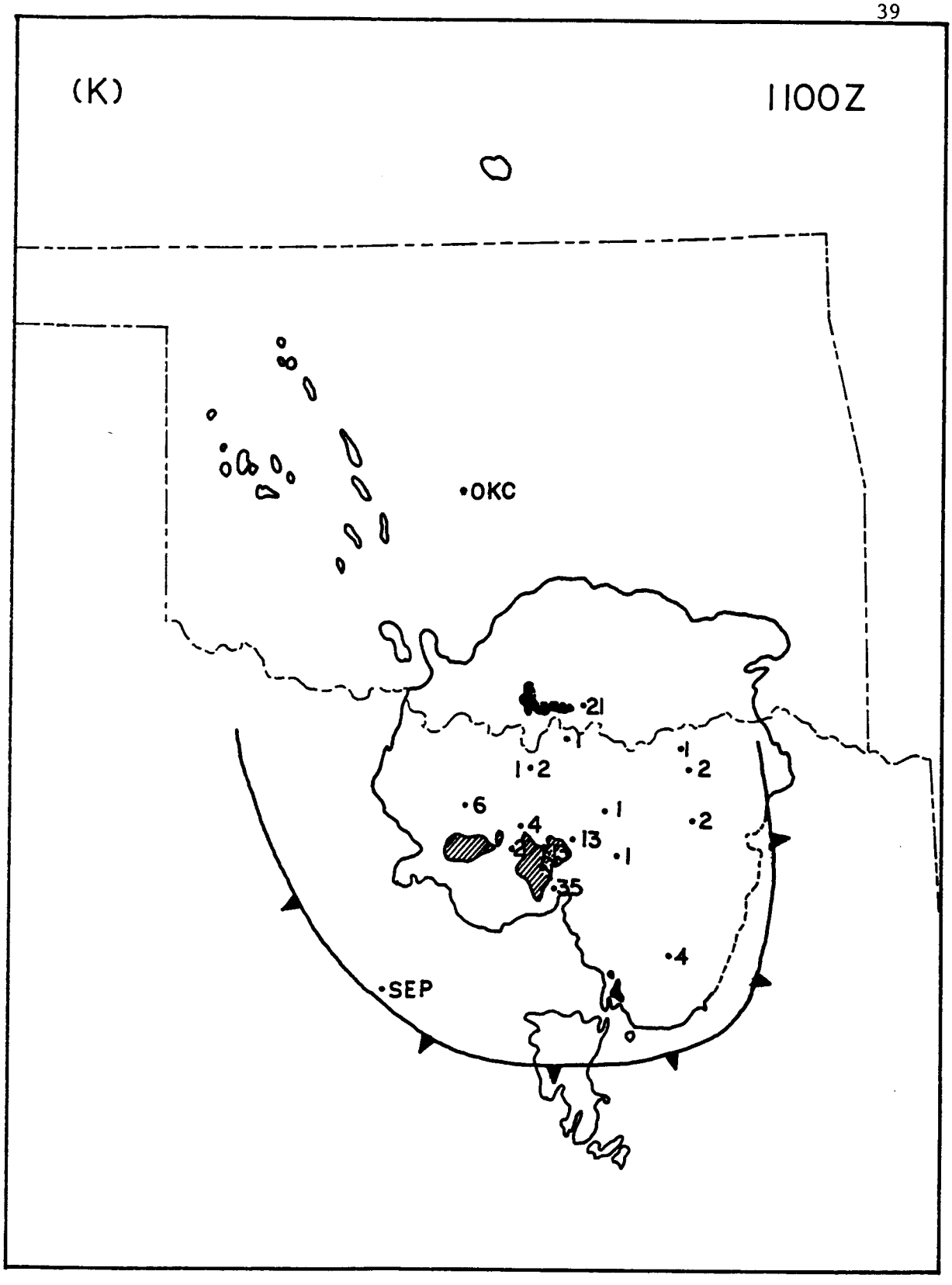

Fig. 13. (Continued)

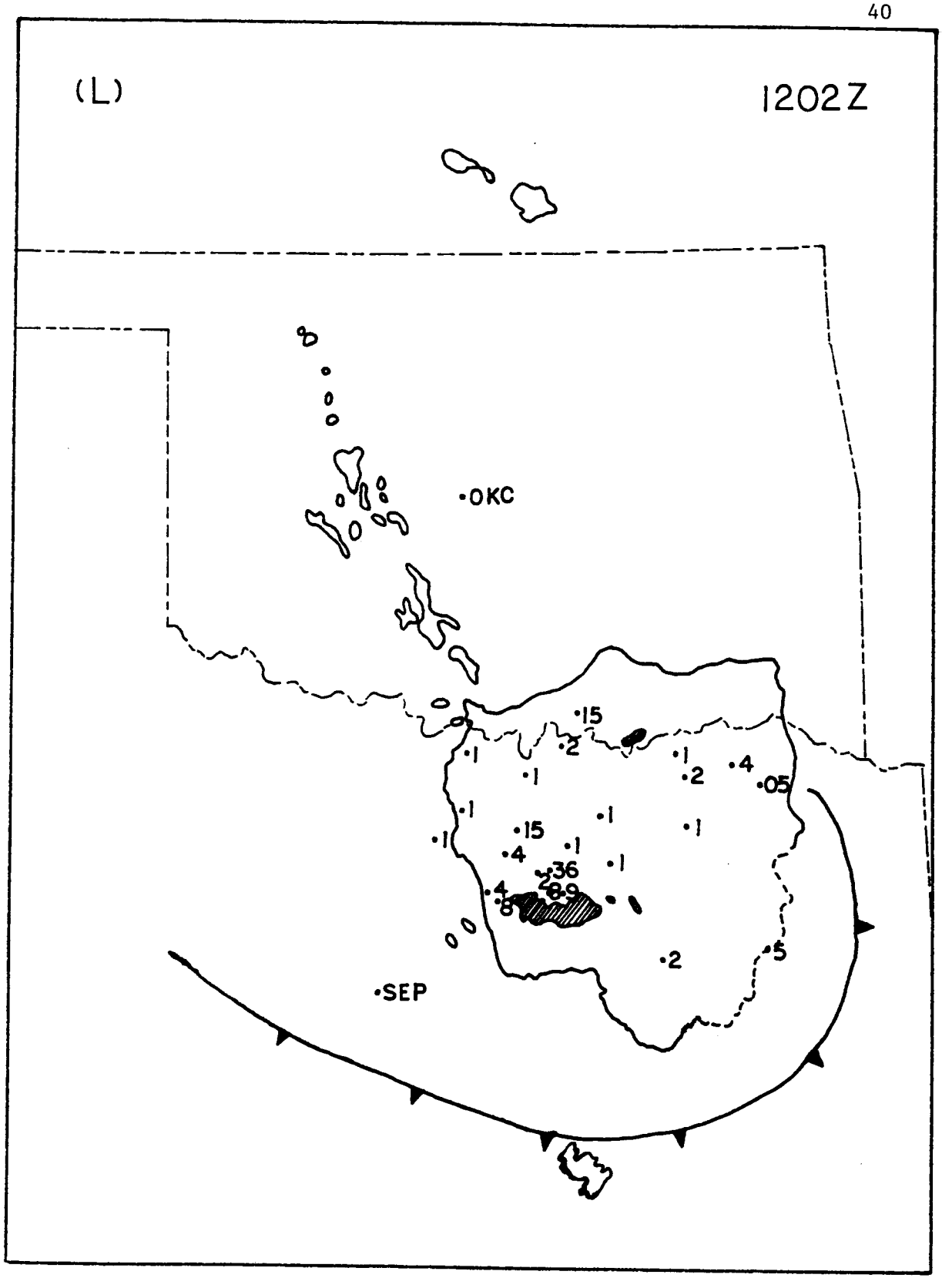

Fig. 13. (continued)

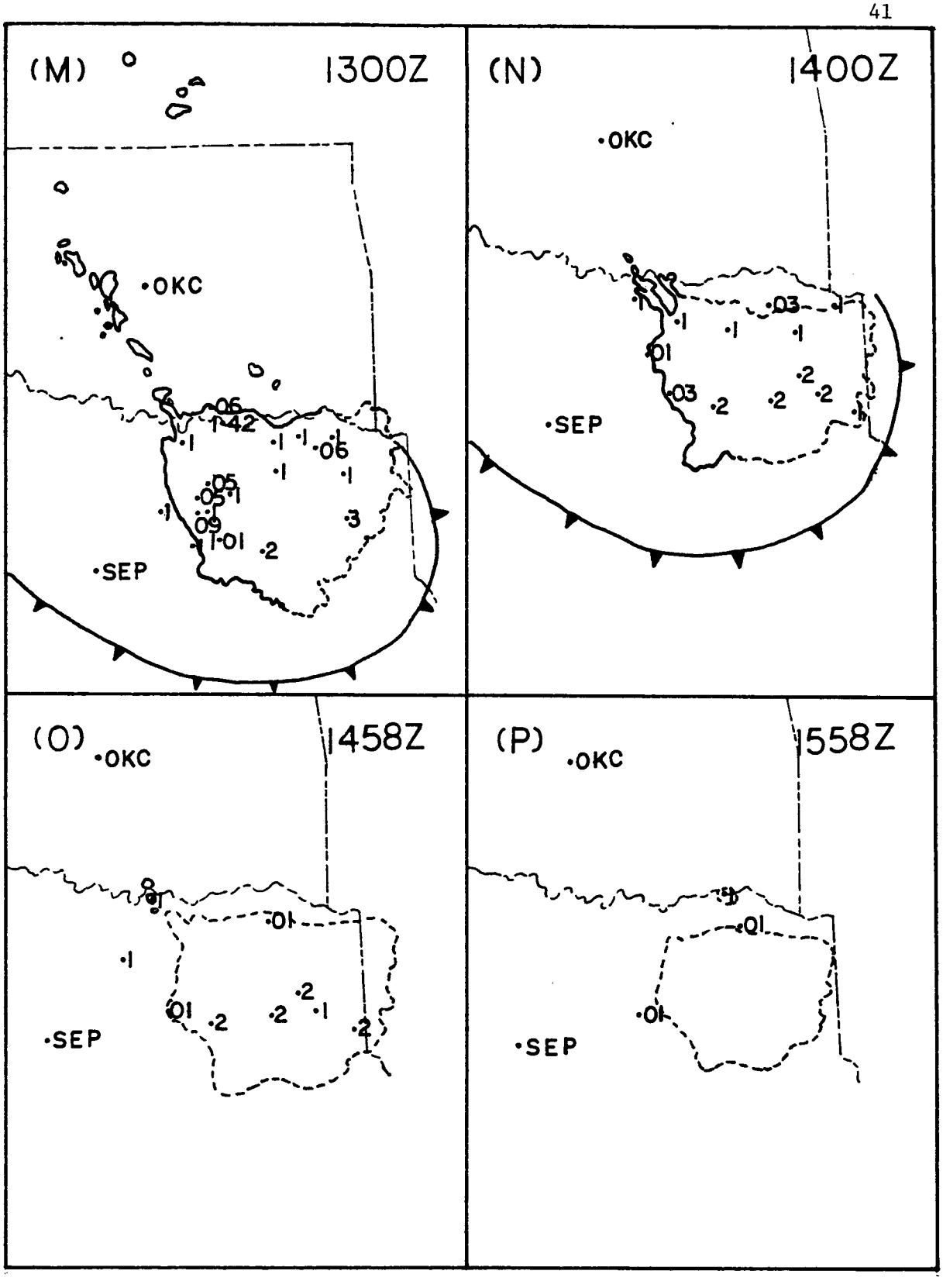

Fig. 13. (Continued)

cells into a larger area of widespread intense reflectivity at Gordonville, TX., rainfall of 1.3 in was recorded (see Fig. 13h). In Figs. 13f-i new cells can be seen to have developed right along the gust front. The MCC rapidly developed after 0800 GMT and the clockwise rotation of the axis of maximum reflectivity, which was mentioned before, can be seen to have taken place between 0600 and 0901 GMT. Very high reflectivity (more than VIP level 3) was observed at 0901 GMT. The strength of the gust front at the same time was revealed by the strong and gusty winds which it produced. At 0935 GMT, as the gust front passed Dallas, TX. a peak wind of 45 kt was recorded.

Figure 13j shows the system at the time of maximum intensity. Although the system was fully developed, the reflectivity was somewhat weaker and there were fewer VIP level 3 cells. Nevertheless, heavy rainfall occurred in the vicinity of the VIP level 3 cells. After 1100 GMT, the gust front moved away from the storm and the system began to dissipate. The dashed boundary on the east side of the wide-spread area of rain in Fig. 131 had to be estimated because of attenuation of both radar beams.

By 1300 GMT, all VIP level 3 or more cells had vanished; however, during the previous hour strong rainfall had occurred in the amount of 1.01 in at Ferris, TX , and 1.42 in at Denison Dam, TX. These heavy rainfalls were produced by the fading VIP level 3 cells at 1202 GMT. Near the termination time of the system, rainfall was wide-spread and light rainfall continued for another 2 h thereafter.

VII. COMBINATION OF SATELLITE IMAGERY AND RADAR OBSERVATION

Figures 14 through 18 represent comparisons of satellite imagery with VIP level 1 and 3 radar patterns at a number of times through the lifetime of the storm of 27 May 1981. Included in these figures are contours of cloud-top temperatures determined from the GOES IR imagery through the use of the McIDAS system at the Marshall Space Flight Center. The reader may wish to compare these figures with Figs. 13g-131 which show the same radar patterns coupled with the gust front positions.

Figure 14 shows the situation at 0700 GMT. On the right-hand side of the figure, the outer line shows the overall cloud shape, as provided by the satellite image on the left-hand side of the figure. The inner, thicker lines depict the cloud top equivalent blackbody temperatures of 240°, 210°, and 205°K.

The satellite image displays a large, nearly circular shield of cloud, as required in Maddox's definition (1980) for an MCC, with coldest tops occurring over the west central portion of the system (compare with Fig. 13g). The radar depiction on the right- hand side of Fig. 14 indicates that the VIP level 1 rainfall at this time was fairly well contained within the 210°K or -63°C isotherm of the storm canopy About half of the VIP level 3 echo fell within the 205°K isotherm. Also, further comparison with Fig. 13g shows that the gust front position in Fig. 13g falls between the 210 and 240°K isotherms shown in Fig. 14. Gurka (1976) found that the gust front generally is

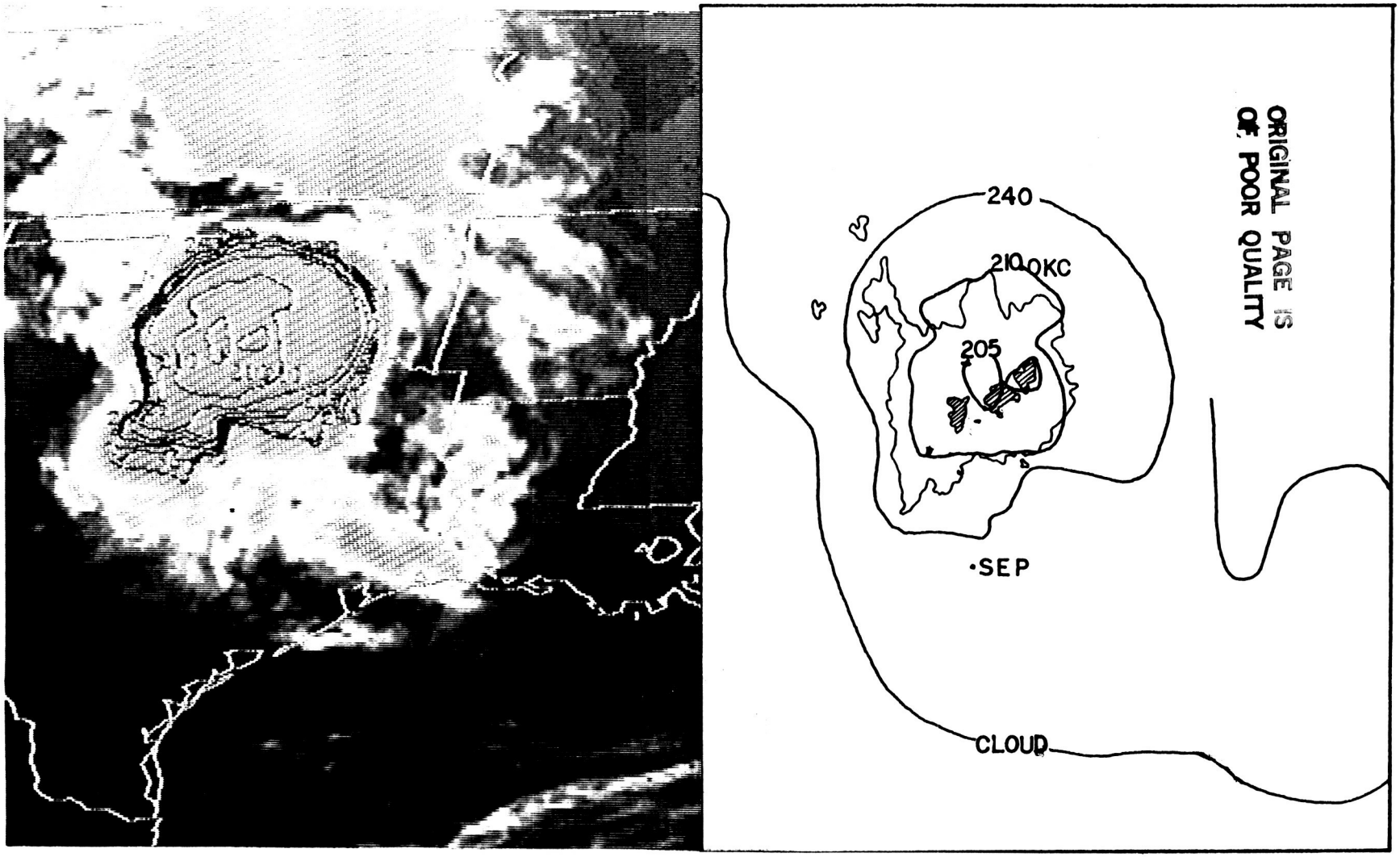

Fig. 14. Simultaneous views of satellite imagery and radar echoes at 0700 GMT. On the left-hand side is the GOES IR image with superimposed equivalent blackbody temperature field (K). On the right the outermost line is the boundary of the cloud shield. Inner lines show IR temperature field superimposed on the radar echo pattern.

located very close to the strongest gradient in IR temperature on the eastern and southern sides of a mesoscale storm

Figures 15 through 18 in general show the same features as noted in Fig. 14. Figures 15 and 16 show good agreement between the 210°K isotherm, the boundary of the VIP level 1 reflectivity region, and the position of the gust front. There is some tendency for the VIP level 3 area to be enclosed by the 205°K isotherm.

At 1001 GMT (Fig. 17), the bands across the satellite image represent radiance data that were lost in transmission from the satellite. This is the time of greatest extent of the storm as measured by the area enclosed by the 210°K isotherm. It is seen that a small appendage of warm-cloud precipitation has developed on the south side of the system; otherwise, the relationships between the temperature values and echo intensities noted earlier still prevail. At this time the gust front on the western side of the storm is moving away from the precipitation area.

By 1202 GMT (Fig. 18) the storm is halfway in time between its time of maximum extent and its termination (the time when it ceased to qualify as an MCC). Figures 18 and 131 show that the gust front has now moved outside the 210°K isotherm on the east side of the system and even outside the satellite image on the west side. The good agreement between the 210°K isotherm and the VIP level 1 reflectivity region also has deteriorated somewhat.

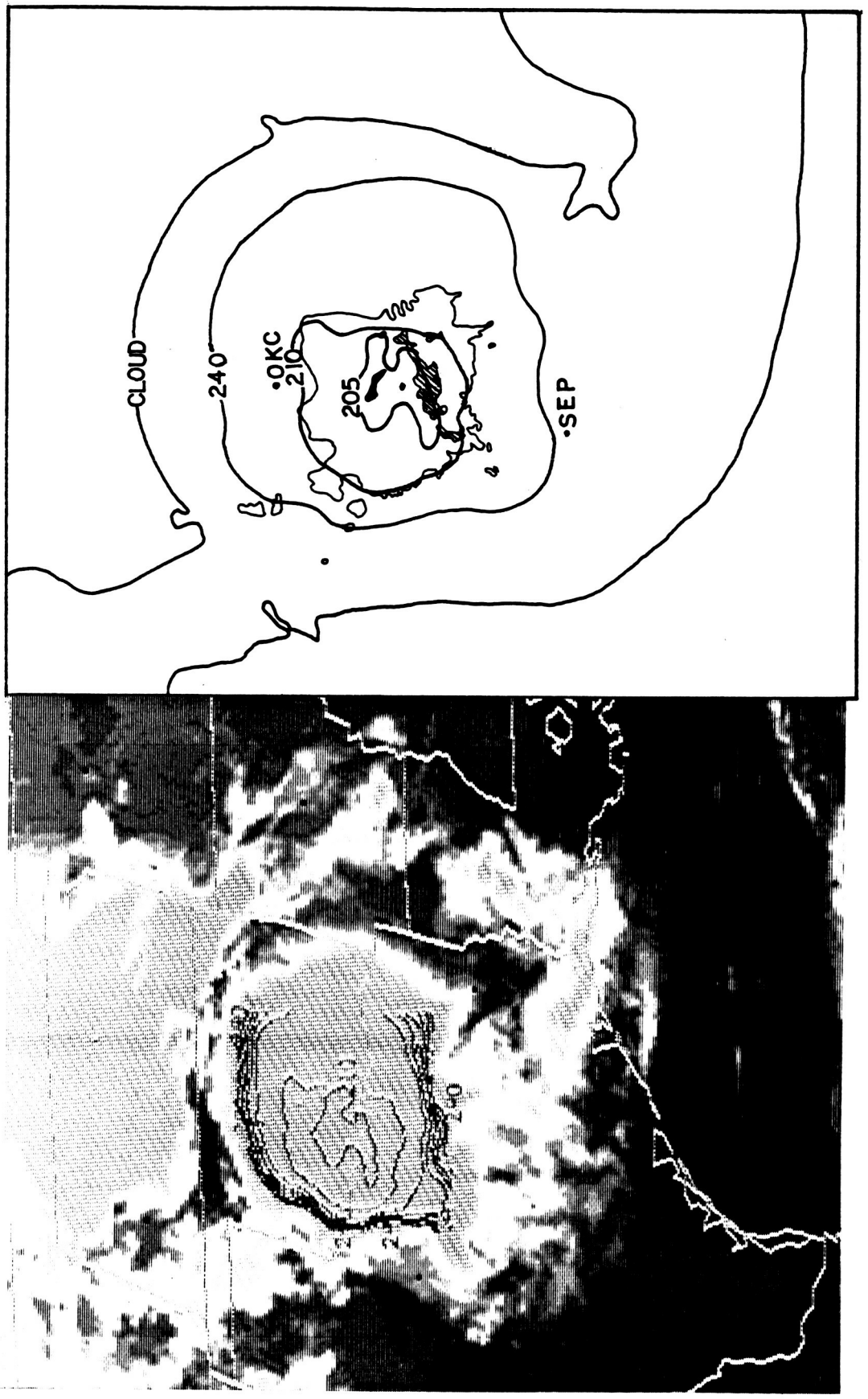

Fig. 15. Simultaneous views of satellite imagery and radar echoes at 0800 GMT. As in Fig. 14.

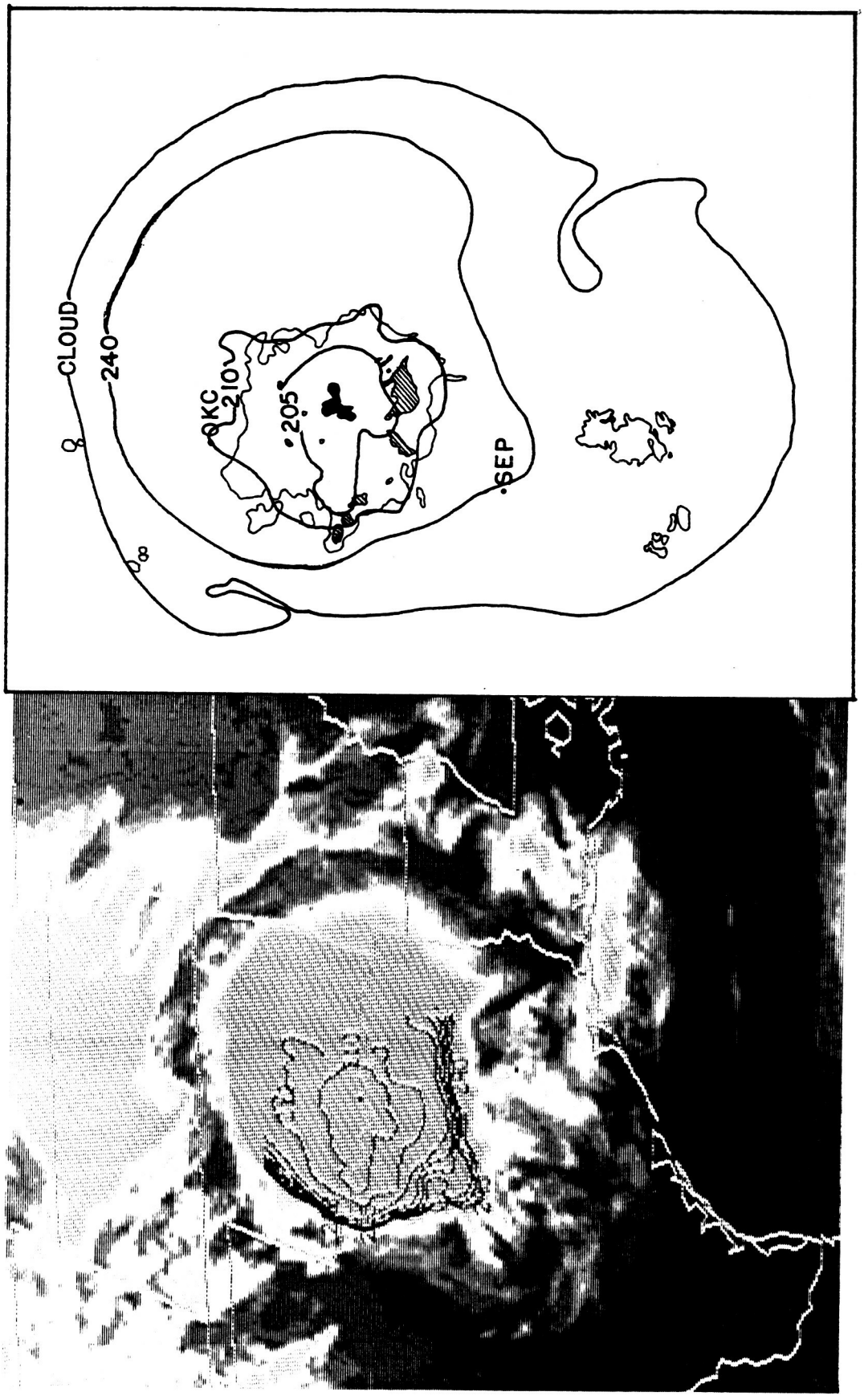

Fig. 16. Simultaneous views of satellite imagery and radar echoes at 0900 GMT. As in Fig. 14.

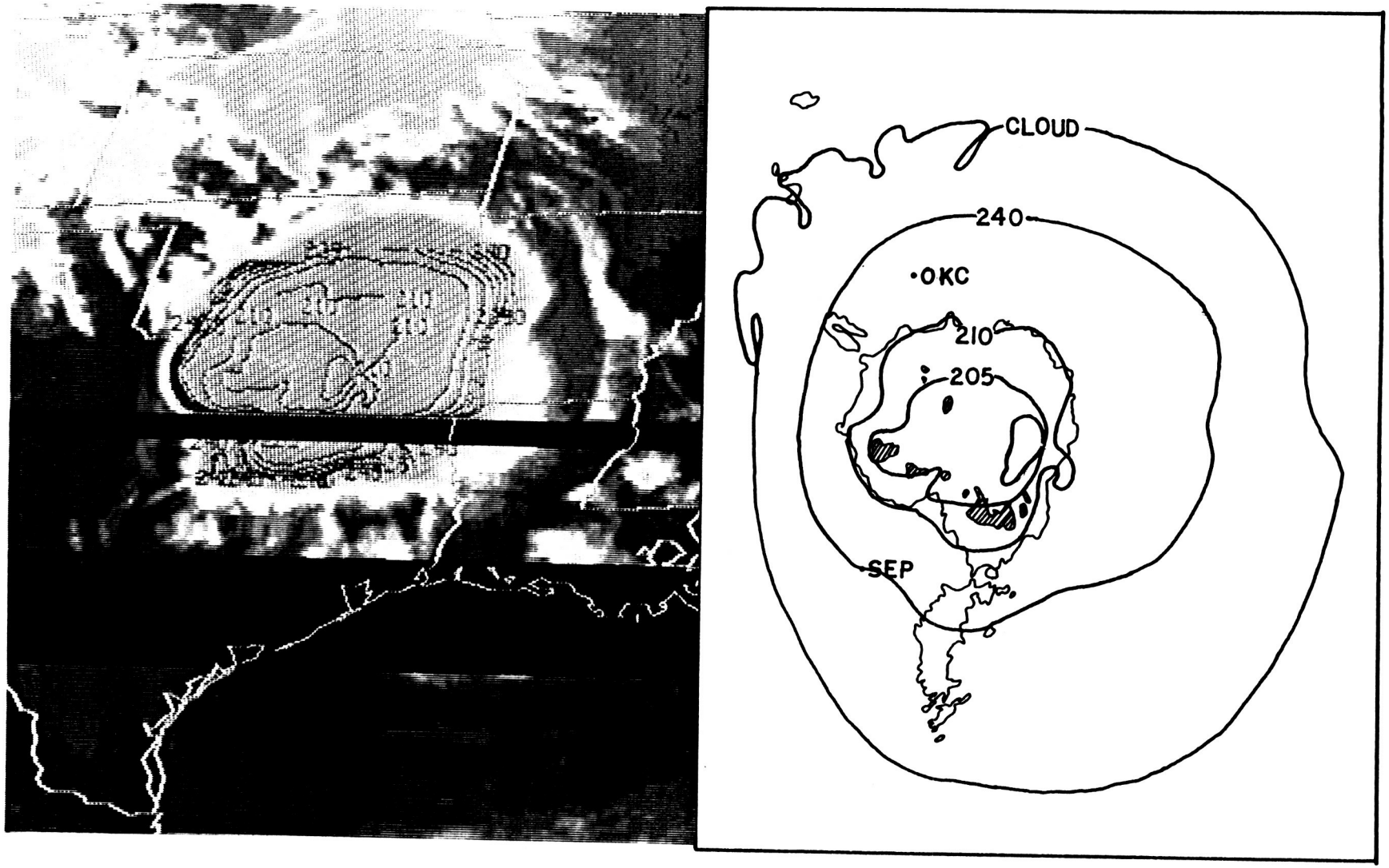

Fig. 17. Simultaneous views of satellite imagery and radar echoes at 1000 GMT. As in Fig. 14 except that some radiance data loss is indicated on the satellite image by black bands.

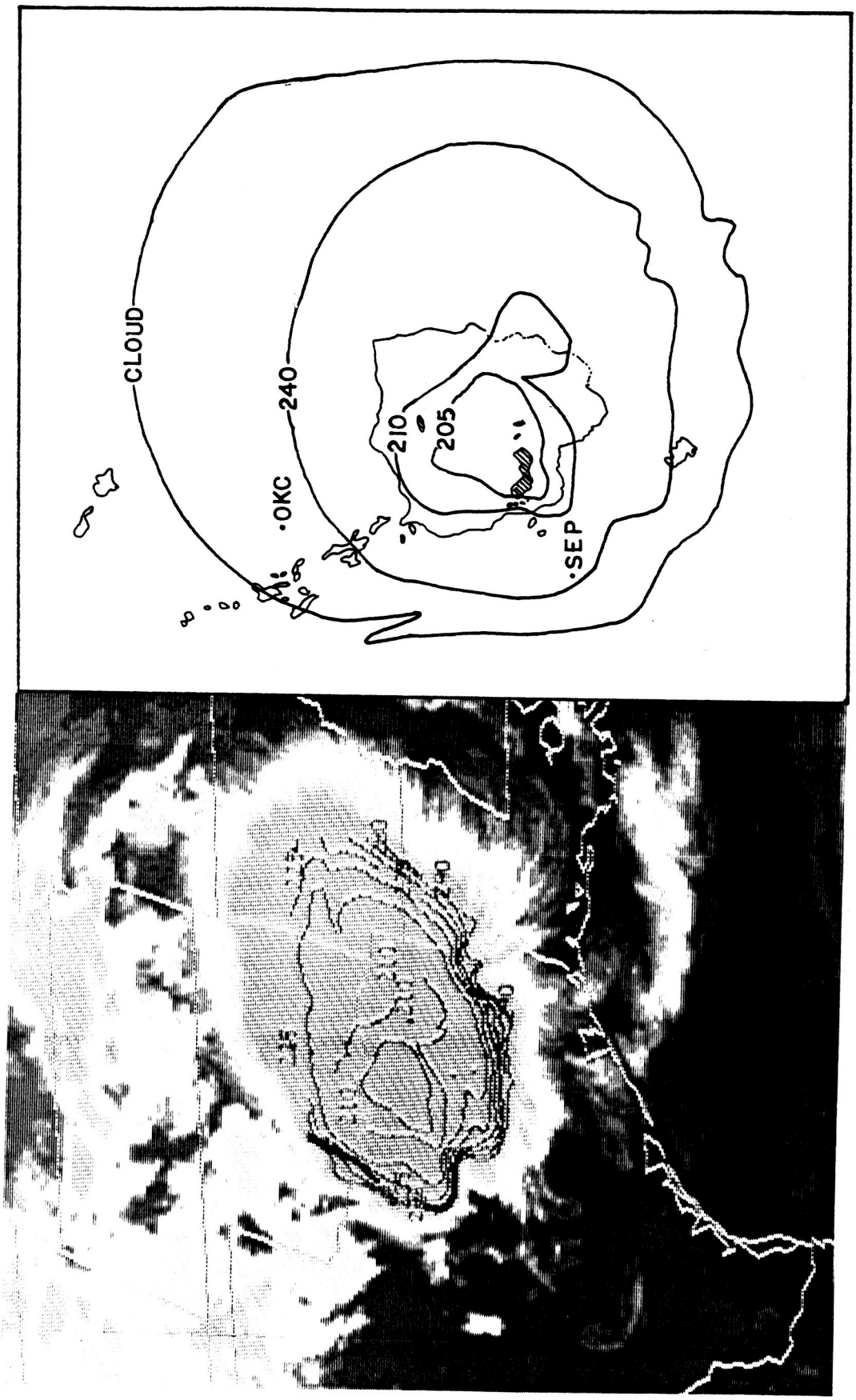

Fig. 18. Simultaneous views of satellite imagery and radar echoes at 1200 GMT. As in Fig. 14.

VIII. CONCLUSIONS AND RECOMMENDATIONS

The MCC of 27 May 1981 developed over southwestern Oklahoma and northern Texas and moved in a eastsoutheasterly direction. A synthesis of radar, satellite, sounding and surface data was used to determine the relationships between system and cell motions relative to the mean cloud layer wind, the relationship between cell development and the gust front, and the relationship between the rainfall patterns and amounts and cloud-top IR temperature structure.

Findings regarding the development and propagation of cells in an MCC are as follows:

1) The direction of cell (VIP level 3 or more reflectivity) propagation was found to be approximately the same as the system (VIP level 1 reflectivity) movement and the ambient wind.

2) Level 3 (or more) cells developed and dissipated on both the north and south ends of the line of maximum reflectivity Thus, the system, as denoted by level 1 reflectivity, grew in size with time. Also, new cells developed to the rear of the line of maximum reflectivity as older cells continued their eastsoutheastward propagation. This led to a clockwise rotation of the line of maximum reflectivity. The resulting pattern of system and cell motion was not consistent with any of the models described by Marwitz (1972) for multi-cell systems.

3) Prior to its becoming an MCC the axis of maximum reflectivity was located near the center of the level 1 reflectivity. After MCC

initiation, this axis was observed to move to a position just behind the leading edge of the precipitation area. This agrees with results found by Leary and Rappaport (1983) using the combination of satellite imagery and radar echoes for an MCC in southwestern Texas. A gust front became identifiable in the surface synoptic data shortly after the initiation of the MCC. Its position in time was found to match well with the boundary of the precipitation area. Level 3 cells were found to form along or just inside the gust front and move with it. Later, as the gust front moved away from the precipitation area, further cell development ceased. These results imply that a synergistic relationship may exist between the system and the gust front in which the downdrafts and outflow from the MCC maintain the gust front, which in turn provides the convergence and updrafts to produce the cells.

Only a small portion of the storm area as seen in satellite imagery represents rainfall of sufficient intensity to be detected by radar. It was found that the 210°K isotherm in the IR satellite imagery tends to encompass this VIP level 1 region. Furthermore, the 205°K isotherm tends to surround a large portion of the heavier rainfall area as denoted by level 3 cells.

These generalizations are drawn from only one MCC and thus may not be representative of MCCs in different synoptic conditions, in different geographical regions, or earlier or later in the convective season.

It is obvious that a better, if not complete, understanding of the internal structure and dynamics of middle-latitude mesoscale systems can only be gained through an elaborate and specialized field study.

Fortunately, plans for such a study have been formulated (Zipser, 1984) and a preliminary, geographically- limited study has been carried out (Cunning, 1986) to test instrumentation and logistics. Until this field study can be accomplished, it is recommended that studies along the lines carried out here be continued. If the results found here can be confirmed, some understanding of MCCs will have been gained which may serve useful in the final planning of a large-scale field program.

REFERENCES

Bartels, D. L., and A. A. Rockwood, 1983: Internal structure and evolution of a dual mesoscale convective complex. Preprints 5th Conf. Hydrometeorology, Tulsa, OK., Amer. Meteor. Soc., 97-102.

Bosart, L. F., and F. Sanders, 1981: The Johnstown Flood of July 1977: A long-lived convective system. J. Atmos. Sci., 38, 1616-1642.

Byers, H. R., and R. R. Braham, Jr., 1949: The Thunderstorm. U. S. Dept. of Commerce Weather Bureau, Washington, D C., 282pp.

Cunning, J. B., 1986: The Oklahoma-Kansas preliminary regional experiment for STORM-Central. Bull. Amer. Meteor. Soc., 67, 1478-1486.

Foster, D. S., and R. M. Reap, 1973: Archiving of manually digitized radar data. Techniques Development Laboratory Office Note 73-6, National Weather Service, Silver Springs, Md., 12pp.

Fritsch, J. M., R. A. Maddox and A. G. Barnston, 1981: The character of mesoscale convective complex precipitation and its contribution to warm season rainfall in the United States. Preprints 4th Conf. Hydrometeorology, Reno, NV., Amer. Meteor. Soc., 94-99.

Fujita, T., and H. A. Brown, 1958: A study of mesosystems and their radar echoes. Bull. Amer. Meteor. Soc., 39, 538-554.

Gurka, J. J., 1976: Satellite and surface observations of strong wind zones accompanying thunderstorms. Mon. Wea. Rev., 104, 1484-1493.

Heymsfield, G. M., and S. Schotz, 1985: Structure and evolution of severe squall line over Oklahoma. Mon. Wea. Rev., 113, 1563-1589.

Howard, K. W., and R. A. Maddox, 1983: Precipitation characteristics of

two mesoscale convective systems. Preprints 5th Conf. Hydrology, Tulsa, OK., Amer. Meteor. Soc., 11pp.

Leary, C. A., and E. N. Rappaport, 1983: Internal structure of a mesoscale convective complex, Preprints 21st Conf. Radar Meteorology, Edmonton, Amer. Meteor. Soc., 70-77.

Maddox, R. A., 1980a; A satellite based study of midlatitude, mesoscale convective complexes. Preprints 8th Conf. Weather Forecasting and Analysis, Denver, CO., Amer. Meteor. Soc., 329-338.

---, 1980b: Mesoscale convective complexes. Bull. Amer. Meteor. Soc., 61, 1374-1387.

---, D. M. Rodgers and K. W. Howard, 1982: Mesoscale convective complexes over the United States during 1981. Mon Wea. Rev., 110, 1501-1514.

---, and K. W. Howard, 1983; Simultaneous radar and satellite depictions of mesoscale convective systems. Preprints 5th Conf. Hydrometeorology, Tulsa, OK., Amer. Meteor. Soc., 10pp.

McAnelly, R. L., and W. R. Cotton, 1986: Meso-β-scale characteristics of an episode of meso-α-scale convective complexes. Mon. Wea. Rev., 114, 1740-1770.

Marwitz, J. D., 1972: The structure and motion of severe hailstorms. Part II: Multi-cell storms. J. Appl. Meteor., 11, 180-188.

Merritt, J. H., and J. M. Fritsch, 1984; Convective complexes. Earth and Mineral Sciences, 54, 1-4.

Miller, M. J., 1978: The Hampstead storm: A numerical simulation of a quasi-stationary cumulonimbus system. Quart. J. Roy. Meteor. Soc., 104, 413-427.

Newton, C. W., and J. C. Fankhauser, 1975: Movement and propagation of multicellular convective storms. Pageogh., 113, 747-764.

Purdom, J. F. W., 1973: Meso-highs and satellite imagery. Mon. Wea. Rev., 101, 180-181.

---, 1976: Some uses of high-resolution GOES imagery in the mesoscale forecasting of convection and its behavior. Mon. Wea. Rev., 104, 1474-1483.

---, 1979: The development and evolution of deep convection. Preprints 11th Conf. Severe Storms, Kansas City, MO., Amer. Meteor. Soc., 143-150.

Rodgers, D. M., K. W. Howard and E. C. Johnston, 1983: Mesoscale convective complexes over the United States during 1982. Mon. Wea. Rev., 111, 2363-2369.

---, M. J. Magnano and J. H. Arns, 1985: Mesoscale convective complexes over the United States during 1983. Mon. Wea. Rev., 113, 888-901.

Welshinger, M. J., 1985: Factors leading to the formation of arc cloud complexes. Masters Thesis, Texas A & M Univ., College Station, TX., 117 pp.

Wilhelmson, R. B., and C. S. Chen 1982: A simulation of the development of successive cells along a cold outflow boundary. J. Atmos. Sci., 39, 1466-1483.

Zehr, R. M. and James F. W. Purdom, 1982: Examples of a wide variety of thunderstorm propagation mechanisms. Preprints 12th Conf. Severe Storms, San Antonio, TX., Amer. Meteor. Soc., 499-502.

Zipser, E. J., 1984: The national STORM program STORM-Central phase

preliminary program design. Prepared by the National Center for Atmospheric Research for the team for STORM-Central, Boulder, CO 80303.

NIGHTTIME ATMOSPHERIC STABILITY CHANGES AND THEIR EFFECTS ON THE TEMPORAL INTENSITY OF A MESOSCALE CONVECTIVE COMPLEX

Jeffrey S. Hovis

and

Kenneth C. Brundidge

Texas A&M University

College Station, Texas

Prepared for George C. Marshall Space Flight Center

under Grant NAG8-043

ABSTRACT

Nighttime Atmospheric Stability Changes and their Effects on the Temporal Intensity of a Mesoscale Convective Complex.

A method of interpolating atmospheric soundings while reducing the errors associated with simple time interpolation was developed. The purpose of this was to provide a means to determine atmospheric stability at times between standard soundings and to relate changes in stability to intensity changes in an MCC. Four MCC cases were chosen for study with this method with four stability indices being included.

At this time, the study of all four cases is incomplete and only the preliminary results for Case 1 are described. The discussion centers on three aspects for each stability parameter examined: the stability field in the vicinity of the storm and its changes in structure and magnitude during the lifetime of the storm, the average stability within the storm boundary as a function of time and its relation to storm intensity, and the apparant flux of stability parameter into the storm as a consequence of low-level storm relative flow. It was found that the results differed among the four stability parameters, sometimes in a conflicting fashion. Thus, an interpolation of how the storm intensity is related to the changing environmental stability depends upon the particular index utilized. Some explanation for this problem is offered.

ACKNOWLEDGEMENTS

The work reported upon here was in part supported by the National Aeronautics and Space Administration under the auspices of the Atmospheric Sciences Division, Space Sciences Laboratory, Marshall Space Flight Center under Grant NAG8-043.

TABLE OF CONTENTS

LIST OF TABLES

LIST OF FIGURES

I. INTRODUCTION

Mesoscale Convective Complexes (MCCs) have recently been receiving considerable attention from the meteorological research community. The research on MCCs seems to have blossomed since these long-lived thunderstorm systems were defined by Maddox (1980) on the basis of their appearance in satellite imagery coupled with cloud top temperatures of their convective elements.

MCCs are important features in the weather of the midwestern section of the United States. Fritsch et al. (1981) found that these storms were responsible for a large percentage of the rainfall in this area. Several researchers (Maddox et al., 1982; Rodgers et al., 1983) have found that they also produce a significant amount of severe weather including flash floods, tornadoes, high winds, and hail, which cause many deaths, injuries, and significant property damage.

Four groups of researchers (Maddox, 1981; Maddox et al., 1982; Rodgers et al., 1983; Rodgers et al., 1985) have studied the life cycle of these storms by using the criteria set up by Maddox (1980). The first storms were found to form, on average, in the midafternoon about 2100 GMT. The storm was found to build in size with time and usually to meet the definition of an MCC at approximately 0300 GMT, which corresponds to the nighttime hours in the midwest. The maximum extent and intensity were reached in the early morning hours at about 0800 GMT. The time of 1230 GMT was the approximate time of termination, in the sense that the storm no longer met the definition of an MCC. Thus, while the average life span of an MCC as such

was about 9 h, convective storm activity associated with the system could last much longer.

Several researchers have shown that upper air observations at 12-h intervals are inadequate for the study of short-lived mesoscale processes. House (1960) concluded that the upper air network with an average spacing between observations of 220 n mi and time spacing of 12 h was insufficient to resolve the mesoscale features that led to the formation, movement, and dissipation of squall lines. Kreitzburg and Brown (1970) showed the mesoscale features within the synoptic scale flow could be linked to the variability of the weather. When looking at a continental occlusion with rawinsonde observations at 90-min intervals they found synoptic-scale features, while having continuity of days in time and around 1000 mi in space, contained mesoscale features with time continuity of a few hours and space continuity of a few hundred miles.

Wilson and Scoggins (1976) studied the atmosphere using rawinsonde observations taken during AVE (Atmospheric Variability Experiment) II. They found that between 30-60% of the total change in atmospheric variables observed over the 12-h period occur within a 3-h interval. In several cases the 3-h changes were larger than those measured over 12 h. As a matter of fact, large changes of vertical motion and potential instability can lead to a change in convective activity by a factor of more than seven over that found in the 12-h data.

Dupuis and Scoggins (1979) used a linear time interpolation scheme to estimate the structure of the atmosphere over the regular 12-h interval between rawinsonde observations. These interpolated values were compared with the actual 3-h observations. They found that the magnitudes of the non-linear changes were largest in areas of convection. The instability increased non-linearly in areas of convection as did low-level convergence and upward vertical motion. This was determined to be important in the release of the potential instability. They concluded that linear time interpolation was inadequate in defining variability over time of atmospheric parameters.

Since vorticity and atmospheric stability are important parameters in convection, Read and Scoggins (1977) used 3-h rawinsonde data from AVE IV to compare the 3-h changes of these parameters to those measured over 12 h for the same time period. Instability was found to be greatest at 3 h prior to thunderstorm development. This would hardly be seen with conventional 12-h observations. Changes in the magnitudes of terms in the vorticity equation also were found to be larger in the 3-h data than that found in the 12-h data. They concluded that the changes in the vorticity, stability, and intensity of the convection over the 3-h periods indicated that studies of convective activity could not be adequately done using 12-h observations.

Vertical motion variability between 3-h and 12-h rawinsonde data has been studied by Overall and Scoggins (1975). Vertical motion had been determined to be important in enhancing and maintaining convective activity by Byers (1944). So, unseen changes in vertical motion could lead to unexplained occurrences of convection. Overall and Scoggins found that

changes in vertical motion for 3-h data could be as large as four times that found when looking at 12-h observations. They also found that the number of mesoscale features that could be analyzed increased as the interval between rawinsonde observations decreased from 12 to 3 h.

Since the MCC is predominantly a nocturnal event, daytime heating does not play an important role in the maintaining of the MCC intensity. So, some other important feature, such as atmospheric stability aloft, must play a significant role in controlling the intensity of the MCC during the nighttime. Considering all this information, research was performed with the following objectives in mind.

(1) to develop a method of interpolating atmospheric soundings to 500 mb between the standard observation times, and

(2) to use these interpolated soundings to examine how the changing stability of the atmosphere in the environment of a Mesoscale Convective Complex (MCC) is related to its temporal intensity changes.

II. PROCEDURE

In order to obtain reasonably accurate interpolated atmospheric soundings, the following was done.

Two AVE-SESAME (Atmospheric Variability Experiment- Severe Environmental Storms and Mesoscale Experiment) data sets were obtained in which radiosonde observations were taken at 3-h intervals for 00 through 12 GMT.

Initially, the data sets were analyzed to separate them into three different groups (storm, non-storm, and all stations). This separation was done by utilizing radar summary maps for the periods involved. If a station had rain or a thunderstorm located within approximately 50 km of it during the period of 2235 GMT from the previous day to 1235 GMT of the day of interest, the station was classified as a storm case. Otherwise, it was a non-storm case. Once this was done, the following interpolation routines were applied to each of these new data sets.

Linear interpolation in time at 25 mb intervals up to 500 mb, not including the surface level, was then performed between the 00 and the following 12 GMT observations to obtain values of temperature and mixing ratio at 03, 06, and 09 GMT. These interpolated values were compared to the actual measured values in order to identify a level of least average error for each of the times.

Vertical interpolation in pressure was then performed using the values at the levels of least average error and the observed values at the surface. This process was carried out from the surface to the 500 mb level at 25 mb intervals also.

In order to incorporate both interpolation methods into one general method, the values obtained from the two interpolations (time and pressure) at each reported time and every level were then matched with the actual measured values to get a least squares fit to the observed data. Three sets of coefficients (storm, non-storm, and all stations) were obtained for use in the resulting interpolation equations. An estimate of the accuracy of the resulting interpolation relationships for temperature and mixing ratio was then obtained by applying them to another AVE-SESAME data set. Also, the results were then examined to see if there is any significant benefit in having separate interpolation equations for storm and non-storm location.

After the interpolation relationships had been determined, they were applied to data sets from areas around MCCs that had previously been identified by Welshinger (1985). Each data set included all upper air stations with available data that were within several hundred kilometers of the location of the MCC.

In order for a station to be used, upper air data, including mandatory and significant levels up to 500 mb, had to be available. Also, the station had of have surface data for 03, 06, and 09 GMT for the time period of interest, including temperature, dewpoint temperature, and sea level pressure or altimeter setting.

Various stability indices were then calculated and plotted on maps showing the air flow in and around the MCC. These indices, including the K index, Total-Totals, CAPE (Convective Available Potential Energy), and the maximum rate of decrease of equivalent potential temperature over a 25 mb layer from the surface to 700 mb (PII- Potential Instability Index), showed the stability of the environmental air feeding the storm and how it changed through the lifetime of the MCC.

The intensity of the MCC as a function of time was indicated by the area enclosed by given values of cloud-top temperatures obtained through satellite measurements. This was in keeping with the criteria established by Maddox (1980).

III. RESULTS

Interpolation Procedure

In an attempt to reduce the errors associated with linear time interpolation, interpolation with respect to pressure was also utilized. This procedure would allow changes at the surface to influence the final soundings. Table 1 shows an example of the errors associated with time interpolation and interpolation with respect to pressure. In the lowest layers, the errors associated with each method are similar. But above that level, time interpolation is much better.

In order to combine the two procedures and reduce the errors to a minimum, a least-squares fit was applied to the interpolated values at various pressure levels and various times. An example of the coefficients for the interpolation equations that resulted after the least-squares fit was applied is given in Table 2. An example of the actual interpolation equation is

$$Q = a_0 + a_1 Q_t + a_2 Q_p$$

where Q_t and Q_p represent the values of the given quantity obtained from time interpolation and pressure interpolation, respectively. Once these coefficients were determined, the interpolation relationships were tested on the original data set to see how much improvement over linear time interpolation was found. Table 3 gives a comparison of the errors resulting from simple time interpolation in comparison to the errors resulting from the new method. For this purpose, the absolute values of the errors on

Table 1. Absolute error analysis of the original data set for the two interpolation methods for temperature at 0600 GMT. All values are in C°.

Pres (mb)	Time interpolation		Pressure interpolation	
	Mean errors	Standard deviations	Mean errors	Standard deviations
1000	0.8	0.56	0.4	0.34
975	1.0	0.65	1.2	1.09
950	1.3	1.05	1.3	1.54
925	1.5	1.24	1.5	1.72
900	1.6	1.65	2.1	2.23
875	1.6	1.86	2.5	2.57
850	1.6	1.68	3.1	2.81
825	1.6	1.52	3.4	2.94
800	1.8	1.56	4.0	3.05
775	1.9	1.68	5.0	2.92
750	1.7	1.30	6.0	2.86
725	1.6	1.08	6.1	2.70
700	1.2	0.93	5.8	2.51
675	1.1	0.91	5.4	2.35
650	0.9	0.74	5.0	1.93
625	0.9	0.74	4.3	1.64
600	1.0	0.97	3.4	1.53
575	1.1	1.01	2.5	1.24
550	1.0	0.80	1.6	0.98
525	1.0	0.89	1.0	0.89
500	1.1	0.91	1.4	1.23

TABLE 2. Least squares coefficients for temperature and mixing ratio to be used to interpolate the 0600 GMT soundings.

	Temperature			Mixing ratio		
Pres (mb)	a_0	a_1	a_2	a_0	a_1	a_2
1000	14.34	0.84	−0.51	2.10	0.72	0.18
975	−0.41	0.71	0.31	−0.52	0.49	0.58
950	0.43	0.56	0.43	0.48	0.18	0.82
925	0.47	0.46	0.55	0.21	0.24	0.80
900	0.92	0.55	0.43	−0.42	0.64	0.44
875	1.51	0.55	0.39	0.00	0.76	0.28
850	0.86	0.73	0.23	1.05	0.94	−0.04
825	0.11	0.85	0.15	0.71	0.72	0.22
800	0.54	0.81	0.20	1.52	0.69	0.11
775	0.13	0.88	0.24	2.49	0.78	−0.28
750	0.17	0.95	0.21	3.32	0.74	−0 48
725	0.48	0.96	0.19	4.21	0.54	−0.63
700	0.56	0.96	0.17	3.70	0.52	−0.60
675	0.53	1.00	0.07	3.23	0.60	−0.67
650	0.83	0.94	0.11	2.23	0.80	−0.61
625	1.15	0.85	0.19	1.12	0.88	−0.42
600	1.11	0.80	0.24	0.96	0.79	−0.43
575	1.68	0.50	0.55	0.30	0.61	−0.08
550	0.74	0.66	0.35	0.20	−1.75	2.22
525	0.35	1.97	−0.96	0.24	0.42	0.20
500	0.15	0.96	0.05	0.13	0.69	0.05

Table 3. Absolute error analysis of the original data set of the two interpolation methods for temperature at 0600 GMT. All values are in C°.

Pres (mb)	Time interpolation		New method	
	Mean errors	Standard deviations	Mean errors	Standard deviations
1000	0.8	0.56	0.1	0.11
975	1.0	0.65	0.8	0.56
950	1.3	1.05	1.1	0.98
925	1.5	1.24	1.3	1.07
900	1.6	1.65	1.6	1.33
875	1.6	1.86	1.6	1.43
850	1.6	1.68	1.6	1.54
825	1.6	1.52	1.5	1.22
800	1.8	1.56	1.7	1.36
775	1.9	1.68	1.8	1.35
750	1.7	1.30	1.5	1.07
725	1.6	1.08	1.3	1.04
700	1.2	0.93	1.0	0.90
675	1.1	0.91	1.0	0.87
650	0.9	0.74	0.8	0.65
625	0.9	0.74	0.7	0.67
600	1.0	0.97	0.9	0.88
575	1.1	1.01	1.0	0.87
550	1.0	0.80	0.9	0.81
525	1.0	0.89	1.0	0.87
500	1.1	0.91	1.0	0.92

each pressure surface were averaged. The reduction in error associated with the new method is significant. If one considers an algebraic average on each pressure surface, the resulting errors are approximately zero (not shown here). This is what we would expect after applying a least-squares fit to the data. However, this does not quarantee the efficacy of the procedure when applied to independent data. Therefore, as a test of the procedure, it was applied to a third AVE-SESAME case. For the new method to be considered good, the errors associated with this new case should be small. Also, the standard deviations should be small. In Tables 4-6, the errors in temperature associated with simple interpolation in time and the new technique are compared. For this purpose, there has been no separation into storm vs non-storm soundings.

At 03 GMT (Table 4), it can be seen that between 1000 and approximately 900 mb, the new method appears to be better than linear time interpolation. Above that level, the two methods have similar errors, with neither providing a distinct advantage. Similar results are seen in Tables 5 and 6.

The results for the mixing ratio (Table 7-9) are quite similar to those for the temperature calculation. Again, the new method shows some advantage in the boundary layer where the influence of values at the surface is the greatest. However, above the boundary level, simple interpolation in time gives somewhat smaller errors.

The conclusion reached from these comparisons was that the smaller errors provided by the interpolation relationships (Table 2) in the boundary layer was of greater significance for the purpose of this study than the slight advantage gained by using linear time interpolation in the upper

Table 4. Absolute error analysis of the two interpolation methods for temperature at 0300 GMT. All values are in C°.

Pres (mb)	Time interpolation		New method	
	Mean errors	Standard deviations	Mean errors	Standard deviations
1000	1.2	0.86	0.5	0.28
975	0.8	0.47	0.7	0.56
950	1.7	2.67	1.5	2.05
925	2.0	2.48	1.7	1.75
900	1.6	1.59	1.5	1.47
875	1.3	0.92	1.2	1.09
850	1.2	0.97	1.3	1.07
825	1.3	0.81	1.3	0.96
800	1.0	0.65	1.0	0.73
775	0.9	0.62	1.2	0.81
750	0.9	0.59	0.9	0.60
725	0.8	0.58	0.8	0.53
700	0.8	0.59	0.8	0.60
675	0.8	0.78	0.9	0.79
650	0.8	0.76	0.8	0.78
625	0.7	0.60	0.8	0.70
600	0.8	0.68	0.8	0.70
575	0.9	0.77	1.0	0.80
550	1.1	1.00	1.2	1.01
525	1.0	0.92	1.0	0.86
500	1.0	0.92	0.9	0.88

Table 5. Absolute error analysis of the two interpolation methods for temperature at 0600 GMT. All values are in C°.

Pres (mb)	Time interpolation		New method	
	Mean errors	Standard deviations	Mean errors	Standard deviations
1000	1.1	0.63	0.9	0.49
975	2.0	1.81	1.6	1.19
950	2.3	2.19	1.9	1.38
925	2.4	2.21	2.2	1.51
900	1.8	1.81	1.8	1.44
875	1.7	1.42	1.7	1.47
850	1.2	1.13	1.3	1.30
825	1.3	0.92	1.5	1.15
800	1.3	0.97	1.3	1.10
775	1.3	1.06	1.3	0.98
750	1.2	1.00	1.0	0.81
725	1.0	0.70	0.9	0.74
700	0.8	0.63	0.9	0.67
675	0.8	0.73	0.8	0.77
650	0.7	0.66	0.8	0.60
625	0.8	0.57	0.7	0.55
600	0.8	0.55	0.7	0.48
575	0.9	0.75	0.9	0.77
550	0.9	0.92	0.9	0.96
525	0.9	0.95	0.9	1.01
500	1.0	1.16	1.0	1.16

Table 6. Absolute error analysis of the two interpolation methods for temperature at 0900 GMT. All values are in C°.

Pres (mb)	Time interpolation		New method	
	Mean errors	Standard deviations	Mean errors	Standard deviations
1000	0.7	0.69	0.7	0.63
975	1.7	1.46	1.6	1.53
950	2.1	1.62	1.8	1.14
925	2.2	1.91	1.9	1.32
900	1.8	1.44	1.8	1.42
875	1.4	1.47	1.4	1.46
850	1.1	0.96	1.1	0.99
825	1.3	1.04	1.3	1.09
800	0.9	0.78	1.0	0.75
775	0.9	0.83	0.9	0.75
750	0.9	0.80	0.9	0.80
725	0.8	0.73	0.9	0.70
700	0.9	0.69	0.9	0.71
675	0.7	0.72	0.8	0.81
650	0.7	0.59	0.8	0.62
625	0.6	0.57	0.7	0.62
600	0.7	0.57	0.8	0.57
575	0.7	0.52	0.7	0.47
550	0.8	0.54	0.9	0.56
525	0.7	0.58	0.9	0.71
500	0.8	0.76	0.9	0.84

Table 7. Absolute error analysis of the two interpolation methods for mixing ratio at 0300 GMT. All values are in g/kg.

Pres (mb)	Time interpolation		New method	
	Mean errors	Standard deviations	Mean errors	Standard deviations
1000	1.6	1.07	0.7	0.66
975	1.2	0.98	1.1	0.88
950	1 2	1.13	1.1	0.90
925	1.3	1.19	1.3	1.06
900	1.1	1.10	1.3	1.09
875	1.2	1.21	1.5	1.10
850	1.5	1.40	1.7	1.54
825	1.5	1.35	1.6	1.36
800	1.5	1.34	1.5	1.25
775	1.2	1.22	1.2	1.10
750	1.1	1.26	1.1	0.96
725	1.1	1.27	1.3	1.44
700	1.2	1.36	1.6	1.38
675	0.9	1.02	1.3	0.96
650	0.7	0.79	1.0	0.78
625	0.6	0.61	1.0	0.73
600	0.6	0.47	0.6	0.56
575	0.6	0.58	0.7	0.64
550	0.6	0.57	0.6	0.60
525	0.4	0.37	0.5	0.43
500	0.3	0.27	0.5	0.40

Table 8. Absolute error analysis of the two interpolation methods for mixing ratio at 0600 GMT. All values are in g/kg.

Pres (mb)	Time interpolation		New method	
	Mean errors	Standard deviations	Mean errors	Standard deviations
1000	1.4	0.63	0.6	0.37
975	1.3	1.18	0.8	0.87
950	1.0	0.84	0.9	1.10
925	1.4	1.23	1.3	1.50
900	1.5	1.27	1.4	1.39
875	1.7	1.30	1.7	1.22
850	1.8	1.71	1.9	1.59
825	1.5	1.20	1.5	1.28
800	1.6	1.66	1.6	1.29
775	1.4	1.44	1.3	1.03
750	1.5	1.51	1.5	1.19
725	1.2	1.07	1.6	1.03
700	1.2	1.07	1.7	1.00
675	1.0	0.95	1.4	0.85
650	0.8	0.80	1.1	0.69
625	0.8	0.73	0.8	0.70
600	0.6	0.57	0.8	0.64
575	0.6	0.41	0.7	0.53
550	0.5	0.42	0.7	0.54
525	0.5	0.41	0.5	0.50
500	0.5	0.38	0.5	0.41

Table 9. Absolute error analysis of the two interpolation methods for mixing ratio at 0900 GMT. All values are in g/kg.

Pres (mb)	Time interpolation		New method	
	Mean errors	Standard deviations	Mean errors	Standard deviations
1000	0.9	0.86	0.5	0.47
975	1.2	0.99	0.9	0.51
950	0.9	1.06	0.7	0.47
925	1.4	1.80	1.2	1.94
900	1.3	1.67	1.2	1.87
875	1.4	1.08	1.4	1.20
850	1.6	1.68	1.8	1.53
825	1.7	2.00	1.9	1.82
800	1.3	1.84	1.5	1.69
775	1.2	1.45	1.4	1.25
750	1.0	0.92	1.1	0.82
725	0.9	0.75	1.2	0.73
700	1.1	0.98	1.3	0.88
675	0.7	0.70	1.1	0.74
650	0.8	0.73	1.1	0.64
625	0.8	0.82	1.0	0.79
600	0.7	0.67	0.9	0.78
575	0.6	0.50	0.8	0.61
550	0.5	0.49	0.6	0.51
525	0.4	0.44	0.5	0.45
500	0.4	0.34	0.5	0.36

levels. Also when comparing the errors associated with the new method applied to separated storm and non-storm cases, there was no distinct advantage found to separation of the cases over performing the interpolation without regard to storm or non-storm sounding. Consequently the combined interpolation technique without separating the soundings was used in the remainder of this study.

Stability Indices

The four MCC cases for the study are listed in Table 10. In these four cases, on average, nine rawinsonde stations were included in the study of each case. Case 1 contained seven stations which was the smallest number while Case 4 had 13 stations.

Table 10. Mesoscale Convective Storm Systems (MCSs) included in study. Initiate and terminate times are after Maddox et al. (1982), Rodgers et al. (1983, 1985).

Case number	Date	Initiate	Maximum extent *	Terminate
1	10/11 Apr 81	2315/10	0300/11	0531/11
2	9 May 81	0115/09	0500/09	1015/09
3	17 May 82	0030/17	0400/17	0730/17
4	10/11 Jun 82	2245/11	0700/11	1530/11

*The times listed are the maximum extent of the area, as depicted on IR satellite imagery, with temperatures $\leq$ -62 C.

After the interpolated soundings were obtained, a variety of stability indices were examined. These were the K, modified K, Total-Totals, modified Total-Totals, CAPE, and Showalter indices along with the maximum rate of decrease of equivalent potential temperature over a 25 mb layer from the surface to 700 mb (PII- Potential Instability Index). The difference between the modified and the regular versions of the K and Total-Totals indices is that in the modified versions, the moisture was averaged between the surface and 850 mb for determination of a dewpoint temperature to be used at 850 mb. In the standard versions, the observed 850 mb dewpoint is used. The justification for this approach is that in many of the soundings, the moisture was confined to the layer below 850 mb. So, the value of the standard index could be misleading in terms of its accounting for lower tropospheric moisture.

After calculating, plotting and examining the fields of these indices, the standard versions of the K and Total-Totals indices along with the CAPE were discarded. The reason for dropping the K and Total-Totals indices was that the fields of these indices were similar in nature to the fields plotted from the modified versions Also, it was felt that that the modified versions were more representative of the actual stability of the atmosphere. The CAPE index, which is a measure of the positive area of the sounding when plotted on a Skew-T, Log-P diagram, was small or even zero throughout the plotted fields. This result is not surprising since the stabilizing effect of nocturnal, radiative cooling was present in the boundary layer.

The Environmental Airflow

To show the airflow in the atmosphere around the MCC, the winds at approximately 1 km above the surface at 00 and 12 GMT were obtained from the rawinsondes. This level was chosen because it is thought to be near the top of the boundary layer and therefore indicates the flow, free of friction, whose stability may be affecting the storm. To get the winds at 03, 60, and 09 GMT, linear time interpolation between the 00 and 12 GMT wind values was used. The movement of each storm was determined from enhanced infrared, satellite images. This motion vector was then subtracted from the 1 km winds to get the storm-relative wind vectors.

Results for Case 1

The analyses of the four cases listed in Table 10 are incomplete at this time. Some of the results for Case 1 are available and are discussed below.

Figures 1a,b,and c deal with the field of modified K index at 00, 03, and 06 GMT, respectively. It can be seen in Table 10 that these times correspond to 45 min after MCC initiation, the time of maximum extent, and 29 min after MCC termination, respectively. Termination refers only to the time that the storm ceased to qualify as an MCC, and not to its actual demise.

In Fig. 1a, the storm position is indicated by the heavy lines indicating the IR equivalent black-body temperature field at the top of the storm. The storm-relative velocity vectors in knots are shown for selected stations and the thin lines represent the modified K values. Figures 1b and 1c show the same quantities. Several features can be observed by a

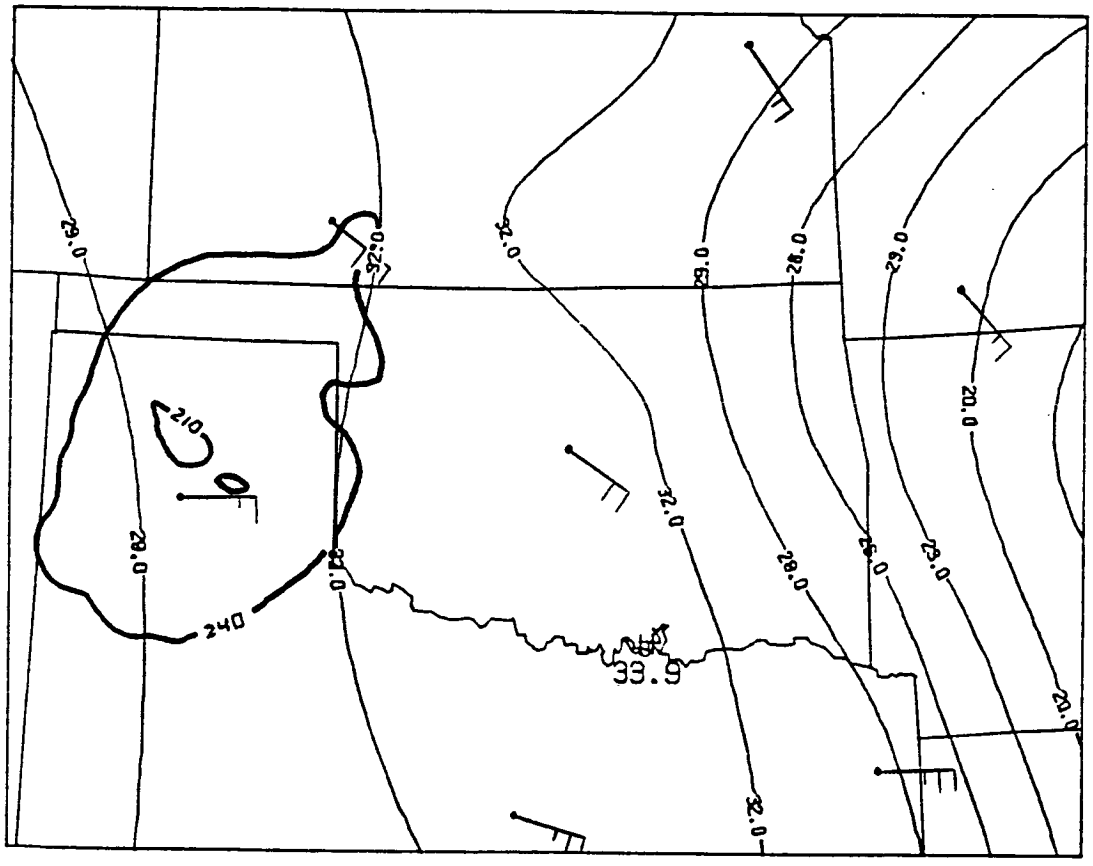

Fig. 1a. Modified K index field for 0000 GMT 11 April 1981.

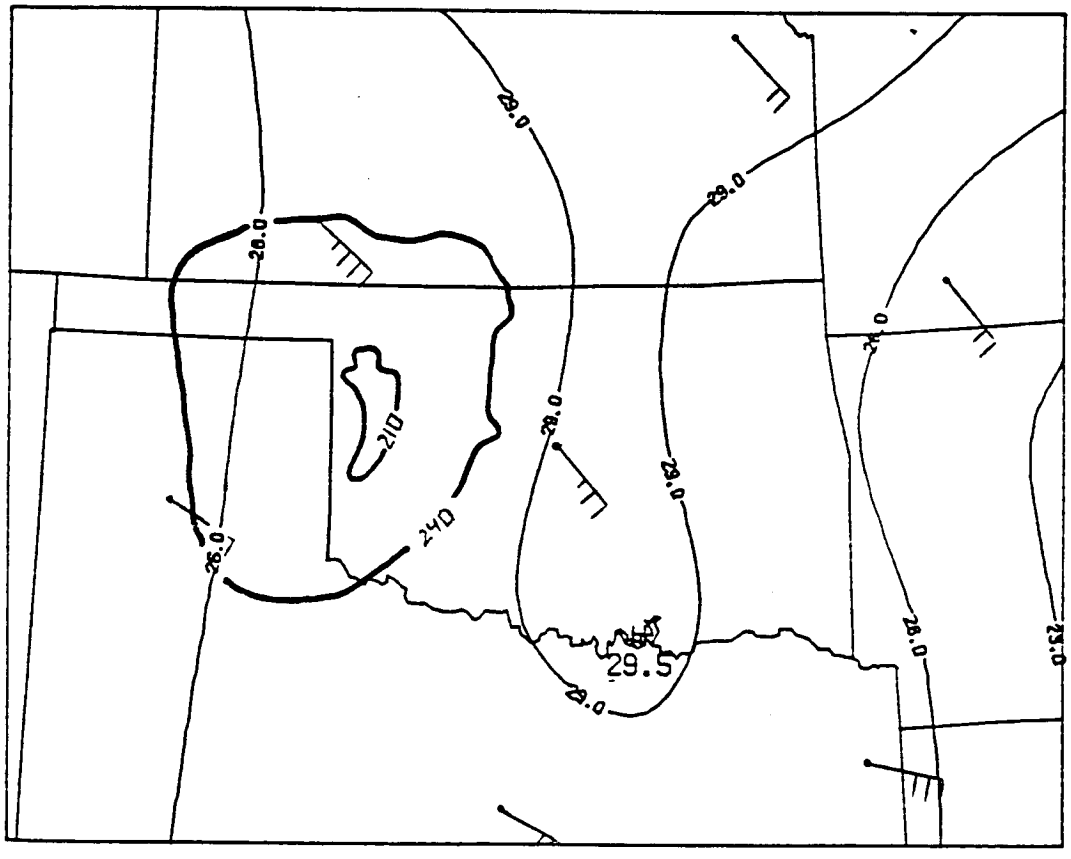

Fig. 1b. Same as Fig. 1a except for 0300 GMT.

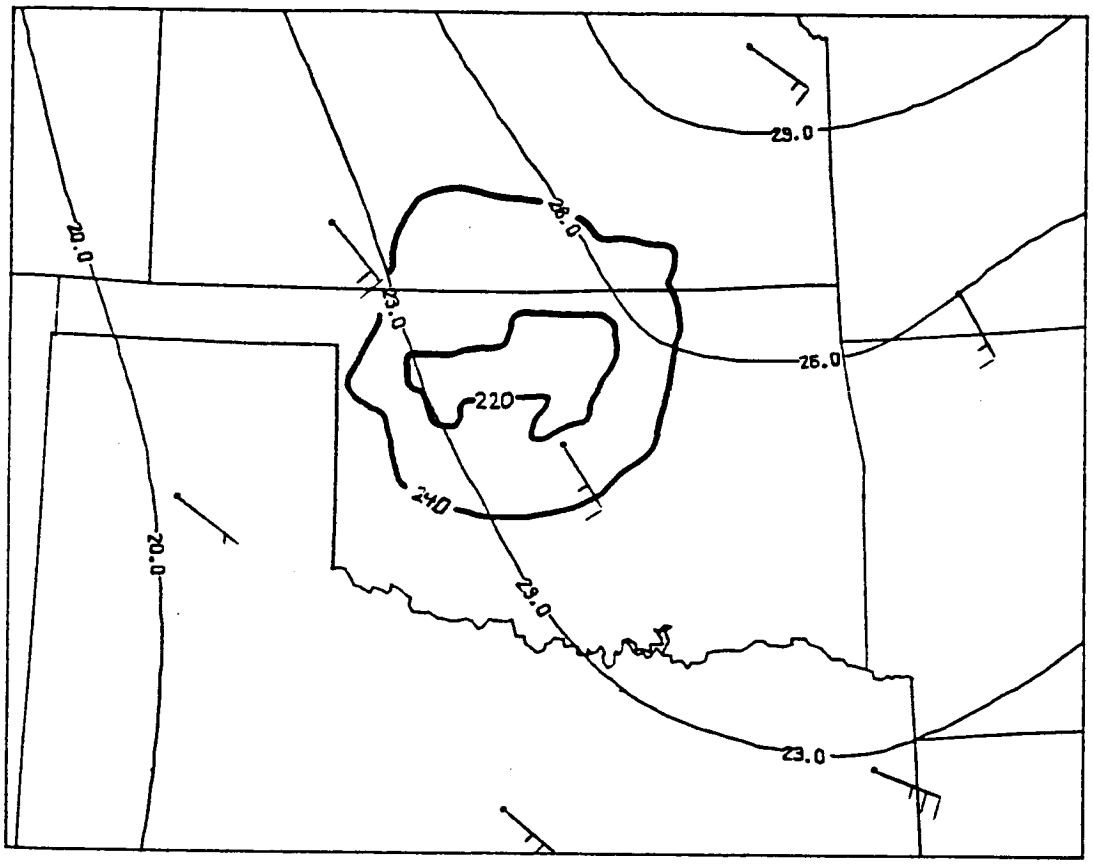

Fig. 1c. Same as Fig. 1a except for 0600 GMT.

comparison of these three figures. First, it is noted that throughout this 6-h period, there is an axis or ridge of larger modified K values to the east of the storm. However, as time goes on, there is a generalized decrease of modified K values across the entire area. This reflects the stabilizing influence of the nocturnal cooling. The relative flow at 00 and 03 GMT indicated an apparent advection of less stable air into the storm area which would seem to explain why the storm reached its maximum extent at 03 GMT. However, a visual examination of the modified K values contained within the 240°K isotherm at each time reveals that the approximate average value went from about 30 at 00 GMT to 27 at 03 GMT and then to about 24.5 at 06 GMT. Thus, it would appear that the radiation effect dominated over the advection effect so that even as the storm was approaching maximum intensity, it was self-destructing in the sense that it was drawing in more-stable air.

Figures 2a b,and c show the situation for the stability field based on the modified Total-Totals index. These figures indicate an altogether different situation than seen in Figures 1a-c. In these figures the most unstable region is to the northwestern side of the storm at 00 and 03 GMT and to the northeast and southwest of the storm at 06 GMT. The relative flow throughout the time period indicates an apparent advection of more stable air into the storm area. A general diminishing of stability across the area occurs only in the period from 03 to 06 GMT. The most unstable approximate storm average value corresponds to the time of maximum extent at 03 GMT. So in this case, the modified Total-Totals field did not

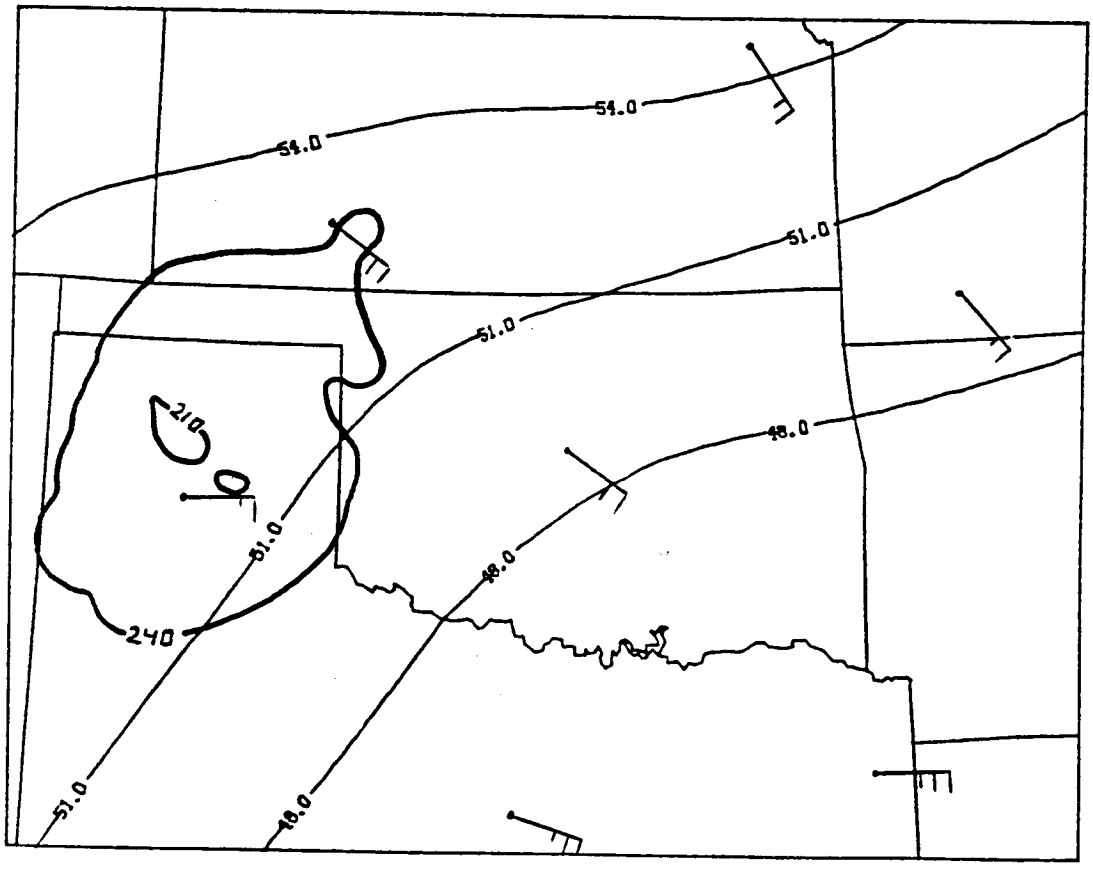

Fig. 2a. Modified Totals-Totals index field for 0000 GMT 11 April 1981.

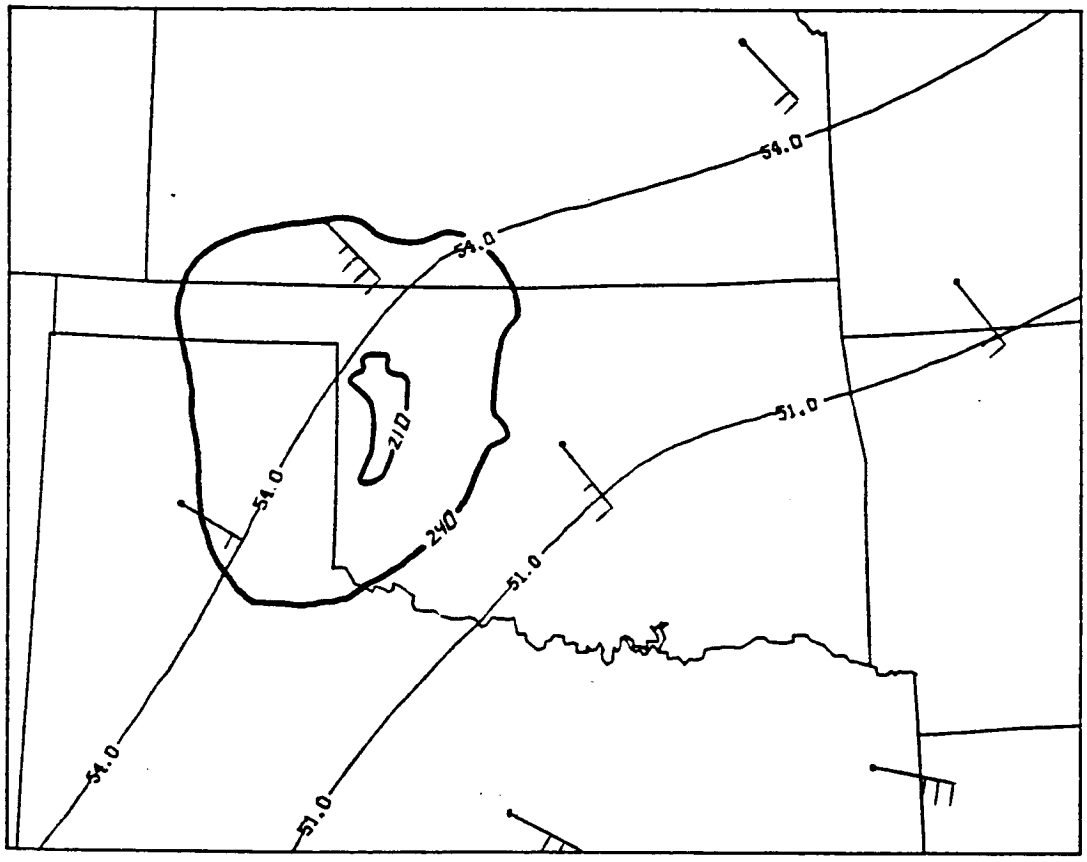

Fig. 2b. Same as Fig. 2a except for 0300 GMT.

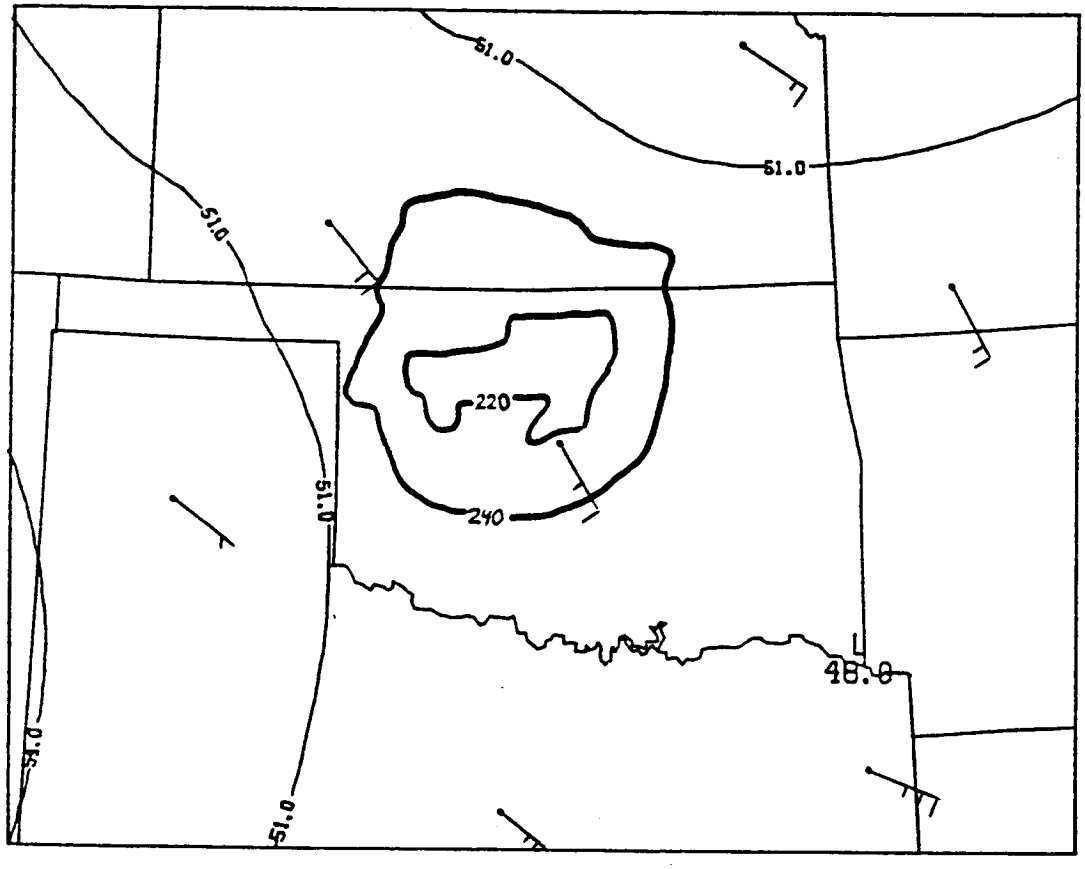

Fig. 2c. Same as Fig. 2a except for 0600 GMT.

immediately indicate the stabilizing effect of nocturnal cooling.

The Showalter index stability fields at 00 through 06 GMT are shown in Figures 3a,b,and c, respectively. These figures show a similar situation to that shown in Figures 2a-c. The most unstable regions from 00 to 06 GMT are located to the north and south of the storm. The relative flow at 00 GMT indicates that the apparent advection at this time is small but is probably moving slightly less-stable air towards the storm area. At 03 and 06 GMT, the apparent advection again is small but indicated movement of somewhat more stable air into the storm area. This initiation in the apparent advection of more stable air into the storm corresponds to the time of maximum extent. The approximate average of the Showalter index within the 240°K isotherm went from about -0.5 at 00 GMT to about -2.0 at 03 GMT and then to -1.0 at 06 GMT. Thus, the most unstable value again corresponded to the time of maximum extent. Again, the effect of the nocturnal cooling in the lower troposphere was not reflected in the Showalter field until 06 GMT.

The PII (Potential Instability Index) stability field is depicted in Figures 4a,b,and c for 00, 03, and 06 GMT, respectively. The most unstable air, according to this index, is located to the north of the storm with an axis of less-stable air to the east of the storm. This axis shifts somewhat westward with time while the storm moves northwestward until it becomes located on the axis at 06 GMT. Also during this period, the entire field of PII undergoes a modification in values indicating greater stability with

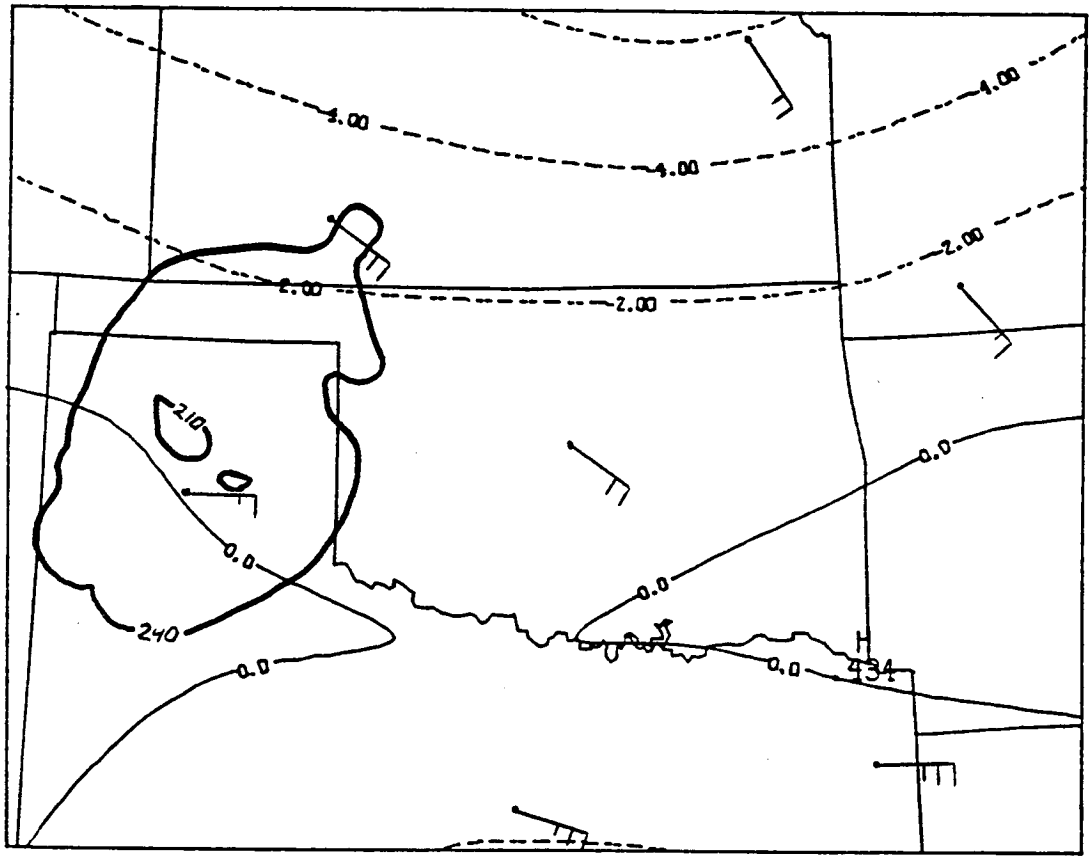

Fig. 3a. Showalter index field for 0000 GMT 11 April 1981.

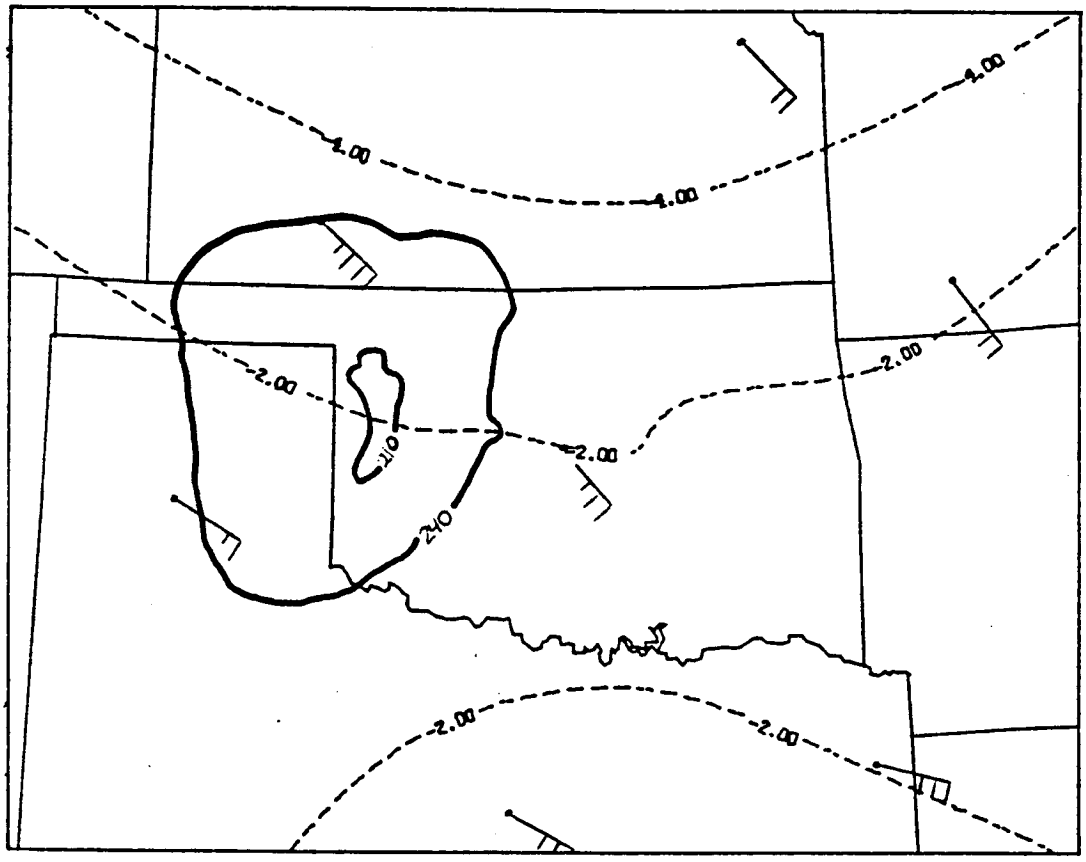

Fig. 3b. Same as Fig. 3a except for 0300 GMT.

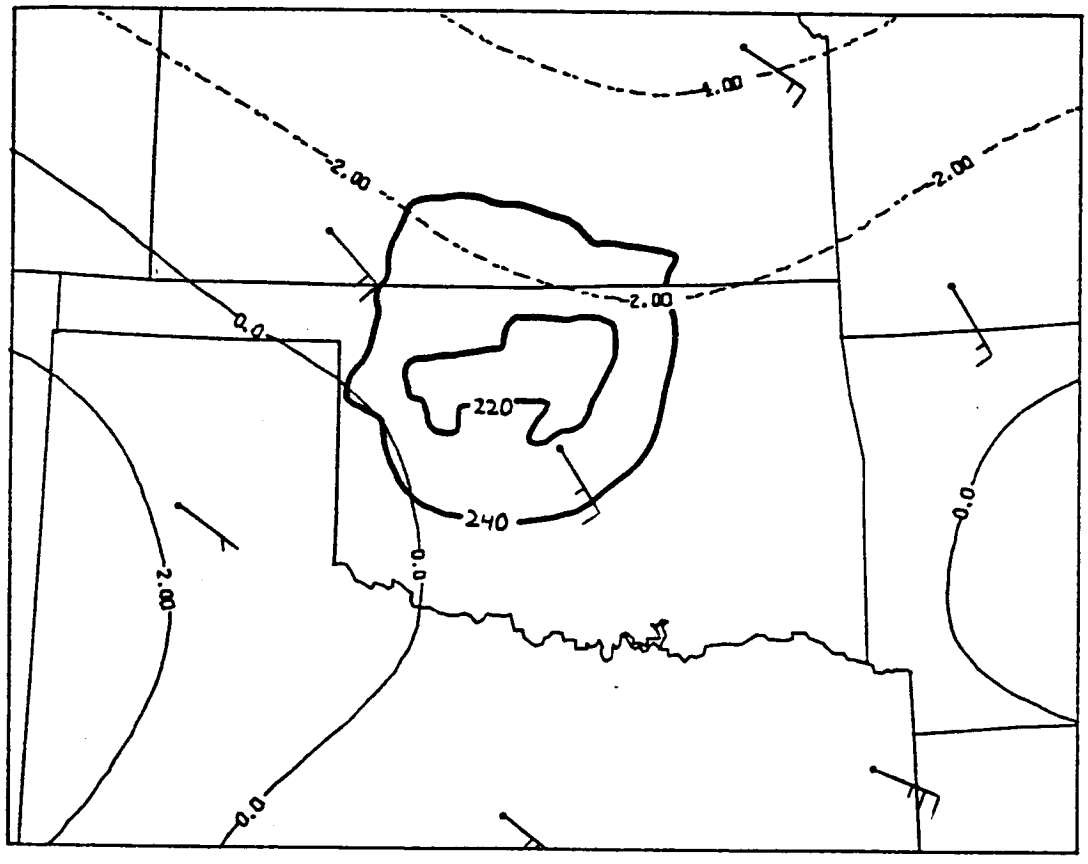

Fig. 3c. Same as Fig. 3a except for 0600 GMT.

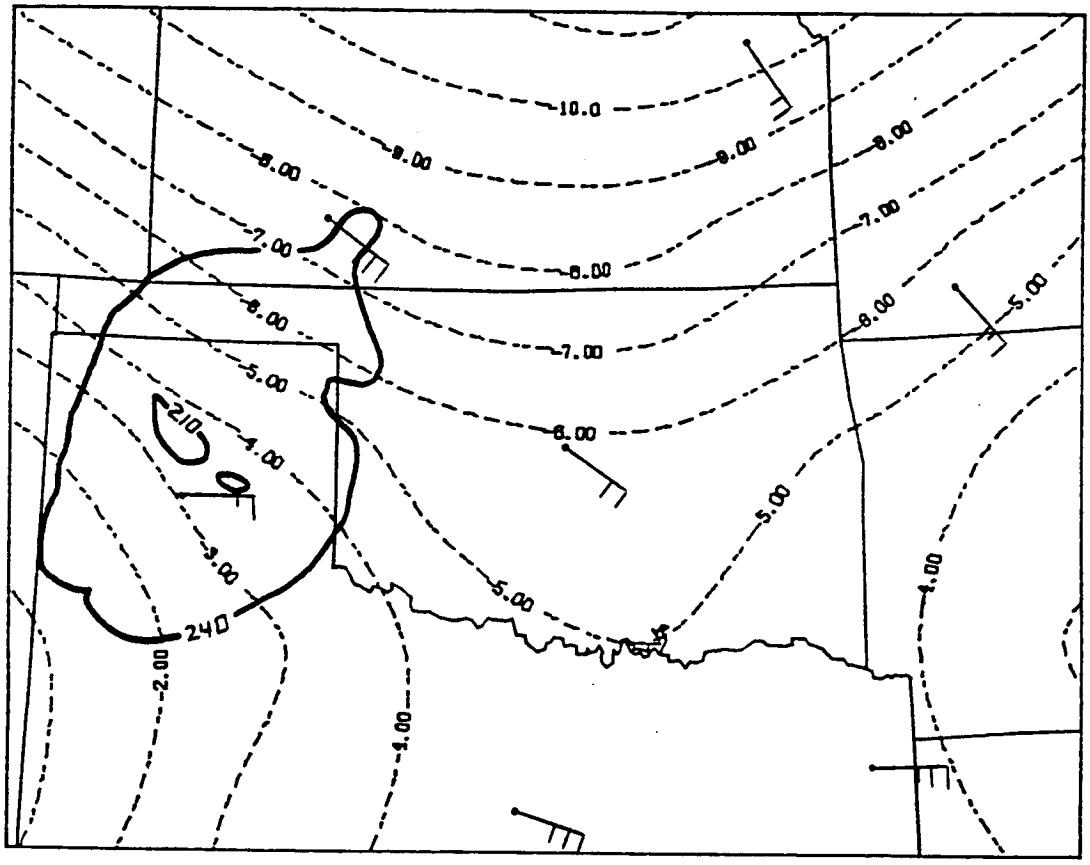

Fig. 4a. Potential Instability Index field for 0000 GMT 11 April 1981.

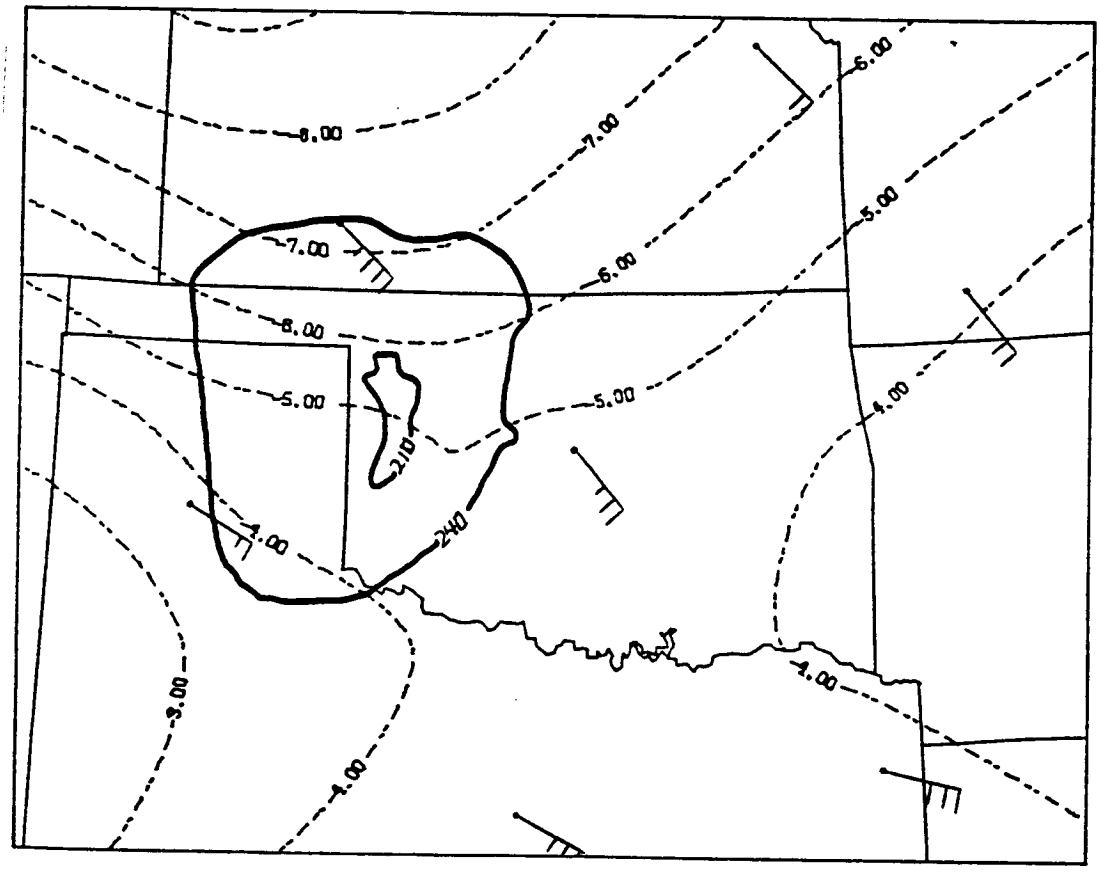

Fig. 4b. Same as Fig. 4a except for 0300 GMT

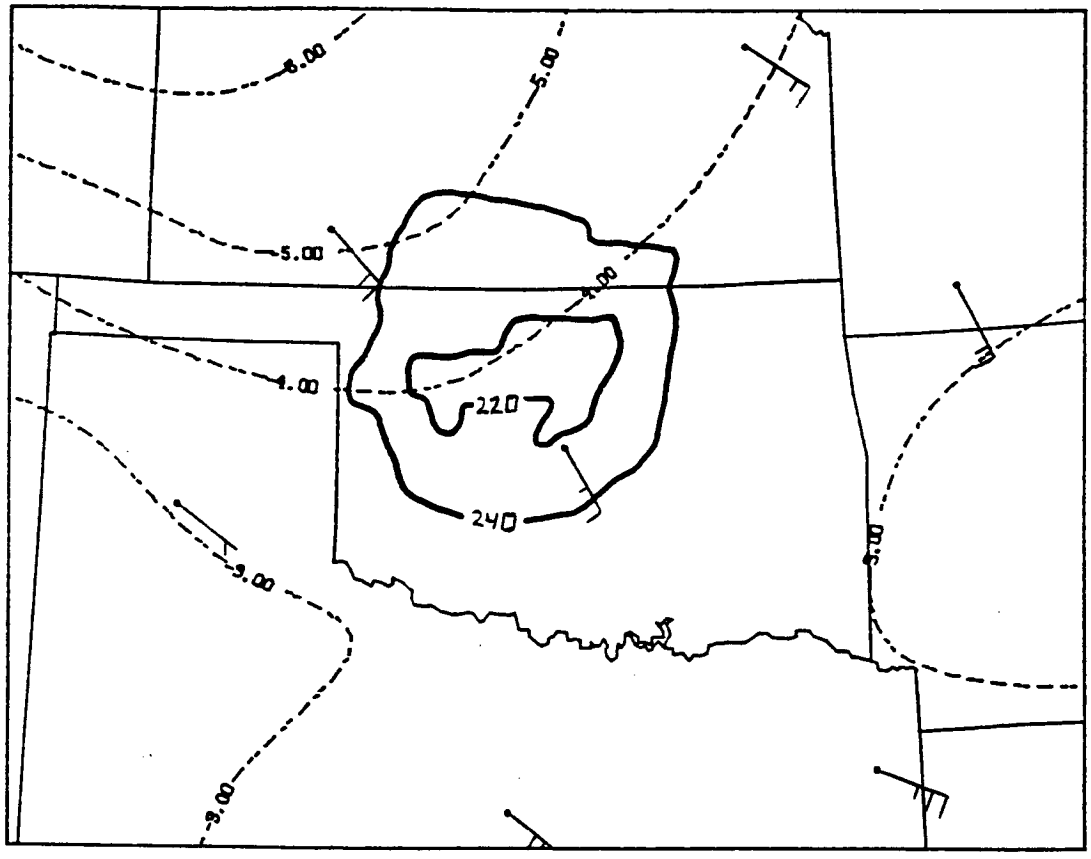

Fig. 4c. Same as Fig. 4a except for 0600 GMT.

time.

At 00 GMT, the average PII value within the 240 K isotherm was approximately -4.5. By 03 GMT, this average has decreased to about -5.5 meaning the area was slightly less-stable. Finally, at 06 GMT, the average was about -4.0. These changes in internal stability correspond nicely with the intensity changes in the storm. The relative flow at 00 GMT suggests a weak flux of less-stable air into the storm. But at 03 and 06 GMT, the flow suggests an apparent flux of stable air into the storm area. Again, this corresponds well to the observed intensity variations of the MCC.

IV. TENTATIVE CONCLUSIONS

One would expect that regardless of the structure of the stability field provided by any of the given indices that certain changes and relationships should be observed to occur during the lifetime of the MCC. These are:

1. The stabilizing influences of the nocturnal radiative cooling should be reflected in the overall stability field becoming more stable with time.
2. The stability within the storm boundary should be reflected in the intensity changes in the storm. Thus, the time of maximum extent of the storm should occur near the time of maximum instability in the storm. Increasing stability of the air in the storm should lead to diminished storm intensity.
3. The storm-relative flow should indicate a flux of less-stable air into the storm as it approaches its most intense stage and a flux of more-stable air into the storm as its termination time is approached.

In fact, the four stability indices examined here differed from one another in some of these aspects while agreeing in others. Only the Potential Instability Index (PII) met expectations in every category listed above. The reason for this is probably a consequence of the quantities which go into the calculation of each of these indices and the extent to which they become modified by the lower tropospheric stabilization provided by the interpolation scheme. The solution to this problem requires additional analysis of Case 1 and the comparison with results from the other

cases under study.

V. REFERENCES

Byers, H. R. 1944: General Meteorology., McGraw-Hill, Inc., New York, NY, 461 pp.

Dupuis, L. R. and J. R. Scoggins, 1979 Differences between measured linearly interpolated synoptic variables over a 12-h period during AVE IV. NASA CR-3150, NASA Marshall Space Flight Center, Huntsville, AL, 126 pp.

Fritsch, J. M., R. A. Maddox and A. G. Barnstron, 1981: The character of mesoscale convective complex precipitation and its contribution to warm season rainfall in the U. S. Preprints, 4th Conf. on Hydrometeorology, Reno, NV, Amer. Meteor. Soc., 94-99.

House, D. C., 1960: Remarks on the optimum spacing of upper air observations. Mon. Wea. Rev., 88, 97-100.

Kreitzburg, C. W. and H. A. Brown, 1970: Mesoscale weather systems within an occlusion. J. Appl. Meteorol., 9, 417-432.

Maddox, R. A. 1980: Mesoscale convective complexes. Bull. Amer. Meteor. Soc., 61, 1374-1387.

_____ 1981: The structure and lifecycle of midlatitude mesoscale convective complexes. Atmos. Sci. Pap. No. 336, Colorado State University 311 pp.

_____, D M. Rodgers and K. W. Howard, 1982: Mesoscale convective complexes over the United States during 1981. Mon. Wea. Rev. 110, 1501-1514.

Overall, J. W. and J. R. Scoggins, 1975: Relationships between motion on isentropic surfaces from 3-h rawinsonde data and radar echoes. NASA CR-2558, NASA Marshall Space Flight Center, Huntsville, AL, 111 pp.

Read, W. L and J. R. Scoggins, 1977: Vorticity imbalance and stability in relation to convection. NASA CR-2819, NASA Marshall Space Flight Center, Huntsville, AL, 111 pp.

Rodgers, D. M., K. W. Howard and E. C. Johnston, 1983. Mesoscale convective complexes over the United States during 1982. Mon. Wea. Rev., 111, 2363-2369.

_____, M. J. Magnano and J. H. Arns, 1985: Mesoscale convective complexes over the United States during 1983. Mon. Wea. Rev., 113, 888-901.

Welshinger, M. J., 1985: Factors leading to the formation of arc cloud complexes. Masters Thesis, Texas A&M Univ., College Station, TX, 110 pp.

Wilson, G. S. and J. R. Scoggins, 1976: Atmospheric structure and variability in areas of convective storms determined from 3-h rawinsonde data NASA CR-2678, NASA Marshall Space Flight Center, Huntsville, AL, 118 pp.